UNIVERSITY "EFTIMIE MURGU" RESITA

Doctoral School of Engineering

DOCTORAL THESIS

Detection of branched cracks in beam-like structures

Author: Eng. Cristian Tufişi

DOCTORAL COMITTEE MEMBERS

President	Prof. univ. dr. eng Dorian NEDELCU	- University „Eftimie Murgu" Reşiţa
Scientific supervisors:	Prof. univ. dr. eng. Gilbert-Rainer GILLICH	- University „Eftimie Murgu" Reşiţa
	Prof. univ. dr. eng. Magd ABDEL WAHAB	- Ghent University, Belgium
Official reviewers:	Prof. univ. dr. eng. Sorin VLASE	- Transilvania University of Braşov
	Prof. univ. dr. eng. Nicolae-Doru STĂNESCU	- University of Piteşti
	Assist. prof. dr. eng. habil. Zoltan-Iosif KORKA	- University „Eftimie Murgu" Reşiţa

REŞIŢA 2020

Acknowledgment

The Ph.D. thesis "Detection of branched cracks in beam-like structures" aims to bring contributions in the field of science and engineering practice, mainly in structural health monitoring by presenting methods of identifying the position and severity of cracks in structures by using natural frequencies and determining the accuracy of these methods in detecting different types of damages.

In achieving the objectives, I had the permanent and competent support of the Doctoral School of the “Eftimie Murgu” University of Resita, but also some specialists from outside the university.

I am especially grateful to the scientific supervisors, Prof.dr.eng. Gilbert-Rainer Gillich and Prof.dr.eng. Magd Abdel Wahab, for the guidance and support, provided throughout the doctoral studies.

I would also like to thank the guidance committee members, namely Prof.dr.eng. Dorian Nedelcu, Prof.dr.eng. Codruta-Oana Hamat and Assist.prof.dr.eng.habil. Zoltan Iosif Korka, for the support provided whenever necessary. I express my gratitude to Prof.dr.eng. Dorian Nedelcu for helping to implement the developed algorithm in the Python-based software PyDAM, and to Assist.prof.dr. Ion Cornel Mituletu for helping with the experimental stage of the thesis.

I would like to send very special thanks to the company, Centrul Prelucrari Mecanice Bocsa, namely to Radu Pantiuc for providing the experimental samples by means of electrical discharge machining.

I would like to express my gratitude to Prof. univ. dr. eng. Sorin Vlase from the Transilvania University of Brașov and to Prof. univ. dr. eng. Nicolae-Doru Stănescu from University of Pitești which, as scientific reviewers, have contributed with competent suggestions and observations to the improvement of the current thesis.

Also, I would like to extend my thanks to my family and friends who were always there to support me in every possible way.

Reşiţa, 23 September 2020 Author: Tufişi Cristian

Contents

LIST OF FIGURES

LIST OF TABLES

SYMBOLS AND ADNOTATIONS

a	[mm]	damage depth
A	[mm^2]	cross section area
B	[mm]	beam width
$c(a)$	[-]	correction coefficient
$c_i^{x_1}$, $c_i^{x_2}$	[-]	pseudo-severity coefficients
$c_{Si}(a, x_1, x_2)$	[-]	enhanced correction coefficient
$c_i^{x_1 - x_2}$	[-]	reduced section coefficient
$COMAC$	[-]	coordinated modal assurance criterion
D_{sem}	[-]	damage identification index
DOF	[-]	degree of freedom
E	[MPa]	longitudinal elasticity modulus
f	[Hz]	natural frequency
$f_{i\text{-}D}$	[Hz]	natural frequency of the damaged beam
$f_{i\text{-}U}$	[Hz]	the frequency for the fault-free beam
FEM	[-]	finite element method
FFM	[-]	fracture mechanism theory
H	[mm]	beam height
i	[-]	vibration mode number
I / Iz	[mm^4]	moment of inertia
Ic	[mm^4]	reduced section moment of inertia
k	[1/mm]	curvature
k_1; k_2	[-]	stress intensity factors
L	[mm]	beam length

m	[kg]	mass
M	[Nm]	bending moment
$M_i(x)$	[Nm]	bending moment
$M_{ci}(x)$	[Nm]	bending moment
MAC	[-]	modal assurance criterion
q	[N]	load
q(x,t)	[N]	normal force distributed on the neutral fiber
R	[mm]	curvature radius
SHM	[-]	Structural Health Monitoring
$s(a)$	[-]	pseudo-severity
t	[s]	time
$T(x)$	[N]	shear force
$T(x)$	[N]	shear force
U_i	[J]	strain energy
U_{Ci}	[J]	strain energy of the damaged beam
v	[mm]	deflection of the neutral axis on the Z direction
x	[mm]	damage position from the fixed end
y	[mm]	distance to neutral axis
Z	[-]	direction of the defined ratio
ε	[mm/mm]	specific linear deformations
ρ	[kg/m^3]	density
γ	[-]	damage severity
δ_{ij}	[-]	Kronecker function
$\bar{\phi}_i''(x)$	[-]	normalized modal curvature
ω	[rad/s]	pulsation

λ_i	[-]	dimensionless wave number for mode number i
ς_i^{0-L}	[-]	strain energy coefficient for a beam of length L
$\varsigma_i^{x_1-x_2}$	[-]	strain energy coefficient for the reduced section interval
$M_{\max}^2$	[-]	magnitude of the bending moment
φ_i^A	[-]	modal shape values for the undamaged structure;
φ_i^B	[-]	modal shape values for the damaged structure;
σ_{ij}	[N]	peak stress
σ_z	MPa	Von Mises stress at crack end
σ_{eq}	MPa	Von Mises equivalent stress
θ	[°]	angle of the crack branch

INTRODUCTION

General background

Damage detection is essential for ensuring the structural integrity and performance of engineering systems, such as mechanical aggregates used in the manufacturing industry or energy sectors, aeronautics, aerospace, and civil structures and infrastructures. In essence, the damages associated with these structures are approached in the current thesis, and they can be described as existing discontinuities in a given material that negatively influences its performance. While there are many nondestructive techniques for evaluating structural systems, existing damage identification methods can be categorized as static and dynamic methods. The current thesis, is focused on damage detection using dynamic methods that rely on the negative impact of damages on the stiffness of a structure, decreasing its capacity to store energy and changing its modal parameters, like natural frequencies, modal curvatures, and damping capacity. The use of natural frequency is the most preferred damage detection characteristic because it offers greater flexibility in measuring the dynamic response of structures. Although modern damage detection methods based on vibration analysis are exponentially developing, most of them handle transverse damages, open or breathing, because these models are simpler to generate. At the same time propagating branched cracks present a higher degree of complexity, and they require much more sophisticated models.

The studies presented in this thesis had as a starting point the need to develop geometries that are altered by branched cracks, the main scope being the connection between the shape and position of the crack by analyzing the modification of the natural frequency induced by the damage. It should be mentioned that in the current research presented in this thesis, the interest is not how the branched cracks develop and propagate, but only the development (design) of models for evaluating complex-shaped damages, by means of simulations and laboratory experiments, considering only isotropic materials because they involve smaller computational resources and technologies for generating more precise damages. In reality, such cracks are manifested mainly in sandwich structures, but can also occur in metal structures due to trans granular and intergranular crack propagation.

Research objectives

The target of the current research is the development of a vibration-based damage detection method that is able to determine the position and depth of a branched crack. The starting point is

the original method developed within the Center for Vibrodiagnostics of the "Eftimie Murgu" University of Resita, which is adapted herein for branched cracks. For this, the following specific objectives have been set:

- analysis of the current state of research on existing methods for detecting and locating damages based on vibration methods with an emphasis on those that use natural frequencies;
- establishing some typologies of branched cracks and parametric analysis in order to establish the influence of various parameters of the crack's geometry (lengths and angles) on the modification of natural frequencies;
- elaboration of analytical models for the identified typologies of branched cracks and their validation by comparing the results obtained with those resulting from simulations;
- elaboration of an algorithm for determining the natural frequencies of beams having branched cracks and its implementation in an application that allows fast calculation for different damage configurations;
- establishing a method for measuring and processing natural frequencies values in beams with and without damages, that would allow us to observe very small changes in frequency;
- validation of analytical models by comparing the obtained results with the experimental results;
- testing and validation of the damage detection method for branched cracks through simulations and laboratory experiments.

In the research presented in this doctoral thesis, the following working hypotheses were established, which do not significantly affect the results obtained, namely:

- the damage-free beam is of rectangular section;
- the width of the beam is small enough so that it does not have a behavior similar to plates;
- the damage is of open type, thus being placed asymmetrically with respect to the neutral fiber;
- the plane in which the transverse branch of the crack is positioned perpendicular to the longitudinal direction;
- the damage extends over the entire width of the beam;
- the dimensions of the damages are so small as not to influence the mass of the beam.

Thesis outline

In order to meet the proposed objectives, the thesis is structured in six chapters, starting from current theories and models known in the literature, continuing with theoretical approaches to the behavior of damaged beams, conducting modal analysis using the finite element method, presentation of the method proposed by the author for detecting, locating and severity evaluation of the damage, validating the concepts through experiments on real beams and finalizing with conclusions and highlighting personal contributions.

Chapter 1: "Current state of research in the field of damage detection by using modal parameters"

This chapter presents the current methods and results obtained in the field of damage detection in beam-like structures using vibration-based methods. In the literature, there are many works that try to solve the problem of detecting damages by vibration. All the methods published and presented in this paper are generally applicable to particular cases for which they have been developed, especially as regards to the boundary conditions; they can be successfully applied to that type of structure, but it is not possible to generalize.

Chapter 2: "Numerical study of damages in beam-like structures"

In the current chapter, the analyzed structure, types of damages studied, and how they affect the natural frequency of the damaged cantilever beam by means of the finite element method are presented. Also, a short description of the workflow needed to define a FEM study using the Ansys simulation software is given.

For the analyzed cases, the first six natural frequencies and the modal shape of vibration were determined for a steel beam of 1 m long, 50 mm wide, and 5 mm high. The values of the eigenfrequencies obtained for the intact beam by the finite element method are given in the presented tables. The considered damages are branched cracks of open type penetrating the entire width of the beam. In order to have a global image of the influence of the damage on the natural frequencies, every analyzed crack was removed by a step of 3 mm starting from the fixed end of the beam, until it reached the free end, and recorded the obtained natural frequency values. Based on these data, the eigenfrequencies curve variation for the damaged structure was plotted, along the entire length of the beam, corresponding to each crack shape and size, respectively corresponding to each vibration mode. The obtained frequency values foot the transverse, L and T-shape cracks were compared, and conclusions were drawn.

In the next subchapter, the study of the influence of different penetration angles of branched cracks, meaning the defined general model of Y-shaped cracks, is presented. At the end of the chapter, the relative frequency shift (RFS) curves were plotted and conclusions were drawn.

The RFS is a method used for evaluating the state of a structure, which should highlight the appearance, location, and information regarding the severity of damages. The relative variation of the eigenfrequencies is, in fact, the ratio between the differences of the eigenvalues of the undamaged beam with the value of the eigenfrequency of the damaged beam divided by the value of the eigenfrequency of the intact beam, expressed as a percentage. The method does not take into account the actual value of the natural frequencies but compares the series of values resulting from the database determined by modal analysis. The graphical representation of RFS values relative to the vibration mode number is called "the tendency of the relative deviation of the natural frequencies". It has no physical significance but allows the detection, localization, and evaluation of the depth of the damage with very good accuracy.

Furthermore, the Damage Location Coefficients are calculated by dividing the values of the RFS for a given case to the biggest value in the series. In general, the RFS for mode one always achieves the value one. This property makes finding the crack location independent of its severity estimation. If the crack position is found using DLCs, by dividing one of the RFSs to the corresponding DLC, one obtains the damage severity.

The conclusions of the method are presented at the end of the chapter.

Chapter 3: "A new predictive model to estimate the frequencies for beams with branched cracks"

In the current study, the author proposed a model with a reduced section that can be trustfully used to calculate the natural frequencies of beams affected by branched cracks when the crack depth, extent and position are known. The algorithm considers the actual bending moment, which is the moment that acts on the constant section beam but having the same effect for the smaller section.

The precision of the algorithm was enhanced, by taking into consideration the stiffness reduction in the affected beam segment, and in addition, the supplementary slope at the ends of the longitudinal component of the crack. Involving this model, one could predict the natural frequencies with high precision, the error being smaller than 1%.

After the comprehension of the algorithm for determining the natural frequencies of beams having branched cracks, it was implemented in an application that allows fast calculation for different damage configurations, named PyDAM.

Different results are shown in the appendix section for T and L -shaped cracks at different locations and depths, denoting the small errors obtained in predicting the natural frequencies using the PyDAM software. This qualifies the proposed model to be used to develop damage patterns as benchmarks to be used in damage detection.

Chapter 4: "Experimental research and validation"

To validate the developed algorithm implemented in the PyDAM application to detect and quantify complex-shaped damages, experimental tests have been conducted in the “Eftimie Murgu” of Resita laboratory for two test beams both in damaged and undamaged state, by measuring their first five natural frequencies and comparing the obtained damage signatures by those obtained using FEM and the developed PyDAM application.

The natural frequency measurements were performed on the two steel beams, cut from a 20x5 mm flat strip with a length of 1000 mm. Thus, for a single beam, two sets of natural frequency measurements were obtained, two for the undamaged beams and two for the damaged ones. The considered damages were of T-shape of known delamination lengths and depth. The RFS’s and DLC curves were plotted and the damage signatures are compared.

Chapter 5: "Conclusions"

In the last chapter, the final conclusions and main personal contributions contained in the current thesis, as well as future research themes are presented.

1. THE CURRENT STATE OF RESEARCH IN THE FIELD OF VIBRATION BASED DAMAGE DETECTION

1.1. Damage detection

Damages can be described as changes occurring in a structure that negatively influences its performance. During operation, mechanical systems, buildings, bridges, dams, railways, or support structures of specific machines, are exposed to the shared or separate effects of dynamic loads, temperature, corrosive environment, material fatigue and other types of phenomena. Early detection of damages in structures is crucial both for safety and economic reasons because cracks during operation are a potential source of disasters. In this respect, structural monitoring deals with the early warning of the integrity alteration of structures, the location, quantification of damages, and the prediction of their remaining life [65].

Structural weakening usually occurs under static loading where the applied load exceeds the critical load. In contrast, most frames are subjected to repeated loads of varying sizes, which are most often below the tensile strength limit and do not exceed the stress levels for which they were designed. Damages can be initiated due to production failures, environmental conditions, and by initiating and increasing cracks caused by repeated loading of the structure, also called fatigue degradation, which generates microscopic inelastic damages in areas with local stress concentration. If enough inelastic damages accumulate, then a small crack occurs, which then propagates through the structure. The damage occurs when the crack reaches a critical size, thus the need to identify it before significant structural damage occurs [37].

Early detection of damage in structures is of great interest for mechanical, spatial and civil engineering fields.

1.1.1. Local methods used in damage detection methods used in damage detection.

Traditional methods of detecting damages fall into the category of nondestructive control abbreviated NDT (nondestructive testing). Nondestructive testing is the process of examining, testing or evaluating materials, parts or assemblies for damages or differences in characteristics without destroying their functionality. In other words, when the inspection or check is completed, the part can still be used.

These methods consist of visual inspections and local damage assessment. They have been studied by a large number of researchers [3] [5]-[6] . The most used NDT methods are:

- visual inspection;
- X-ray radiography;
- ultrasound;
- penetrating liquids;
- magnetic testing;
- the turbulent current.

All these methods obviously have the limitation that it is necessary to envisage the damages' locations and require that the examining part of the structure is accesible. In addition, this approach is not practical as it requires significant time and preparation work.

1.1.2. Global methods used for damage detection.

In order to meet the limitations presented by the local control approaches, it was necessary to develop global methods that are based on the analysis of the dynamic behavior of structures during operation. These methods have the advantage that they can be applied to complex and partially inaccessible designs.

The principle of global damage detection methods assumes that the modal parameters are directly proportional to the physical parameters of a structure, such as mass, stiffness, and damping matrix, which results in changes of the physical parameters, such as the overall rigidity due to the occurrence of invisible cracks, which cause changes in the modal parameters of the structure. Thus, a new concept called "Structural Integrity Assessment" or "Structural Health Monitoring" (SHM) was born, and the purpose of this concept was defined in work published by Balageas et al. as a process of monitoring and diagnosing the condition of structures [6], performed during operation.

SHM is an active field of research, based on the need to complement the traditional methods of damage assessment in structures by evaluating them, using global methods of nondestructive control through physical measurements and computer-aided analysis. Structural monitoring is a cheap and easy-to-implement technology capable of providing useful information about the safety of structures. This process involves observing a structure or mechanical system over time using periodic measurements. It extracts the deterioration-sensitive features from these measurements, and statistical analyses of these features to determine the current state of system integrity [7].

A well-known classification of fault identification methods presented by Rytter, which defines four levels of structural integrity monitoring, is described [6], [87]:

Level I: Detection - determines the existence of the damage.

Level II: Detection + Localization - determines the location of the damage.

Level III: Detection + Localization + Quantification - determines the depth of the damage.

Level IV: Detection + Localization + Quantification + Prediction - determines the remaining life of the structure.

The problem of detecting damages (level 1) is substantially equivalent to detecting a change in the dynamic characteristics of structures, such as natural frequencies.

There are two approaches to extending vibration-based methods beyond level 1. In a first approach, a large number of sensors are needed to enable the detection of cracks based on the detection of the modal shape change. A second approach requires a fewer number of sensors, but an analytical model of the structure is needed. The parameters of the model that are influenced by damages are updated so that the dynamic characteristics of the model correspond to the measurements.

The detection at level IV in structural systems is associated with the fields of fracture mechanics, fatigue resistance analysis, or structural design.

1.1.3. Methods based on modal analysis

The technique of damage identification by vibration analysis represents a new concept of SHM, more advantageous than the conventional detection techniques. The principle of these methods is based on the analysis of the behavior of the structures subjected to vibrations. Damages modify the physical properties of a structure (mass, rigidity), and its dynamic characteristics (natural frequencies, degree of damping and modal shapes). Therefore, by examining the dynamic properties of a structure from its vibrations, any type of damage can be identified, including their location and severity [53]. Significant work has been done regarding damage localization using vibration-based techniques [104]. There are two variants of vibration-based crack detection methods: frequency analysis and modal analysis. A straightforward method is to compare the measured frequencies with the predicted frequencies of a damaged structure to determine the presence of the damage. Other methods are involved in defining parameters (indicators) that are related to frequency changes to delimit the size and/or location of the crack.

The detection methods by using modal analysis are cheap and fast; they allow to identify damages located in less accessible areas and can be classified into four broad categories based on the data needed for detection [87]:

- Methods based on natural frequencies;
- Methods based on modifying their natural modes of vibration;

- Methods based on the shape of the deformation curve;
- Other methods based on modal parameters.

1.1.4. Damage detection using natural frequencies

There are two types of frequency analysis, the direct method and the inverse method of identification that can be used to detect damages [4]. Both methods assume that the natural frequencies of a structure change when the physical properties of the structure change.

Natural frequencies are inherent properties of a structure determined by its physical properties, such as rigidity and mass. Each system can be described in terms of the stiffness matrix that connects the displacements (or system response) and the forces (or system inputs); for example, the frequencies for a simply supported beam are given by the relation:

$$\omega_n = \left(\frac{n\pi}{L}\right)^2 \left(\frac{EI}{m}\right)^{\frac{1}{2}}, n = 1,2,3 \ldots \quad (1.1)$$

where: L - the length of the beam;

EI - rigidity;

m - mass;

n - vibration mode number.

The sensitivity of a structure to a local deterioration can be easily seen from equation (1.1) for the natural frequency of uneven linear beams, with the square section and known material properties. When a crack occurs, this will lead to a change in the moment of inertia I, or perhaps even the mass, and therefore to changes in the natural frequencies, these are also known as the resonant frequencies.

Most structures can be made to resonate, i.e., vibrate with an excessive oscillating motion. Based on this point, changes in natural frequencies occupy an essencial place in the methods of global damage detection since they are relatively easy to determine.

Currently, there are many works in the specialized literature on damage detection using changes in natural frequencies. Most of the older works were based on simple structures and structural elements. Some studies consist of calculating frequency changes from a known type of damage. Typically, the deterioration is mathematically modeled. The measured frequencies are compared with the estimated frequencies to determine the presence of damages.

One of the most frequently cited works on the use of natural frequencies in damage detection is the study made by researchers Cawley and Adams [11], in whom they demonstrated both analytically and experimentally, that a single point in a structure can be used to detect and quantify

damages. The main idea in their method is to use the measured frequency ratio, two modes of vibration as a function of damage locations. The positions in which this determined theoretical ratio is equal to the value measured experimentally are considered possible areas of deterioration.

Vandiver [100] investigated the frequency changes for the first two bending and torsional modes of a light tower to identify existing damages. The numerical analysis indicated that the changes in the effective mass of the tower resulting from the reversals of the water in the deck-mounted tanks would produce only a 1% change in frequencies for the first three modes of vibration, and the damage of the component structures would produce more considerable resonance changes of 1%, and thus the detection of damage is possible.

A different opinion was presented by Banks et al. [7], who stated that the use of natural frequency to detect damages in structures depends on the geometry of the cracks. For some types of damage, the method may be suitable, but for other configurations, the method is not sufficient. The low sensitivity of frequency changes due to cracks requires either very precise measurements or a high level of deterioration.

Kenley and Dodds, in their paper [55] present a study regarding the frequency changes that occurred due to the appearance of damages in a decommissioned maritime platform. They found that the damage had to produce a 5% decrease in total stiffness before being detected.

Abdel Wahab and De Roeck, in their study [100] investigated the effect of temperature fluctuation on the modal parameters of a pre-compressed concrete highway bridge. The bridge, named B15 and built-in 1971, has a total length of 124.6 m (35.8 + 53.0 + 35.8). The beams have a width of 9.4 m, varying in depth between 1.0 and 2.5 m. The width of the bridge was 13.0 m with two lanes. The structure was supported at the two ends by neoprene supports, which allow lateral movements. The dynamic response of the structure was measured twice: in spring, May 1996 (temperature about 15ºC), and in winter, in January 1997 (temperature about 0ºC). The modal parameters of the bridge (i.e., the natural frequencies, the degree of damping, and the modal shapes) were extracted from the measured data, using a time duration in the form of a vector autoregressive model. The results showed that the natural frequencies, due to the increase of the temperature, showed a decrease of about 4-5%. The researchers concluded that when natural frequencies values are used to evaluate damages in a structure, the effects of temperature must be taken into account.

In his doctoral thesis [52], Horia Furdui presented the effects of the influence of external factors on the analyzed beams, with emphasis on the temperature variation. Based on the analytical results and the experiments, made using the finite element method in comparison with

measurements made on a real structure, the author highlighted new aspects regarding the vibration of the beams subjected to axial loads, mathematical relationships and algorithms were developed regarding the elimination of the effect of temperature variation during the structural integrity monitoring.

Kim and Stubbs [57] - [59] formulated a crack location model that can estimate the size and location of the damage in the beams by using natural frequencies. The method can locate the crack and estimate its size. However, the limitation of the method is that it was applied only to beams, and it is not clear whether the method will work for different types of damages or structures.

Kessler et al. [56] further studied the effect of various types of damage (holes, delamination, impact damages, cracks induced by bending and fatigue) on composite plates based on natural frequencies. The authors found that the frequency-based method is usually reliable for detecting the presence of damage in a simple composite structure, while important information about the size and type of damage, location, and orientation cannot be obtained only by this simple method because of the large number of variables that can cause changes in natural frequencies.

Natural frequency-based methods have been used to detect cracks, characterize delamination and determine elastic constants [15], [74], [91], [20]. These methods use the natural change of the frequencies of the structures as a basic element for damage detection; it is attractive because the natural frequencies can be conveniently measured from only a few accessible points of the structure, and the results are usually less contaminated. But it has some limitations, such as the complexity of structural modeling and the deterioration and non-uniqueness of the solutions.

Recent research by Gillich et al., published in the papers [35] - [44], proposes direct and indirect methods based on natural frequency to identify multiple cracks in beams. Direct methods include a simplified definition of natural frequency decreases caused by cracks. The ratios between the natural frequencies obtained from the defective and the unpaired beams are determined by an approach that uses the local crack flexibility model. This approach does not take into account the effects of nonlinear cracks that can be easily overlooked when the number of cracks is not excessive. A mathematical relation is presented that allows the prediction of the frequency changes of the beams if a crack occurs in which produces a sharp decrease of the rigidity in the structure. In the first phase, the analysis was performed for damages by reducing the rigidity of the plate subjected to the highest bending moment. From this analysis, it was discovered the evolution of the severity of the damage and the effect of the damage on its position, reflected by a decrease in frequency. The reliability of this relationship was tested with the results obtained by the finite element method and the experimental results.

The crack detection methodology is also validated by experimental analysis; the results show that the reports of the locations and the depth of cracks are successfully anticipated by using the methods presented in the paper; if the damage appears in a structure, it will vibrate differently; therefore, the comparison of natural frequencies of the structure in the current state with those of the integral state can offer a perspective on the existence of damages.

The use of natural frequency as a characteristic of sensitivity to deterioration offers a cheap and efficient evaluation technique in most structures; in addition, the global nature of the method offers greater flexibility in measuring the dynamic response of the structure and allows the measurement points to be customized.

1.1.5. Methods based on the change of the modal curvature values

The vibration modes are characteristic properties of a structure and are determined by the properties of materials such as mass, damping capacity, rigidity, and boundary conditions of the structure. Each mode is defined by a natural frequency value, modal damping, and shape. If the properties of the materials or the boundary conditions of a structure change, the vibration modes will change.

Modal shapes represent a specific deformation pattern of a mechanical system at specific frequencies.

The methods based on the modification of the vibration modes are an advantageous tool for the evaluation of structures, the results being less influenced by the environmental conditions [18], also containing spatial information that can be used to locate the damages.

Two sets of parameters, called the modal assurance criterion (MAC), and the coordinated modal assurance criterion (COMAC), were introduced by Allemang [78], Levine et al. [10]. These parameters can be adapted to compare two sets of modal shapes in order to express the degree of correlation between them. The values recorded by the two methods can be used to give indications about the presence and location of damages in a structure.

The MAC values for two sets of modal shapes are given by the relation:

$$MAC_{A,B} = \frac{\left|\sum_{i=1}^{n} \varphi_i^A \varphi_i^B\right|^2}{\sum_{i=1}^{n}(\varphi_i^A)^2 \sum_{i=1}^{n}(\varphi_i^B)^2} \tag{1.2}$$

where:

φ_i^A – modal shape values for the undamaged structure;

φ_i^B - modal shape values for the damaged structure;

The MAC factor indicates the degree of correlation between two modes, and its values range from 0 to 1; that is, if two modal vectors are identical, the value will be 1, and any deviation from this value can be interpreted as structural damage.

Similarly, the COMAC factor can be defined to detect the differences between the degrees of freedom (DOF) of two modal vectors.

For a degree of freedom i, the COMAC factor is defined as:

$$COMAC_{i,A,B} = \frac{\left|\sum_{j=1}^{n} \varphi_{i,j}^{A} \varphi_{i,j}^{B}\right|^2}{\sum_{j=1}^{n} (\varphi_{i,j}^{A})^2 \sum_{j=1}^{n} (\varphi_{i,j}^{B})^2} \tag{1.3}$$

If the modal shift of the coordinate *i* for two measurements is identical, the COMAC value is equal to 1. Any deviation from the value one can be interpreted as an indicator of the damage in the structure.

It can be concluded that modal shapes contain information that can be used to detect and locate damages. A significant disadvantage of using modal assurance criteria is the laborious methods necessary to obtain the vibration modes shapes experimentally [31].

1.1.5.1. Methods based on the modification of the shape of the modal curvature

An alternative to using modal shapes to obtain spatial information about vibration changes in structures is the use of modal shape derivatives, such as curvature. It is noteworthy that, for the beams, the curvature and the bending deformation, shown in Figure 1 [82] are directly related and are expressed by the relation:

$$\varepsilon = \frac{y}{R} = ky \tag{1.4}$$

where:

ε – represents the deflection;

R – *curvature radius*;

k – curvature;

y – distance to the neutral axis.

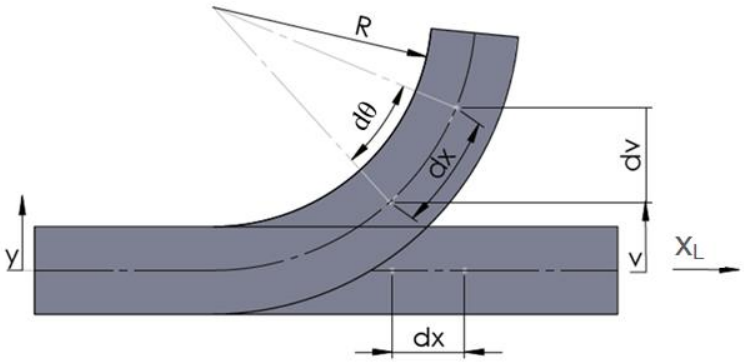

Figure 1.1. Curvature and bending deflection of a beam

Starting from the Euler-Bernoulli general equation, which in the case of beams of constant section becomes:

$$EI\frac{\partial^4}{\partial x_L^4} + \rho A\frac{\partial^2 v}{\partial t^2} = q(x_L, t) \tag{1.5}$$

where: E [N/m^2] longitudinal modulus of elasticity, or Young's modulus;

I [m^4] –moment of inertia;

A [m^2] – transversal section area;

ρ [kg/m^3] – material density.

v [m] – vertical displacement of the neutral axis;

x_L [m] – axial displacement;

t [s] – time variable;

q (x, t) [N/m] – neutral fibre distributed load

For the case when the distributed load on the neutral axis is equal to zero, the equation for transversal beam vibration is obtained:

$$\frac{\partial^4 v}{\partial x_L^4} + \frac{\rho A}{EI} * \frac{\partial^2 V}{\partial t^2} = 0 \tag{1.6}$$

In case of free vibrations $q(x_L, t)=0$, $v(x_L,t)$ defines a synchronous harmonic movement:

$$v(x_L, t) = X(x_L)\sin(\omega t + \phi) \tag{1.7}$$

Replacing the solution in the equation, results:

$$\frac{\partial^4 v}{\partial x_L^4} - \omega^2 * \frac{\rho A}{EI_z} v = 0 \tag{1.8}$$

The general solution is presented in the form:

$$v(x) = A\sin(\alpha x) + B\sin(\alpha x) + Csh(\alpha x) + Dch(\alpha x) \tag{1.9}$$

The four integration constants A, B, C, and D are determined from the initial boundary conditions. After writing the three derivatives of the function, and depending on the resting conditions applied at the ends of the beam; one can obtain the solutions α respectively, the own forms of the vibration modes.

$$\begin{cases} v(x) = A\sin(\alpha x) + B\cos(\alpha x) + Csh(\alpha x) + Dch(\alpha x) \\ v'(x) = \alpha\big(A\cos(\alpha x) - B\sin(\alpha x) + Cch(\alpha x) + Dsh(\alpha x)\big) \\ v''(x) = \alpha^2\big(-A\sin(\alpha x) - B\cos(\alpha x) + Csh(\alpha x) + Dch(\alpha x)\big) \\ v'''(x) = \alpha^3\big(-A\cos(\alpha x) + B\sin(\alpha x) + Cch(\alpha x) + Dsh(\alpha x)\big) \end{cases} \tag{1.10}$$

Pandey et al. [32] analyzed the changes in the curvature of the modal shape for a beam by the finite element method (FEM). The curvature values were calculated by moving the modal shape for a mode i and a degree of freedom q. There are two options for obtaining the curvature: calculation of modal displacements or direct measurement of curvature/deformation. If a crack resulting from bending occurs, there is a decrease in bending stiffness (EI), and this should cause a local increase in curvature, which is equal to the bending moment divided by the bending stiffness. The curvature values are calculated based on the shapeshift.

The methods of detecting and evaluating damages based on the modification of the curvature of the shapes of the vibration modes are used as alternative methods of those that use the modification of the modal shapes due to the indications that are more sensitive to the appearance of faults.

There are two options for obtaining curvature: calculation of modal displacements or direct measurement of curvature/deformation. If a crack resulting from bending occurs, there is a decrease in bending stiffness (EI), and this should cause a local increase in curvature, which is equal to the bending moment divided by the bending stiffness. The curvature values are calculated based on the shapeshift.

From the literature, it was concluded that the method for modifying the curvature of the vibration modes is a good damage indicator. It is known that the forms of the vibration modes are functions of them; the use of the method is limited by the difficulties that arise in the measurement process, the variation of environmental factors, and the uncertainties regarding the boundary conditions.

1.1.5.2. Frequency response function (FRF)

The FRF method has been shown to be a sensitive indicator for the prediction of damages in different structures. Wang, Lin, and Lim [101] formulated a new damage detection algorithm using a measured natural frequency function.

The principle underlying the techniques for detecting structural damage is that the vibration signature, e.g., modal properties or frequency response function (FRF), is a sensitive indicator of physical, structural integrity and can thus be used to detect cracks. As the modal data indirectly measured contain accumulated errors generated by the extraction of the modal parameters and provide much less information than the FRF data, it is more reasonable and reliable to use directly measured FRF data to detect structural damage. Based on the nonlinear perturbation equations of FRF data, an algorithm has been derived that can be used to determine a destruction vector indicating both the location and magnitude of cracks.

The absolute differences between the response frequency curves of the damaged structures, compared to the integral ones at location *x*, for the chosen frequency range, is calculated by applying a force at a point *j*, defined by the relation:

$$\Delta\alpha''_{x,j} = \sum_{\omega} \left| \alpha''_d(\omega)_{x,j} - \alpha''(\omega)_{x,j} \right| \tag{1.11}$$

Research shows that the frequency response method of FRF has had good results in detecting, locating, and quantifying damages; although this method must be further developed and better characterized, it was concluded that the method for detecting proposed faults could not be applied to identifying damages on a small scale, because changes in vibration data caused by minor cracks may not be detectable in the presence of noise.

Its main advantage is simplicity, due to the fact that there is no need to carry out a modal analysis to identify modal shapes or frequencies, as with other methods.

1.1.5.3. Methods based on the modification of potential energy (deformation)

The concept of this method was introduced by Stubbs, Kim & Topole [88]. They developed a method based on the reduction of the modal deformation energy caused by damages in an area between two degrees of structural freedom, as it results from the measured curve of the shape of the module. This method is mentioned in the literature as a damage index method and is based on the connection between the deformation energy d_{Ui} , which is stored in section *x* of the structure [87], and the curvature of the shape of the vibration mode *i* ϕ_i in the same section. expressed mathematically as a function of the modulus of elasticity *E* of the material and the moment of inertia of the cross-section *I*, in the form:

$$dU_i(x) = \frac{1}{2} EI[\Phi_i''(x)]^2 dx \tag{1.12}$$

The deformation energy corresponding to the shape of the vibration mode *i* in section *A* is directly proportional to the square of the curvature of the shape of the vibration mode, respectively, for the same section.

The damage detection index based on this method is defined as the absolute difference between the square of the measured data and the square of the modal curvature value.

$$D_{sem}(x,y) = \left| k_{măsurat}(x,y)^2 - k_{fitting}(x,y)^2 \right| \tag{1.13}$$

Stubbs and Kim [60] applied this method to a steel bridge. In these studies, the damage was successfully localized using the first three modes of vibration.

1.2. Types of damages

The basic idea of vibration detection methods is to measure the dynamic characteristics over the entire operating life of a structure and to use these features as a basis for detecting the position and severity of cracks. However, the successful detection of damages by measuring dynamic characteristics depends very much on the exact modeling of the crack. Previously it was presented that the presence of damages negatively influences the rigidity of the structures, diminishes the natural frequencies, and modifies the modal shapes. These parameter changes depend directly on the type, size, and position of the crack in the structure, and the exact modeling of these parameters is a very important factor in determining the dynamic characteristics of a damaged structure.

Crack modeling can be divided into two wide categories, open cracks that are characterized by the fact that they remain open during vibration, and closed cracks, which close and open during vibration.

The decrease of the structural rigidity due to an open crack is constant. A number of analytical methods have been developed to investigate the decrease in stiffness due to an open crack; these methods include analysis on a model of a short beam, estimate the increased flexibility, due to the crack, by using an expression of the stress intensity factor in the rupture mechanics.

The alternating cracks close and open during the harmonic vibration of a structure. To date, very few studies have explicitly examined the effects of effective opening and closing of cracks on the rigidity and dynamic response of a structure. It is assumed that structures containing cracks that close and open to vibration have two characteristics of rigidity, a higher value when the damage closes, and a lower value when it opens. Krawczuk and Ostachowicz [62] assumed a time-

dependent function for opening and closing the cracks during the vibration period. Other researchers [1,63,72, 77], due to the complex nature of the equations and the difficulty of obtaining exact analytical solutions, carried out experimental investigations using the dynamic response to the nonlinearity associated with the opening and closing of cracks. It has been observed that the opening and closing cracks make the rupture more rigid than it already is; this will indicate the crack depth to be much smaller than in reality. These papers have shown that it is difficult to relate the size and location of the crack directly from the measured cracking indicators.

During the last three decades, extensive research has been carried out to identify faults in mechanical systems and civil engineering based on natural vibrations, and thus significant progress has been made in this area. To solve the various problems, a wide range of techniques, algorithms, and methods have been developed starting from basic structural components (beams, plates) to complex structures (bridges, buildings).

There are two main reasons why damage detection research is focused on simple structures:

- most structures or components thereof in civil and mechanical engineering can be considered as bar or plate type;

- the identification of the damage in a bar, respectively, the plate provides an important indication for the efficiency and accuracy of the techniques for identifying the crack. [70]

1.2.1. Propagation of damages in isotropic structures

In structures, there can be many types of damages, of different irregular shapes and sizes, caused by the fatigue of the material, and delamination's in the interface area of the composite materials, faults due to inadequate production, superficial damages caused by strokes or corrosion. During the operation of a mechanical system or structure, cracks can take a complex form by propagating them, making their detection and evaluation more difficult by global nondestructive control methods.

The range of stresses at the tip of a crack for a homogeneous, isotropic elastic material is given by the general formula:

$$\sigma_{ij} = K_I(2\pi r)^{\frac{1}{2}} * \sigma_{ij}^{I}(\theta) + K_{II}(2\pi r)^{-\frac{1}{2}} * \sigma_{ij}^{II}(\theta) + T\delta_{i1}\delta_{j1} \quad (1.14)$$

where:

δ_{ij}- Kronecker delta function;

r and θ are the peak central polar coordinates.

For homogeneous solids, the breaking resistance is defined as the critical value of the intensity factor of the K_I voltages or the energy lost by the system due to the propagation of the crack G determined by a test of a mode I sample.

Lichun Bian and Farid Taheri [64] proposed a maximum ratio criterion applied to the mixed propagation of cracks caused by the fatigue of the material. They studied experimentally and theoretically the initiation and propagation of cracks in rectangular magnesium plates containing a sloping crack. Based on the complex state of stresses at the tip of the crack, a maximum ratio criterion is developed to determine the propagation of the cracks for a given angle of inclination, through a theory of the opening mode. It is assumed that the damage starts to spread when the maximum value of the ratio approaches its critical value, and the cracking direction coincides with the direction of the maximum defined ratio, given by the relation:

$$Z = \frac{1}{\sqrt{2\pi r}} * \frac{\sigma_z^2(k_1, k_2, \theta)}{\sigma_{eq}(k_1, k_2, \theta)} \tag{1.15}$$

where:

σ_z- Von Mises stress at the crack tip;

fσ_{eq} - equivalent Von Mises stress;

θ – propagation angle;

K_1 and K_2 – intensity factors.

The results obtained using the criterion of the proposed maximum ratio are, in some cases, in a better agreement with the experimental data compared with the results obtained using the corresponding breaking criteria. It is found that the new criterion proposed, i.e., criterion *Z*, is efficient and offers an acceptable estimate in predicting the propagation of cracks in fatigue.

From the specialized studies, it was observed that if a crack is on the interface between two different elastic solids, but isotropic, due to the dissimilarity in the elastic properties, there will usually be an asymmetry near the crack tip even though the geometry and loading are symmetrical. By their nature (and because of the loads), the interface cracks tend to be mixed.

Whether a crack will propagate in the interface or develop in any of the adjacent materials depends on the energy potential released depending on its inclination and the relative resistances of the interface and adjacent materials.

The phenomenon of bifurcation of cracks in brittle materials, that is, in dividing a single primary crack into two or more branches, is well known: Schardin [83], Clark, Irwin [14.], Kerkhof [54]. In the simplest case where a crack is separated into two secondary cracks, the angle of

connection (between the line of symmetry and a branch) is roughly constant and measured up to around 15 °.

Andersson [46] calculated the stress intensity factors for cracks with defined length branches and determined the branch angle. In order to investigate the mutual influence of the crack's branches, the static stress analysis was performed for two symmetric branches centered on the edge of the plate under uniaxial tension. The geometry of this model can be conveniently treated by mathematical analysis and includes important features to be investigated.

1.2.2. Propagation of damages in composite geometries

Tahreer M. Fayyad and Janet M. Lees [89] investigated the development of cracks in reinforced concrete beams using digital image correlation methods. Specifically, the purpose of the paper was to investigate the relationships between the height of the beam with known damage, the reinforcement ratio, the ductility, and the onset of crack branches. The beams were tested by bending at three points, and the surface deformations and crack opening were deduced using the digital image correlation (DIC) presented by the authors in figure 2.

The authors note that in the reinforced concrete, the crack initially propagates as a single narrow strip, slightly curved, but the presence of the reinforcement prevents the premature fracture and results in the development of the crack branching-the combination of this bifurcation and propagation of the crack results in the deterioration of the compression zone.

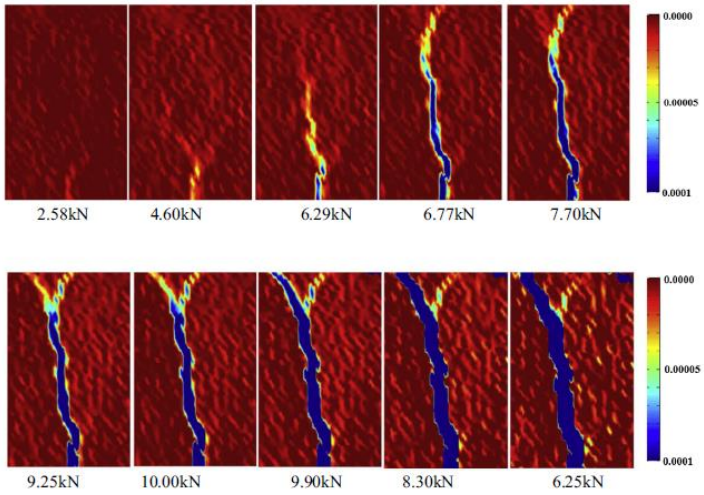

Figure 1.2. The correlation of digital images (DIC) presented by the authors regarding the development of cracks in reinforced concrete beams [89]

Bermejo and Danzer [79] analyzed the mechanism of bifurcation of delamination in the area with weak interfaces in stratified ceramics, the conditions under which a crack penetrates or deflects along with the interface of two materials.

Sevectek et al. [71], in their work, have experimented with crack propagation in laminated ceramic composites designed with residual stresses. Unlike the direct propagation of cracks in the monolith, the path of the cracks in the laminates is influenced by the magnitude and location of the compression efforts in the inner layers. A semi-analytical model based on the Fracture Mechanism (FFM) theory was developed to describe and predict the propagation of cracks in symmetrical laminates formed of alternating layers. It has been found that an optimal concept that favors the crack bifurcation mechanisms followed by the delamination of the interface is strongly dependent on:

(a) the compression level (depending on the thickness ratio of the layer and the differential interface between layers);

(b) the combination of the layer, the thickness, and the compression stresses that cause the crack bifurcation;

(c) the inclined angle of the crack bifurcation is favored by the elastic mismatch between the layers.

Doquet and Bertolino [17] developed a local method for predicting the mechanism of propagation of cracks caused by material fatigue, based on the calculations in the elastoplastic domain, by applying at the tip of the crack two critical criteria dominated by tensile or shear stresses.

In their work, Zhang et al. [103] presented a vibration-based monitoring method for laminated composites made of polymeric fibers with delamination damages that may not be visible from the surface but have a significant adverse effect on the rigidity and loading capacity of the structure. Therefore, it is crucial to detect the presence of delamination at an early stage. They proposed a graphical method for detecting delamination in composites using natural frequencies. It was shown by means of the finite element method that this method could be used successfully to predict the size of the crack, the longitudinal position, and the interface at which the delamination occurs, with considerable precision. Location and size prediction errors are within 0.35%, except for one case. The interface location prediction is correct in eleven of the twelve cases; this is explained by the fact that at the turning points of the composite beam, there are no bending moments; thus, the crack has no effect.

Soham et al. [85] present an article on the detection of cracks in glass-epoxy composite beams with dimensions 550 mm × 50 mm × 10 mm. The transverse cracks were created in different

positions, with variable depth, using a saw. The bar is excited to obtain the natural frequencies, and the dynamic responses of the beam are measured. From this study, it can be observed that the natural frequencies for the composite beam decrease with the introduction of a crack or with the increase of the crack depth.

The natural frequency of the beam decreases as the crack length increases from the fixed end to the median area and begins to grow again towards the free end.

Praisach et al. present in the paper [33] a study in which he develops an algorithm for the evaluation of transverse cracks in composite structures based on natural frequency changes due to damages. The evaluation is carried out in two stages; first, the location of the crack is found, and then an evaluation of its severity is performed. The technique is based on a mathematical relation that offers the exact solution for frequency changes of bending vibration modes, taking into account two terms. The first term is related to the strain energy stored in the beam, and the second term considers the increase in flexibility due to damages.

By knowing that a crack produces a decrease of the natural frequencies in a beam section subjected to bending, it results that for a mode *i* of vibration, the eigenfrequency drop due to damage depends on the capacity of the impaired section to store energy, that is the square of the modal curvature shape it is possible to find the influence of the crack on any other position considering the normalized stored energy in that location.

Based on these observations, the authors established a relationship indicating the change in frequency for any vibration mode *i*, damage depth a, location x, and any type of bar fixation.

$$f_{i-D}(x,a) = f_{i-U} * \left[1 - \gamma(0,a) * (\bar{\phi}_i''(x))^2\right] \quad (1.16)$$

where:

f_{i-U} - natural frequency of the undamaged beam;

$f_i(x, a)$ – natural frequency for a beam with a crack of depth a and position x;

$\gamma(a)$ - damage severity

$\bar{\phi}_i''(x)$ normalized modal curvature, having values between -1 and 1.

2. NUMERICAL STUDY OF DAMAGED BEAMS

2.1. The analyzed structure

The research aims to find the effect of different shaped cracks on the natural frequencies of structures by means of finite element analysis. For this purpose, for all studies in this thesis, a steel beam was considered, fixed on the left end and free at the other one (cantilever beam) both in intact and damaged states.

The beam geometry is modeled using the SolidWorks design software, with its main dimensions described as length *L*, width *B*, and thickness *H*, shown in Figure 1.

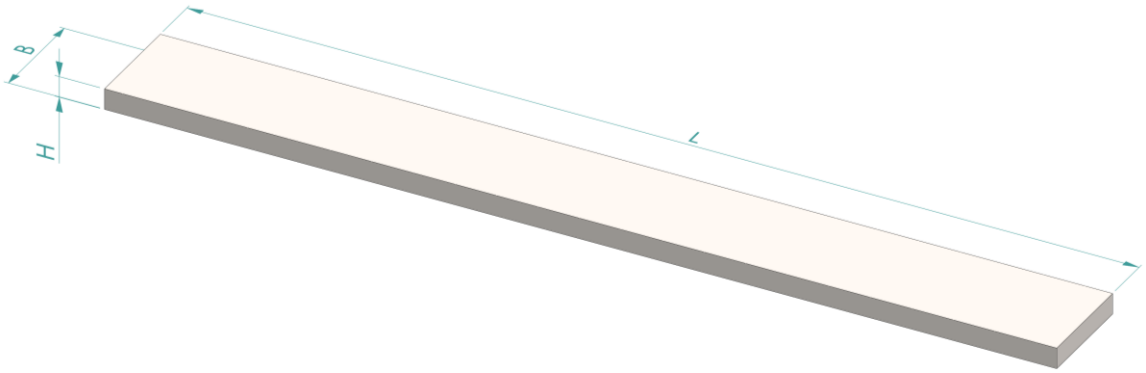

Figure 2.1. Main dimensions of the studied model

The assigned material for the beam is Structural Steel, with physical-mechanical properties defined in the ANSYS library. The beam's properties and dimensions are presented in Table 2.1.

Table 2.1. Physical-mechanical properties of the structural steel used

Length *L* [mm]	Width *B* [mm]	Thick. *H* [mm]	Mass density [kg/m^3]	Young modulus [N/m^2]	Poisson ratio [-]	Tensile strength [MPa]	Yield strength [MPa]	Min. elongation [%]
1000	50	5	7850	$2 \cdot 10^{11}$	0.3	470-630	355	20

The static and modal analyses are performed by involving the ANSYS simulation software; In general, hexahedral mesh elements with the maximum edge size of 2 mm have been used.

For the cantilever beam, the following equation derived from Euler-Bernoulli beam theory gives the natural frequencies and the mode shapes [105]:

$$f_i = \frac{\lambda_i^2}{2\pi}\sqrt{\frac{EI}{\rho A L^4}} \tag{2.1}$$

The modal shapes for the cantilever are given by the following relation:

$$\phi(x) = \frac{\cos(\alpha_n L) + \cos(\alpha_n L)}{\sin(\alpha_n L) + \sin(\alpha_n L)} * [\sin(\alpha_n L * x) - \sin(\alpha_n * x)] - \cos(\alpha_n * x) + \cosh(\alpha_n * x) \tag{2.2}$$

The squared modal curvature is given by the relation:

$$\bar{\phi}_i''(x) = \cosh(\alpha x) - \cos(\alpha x) - \frac{\cos(\alpha L) + \cos h(\alpha L)}{\sin(\alpha L) + \sin(\alpha L)} * [\sin(\alpha x) - \sin(\alpha x)] \tag{2.3}$$

2.2. Types of damages studied

In structures, there are many types of damages of different irregular shapes and sizes. They arise due to material fatigue, delamination in the boundary area of composites, faulty materials due to inadequate production, superficial defects caused by impacts, or corrosion.

During the functioning of a mechanical system or structure, damages can take a complex form by propagation.

Based on the models presented in the literature, it was proposed in the current thesis to study higher complexity damages, which comprehend most of the crack types that can be present in structures, so that one can easily create a database for structural health monitoring. An "Y-shaped" crack type is described, with different angles of penetration of the branches in the structure with the damage as schematically presented in Figure 2.2.

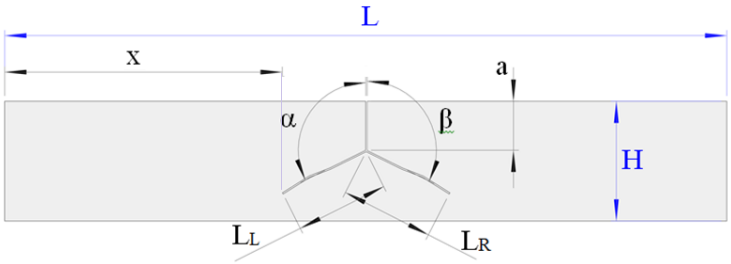

Figure 2.2. A zoom on a steel beam having a Y-shaped crack

The Y-shaped crack type comprehends all other damages studied so that in the current paper, all damages will be described according to the schematic of the generalized crack illustrated in Figure 2.2.

In Table 2.2, the types of damages studied with their dimensions presented relative to the general damage schematic are illustrated.

Table 2.2. Idealized crack dimensions

Crack shape		Crack length		Crack depth	Crack angle		Crack geometry
		L_L [mm]	L_R [mm]	a [mm]	α	β	
a	Transv.	no	no	yes	no	no	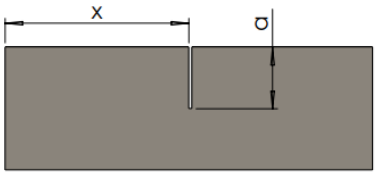
b	L_R	0	yes	yes	no	90	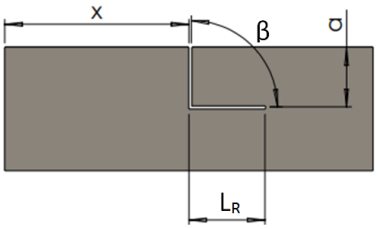
c	L_L	yes	0	yes	90	no	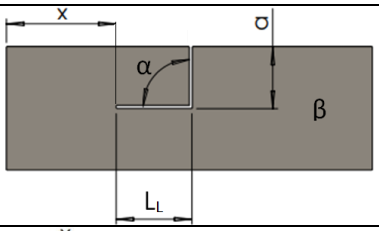
d	T	yes	yes	yes	90	90	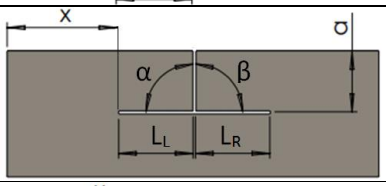
e	Y	yes	yes	yes	yes	yes	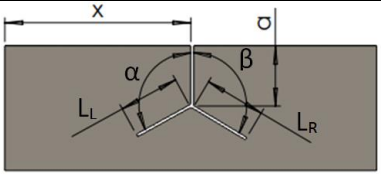

In this thesis, studies made on cantilever beams having breathing transversal cracks were carried out, and starting from these types of damages a more complex shaped crack is modeled, resulting in a delamination or multiple branched cracks with different angles of penetration [82].

The most common defect types found in structures are transversal cracks with their main dimensions presented in Figure 2.3.

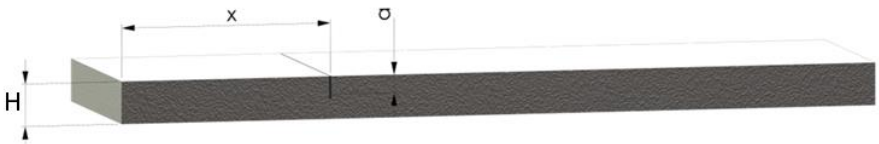

Figure 2.3. A zoom on a steel beam having a transversal crack

Composite materials can present more complex damages than transversal, i.e., they can further evolve to branched cracks.

Starting from transversal cracks, several scenarios have beencreated, i.e., a transversal crack followed by one or two longitudinal extents. For the first two cases, the shape of the damage consists of a crack in a transverse direction with a branch in the horizontal direction, oriented to the right indicated as L_R for the first case and to the left indicated as L_L for the second case, as shown in Figures 2.4 and 2.5.

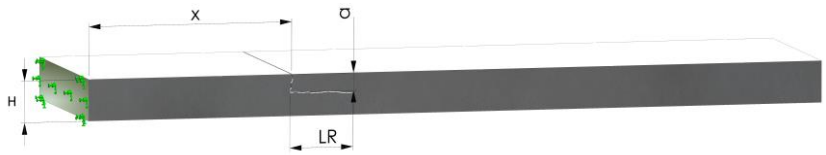

Figure 2.4. A zoom on a steel beam having an L-shaped crack oriented to the right L_R

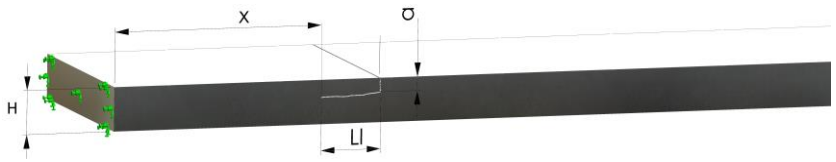

Figure 2.5. A zoom on a steel beam having an L-shaped crack oriented to the left L_L

In the latter cases, the influence of T-shaped damages presented in Figure 2.6 was analyzed, which consists of a transverse crack and two branches at the angle of 90º. For all cases, the longitudinal branch penetration size was taken from 10 mm to 50 mm.

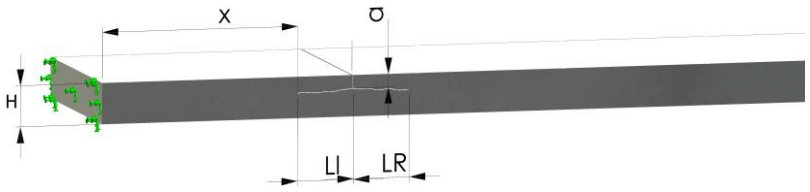

Figure 2.6. A zoom on a steel beam having a T-shaped crack

2.3. Finite element method

In the current subchapter, Finite Element studies were carried out for finding the natural frequencies, modal shapes, deflections under own weight, and stress distribution for the analyzed structure with and without damages.

Finite Element Analysis (FEA) is the mathematical description by involving the integration of differential equations for known boundary conditions of any given physical phenomenon for

finding the exact solution of a problem, also called Finite Element Method (FEM). The described method is used for reducing the overall costs of designing prototypes, experimental stands and to optimize already produced systems.

FEM requires as a starting point an integrated model of the studied phenomen, which is applied separately for a series of small elements produced using the meshing technique, also named discrete elements linked between themselves by nodes.

It is mandatory to know that FEM only gives an estimated solution to a given problem and the precision of the obtained results is directly related to the reconstruction accuracy of the studied assembly or model . FEM is a numerical method used to forecast how a part or assembly performs under given situations. The simulation results obtained using FEM are usually represented using a color scale [105].

Modal analysis is the study of the vibrational behavior of given structures, like the vibration of civil constructions, buildings, roads and bridges, mechanical systems and support structures of certain machines.

In mechanics, the modal analysis uses the mass and stiffness matrix of a structure to find the natural frequencies of given models. The natural frequencies are important for defining the seismic resistance of structures and making sure that the resonant frequencies do not match the environmental excitation frequency, that may be caused by earthquakes, cars, people walking, or other types of deviations.

The analysis type Static allows time-invariant calculation of the displacements as well as the stresses and strains in one or multiple solid bodies caused by the applied constraints and loads, e.g., bearings, gravity, forces. The results enable us to evaluate whether a component is deformed in an undesired manner or if a critical stress state occurs at some specific detail of the geometry. Another study approach is to modify a design based on the results of a simulation to meet the requested properties and test the new construction again [106].

2.4. ANSYS simulation workflow

The analyses in this report were performed using FEM, through the help of ANSYS version 14.5 software. The finite element model used must allow accurate processing information as much as possible. Under ANSYS, one can perform the following types of structural analysis: static analysis, modal analysis, transient dynamics, spectral analysis, buckling analysis, explicit dynamic analysis, and some special-purpose analyses.

The ANSYS software also ensures the necessary flexibility for using in different desing projects by implementing besides structural mechanics other modules like fluid dynamics or electromagnetics.

For determining displacements, stresses, distortions, and other forces in the structure being analyzed, the linear static analysis is used. In static analysis, loads that can be applied refer to applied external forces and pressures, inertial forces in the stationary state (such as gravity or rotational speed), temperatures.

Modal analyses determine the vibration characteristics (natural frequencies and mode shapes) of mechanical systems. They are used for determining the *n* resonant frequency of a given geometry, which are related to the shape, stiffness, and the way the geometry is constrained, but it is not related to loading.

For performing a FEM simulation, the following steps are implied:

• preprocessing;

• the solution determination phase;

• post-processing.

The preprocessing stage specifies the type, name of the study and the analyzed geometry. In this stage, the mesh is generated, materials, constraints, and loads are defined, Figure 2.7.

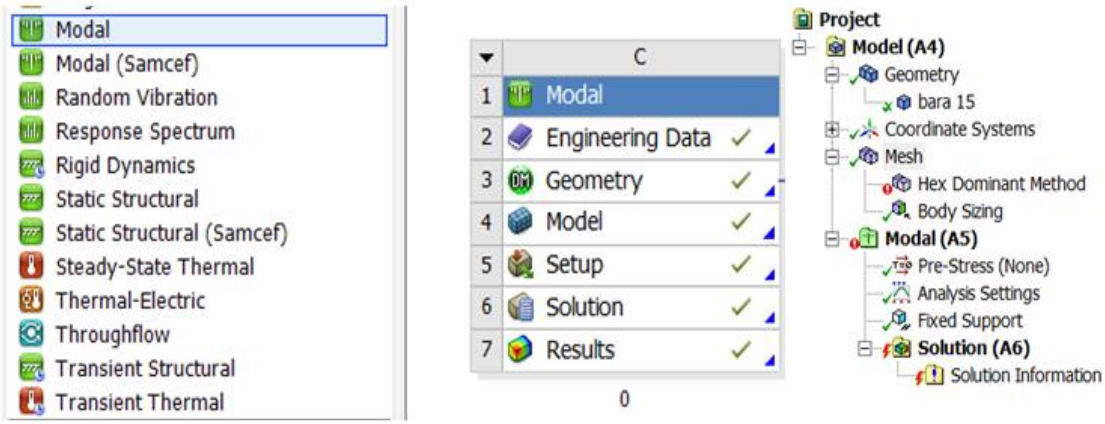

Figure 2.7. Preprocessing interface of the ANSYS software

The analyzed model can be generated directly in the ANSYS software by using the integrated design modeler or by importing the geometry from third-party software, like Solid Works. In the current thesis both methods have been used, depending on the number of damage positions.

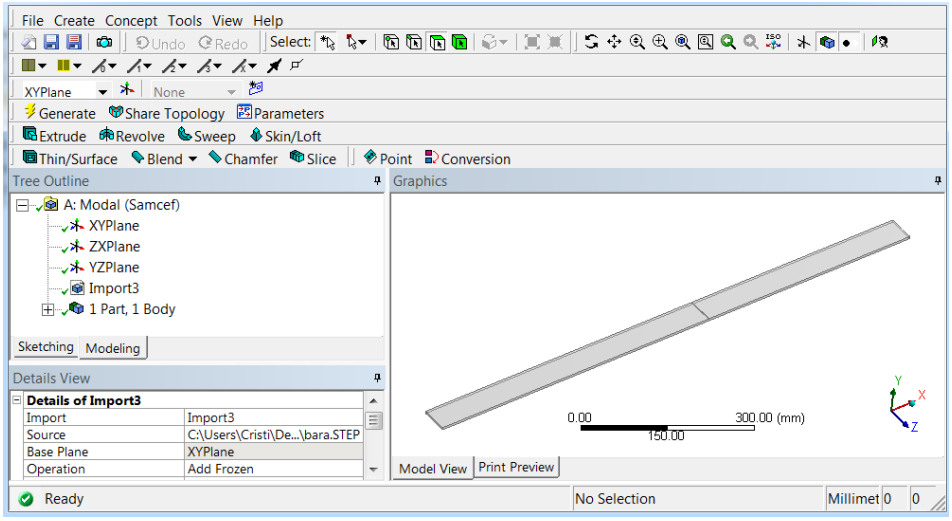

Figure 2.8. ANSYS graphical interface

In the current study, because of the large number of different damage locations and size, it is easier and faster to parameterize the model for FEM analysis. For this purpose, the position and general dimensions of the cracks have been set up so that they can be defined using table input data. The dimensional parameters are shown in Figure 2.9, where *H1* is the delamination length L_R, *H6(P18)* is the damage location *x(P1)*, and *V2* is the damage depth *a(P2)*.

H1	20 mm
H3	0.04 mm
H6	10 mm
V2	2.5 mm
V5	0.04 mm

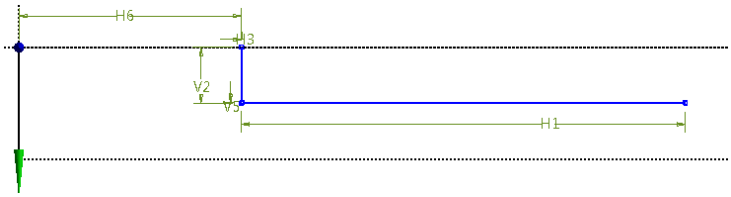

Figure 2.9. Parameterized dimensions

Using the described method makes it easy to introduce all required dimensions necessary for all damage scenarios, as presented in Figure 2.10:

Name	Update Order	P1 - pozitie	P2 - adancime	P18 - delaminare	P4 - Body Sizing Element Size
Units					mm
Current	1	10	2.5	20	2
DP 1	2	20	2.5	20	2
DP 2	3	30	2.5	20	2
DP 3	4	40	2.5	20	2
DP 4	5	50	2.5	20	2
DP 5	6	60	2.5	20	2
DP 6	7	70	2.5	20	2
DP 7	8	80	2.5	20	2
DP 8	9	90	2.5	20	2
DP 9	10	100	2.5	20	2
DP 10	11	110	2.5	20	2

Figure 2.10. Parameterized dimensions using table input data

After the definition of geometry, all the necessary loads and constraints are imposed, and the model is ready for meshing. It was found that in order for the analysis to be more accurately, it is necessary to use a fine mesh of hexahedral elements with a maximum edge size of 2 mm, as shown in Figure 2.11:

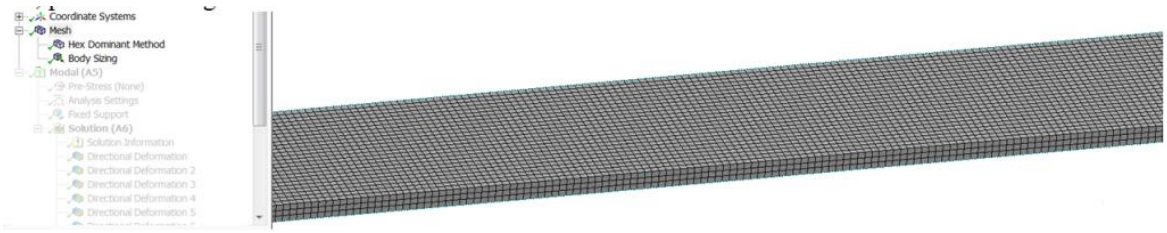

Figure 2.11. A zoom on the meshed geometry of a beam

After completing the preprocessing step, the simulation is run, and the solution is calculated. All results can be evaluated in the post-processing stage with the help of the ANSYS Multiphysics interface, presented in Figure 2.12.

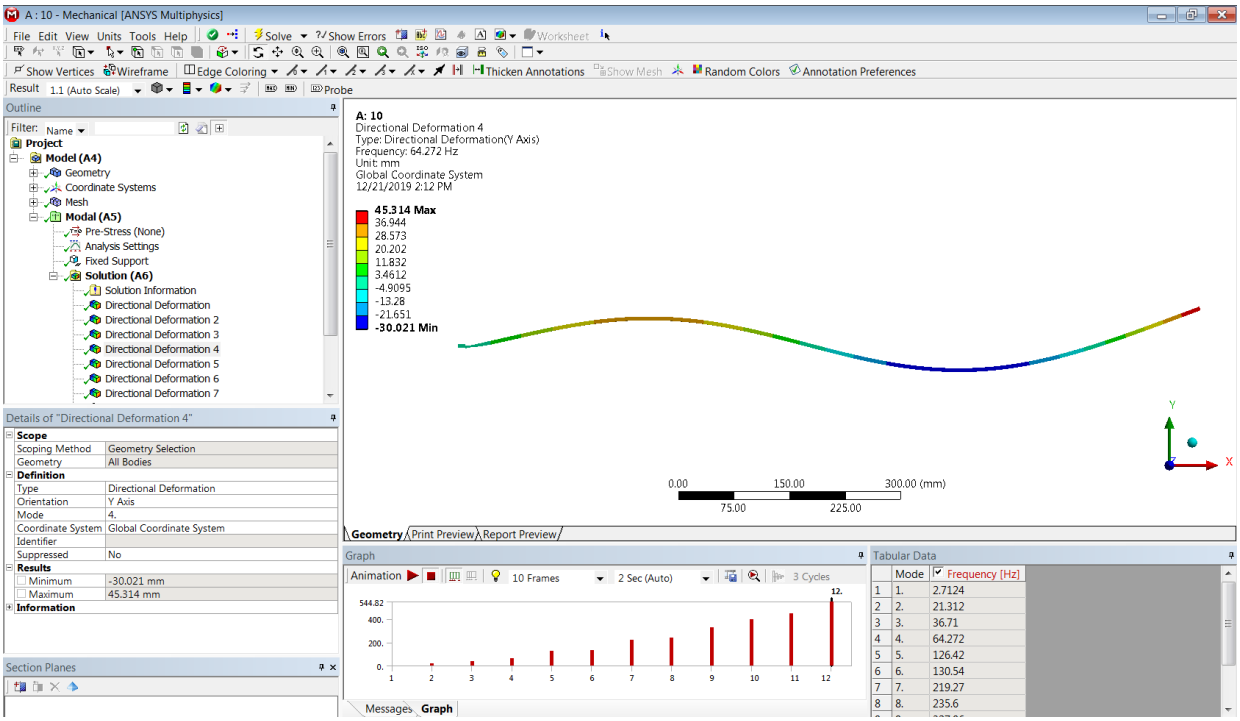

Figure 2.12. Results viewing interface

2.5. Modal analysis of damaged cantilever beams

2.5.1. Transversal damage

To profoundly understand the frequency shift phenomena that occur due to different damage types, first, the natural frequency curves for the undamaged cantilever with the dimensions presented in Table 1.1, was plotted.

For the undamaged beam, the natural frequencies for the first six modes of transversal vibration are presented in Table 2.3:

Table 2.3. The natural frequency values for the undamaged beam

Mode no.	1	2	3	4	5	6
Frequency [Hz]	4.09	25.627	71.757	140.63	232.53	348.21

After this, it was considered that the damaged cantilever with a transversal breathing crack, first having the depth *a=1* mm extending from the upper surface, and for the second transverse damage scenario, the crack depth is defined *a=2,5* mm. For both damage scenarios, the crack was iteratively removed with a step of *s=3* mm along the whole length of the beam, starting from the fixed end.

Table 2.4. The transversal crack dimensions and geometry

Crack shape	Crack length		Crack depth	Crack angle		Crack geometry
	L_L [mm]	L_R [mm]	a [mm]	α [º]	β [º]	
Transversal	-	-	1	-	-	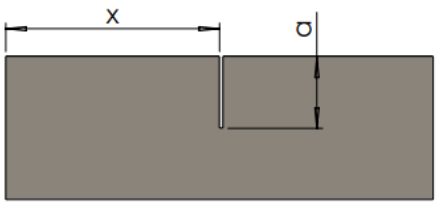
			2.5			

For investigating the effect of the crack severity, the natural frequency shift for the two damage cases were compared with those of the undamaged beam. The fixed end of the cantilever beam has been taken as reference, and the natural frequency curves for the first six bending vibration modes have been plotted and illustrated in Figure 2.13.

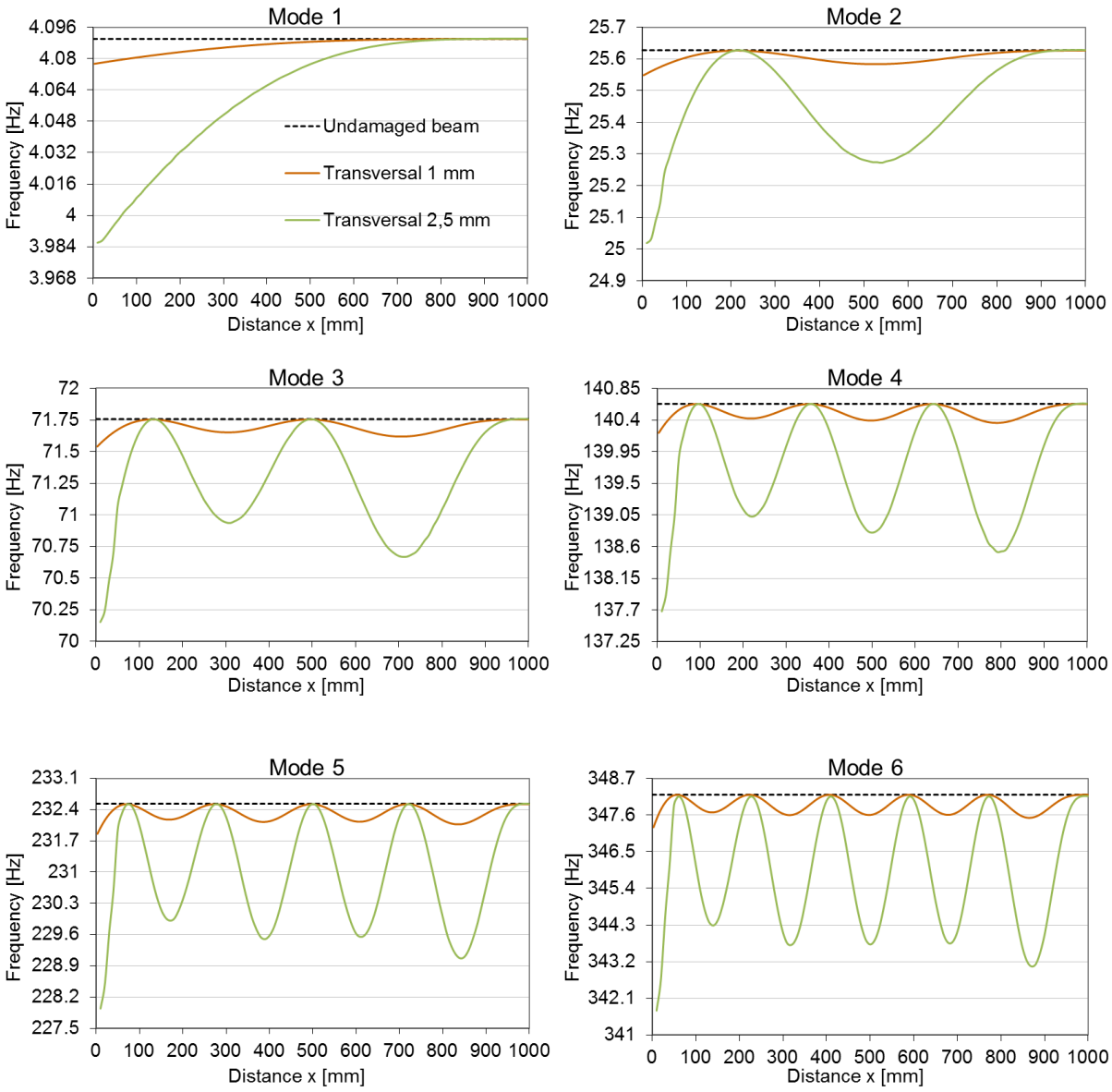

Figure 2.13. Frequency versus crack location for the transversal cracks of depth *a=1* mm and *a=2.5* mm

From this study, it is clear that the frequency of a beam decreases, in the event of a crack, due to the fact that it loses its stiffness and thus, cannot anymore accumulate the same amount of energy as in the healthy state.

The crack depth determines the damage severity, which is a parameter independent of the crack location. Hence it controls the amplitude of the frequency shift curves. On the other hand, the shape of these curves is controlled by the crack location and the vibration mode number. A crack with a given depth differently affects the natural frequency of a vibration mode if it is placed in different beam slices.

One can observe that there are locations where the crack produces no energy decrease, and consequently, it has no effect on the natural frequencies. This happens when it is located on inflection points. On the other hand, it produces main frequency alteration when it is positioned on the local maxima of the modal curvature. Regarding the crack with defined depth and position, it differently affects the natural frequencies of different vibration modes.

2.5.2. L-shaped damage

The next sections are dedicated to the study of complex-shaped cracks, described with the help of the general damage schematic (Figure 2.2), consisting of a transverse extension followed by delamination.

The crack geometry is described in this case as an L-shaped crack, with its branch oriented to the right.

Table 2.5. The L_R crack dimensions and geometry

Crack shape		Crack length		Crack depth	Crack angle		Crack geometry
		L_L [mm]	L_R [mm]	a [mm]	α [°]	β [°]	
b	L_R	-	50	2.5	-	90	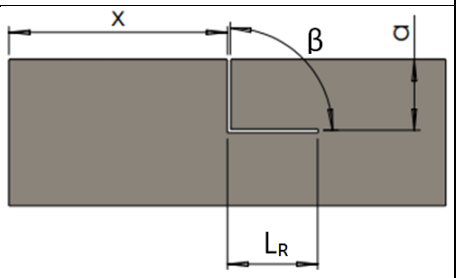

Table 2.5 illustrates the real crack with its main dimensions. The crack position is described by the distance *x*, which is always considered between the fixed beam end and the left end of the crack.

The damage case was described as L_{R50}, according to Table 2.2, which represents an L shaped crack; it has a transverse branch, with depth $a = 2.5$ *mm* and a longitudinal branch of 50 mm localized at a distance *x* from the fixed end. The damage was also removed iteratively with a step of *s=3mm*.

The curves, plotted for the first six weak-axis bending vibration modes, are depicted in Figure 2.14 and compared to the natural frequencies of the undamaged beam and the damaged beam with a transversal crack of $a = 2.5$ *mm*.

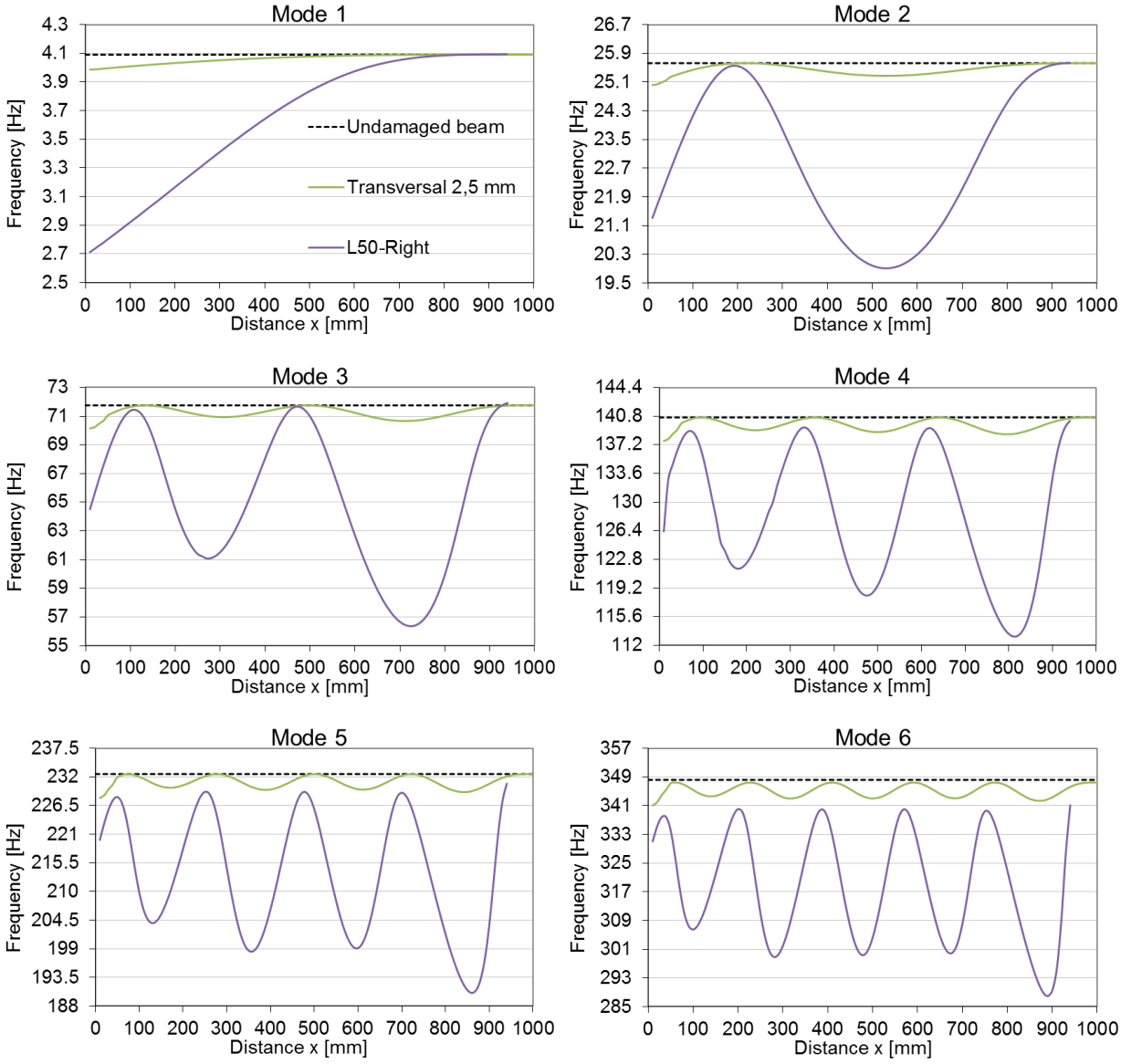

Figure 2.14. Frequency versus crack location for two types of damages (transversal and L_R-shaped) for six vibration modes.

It was found that the two crack types produce different shifts, but the curves representing these shifts are somehow similar. The curves for the L_R-shaped crack shift to the fixed end; thus, the inflection points do not coincide with these of the transverse crack. From Figure 2.15, it is easy to see the natural frequency decrease between the transversal crack and a crack with a 50 mm delamination.

In the next case the same type of damage was generated, but this time, the crack is oriented to the left, with its dimensions and shape presented in table 2.6.

Table 2.6. The L_L crack dimensions and geometry

Crack shape		Crack length		Crack depth	Crack angle		Crack geometry
		L_L [mm]	L_R [mm]	a [mm]	α	β	
c	L_L	50	-	2.5	90	-	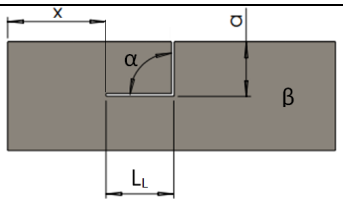

The curves, plotted for the first six weak-axis bending vibration modes, are depicted in Figure 2.15 and compared to the natural frequencies of the undamaged beam and the damaged beam with a transversal crack of $a = 2.5\ mm$.

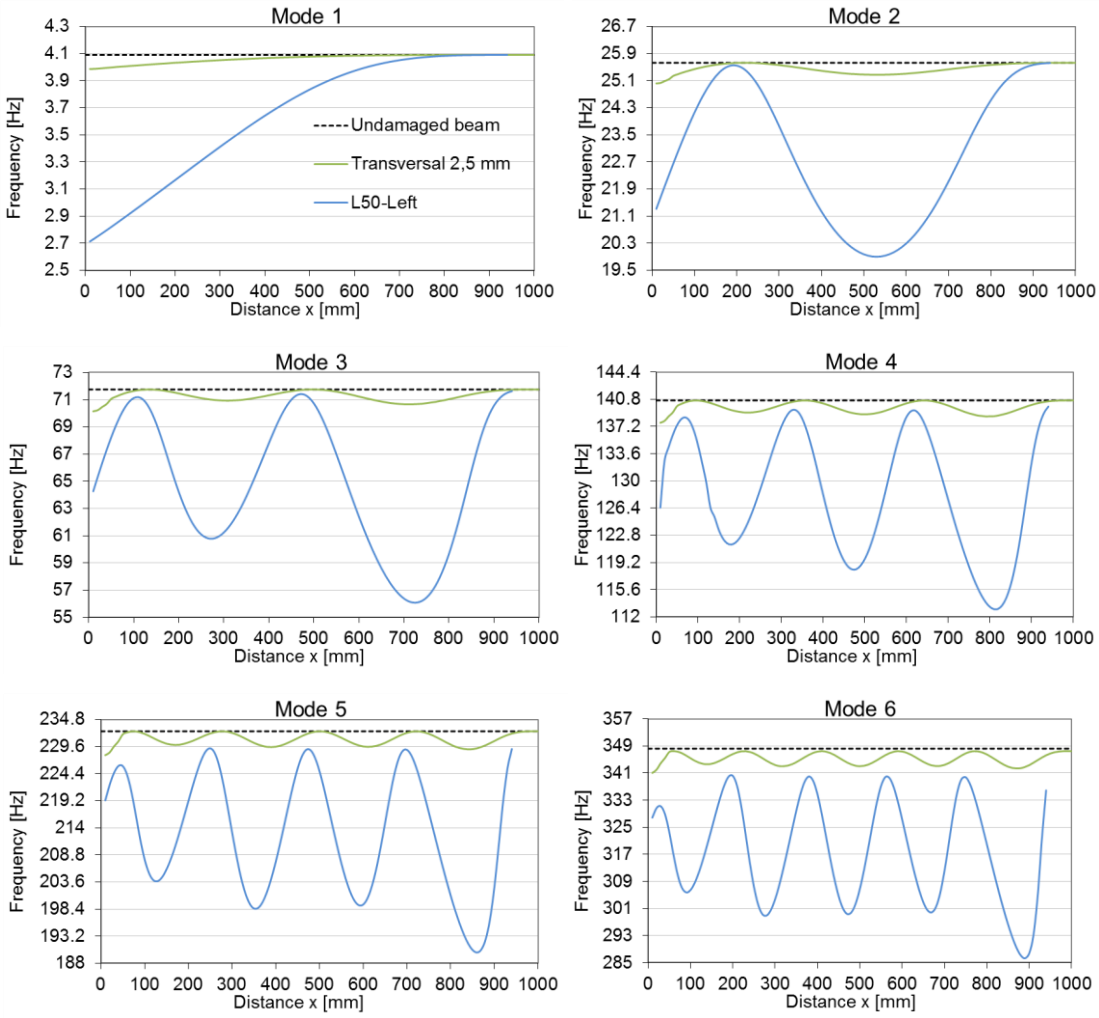

Figure 2.15. Frequency versus crack location for two types of damages (transversal and L_L-shaped and transversal) for six vibration modes.

Figure 2.16 illustrates the obtained natural frequencies curves for the beam with a transversal crack with depth a=2.5 mm in comparison with the L_{R50} crack and L_{L50} crack described in tables 2.5 and 2.6. From this comparison, it was observed that the natural frequencies present small differences for the same crack, but with different longitudinal element orientation. Dissimilar to the beam with a transverse crack, which achieves the healthy beam's frequency when the crack is located on an inflection point, the maximum frequency value achieved by the beam with an L-shaped crack is always lower than the frequency of the healthy beam. This is more evident for higher modes and if the crack is closer to the fixed end.

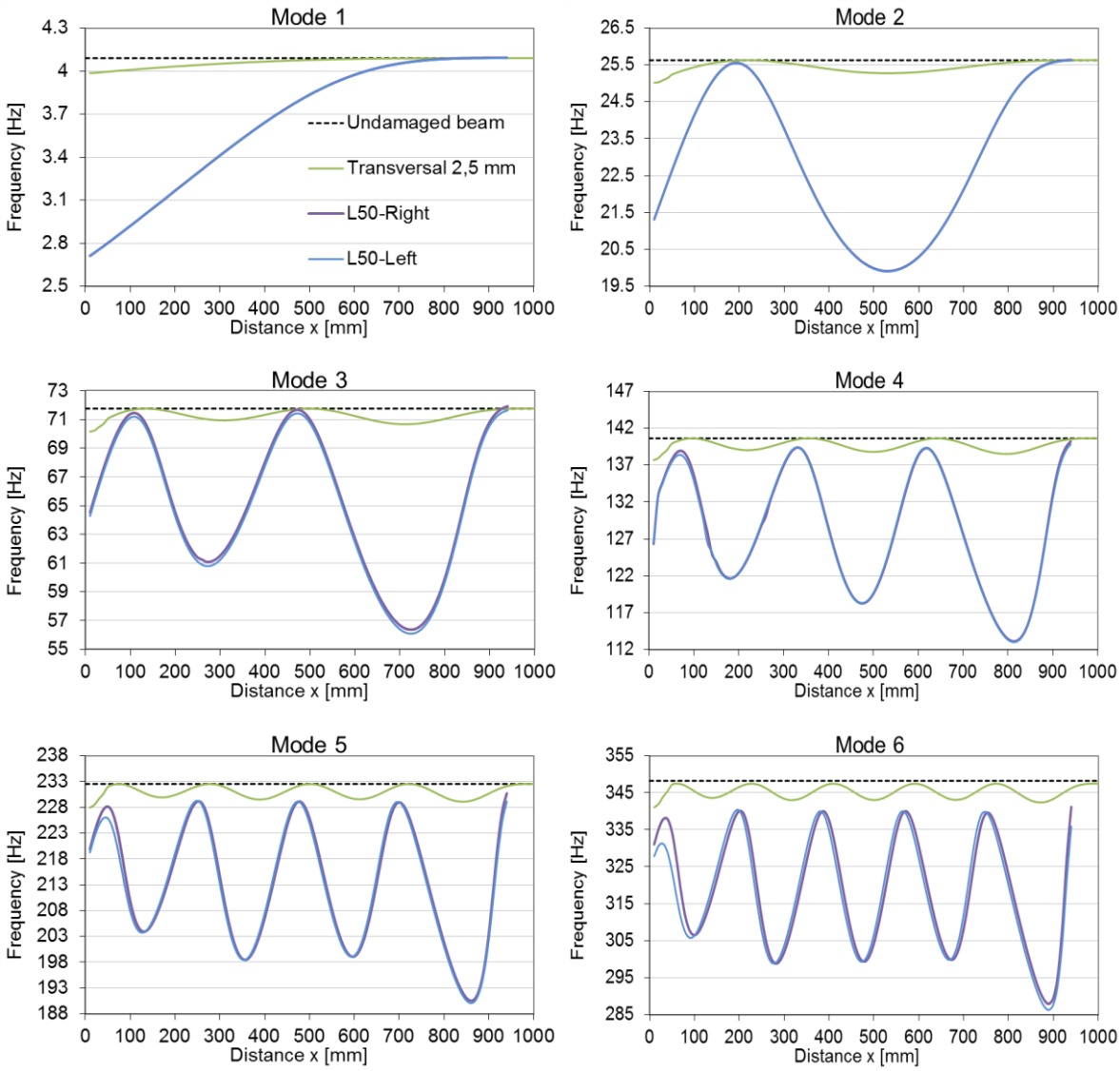

Figure 2.16. Frequency versus crack location for three types of damages (transversal, L_{R50}-shaped and L_{L50}-shaped) for six vibration modes.

Furthermore, the analyzed effect of L-shaped cracks having different delamination length is presented.

The crack position is described by the distance *x*, which is always considered between the fixed beam end and the left crack component. The depth of the crack is for all studies *a*=2.5 mm, the variables baying: the delamination length, orientation (left or right), and crack position. The crack end is considered because the longitudinal component is the relevant one. In this way, the compatibility of the achieved results are assured.

The first evaluation focused on the influence of the crack position, while the second one was on the influence of the longitudinal crack extent. For clarity, a detailed description of the cracks involved in the analyses is given in table 2.7.

Table 2.7. The L_R and L_L cracks with different delamination dimensions

Crack shape		Crack length L_L [mm]	Crack length L_R [mm]	Crack depth *a* [mm]	Crack angle α [°]	Crack angle β [°]	Legend	Crack geometry
b	L_R	-	50	2.5	-	90		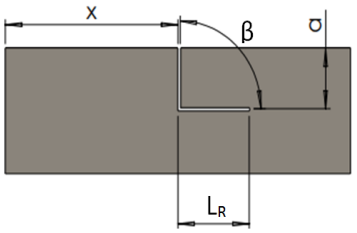
		-	40	2.5	-	90		
		-	30	2.5	-	90		
		-	20	2.5	-	90		
		-	10	2.5	-	90		
c	L_L	50	-	2.5	90	-		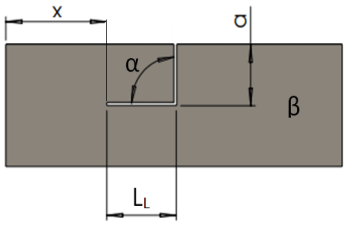
		40	-	2.5	90	-		
		30	-	2.5	90	-		
		20	-	2.5	90	-		
		10	-	2.5	90	-		

For all damage scenarios, the crack was iteratively removed by a step of *s =10* mm along the beam starting with a distance of 10 mm from the fixed end to the left longitudinal extent of the crack. The acquired results are the values of the natural frequencies for the first six bending vibration modes.

Figure 2.17 illustrates the comparison between the L_R and L_L damages for the different delamination lengths, presented in table 2.7:

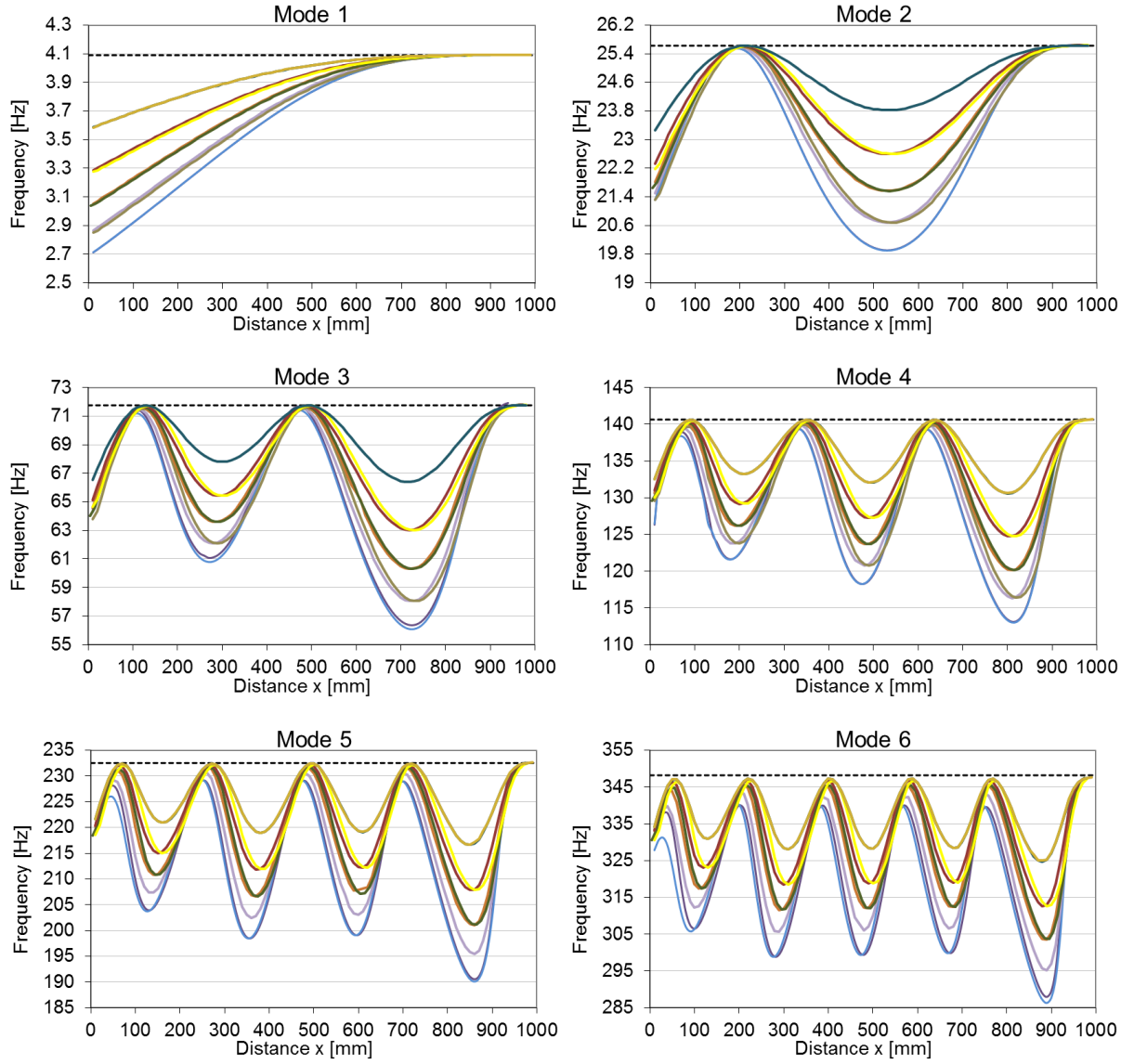

Figure 2.17. Frequency versus crack location for L_R-shaped and L_L-shaped cracks

From this comparison, one can observe that the natural frequencies present small differences for the same crack length, but the plotted curves are shifted, matching the delamination orientation. All crack positions have been defined starting from the left end of the beam to the transversal element of the crack. The plotted charts show a symmetrical shift for every pair of L_R and L_L cracks.

2.5.3. T-shaped damage

Next, the evaluation of the damage severity is studied by comparing the effect of the cracks with a *T* shape, all having the transverse branch with a similar depth, but having different dimensions of the longitudinal branches, as presented in Table 2.8. The way how these cracks diminish the natural frequencies is presented in Figure 2.19.

Table 2.8. The T-shaped crack dimensions and geometry

Crack shape		Crack length L_L [mm]	Crack length L_R [mm]	Crack depth a [mm]	Crack angle α	Crack angle β	Crack geometry
d	T_{50}	25	25	2.5	90	90	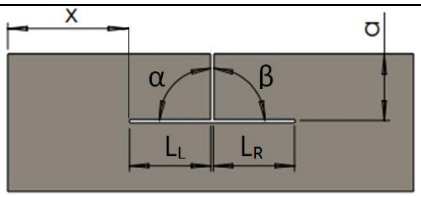
e	T_{40}	20	20	2.5	90	90	
f	T_{30}	15	15	2.5	90	90	
g	T_{20}	10	10	2.5	90	90	
h	T_{10}	5	5	2.5	90	90	

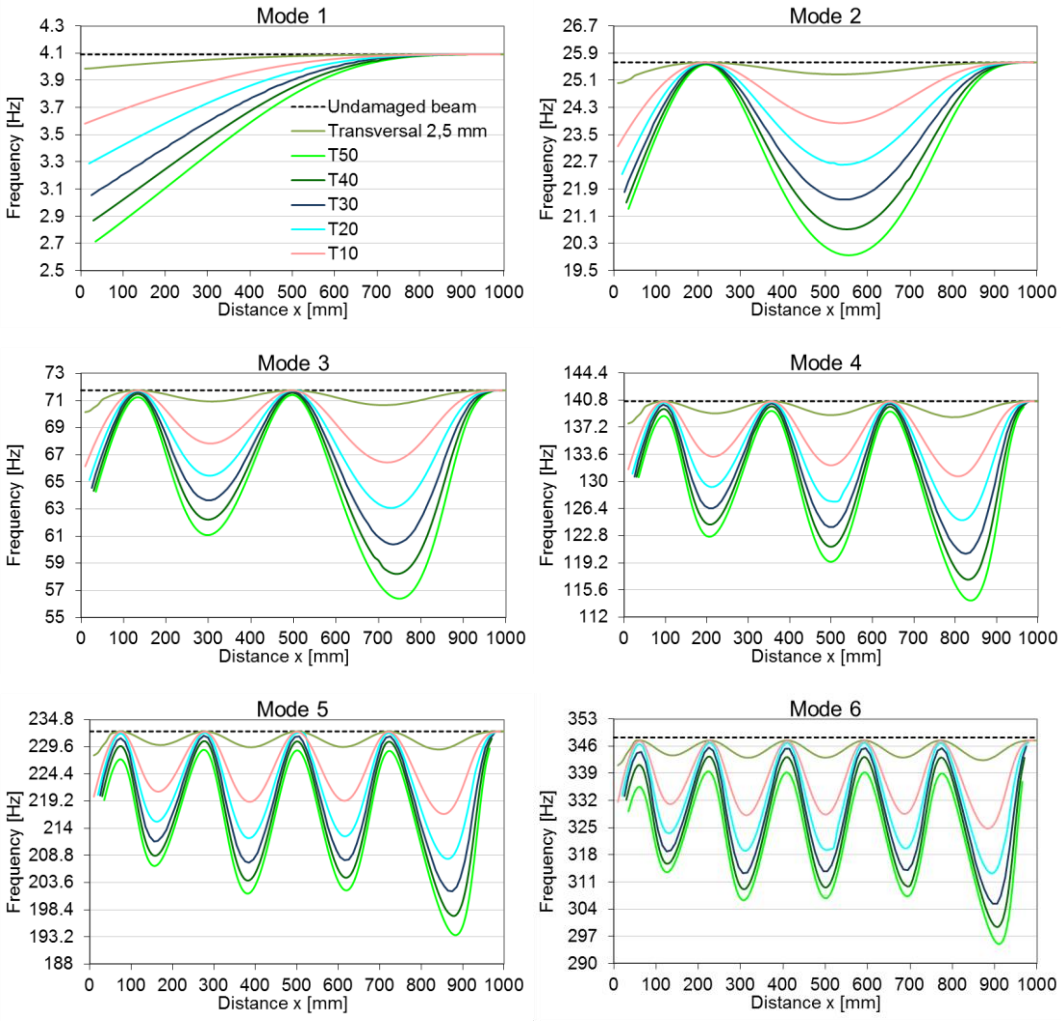

Figure 2.18. Frequency Shift Curves (FSC) for damages of type T_{50}, T_{40}, T_{30}, T_{20}, T_{10}

From Figure 2.18, it indeed results that the five damages considered have different behavior since the frequency drop is more significant as the longitudinal component is increased. Near the free end of the beam, one can observe that minor differences between frequencies occur for

the first three modes of vibration, but at higher modes, the influence of the damage extent is easy to observe. From this study, it was concluded that the transversal component of the crack has an influence on the damage severity; the longitudinal component should also be taken into account to express the severity for all vibration modes.

2.5.4. Comparison of T and L-shaped cracks

Furthermore, the results obtained for the L-shaped cracks located in the same beam geometry described in Table 2.1 are compared to the T-shaped cracks having the dimensions of the general damage schematic. The crack dimensions are presented graphically in Table 2.9. By investigating the effect of the crack position, for both *L* and *T* shaped cracks, the left crack end was taken as reference. As presented in Table 2.9, for the two damage cases, the longitudinal crack components have the extent 50, 30, and 10 mm, respectively.

Similarly, simulations were made to find the frequencies for the damage cases presented.

Table 2.9. The L_R, L_L, and *T* cracks with different delamination dimensions

Crack shape		Crack length L_L [mm]	Crack length L_R [mm]	Crack depth *a* [mm]	Crack angle α	Crack angle β	Legend	Crack geometry
b	L_R	50	-	2.5	-	90		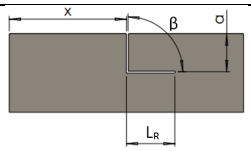
		30	-	2.5	-	90		
		10	-	2.5	-	90		
c	L_L	50	-	2.5	90	-		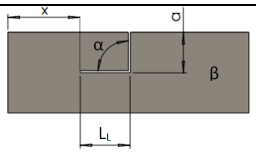
		30	-	2.5	90	-		
		10	-	2.5	90	-		
d	T	50	-	2.5	90	90		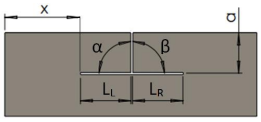
		30	-	2.5	90	90		
		10	-	2.5	90	90		

The comparison is presented for the *T* and *L* shaped cracks, in Figures 2.19 for the 50 mm delamination damages, in Figure 2.20 for the 30 mm delamination damages, and in Figure 2.21 for the 10 mm delamination.

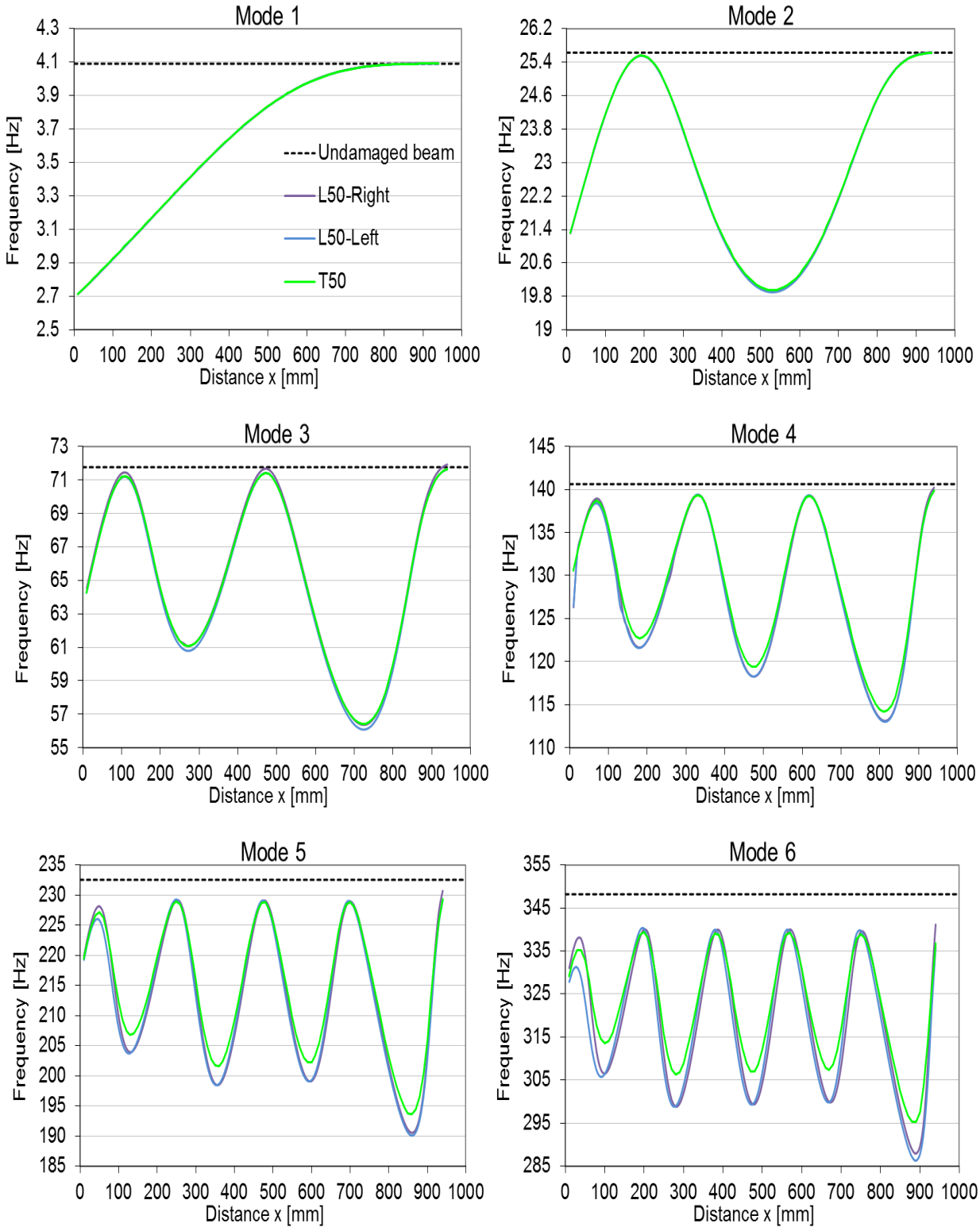

Figure 2.19. Frequency Shift Curves (FSC) for damages of type T_{50}, L_{R50} and L_{L50}

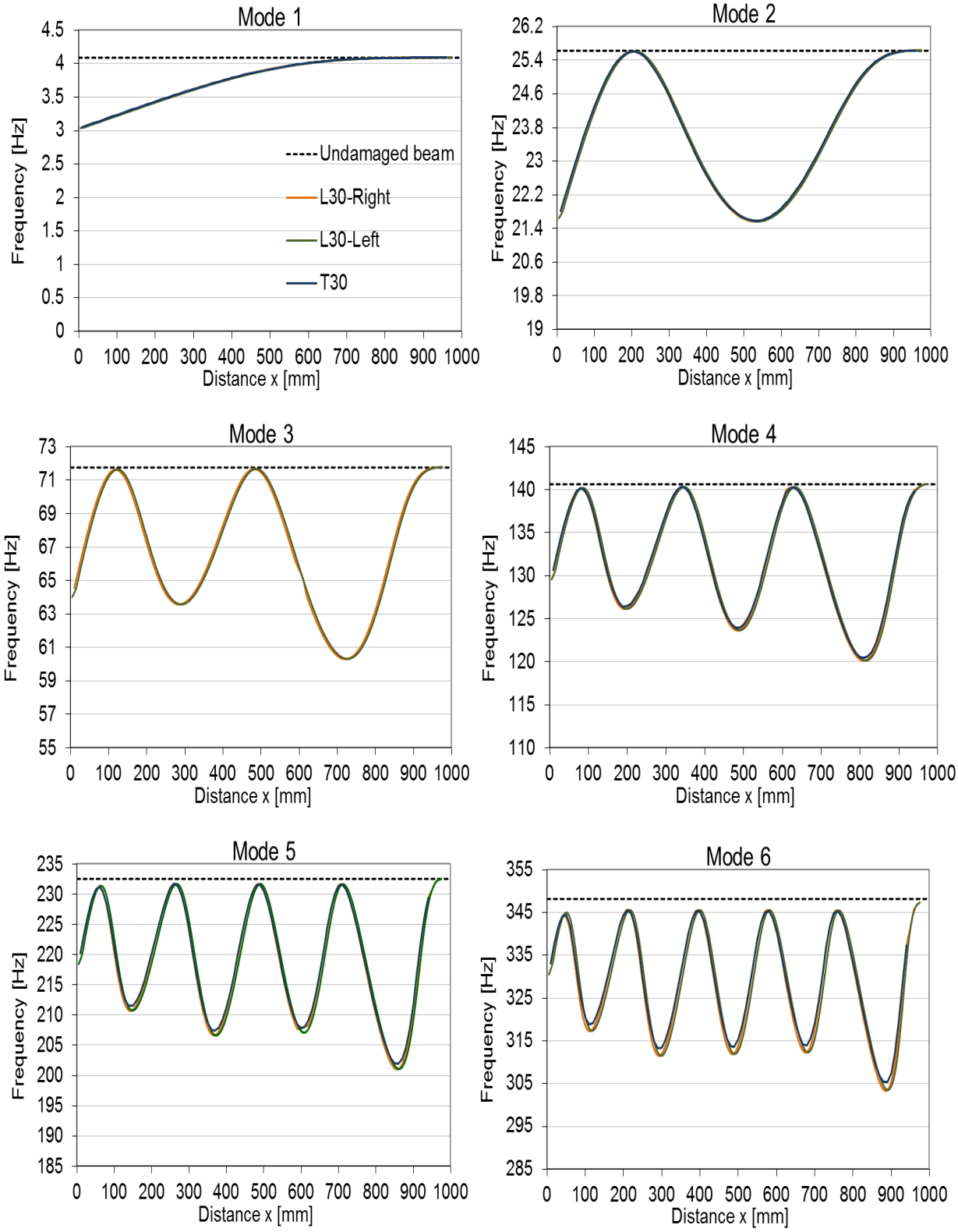

Figure 2.20. Frequency Shift Curves (FSC) for damages of type T_{30}, L_{R30} and L_{L30}

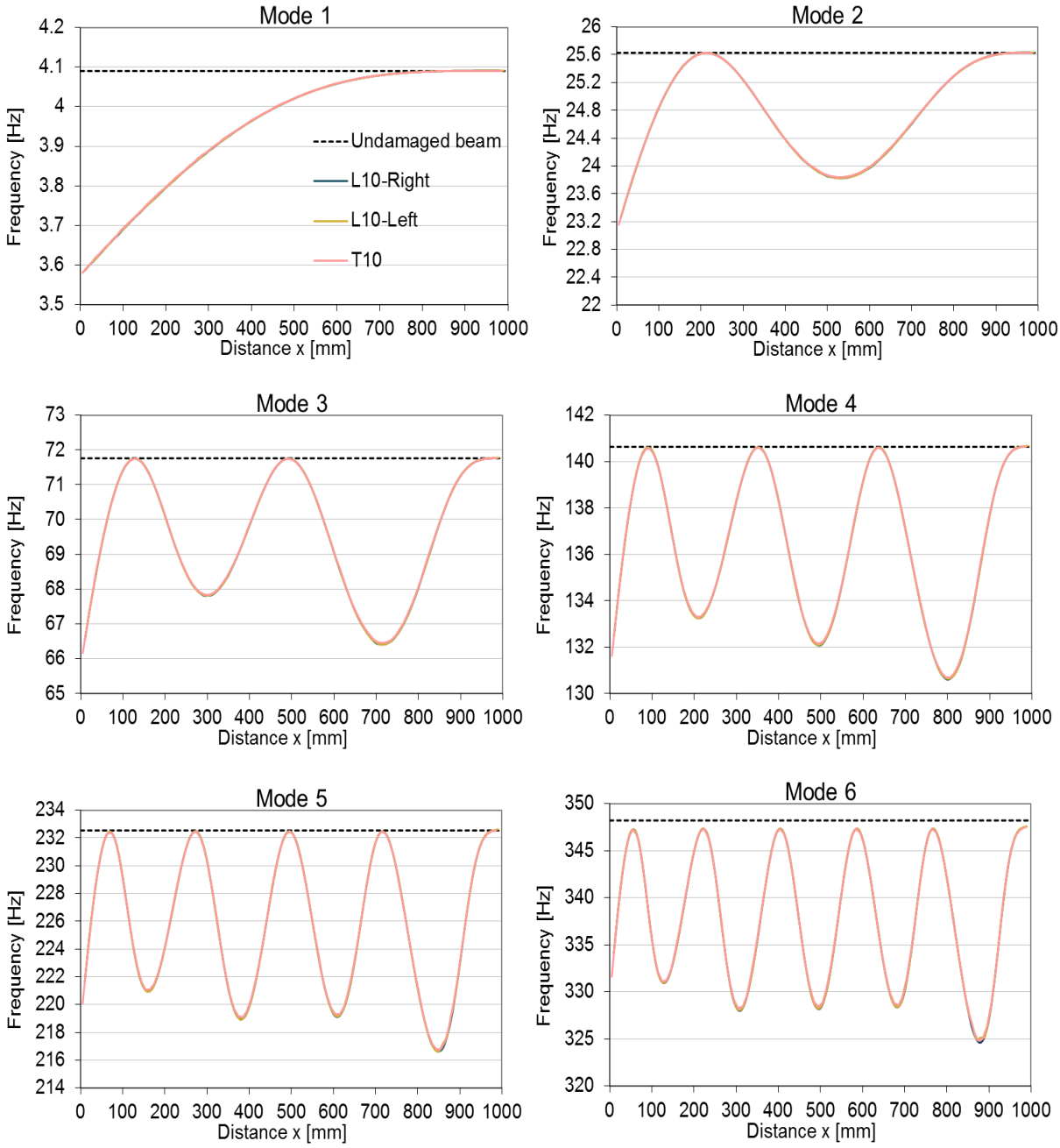

Figure 2.21. Frequency Shift Curves (FSC) for damages of type T_{10}, L_{R10} and L_{L10}

From Figure 2.19, and 2.20, it can be seen that the three damages of type L_L, L_R, and T with 50-, and 30-mm delamination, considered in this sub-section, have a quite similar effect upon the first three vibration modes. Starting from the fourth mode, a behavioral differentiation is observed, since the frequency drops for the beam affected by an L crack are more significant as those of the beams affected by T-type cracks. In addition, near the fixed end, minor differences between frequencies of the beams carrying L_{L50} and L_{R50} cracks are observed. Also, the curves shift differently in relation to the delamination orientation. From Figure 2.21, one can conclude that for the 10 mm

delamination, the natural frequency values are very close for all three types of cracks, but the curves do shift a minimal amount due to the orientation of the delamination.

These observations permit concluding that the longitudinal damage branch is relevant for the behavior of a damaged beam, and it should be considered when defining damage patterns for vibration-based nondestructive structural health assessment. The transversal crack branch has the primary effect on the frequency drop if it is located at one end of the longitudinal crack branch. Intermediate positions of the transversal crack branch lead to lower frequency drops if the delamination length is approximately four times bigger than the transversal element. The lowest drop is obtained if the transversal element is situated in the center of the longitudinal crack branch.

2.6. Complex shaped cracks with different branch orientations

2.6.1. Damages with different branch orientations positioned on different locations along the beam

The current research is focused on finding a mathematical relationship with a large degree of generality, and it wasw succeeded in the current thesis, by developing a relationship that can be applied to any beam-like structure if it is subject to a transverse crack [13]-[16].

The current subchapter is fixated on cracks with Y-shaped [84], which have increased complexity and, therefore, more parameters that influence the frequency changes. This makes approaching such structures more difficult. For the next analysis, models are created in which the two branches of the crack propagate at various angles. The cross-sectional component is placed in characteristic locations of the structure in out of plane vibration. The simulation results are aimed to demonstrate that the crack propagation direction has a significant effect on the eigenfrequency values [27].

The assigned material for the beam is Structural Steel, and the main dimensions presented in Table 2.1 besides the width *B*, which is for this study *B=20* mm.

The damage geometry is described as a Y-shaped crack resulting from a transverse component followed by two oblique ramifications. It matches the idealized crack with its general dimensions described in table 2.10 and having the angular values according to table 2.11. The damaged is placed in three well known positions, *x*=10, *x*=300, *x*=480 mm [11]. The positions of the crack have been selected as such that in mode 3 of transversal vibration the *x*=10 is at the maximum point of the curve, *x*=300 is at an intermediate point and *x*=480 at an inflection point.

Table 2.10. Dimensions of the Y-shaped crack

Crack shape		Crack length		Crack depth	Crack angle		Crack geometry
		L_L [mm]	L_R [mm]	a [mm]	α [°]	β [°]	
e	Y	3	3	1	see table 10	see table 10	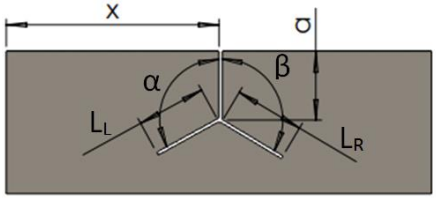

The investigation presented in this chapter is a numerical study destined to find the dynamic response of beams with branched cracks, in particular, to define the effect of the position of the transverse crack component relative to the longitudinal crack component.

Table 2.11. Dimensions of the Y-shaped crack

α [°]	β [°]	β [°]	β [°]	β [°]
	90	120	150	180
90	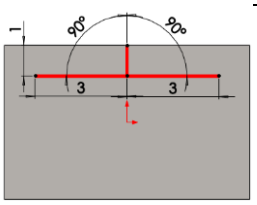	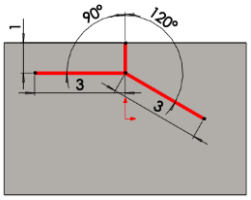	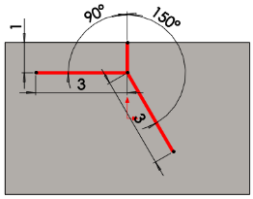	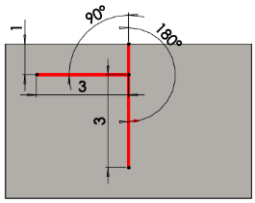
120	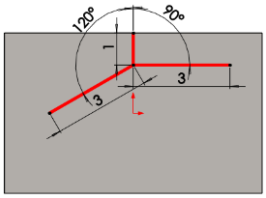	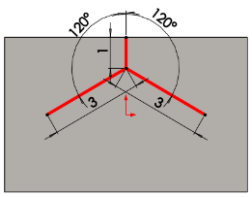	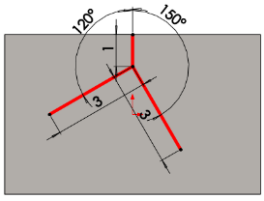	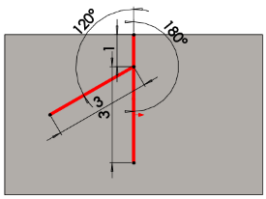
150	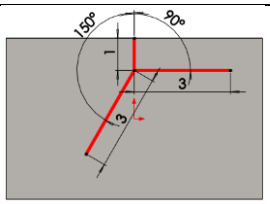	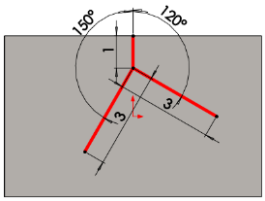	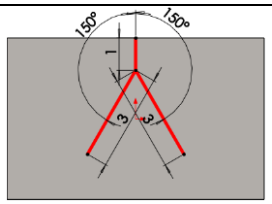	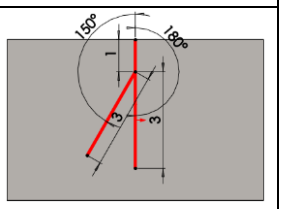
180	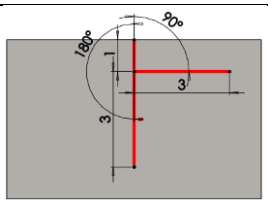	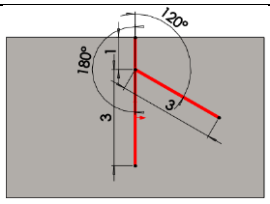	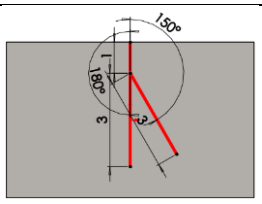	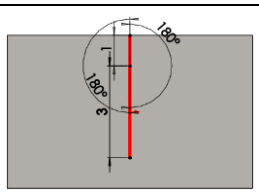

The acquired results for the beam in a healthy and damaged state are the eigenfrequencies' values for the first six modes of out-of-plane vibration. In Figure 2.22, the stress distribution for the three key positions of the crack for the third vibration mode, is illustrated, where *x=10* mm represents the crack positioned near the fixed end, *x=300* mm the position of the crack where the beam deflection is maximal, and *x=480* mm at an inflection point.

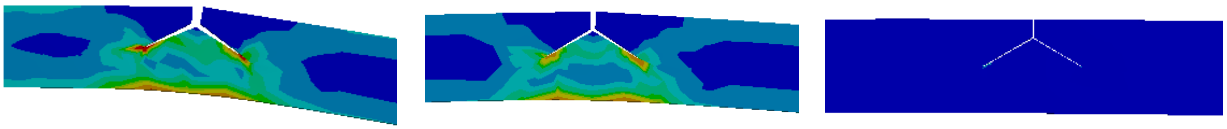

a b c

Figure 2.22. A zoom on the 3 crack locations: (a) *x* = 10 mm; (b) *x* = 300 mm; (c) *x* = 480 mm

In order to understand the phenomena of frequency shift due to the different types of cracks in a cantilever beam, the frequency shift curves were plotted for all damage cases for the first six vibration modes. In Figures 2.23 to 2.28, the plotted frequency shift curves for the vibration modes one to six are illustrated.

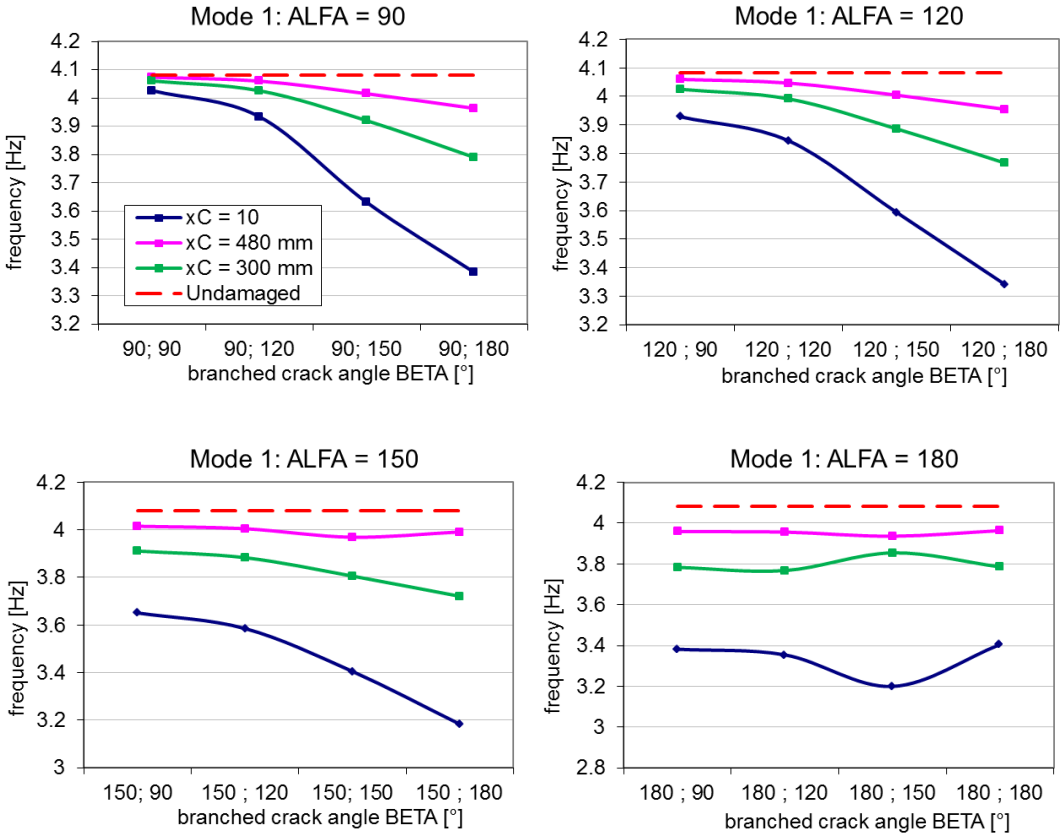

Figure 2.23. Frequency shift curves for the first vibration mode for the three damage positions: 10 mm, 300 mm and 480 mm

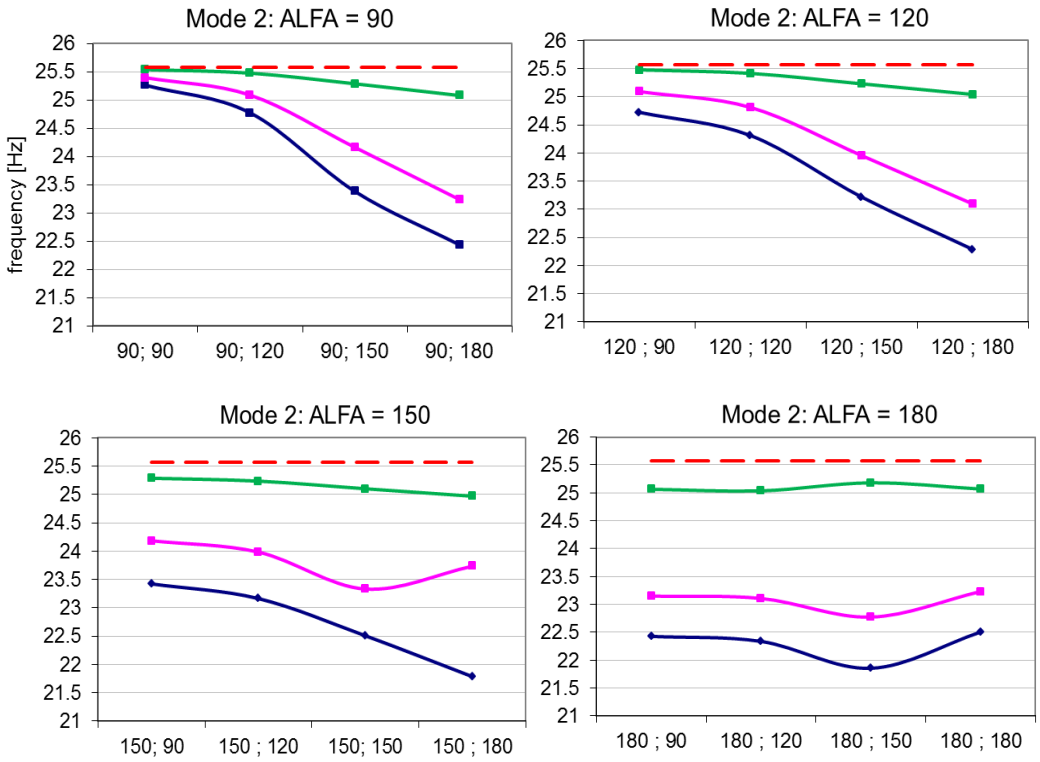

Figure 2.24. Frequency shift curves for the second vibration mode for the three damage positions:10 mm, 300 mm and 480 mm

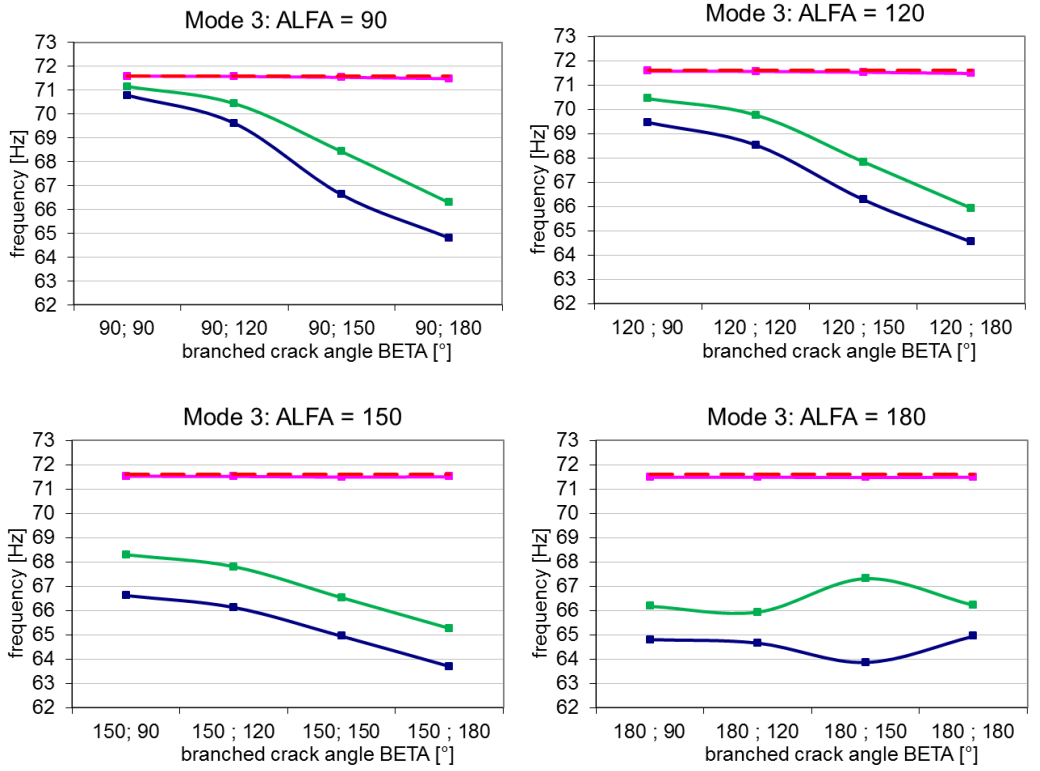

Figure 2.25. Frequency shift curves for the third vibration mode for the three damage positions:10 mm, 300 mm and 480 mm

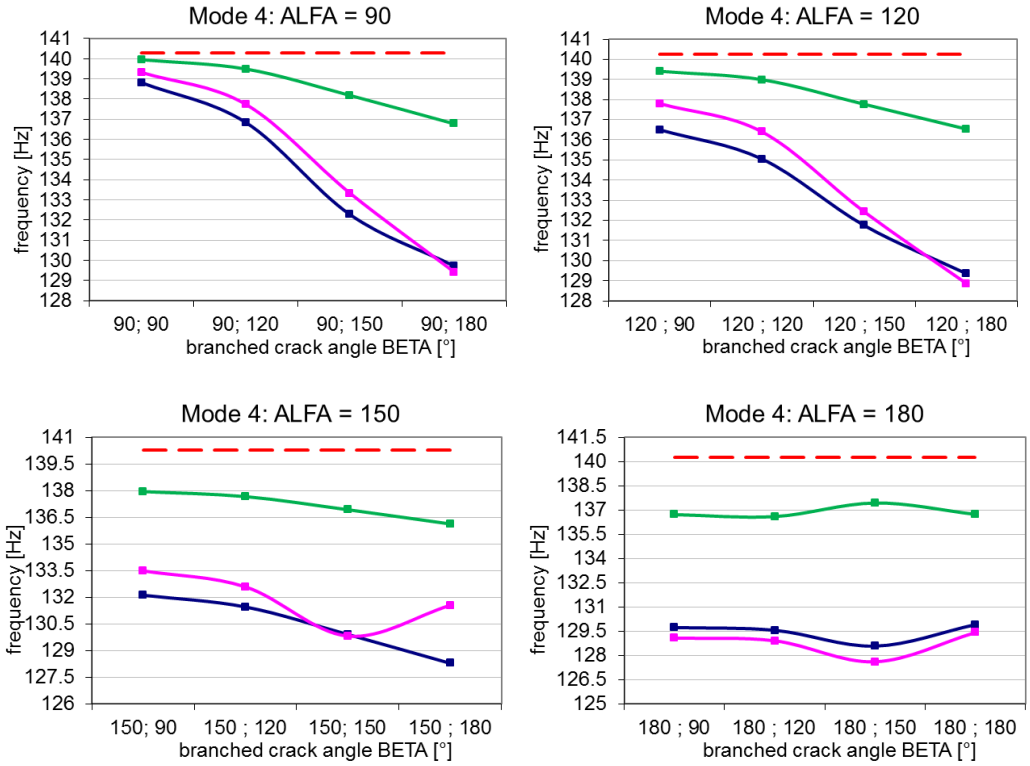

Figure 2.26. Frequency shift curves for the fourth vibration mode for the three damage positions:10 mm, 300 mm and 480 mm

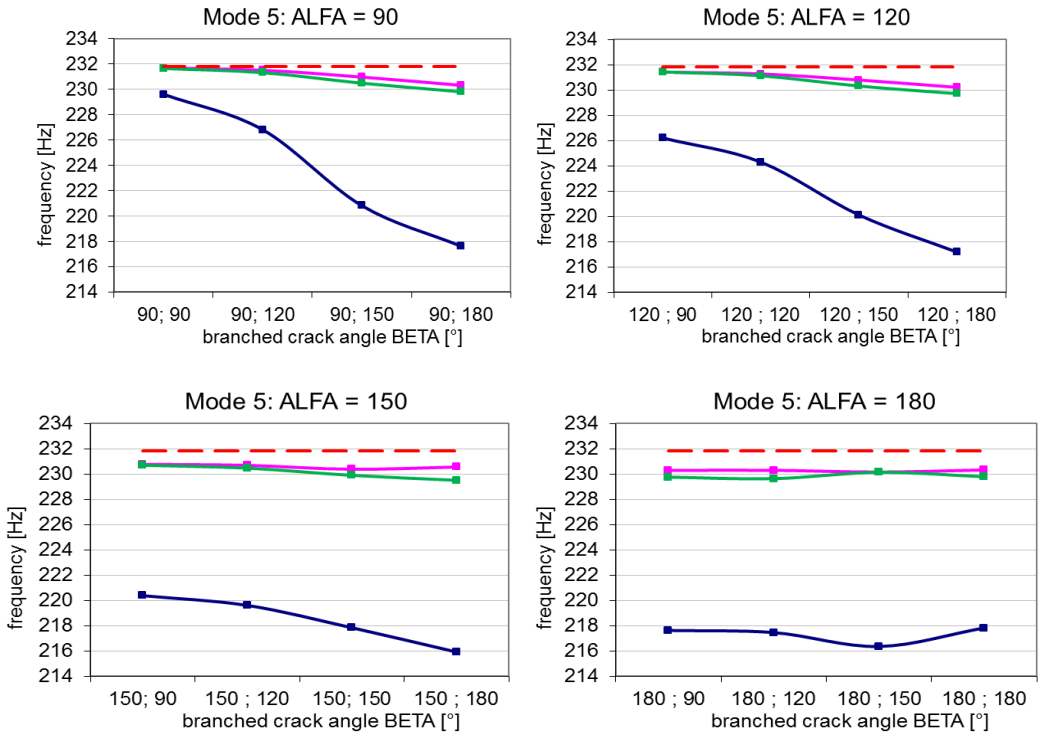

Figure 2.27. Frequency shift curves for the fifth vibration mode for the three damage positions:10 mm, 300 mm and 480 mm

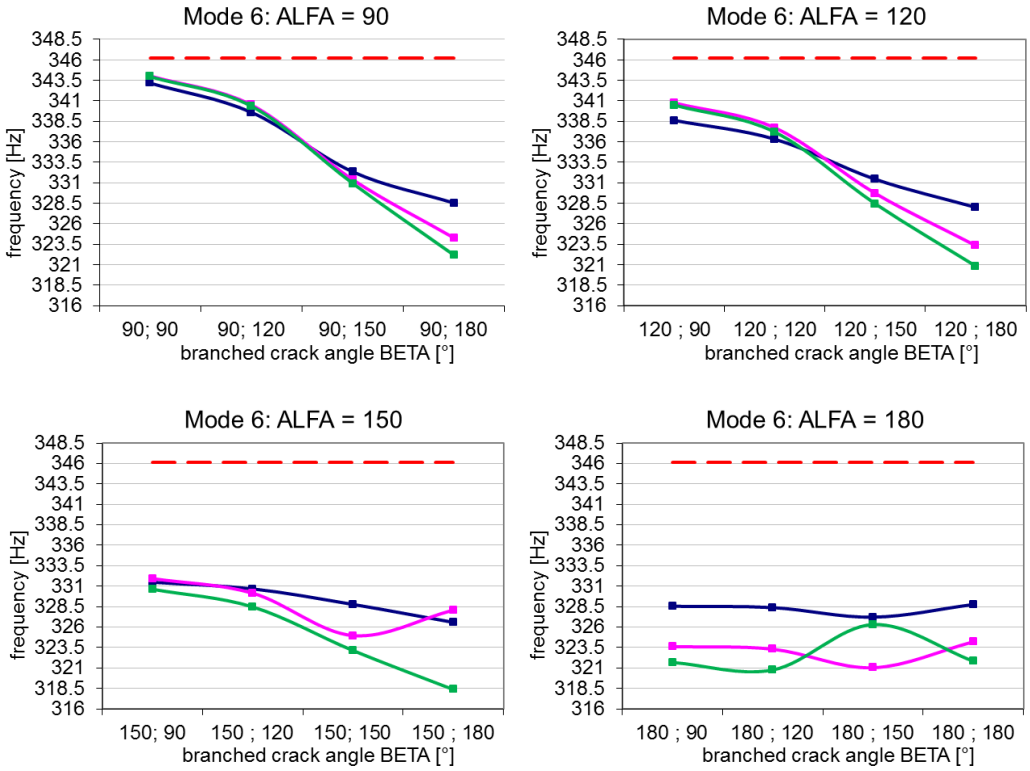

Figure 2.28. Frequency shift curves for the six-vibration mode for the three damage positions:10 mm, 300 mm and 480 mm

The first evaluation focused on the influence of the different propagation angles of the crack, while the second one was on the influence of the crack position for the third vibration mode.

The way that a Y-shaped crack diminishes the eigenfrequencies of the beam is shown by comparing the evolution of the frequency shift on different locations and geometry of the crack. One can observe that, in comparison, the position of the crack with the most influence on the modal parameters is located near the fixed end, which demonstrates that for a cantilever, the location with the highest bending moment is at the fixed end.

After comparing the values obtained for all damage scenarios, one can assume that the presence of a Y-shaped crack with branches at 60˚ and 90˚ has the most substantial effect on the frequency drop irrespective of the crack location.

Since the frequency shifts are in direct relation with the mode shape curvatures or bending moments from the plotted values, one can observe that the beam achieves different frequency shifts at different locations. For the damaged case with the crack located at an inflection point, as expected, the obtained values indicated a low-frequency drop. This happens because no stress is present in the crack region, as shown in Figure 2.22-c. The results of the damaged beam, as well

as the results on the healthy beam obtained by FEM analysis, are presented in Table 2.12 for conformity. It can be easily observed that the shift is less than 1%.

Table 2.12. Comparison between the frequencies of the undamaged beam f_{iU} and the beam with a crack f_{iC} positioned at x_c= 480 and x_c=300 mm for mode 3

f_{iU} [Hz]	α [˚]	β [˚]	$f_{iC\text{-}480}$ [Hz]	difference [%]	$f_{iC\text{-}300}$ [Hz]	difference [%]
71.597	0	0	71.588	0.01	71.157	0.61
		30	71.577	0.03	70.439	1.62
		60	71.538	0.08	68.42	4.44
		90	71.484	0.16	66.285	7.42
	30	0	71.569	0.04	70.436	1.62
		30	71.559	0.05	69.763	2.56
		60	71.524	0.10	67.833	5.26
		90	71.474	0.17	65.93	7.92
	60	0	71.52	0.11	68.292	4.62
		30	71.514	0.12	67.802	5.30
		60	71.488	0.15	66.524	7.09
		90	71.503	0.13	65.263	8.85
	90	0	71.481	0.16	66.17	7.58
		30	71.482	0.16	65.932	7.91
		60	71.469	0.18	67.305	5.99
		90	71.484	0.16	66.21	7.52

This study found that the branch penetration angle of the crack produces different frequency shifts.

It was also observed that the most considerable shift and stress are found at the fixed end, for all six modes of vibration. The smallest frequency changes, as expected, were found at inflection points where the beam faces less stress; thus, the crack has a low effect. After comparison of the eigenfrequencies values for the different penetration angles of the damage, it was found that the geometry formed by a transverse crack with one branch propagating in the same transverse direction and the other at 60˚ degrees presents the largest frequency drop, no matter of the crack position in the beam.

2.6.2. Influence of the branch orientation of L and T-shaped cracks

To create diverse damage scenarios, a branched crack that has the transverse component located at a distance *x=6 mm* from the fixed beam end was considered. The cantilever beam has the dimensions presented in Table 2.1. In the first case, the crack is modeled with a transverse component of depth a=1,5 mm, followed by a branch of length L_R=1,5 mm that forms an angle α_0=90º with the other crack component. This is, in fact, the L-shaped crack presented earlier, which

has the horizontal branch oriented to the right, but with different dimensions. This crack was denoted, initially as L_R, and it is presented in Figure 2.29 with a red line. For the entire damage scenarios, with blue line the iterative positions of the initial longitudinal branch was shown; basically the branch is reoriented for every damage case with a step of $\Delta\alpha = 15°$ [49].

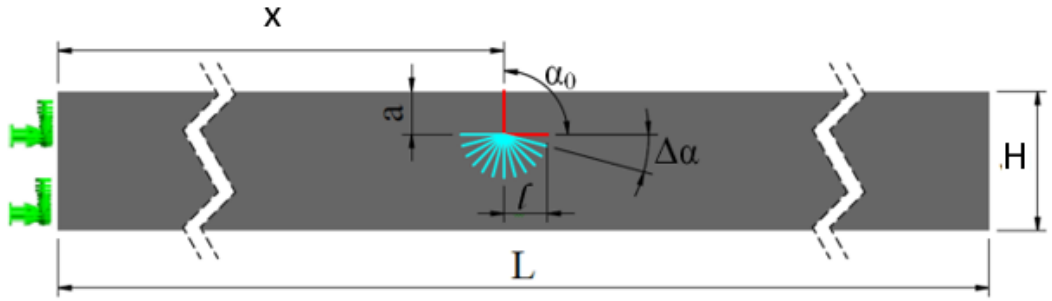

Figure 2.29. Branched crack geometry: L – shaped crack

For the second case, a T crack was considered, modeled with a transverse component that has the same depth a =1.5 mm, but followed by two branches of equal length L_R=L_L=1.5 mm spread in the horizontal direction.

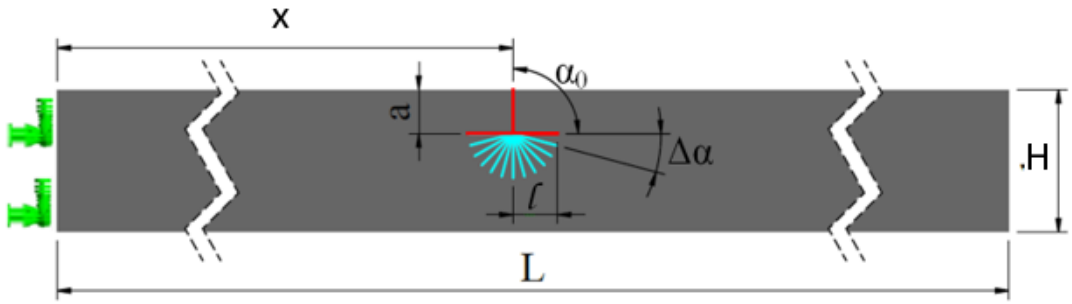

Figure 2.30. Branched crack geometry: T – shaped crack

In order to evaluate the effects of the orientation of the crack branches on the beam's eigenfrequencies, the right branch of the crack was iteratively removed in the clockwise direction with a step $\Delta\alpha = 15°$ for both damage cases. Therefore, the right branch has different angles, as presented in Figure 2.29 for the initial L_R crack and Figure 2.30 for the initial T crack.

From the modal analysis, the eigenfrequencies for the healthy beam and the beam with the cracks described in the previous section were found. The results are presented in Figure 2.31. From this figure, one can observe that in all cases the crack produced a frequency drop. It can also be noticed that the L-shaped crack produces quite similar frequency drops as the T-shaped crack, with the observation that for the latter, a slightly bigger frequency drop was obtained. This is justified by the supplementary left crack branch. However, the contribution of this additional branch was proved to be low.

It was necessary to point out the two particular positions of the branch of the crack that rotates. The first refers to the L_R crack that has $\alpha = 180^{\circ}$, which is actually a transverse crack with the depth 3 mm. Similarly, it is the case of the T crack, which is a transverse crack with the depth 3 mm and a longitudinal branch oriented to the fixed end. For this particular branch angle, the highest frequency drop is obtained for both crack types. The second case is the angle $\alpha = 270^{\circ}$, where the two cracks are similar, actually being an L-shaped crack with the delamination oriented to the left. Here, the same frequencies are obtained for both crack types.

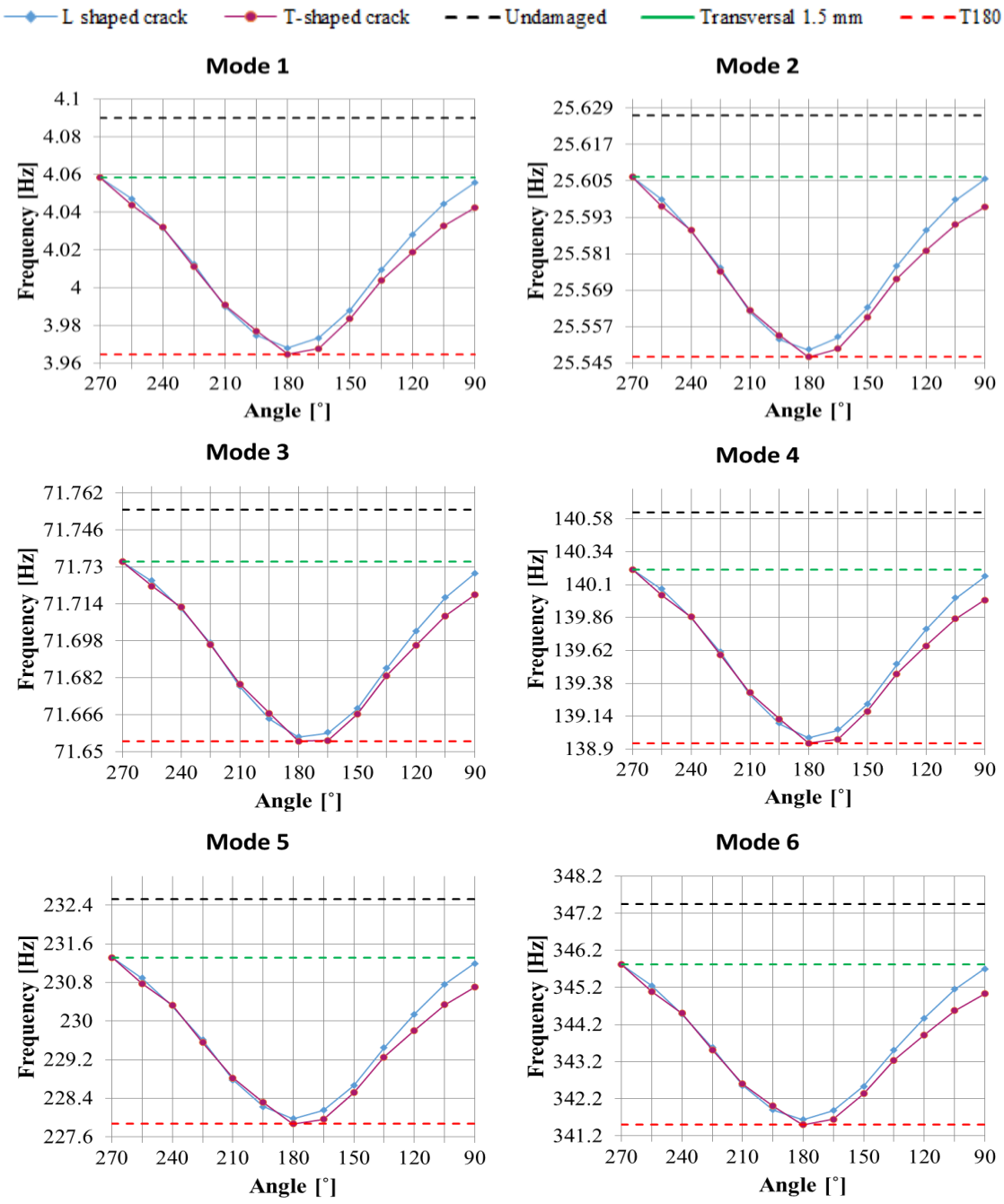

Figure 2.31. Frequency evolution with the crack branch rotation.

Table 2.13. Comparison of frequencies obtained directly from FEM and calculated involving the hybrid method for T-shaped crack

T_{90} analytical	T_{90} FEM	Percent diff.	T_{180} analytical	T_{180} FEM	Percent diff.
4.043	4.042	0.02%	3.97	3.96	0.08%
25.33	25.59	1.04%	24.86	25.5	0.03%
70.93	71.72	1.11%	69.61	71.65	0.03%
139.02	139.99	0.70%	136.42	138.94	0.02%
229.86	230.70	0.37%	225.57	227.86	0.01%
343.47	345.03	0.45%	337.08	341.49	0.01%

The differences presented in table 2.13, resulted by comparing the eigenfrequencies achieved analytical and with the help of FEM, are quite similar. In general, differences less than 1.2% were found, excepting the L180 crack, these are up to 2.85%.

2.7. Damage patterns

2.7.1. Relative frequency shifts (RFS)

In order to evaluate the results of FEM modal analyses, for the previous described damage cases, the term relative frequency shift (RFS) is introduced, defined with the relation contrived by our research group [49]:

$$RFS_i(x,a) = \Delta\bar{f}_i(x,a) = \frac{f_{iU} - f_{iD}(x,a)}{f_{iU}} \tag{2.4}$$

In the above relation, f_{iU} and f_{iD} represent the natural frequencies of mode i for the healthy beam and damaged beam case, respectively.

The normalized frequency shift for a transverse vibration mode is nominated Relative Frequency Shift (RFS). The RSF for the i-th vibration mode is calculated, with the mathematical relation (2.4).

The natural frequency shifts of beams due to damages constitute a reliable indicator, signalizing the appearance of damage and information about the position and severity.

The crack depth determines the damage severity, which is a parameter independent of the crack location; hence it controls the amplitude of the frequency shift curves. On the other hand,

the shape of these curves is controlled by the crack location and the vibration mode number. A crack with a given depth differently affects the natural frequency of a vibration mode if it is placed in different beam slices. Regarding the crack with defined depth and position, it differently affects the natural frequencies of different vibration modes. As described in papers [36] [96] [25], a sequence of RFS values derived for a specific crack can be used as a pattern to determine the damage signature.

2.7.2. L-shaped cracks RFS

In Figures 2.32 to 2.37, the Relative Frequency Shift curves plotted for the first six bending vibration modes for the damage cases L_{L10}, L_{R10}, L_{L30}, L_{R30}, L_{R50}, and L_{L50} are illustrated. Here, the frequency shifts for the crack location x=300 mm are highlighted with a red dotted line and the results are depicted.

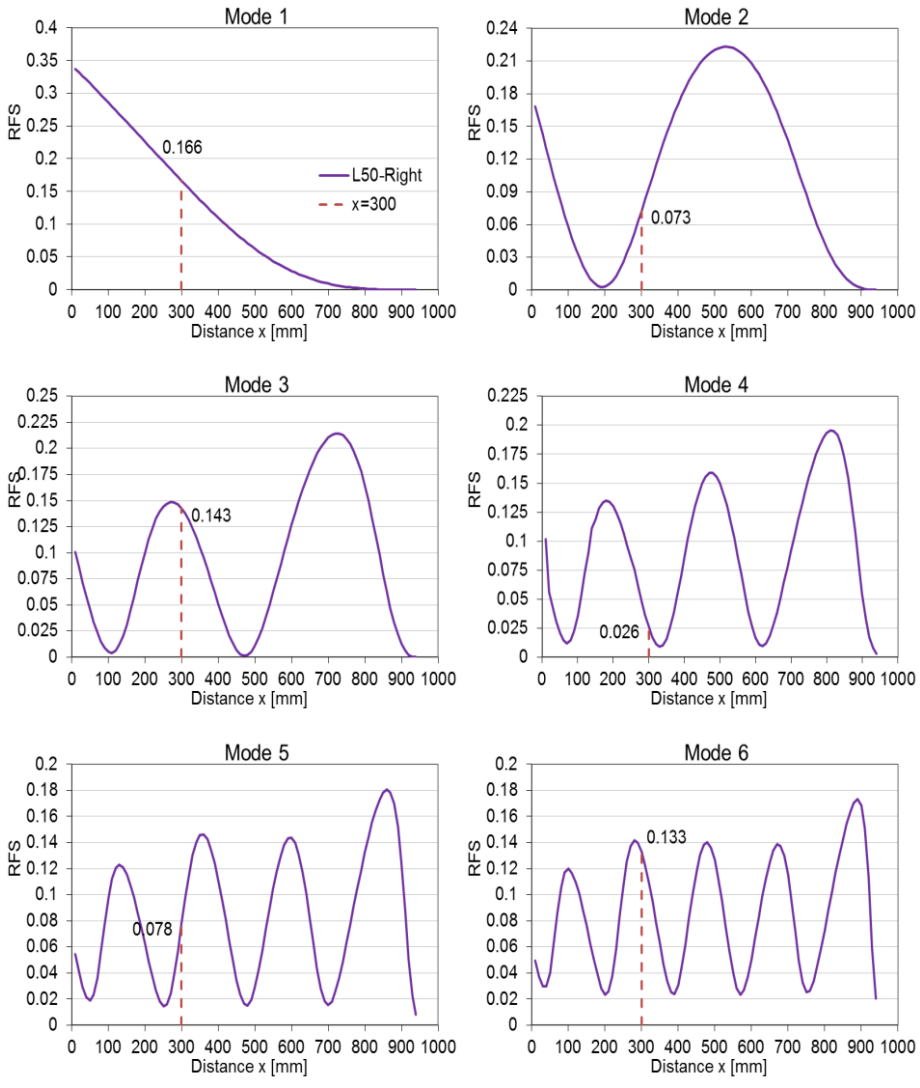

Figure 2.32. RFS curves for the first six vibration modes for damage case L_{R50}.

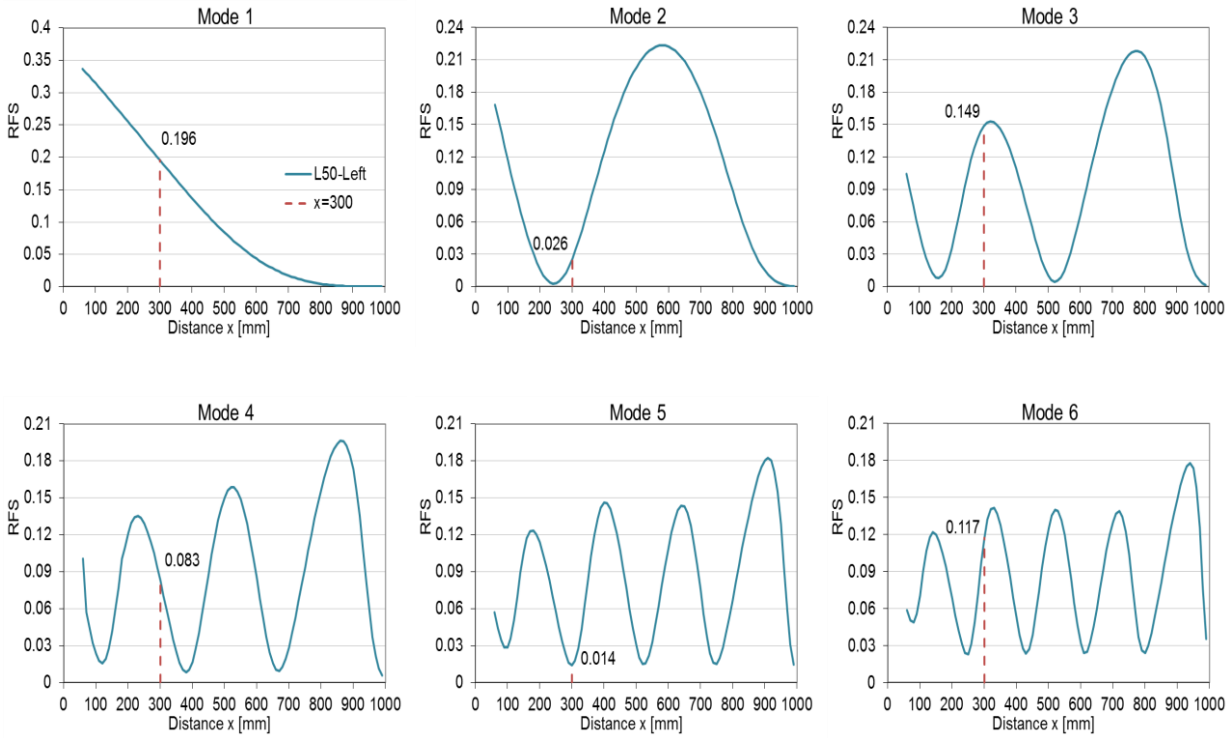

Figure 2.33. RFS curves for the first six vibration modes for damage case L_{L50}.

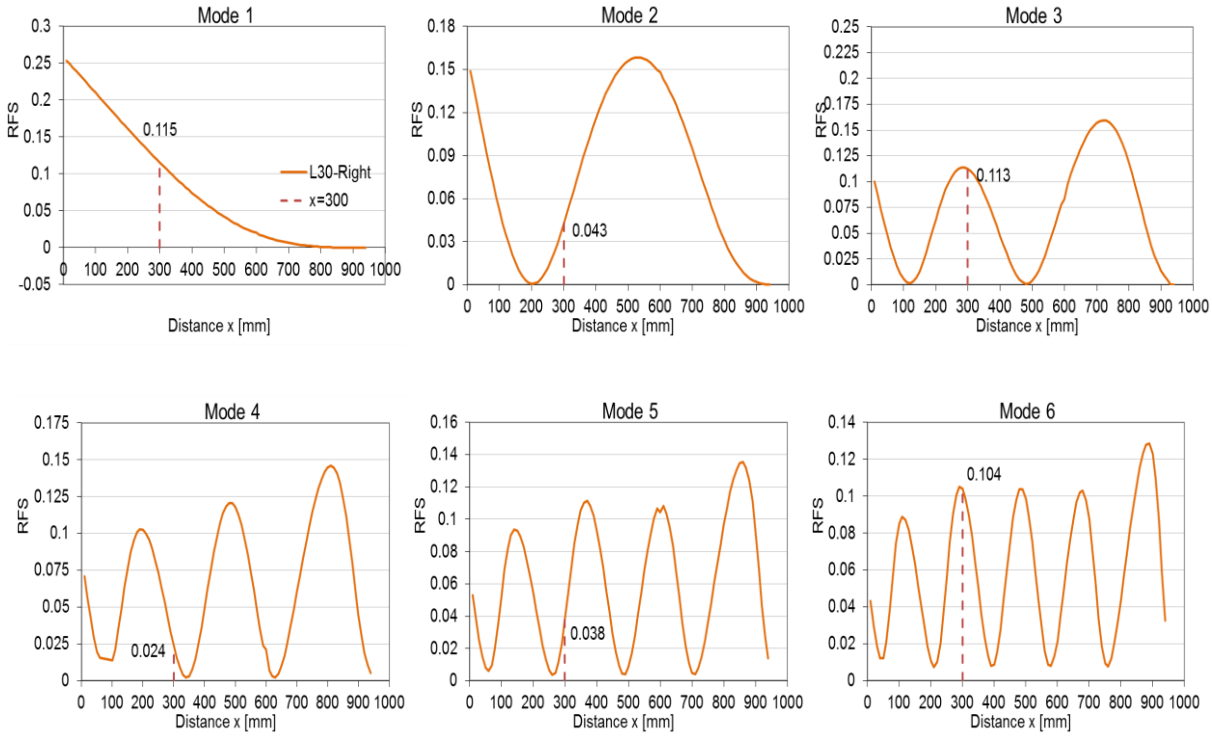

Figure 2.34. RFS curves for the first six vibration modes for damage case L_{R30}.

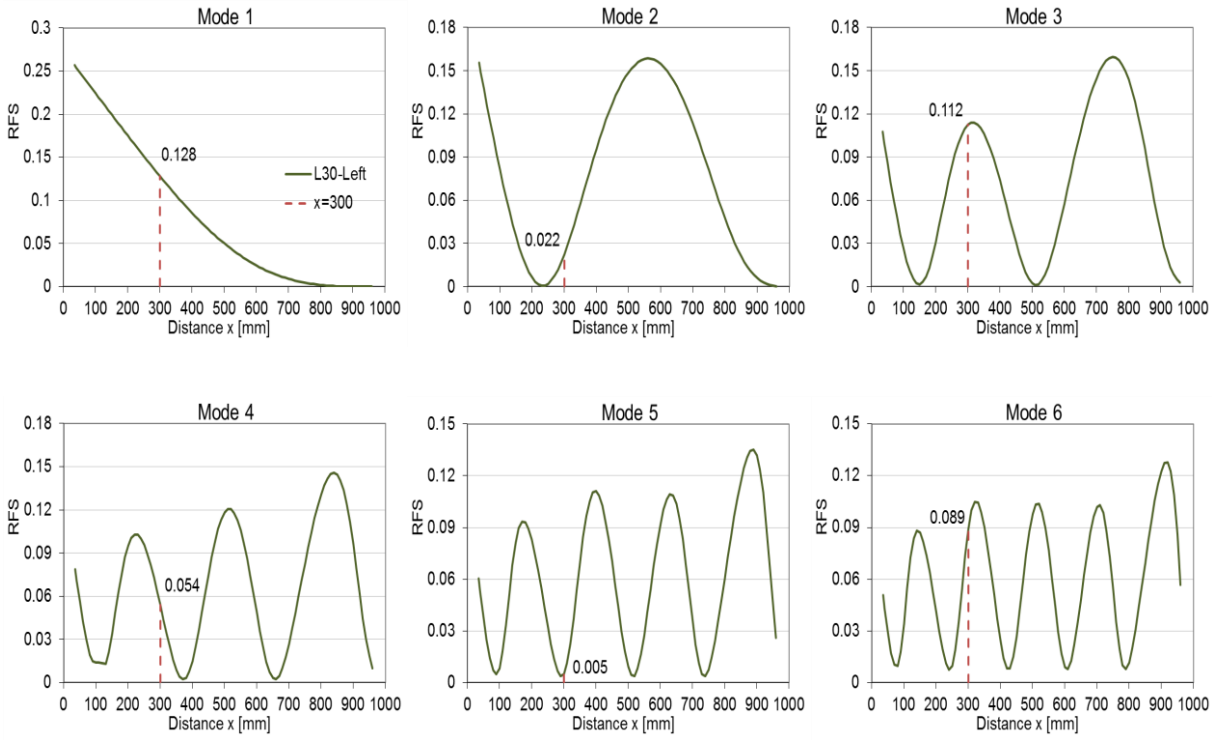

Figure 2.35. RFS curves for the first six vibration modes for damage case L_{L30}.

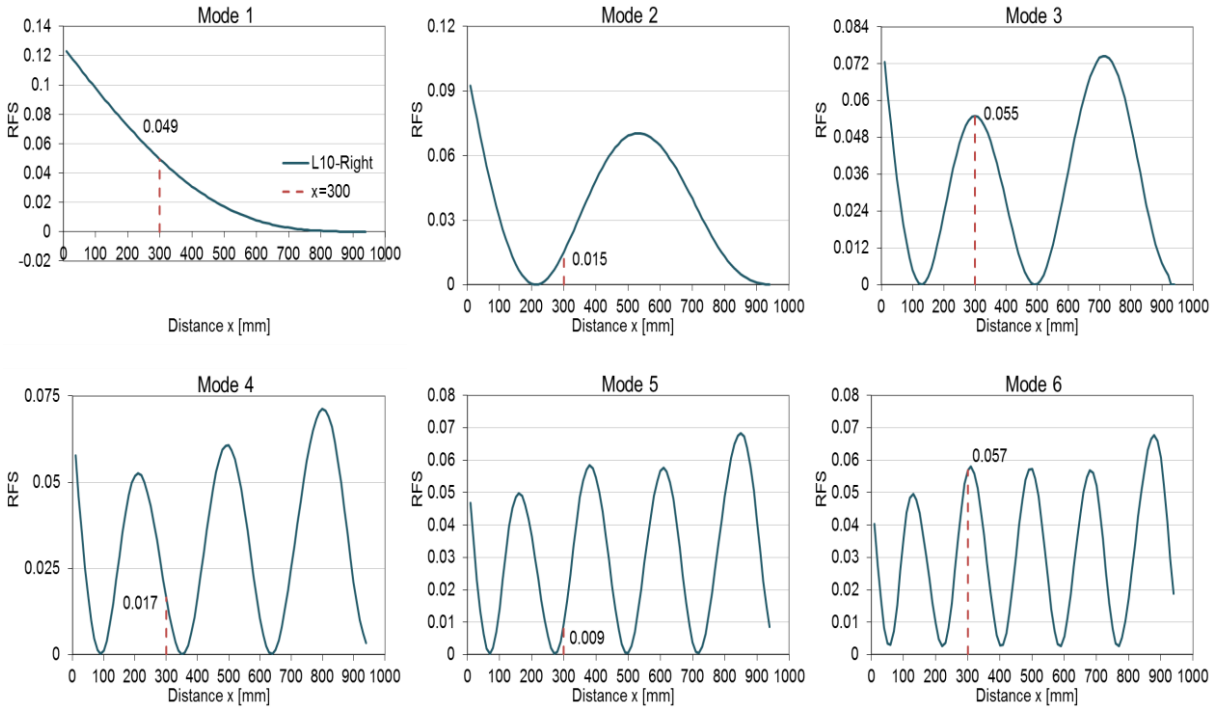

Figure 2.36. RFS curves for the first six vibration modes for damage case L_{R10}.

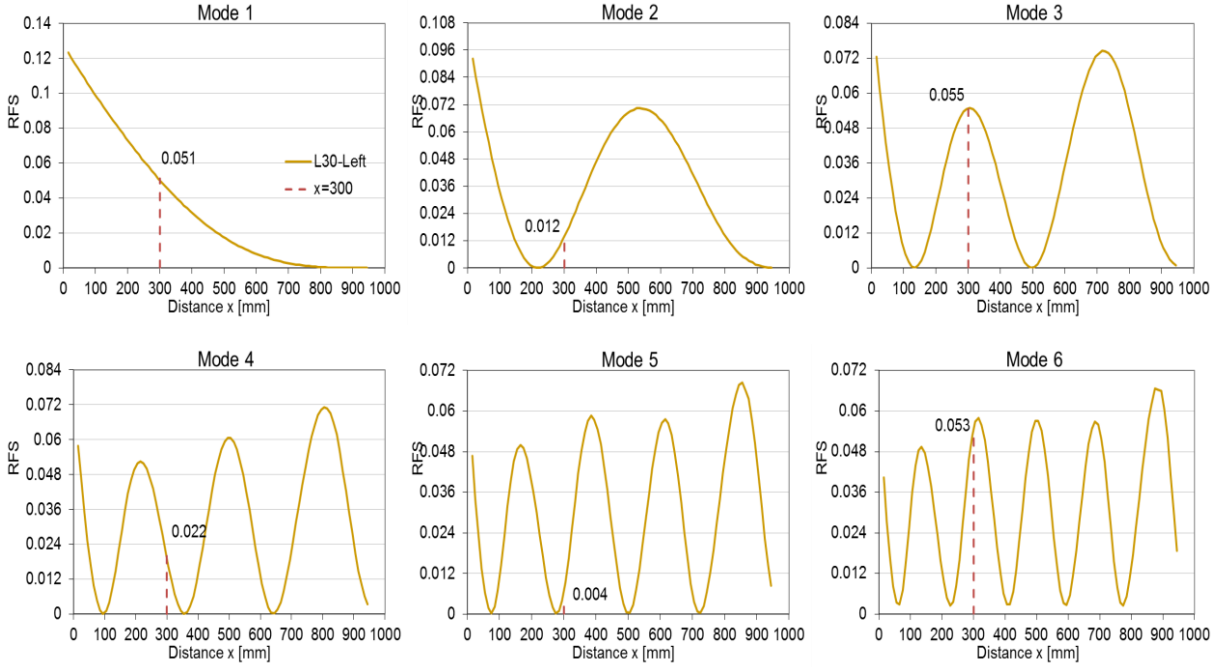

Figure 2.37. RFS curves for the first six vibration modes for damage case L_{L10}.

2.7.3. T-shaped cracks RFS

In Figures 2.39 to 2.41, Relative Frequency Shift curves plotted for the first six bending vibration modes for the damage cases T_{10}, T_{30}, and T_{50} are illustrated. Here, the frequency shifts for the crack location x=300 mm are highlighted with a red dotted line, and the results are depicted.

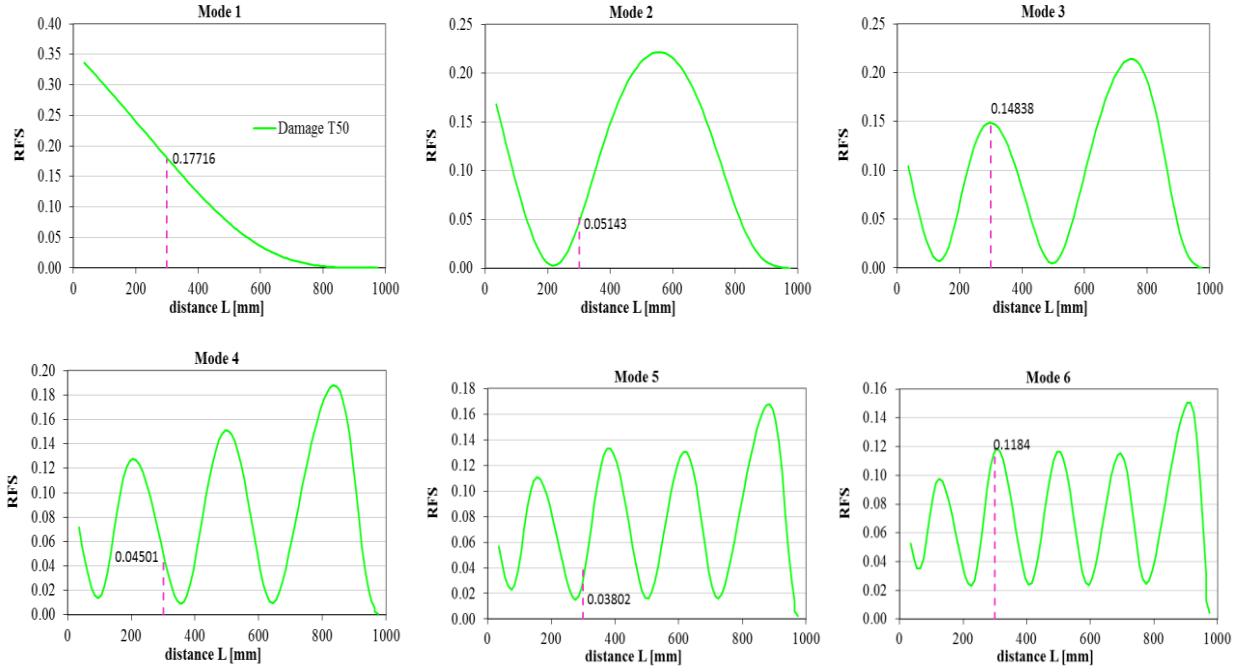

Figure 2.38. RFS curves for the first six vibration modes for damage case T_{50}.

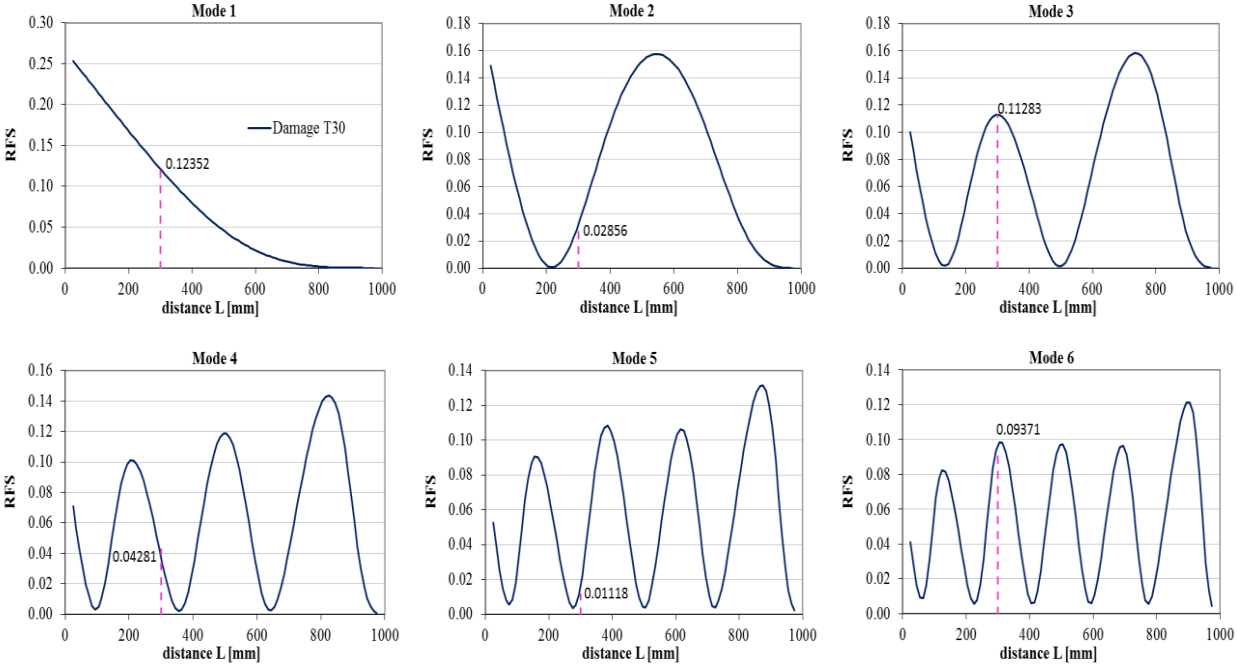

Figure 2.39. RFS curves for the first six vibration modes for damage case T30.

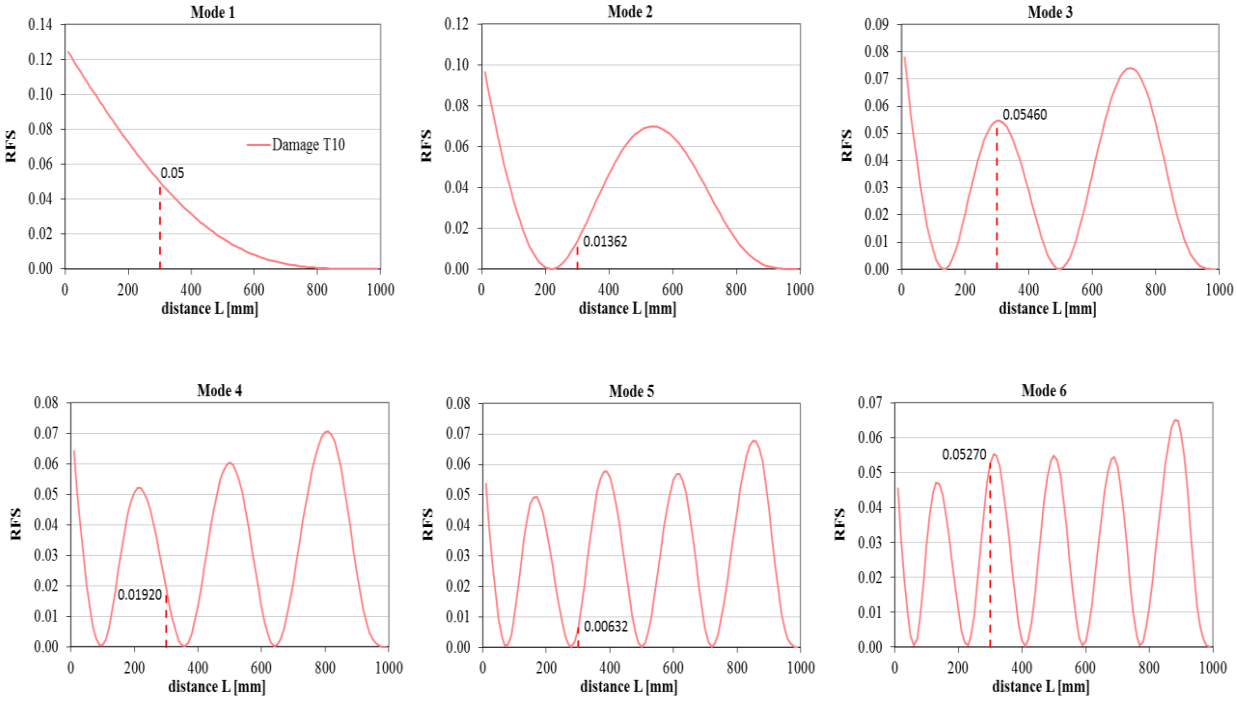

Figure 2.40. RFS curves for the first six vibration modes for damage case T_{10}.

Based on these values, the histograms representing the RFSs for x=300 mm are shown in Figure 2.41.

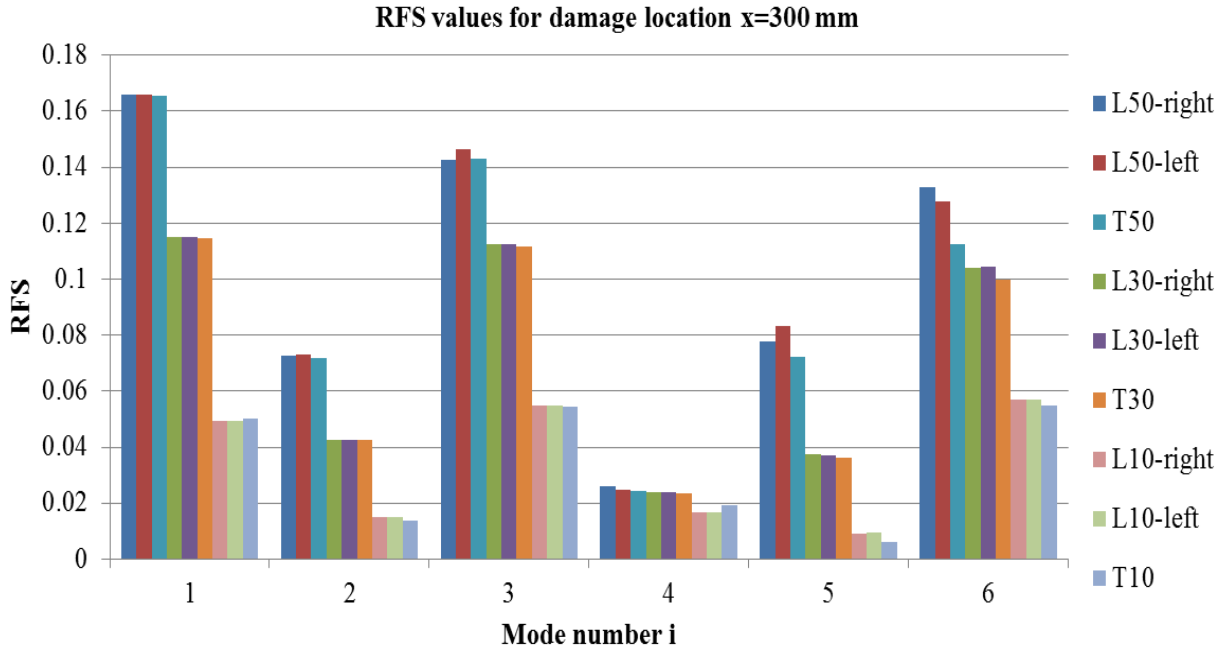

Figure 2.41. Histograms build for RFS values representing the cracks at location x = 300 mm

2.7.4. Y-shaped cracks RFS

The research is conducted by using the finite element method to describe the dynamic response of a structure affected by a transversal open crack followed by one or two branches, each oriented at different angles. These cracks are traditionally referred to as a Y-shaped crack. After calculating the relative frequency shifts for the first six transverse vibration modes and recorded the damage signature for the considered branched crack position. The damage signatures can be used as patterns in damage detection methods, converting the procedure of detecting the crack location and severity from the natural frequency drop in an inverse problem.

The RFS values are calculated, for the cases presented in Figures 2.29 and 2.30, meaning the beam having an L_R crack and a T-shaped crack with a rotating branch initially, for all positions of the rotated branch.

With the frequency values plotted in Figure 2.42, the evolution of the RFSs with the branch rotation α was depicted. The obtained values are used to plot Figure 43. The particular cases of L_R, respectively, T-shaped crack are explicitly presented in Tables 2.4 and 2.5. For comparison reason, in Figure 2.43, the RFS for a transversal crack of depth a=1.5 mm is also presented.

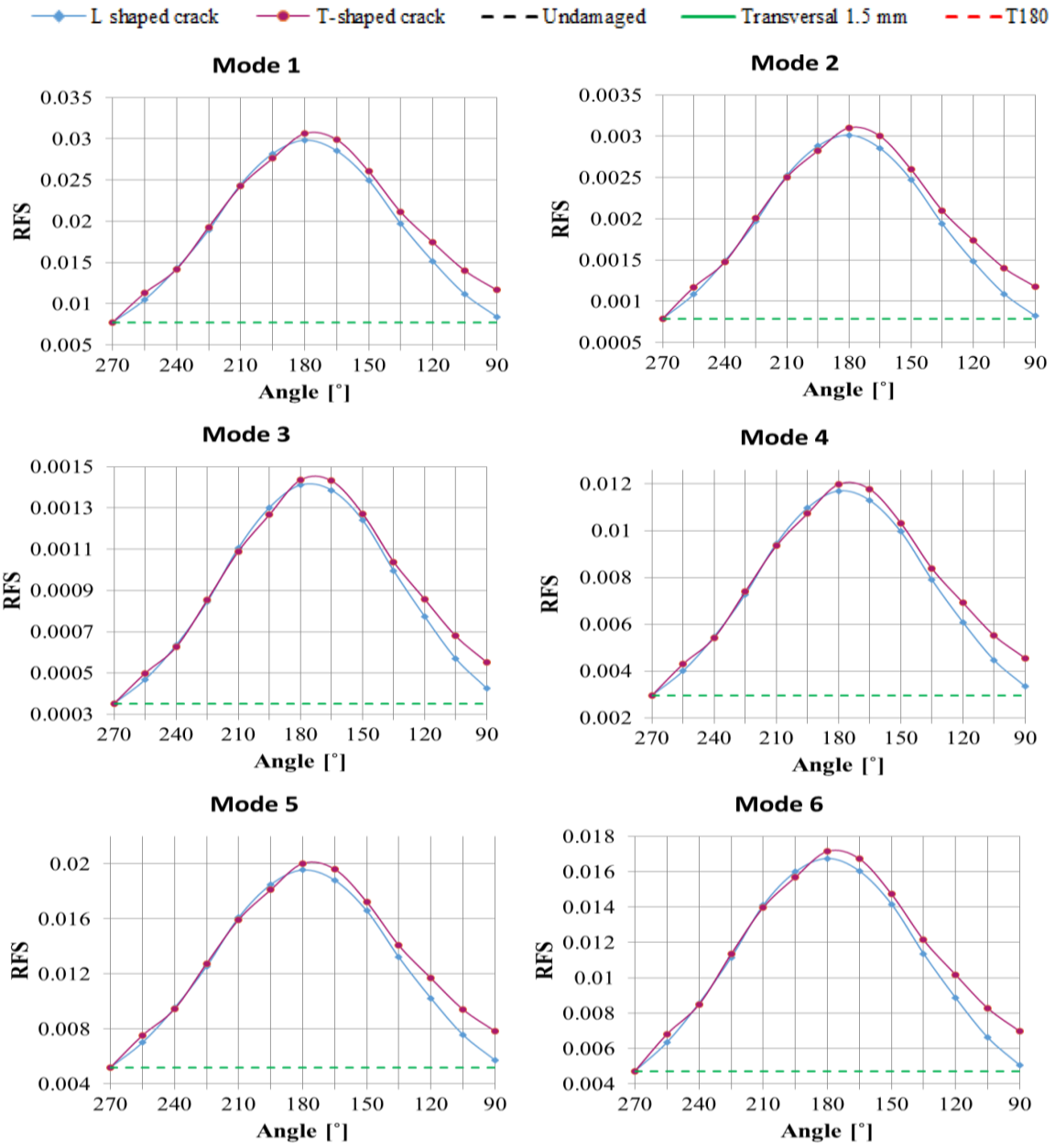

Figure 2.42. RFS evolution with the crack branch rotation.

2.8. Damage Location Coefficients (DLC)

The Damage Location Coefficients are calculated by dividing the values of the RFS for a given case to the biggest value in the series [25]. In general, the RFS for mode one always achieves the value one. This property makes finding the crack location independent of its severity estimation. If the crack position is found using DLCs, by dividing one of the RFS to the corresponding DLC, one obtains the damage severity. This should be preferably made for the biggest RFS, to avoid small numbers, which are most susceptible to introduce errors.

To have comparable values, it is convenient to work with normalized frequency values, which means that the frequency of the healthy beam for any mode is one.

For the L and T-shape cracks located at a distance from the fixed end x=300 mm, the values of the Relative Frequency Shifts from Figures 2.32 to 2.40 are normalized by dividing them to the highest value of every series, and the Damage Location Coefficients are obtained as shown in Figure 2.43.

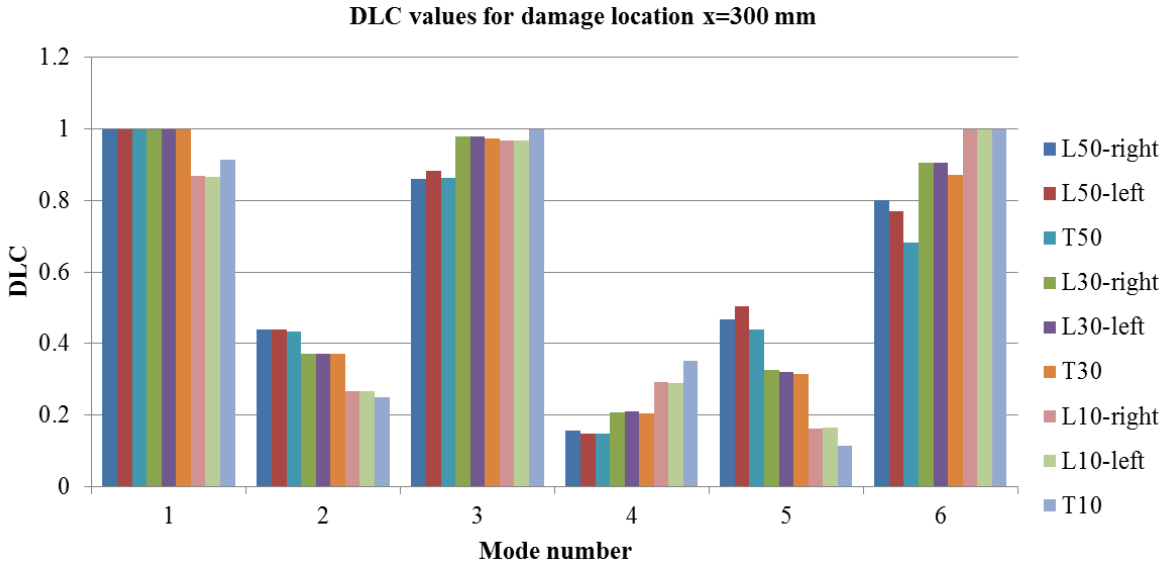

Figure 2.43. DLC for the beam having the cracks at distance x=300 mm.

In Figures 2.44 to 2.45 the DLC's from Figure 2.43 are plotted in pairs, for every delamination length.

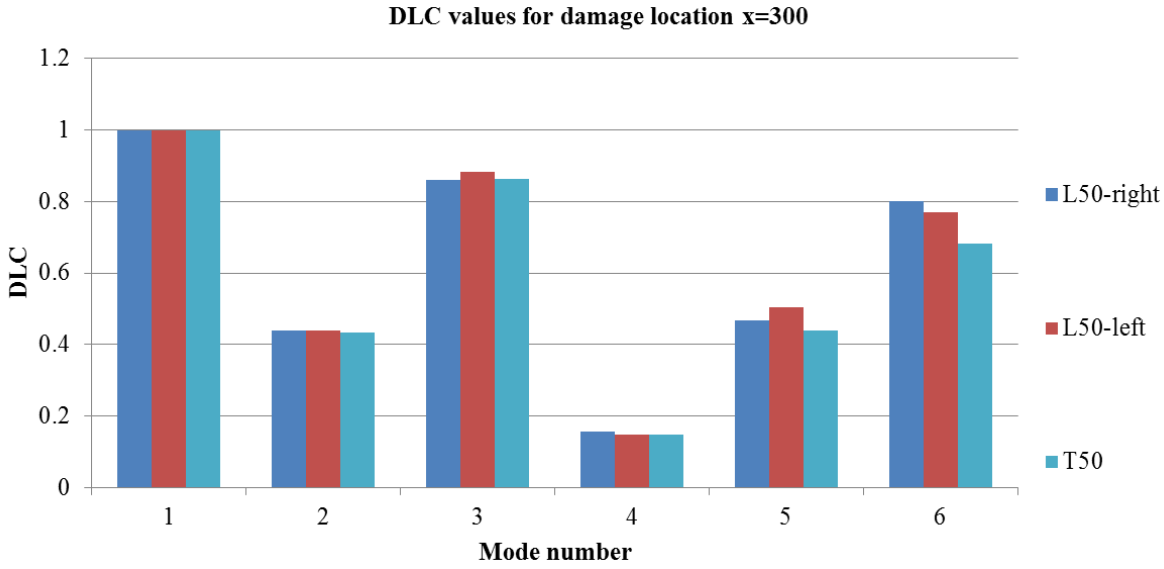

Figure 2.44. DLC for the beam having L_{R50}, L_{L50} and T_{50} crack at distance x=300 mm.

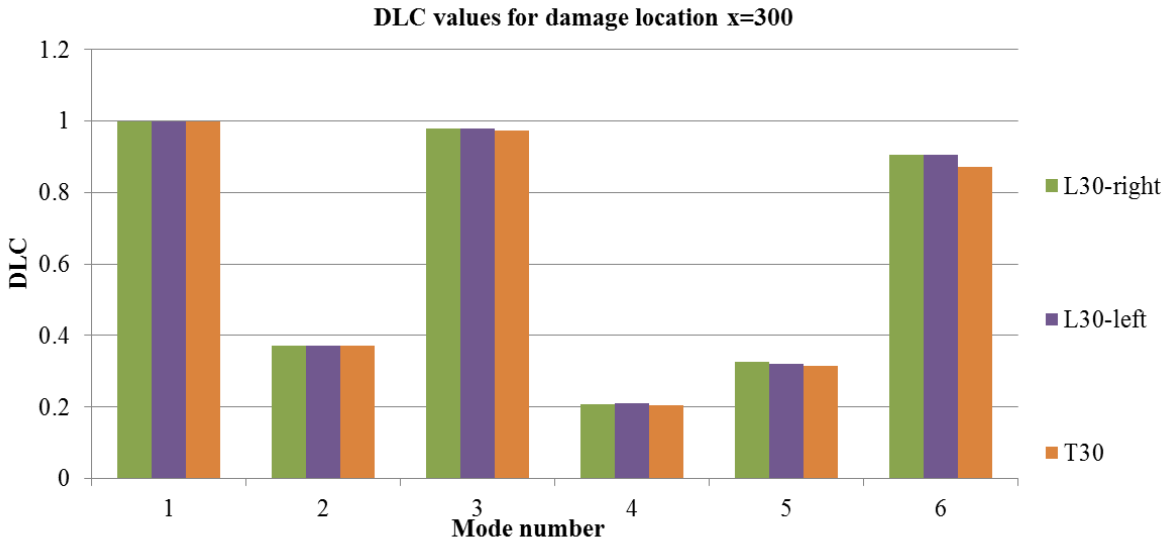

Figure 2.45. DLC for the beam having L_{R30}, L_{L30} and T_{30} crack at distance x=300 mm.

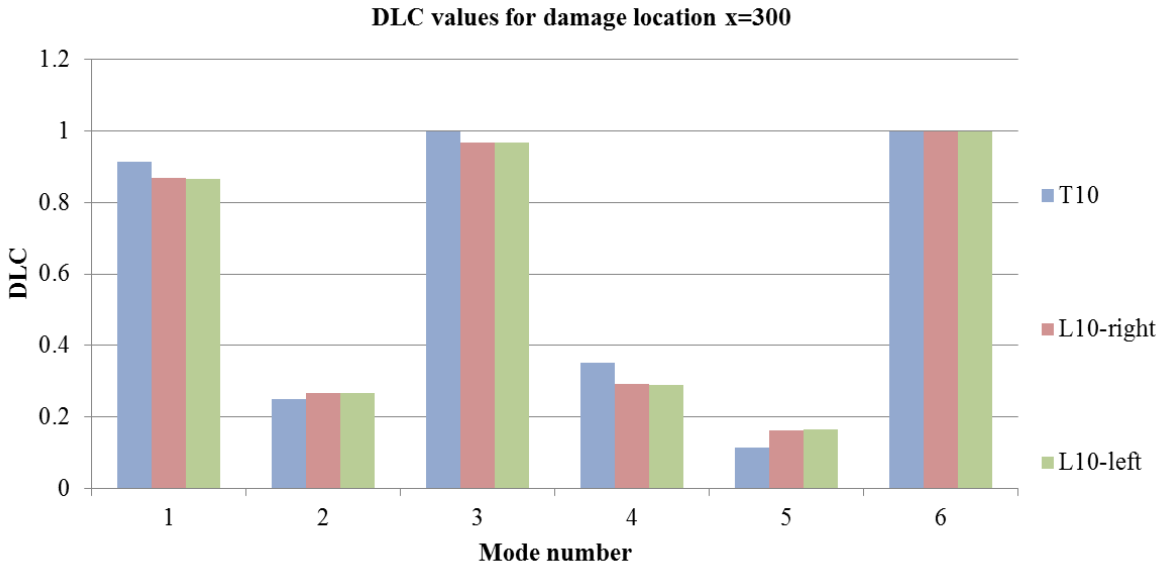

Figure 2.46. DLC for the beam having L_{R30}, L_{L30} and T_{30} crack at distance x=300 mm.

From Figures 2.46 it was concluded that the DLC's are quite similar irrespective to the transversal damage position and have pointed out the ability of patterns derived from simulations involving the FEM to indicate the damage position for any geometry and size of the L and T-shaped crack.

Considering now, the conclusion traced for the DLC values in Figures 2.44 to 2.46 one can conclude that the severity increases with the shifting of the transversal crack extent of the damage does not influence the damage pattern.

All these values can be found, so a database can be created for any imaginable damage scenarios. These are finally compared with the measurement results to locate the crack and quantify its dimensions [25].

The second aspect of this study is focused on finding if the DLC's for branched cracks oriented at different angles are similar, and how the severity is affected when the crack propagates in various directions. This is made by comparing the DLC's for the different values of the angle α for the damage scenarios presented in Figures 2.29 and 2.30.

Furthermore, the RFS's for the beam with an L_R crack were calculated, for all positions of the rotated branch, and represent the achieved values in Figure 2.42. One can observe that the pattern for this crack type does not change since the ratios between the RFS amplitudes are the same irrespective to the angle α. This is even better illustrated in Figure 2.47, where the Damage Location Coefficients are calculated by dividing the values of the RFS for a given case to the biggest value in the series [25]. The absolute amplitudes of the RFS depend on the branch orientation because different severities are obtained for different angles α. If the crack position is found from the DLCs, by dividing one of the RFSs to the corresponding DLC one obtains the damage severity. This should be preferably made for the biggest RFS, to avoid small numbers, which are most susceptible to introduce errors.

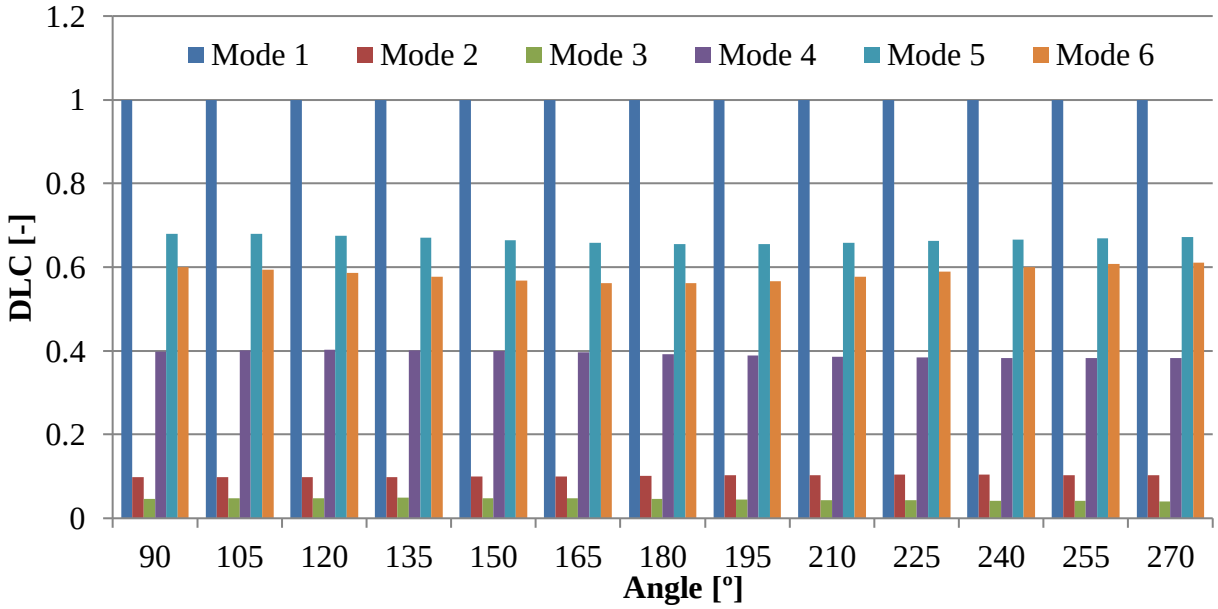

Figure 2.47. The Damage Location Coefficients for the beam with an L_R-shaped crack

Comparing Figure 2.47 with Figure 2.48 clearly results that the DLCs are similar, which shows that the DLCs are in connection with the damage location only.

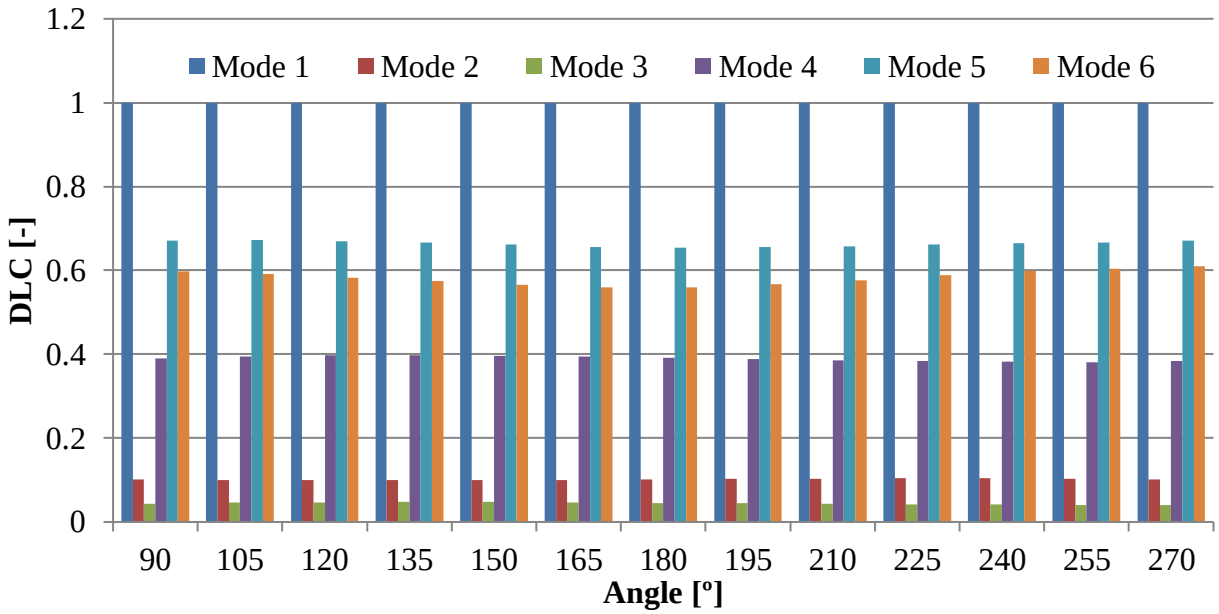

Figure 2.48.The Relative Frequency Shifts for the beam with a T-shaped crack.

The same comments as for the L-shaped crack are valid for the T-shaped crack too. Moreover, the DLC's are similar to that of a transverse crack. This is proved by the crack L_{180}, which is actually a transverse crack with depth $a+l = 3$ mm.

3. A NEW PREDICTIVE MODEL TO ESTIMATE THE FREQUENCIES FOR BEAMS WITH BRANCHED

3.1. Materials and methods

The current chapter aims to describe an algorithm developed, for calculating the natural frequencies of beams with reduced sections obtained by applying a stiffness reduction model. The results obtained show that by using the squared modal curvature and by taking into account the bending moments produced by the stiffness reduction, lead to a precise reading of the natural frequencies of beams with complex shaped damages.

The developed algorithm takes into account the severity of branched cracks with different depth of the transversal component and length of delamination based on the stiffness decay of the affected beam segment. Then, taking into consideration the supplementary slope at the delamination ends of the complex-shaped crack, correction coefficients we proposed in order to find an accurate model to predict the natural frequencies of cantilever beams having complex-shaped cracks with different depths and placed on different locations along the beam. The developed algorithm using the three features is embedded in a desktop software with the help of the Python programming language, and the depicted natural frequencies are compared with the values obtained by modal FEM simulations using the ANSYS software.

A linear elastic cantilever beam was considered, fixed at the left end, with its dimensions presented in Table 3.1 in reference to the notations presented in Figure 1.1.

Table 3.1. Beam dimensions

Length L [mm]	Width B [mm]	Thick. H [mm]
1000	20	5

The physical-mechanical properties of the material used are presented in Table 4.2.

Table 3.2. Physical-mechanical properties of the structural steel used

Area A [mm^2]	Moment of inertia $I_y=BH^3/12$ [mm^4]	Mass density ρ [kg/m^3]	Young modulus E [N/m^2]	Poisson ratio [-]	Tensile strength [MPa]	Yield strength [MPa]	Min. elongation [%]
125	520.0833	7850	$2\cdot10^{11}$	0.3	470-630	355	20

3.1.1. Theoretical background

Knowing that the relationship between a beam's deflection and the applied load is described by the Euler-Bernoulli equation: [105]

$$\frac{d^2}{dx^2}\left(EI\frac{d^2w}{dx^2}\right) = q \tag{3.1}$$

and by applying distributed pseudo inertial forces in respect to d'Alembert's principle, the motion of the beam can be described as:

$$q = -\ddot{w}\frac{dm}{dx} = -\rho A\ddot{w} \tag{3.2}$$

By equalizing equations 3.1 and 3.2 results in:

$$\frac{d^2}{dx^2}\left(EI\frac{d^2w}{dx^2}\right) = -\rho A\ddot{w} \tag{3.3}$$

For the particular case where the modulus of elasticity E and moment of inertia I_y are constant, the general solution becomes:

$$w(x,t) = \phi(x)T(t) \tag{3.4}$$

By substituting in 3.3:

$$\frac{d^2\phi}{dx^4}\left(\frac{\rho A}{EI_y}\omega^2\right)\phi = 0 \tag{3.5}$$

Where ω is the pulsation of the beam.

The general solution for the differential equation is [45]:

$$\phi(x) = A\sin(\alpha x) + B\cos(\alpha x) + C\sinh(\alpha x) + D\cosh(\alpha x) \tag{3.6}$$

The constants A, B, C, D are determined by applying the boundary conditions.

The coefficient α represents the dimensionless wave number and it is determined as:

$$\alpha = \sqrt[4]{\frac{\rho A}{EI_y}\omega^2} \tag{3.7}$$

The angle between the deformed neutral fiber and the undeformed beam's direction axis, for small deformations, can be described by the tangent of the angle with the deformed neutral fiber slope:

$$\theta(x) = \frac{d\phi}{dx} = \alpha[A\cos(\alpha x) - B\sin(\alpha x) + C\cosh(\alpha x) + D\sinh(\alpha x)] \quad (3.8)$$

The bending moment is expressed as:

$$M(x) = \frac{d^2\phi}{dx^2} = -EI_y\alpha^2[-A\sin(\alpha x) - B\cos(\alpha x) + C\sinh(\alpha x) + D\cosh(\alpha x)] \quad (3.9)$$

And the shear force is expressed:

$$T(x) = \frac{d^3\phi}{dx^3} = -EI_y\alpha^3[-A\cos(\alpha x) + B\sin(\alpha x) + C\cosh(\alpha x) + D\sinh(\alpha x)] \quad (3.10)$$

For the cantilever beam of length L, the boundary conditions are:

For the fixed end, rotation and deflection are zero:

$$\begin{cases} \phi(0) = 0 \\ \phi(0) = 0 \end{cases} \quad (3.11)$$

For the free end, shear force and bending moment are zero:

$$\begin{cases} \phi^{"}(L) = 0 \\ \phi^{"}(L) = 0 \end{cases} \quad (3.12)$$

By deriving equation 3.6 one obtains the following:

$$\phi'(x) = \alpha[A\cos(\alpha x) - B\sin(\alpha x) + C\cosh(\alpha x) + D\sinh(\alpha x) \quad (3.13)$$

$$\phi^{"}(x) = \alpha^2[-A\sin(\alpha x) - B\cos(\alpha x) + C\sinh(\alpha x) + D\cosh(\alpha x) \quad (3.14)$$

$$\phi'''(x) = \alpha^3[-A\cos(\alpha x) + B\sin(\alpha x) + C\cosh(\alpha x) + D\sinh(\alpha x) \quad (3.15)$$

By applying the boundary conditions from 3.11 and 3.12 from relations 3.6, 3.13-3.15 the following system results:

$$\begin{cases} \phi(0) = A\sin(0) + B\cos(0) + C\sinh(0) + D\cosh(0) = 0 \\ \phi'(0) = \alpha[A\cos(0) - B\sin(0) + C\cosh(0) + D\sinh(0) = 0 \\ \phi^{"}(x) = \alpha^2[-A\sin(\alpha L) - B\cos(\alpha L) + C\sinh(\alpha L) + D\cosh(\alpha L) = 0 \\ \phi'''(x) = \alpha^3[-A\cos(\alpha L) + B\sin(\alpha L) + C\cosh(\alpha L) + D\sinh(\alpha L) = 0 \end{cases} \quad (3.16)$$

It is noted:

$$\alpha * L = \lambda \quad (3.17)$$

By replacing with λ in the last two relations 3.16:

$$\begin{cases} \phi^{"}(x) = -A\sin\lambda - B\cos\lambda + A\sinh\lambda + B\cosh\lambda = 0 \\ \phi'''(x) = -A\cos\lambda + B\sin\lambda - A\cosh\lambda - B\sinh(\alpha x) = 0 \end{cases} \quad (3.18)$$

By multiplying the first relation from 3.16 with -1:

$$A = -B\frac{(\cos\lambda + \cosh\lambda)}{\sin\lambda + \sinh\lambda} \quad (3.19)$$

Thus, the modal shape is given by the function [2]:

$$\phi(x) = \cosh(\alpha x) - \cos(\alpha x) - \frac{\cos\lambda + \cosh\lambda}{\sin\lambda + \sinh\lambda}[\sinh(\alpha x) - \sin(\alpha x)] \quad (3.20)$$

By replacing relation 3.19 in the second equation from 3.18 the characteristic equation for the cantilever is obtained:

$$1 + \cos\lambda * \cosh\lambda = 0 \quad (3.21)$$

The dimensionless wave numbers for the first six modes of transversal vibration for the cantilever beam are presented in Table 3.3

Table 3.3. Dimensionless wave numbers for the cantilever

Mode *n*	**1**	**2**	**3**	**4**	**5**	**6**
λ	1,875104	4,694091	7,854757	10,99554	14,137168	17,278759

The pulsation is given by the relation:

$$\omega = \frac{\lambda_i^2}{L^2}\sqrt{\frac{EI_y}{\rho A}} \quad (3.22)$$

Knowing that:

$$\omega_i = 2\pi * f_i \quad (3.23)$$

The natural frequencies of the beam for any boundary condition is described as:

$$f_i = \frac{\lambda_i^2}{2\pi L^2}\sqrt{\frac{EI_y}{\rho A}} \quad (3.24)$$

The normalized modal shape is obtained by replacing the A, B, C, D coeff. in relation 3.6:

$$\bar{M}_i(x) = \bar{\phi}_i(x) = 0.5\left\{\frac{\cos\alpha_i L + \cosh\alpha_i L}{\sin\alpha_i L + \sinh\alpha_i L}\left[\sin(\alpha_i x) - \sinh(\alpha_i x)\right] - \cos(\alpha_i x) + \cosh(\alpha_i x)\right\} \quad (3.25)$$

3.1.2. Stiffness decrease method

Here, a method for determining the effect of the stiffness degradation on the natural frequencies of beams is presented. The first step is to consider a model with decreased stiffness, as illustrated in Figure 3.1. The current method intends to predict the impact of the stiffness variation on the natural frequencies of the cantilever beam.

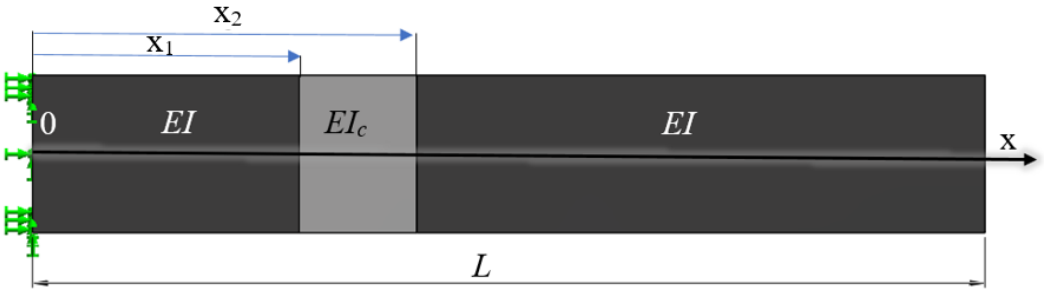

Figure 3.1. The reduced section model.

The strain energy is expressed with the well-known relation [45]:

$$U_i^{0-L} = \frac{M_{\max}^2}{2EI}\int_0^L \left[\bar{M}_i(x)\right]^2 dx \tag{3.26}$$

where A is the magnitude of the bending moment.

Let us denote the integral in Eq. (3.26) as the strain energy coefficient. It is calculated, for the whole intact beam and for all vibration modes, as [45]:

$$\varsigma_i^{0-L} = \int_0^L \left[\bar{\phi}_i''(x)\right]^2 dx = 0.25 \tag{3.27}$$

For a segment x_1-x_2, the stiffness decrease coefficient becomes:

$$\varsigma_i^{x_1-x_2} = \int_{x_1}^{x_2} \left[\bar{\phi}_i''(x)\right]^2 dx \tag{3.28}$$

Let us consider the rigidity of the damaged segment x_1-x_2 of the beam to be EI_C. Between the bending moment $M_{Ci}(x)$ acting on the damaged beam that produces the same effect (deflection) as the real moment $M_i(x)$ on the intact beam is [45]:

$$\bar{M}_{Ci}(x) = \frac{I_C}{I}\bar{M}_i(x) \tag{3.29}$$

The energy stored in the intact beam is [2]:

$$U_i^{0-L} = \frac{M_{\max}^2}{2EI}\int_0^{x_1}\left[\bar{M}_i(x)\right]^2 dx + \frac{M_{\max}^2}{2EI}\int_{x_1}^{x_2}\left[\bar{M}_i(x)\right]^2 dx + \frac{M_{\max}^2}{2EI}\int_{x_2}^{L}\left[\bar{M}_i(x)\right]^2 dx \tag{3.30}$$

while the energy stored in the damaged beam, calculated considering Eq. (3.29), which is obviously lower, is [45]:

$$U_{Ci}^{0-L} = \frac{M_{\max}^2}{2EI}\int_0^{x_1}\left[\bar{M}_i(x)\right]^2 dx + \frac{M_{\max}^2}{2EI}\frac{I_C}{I}\int_{x_1}^{x_2}\left[\bar{M}_i(x)\right]^2 dx + \frac{M_{\max}^2}{2EI}\int_{x2}^{L}\left[\bar{M}_i(x)\right]^2 dx \tag{3.31}$$

It is known that the natural frequency for a vibration mode is proportional with the energy stored in the beam in that mode ($f_i \approx U_i^{0.5}$). In consequence:

$$\frac{f_{Ci}}{f_i} = \left(\frac{U_{Ci}^{0-L}}{U_i^{0-L}}\right)^{0.5} \tag{3.32}$$

It is observed that, if substituting Eq. (3.30) and (3.31) in Eq. (3.32), is possible to reduce the term $A^2/2E\mathrm{I}$ and the frequency for the damaged beam can be calculated involving the frequency of the intact beam f_i, the ratio between the moments of inertia for the two cross-sections I and I_C, and the strain energy coefficients ς_i for the different beam segments. Hence, the frequency for the damaged beam becomes [45]:

$$f_{Ci} = f_i\left(\frac{\varsigma_i^{0-x_1} + \frac{I_C}{I}\varsigma_i^{x_1-x_2} + \varsigma_i^{x_2-L}}{\varsigma_i^{0-L}}\right)^{0.5} = c_i^{x_1-x_2}\cdot f_i \tag{3.33}$$

and can be calculated known the beam parameters and the crack shape and position.

The coefficients ς_i are calculated with Eq. (3.21). An example of strain energy distribution in mode 3 for the intact beam and the damaged beam is given in Figure 3.2.

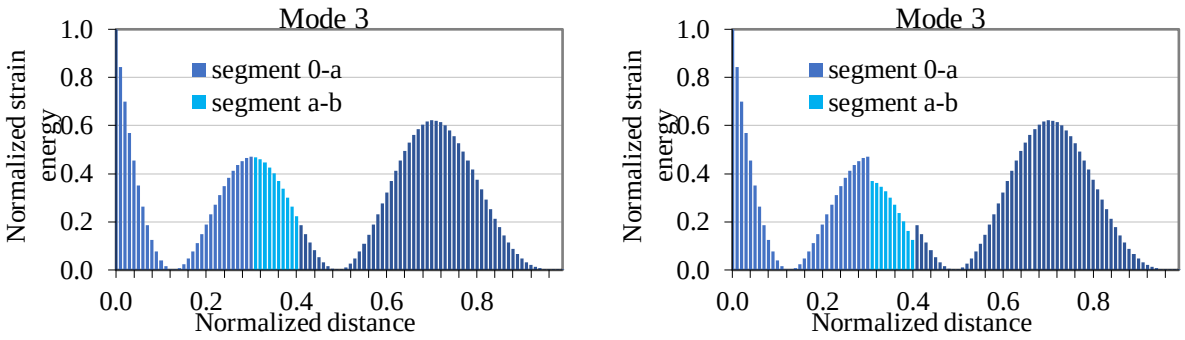

Figure 3.2. Strain energy distribution for the intact beam (a) and the damaged beam (b).

In order to test the reliability of the stiffness reduction method the results obtained by calculus are compared with the natural frequencies obtained through FEM simulations for a cantilever beam, with its dimensions described in Figure 3.1 and Table 3.1, having a T-shaped crack with

different depths *a* and on different positions along the beam. The crack shape and dimensions are presented in Table 3.4:

Table 3.4. The T-shaped crack dimensions and geometry

Crack shape		Crack length		Crack depth	Crack angle		Crack geometry
		L_L [mm]	L_R [mm]	*a* [mm]	α	β	
d	T_{50}	25	25	0.2 to 1.2	90	90	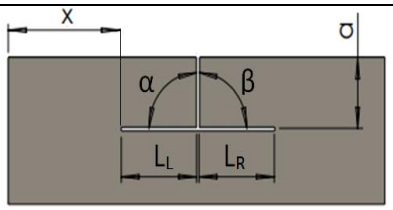

The first step was to determine the stiffness decrease coefficients for the reduced section, meaning the damage intervals and depth. The stiffness reduction coefficients and ratio between the moments of inertia for the two cross-sections *I* and I_C have been depicted, for the first five modes of transversal vibration, and the natural frequencies of the damaged cantilever have been calculated. In order to demonstrate the precision of the developed method, modal simulations were made using FEM for the same damage scenario and compared to the results obtained with the developed stiffness reduction method. The comparison between the results obtained by applying the developed method and the ones obtained by means of FEM for the described T-shape crack having depths of *a*=0.2, 0.6, and 1 mm positioned at *x*=250 mm, meaning the damage extremities x_1-x_2=250-300, are shown in Tables 3.5 to 3.7.

Furthermore, the comparison between the results obtained for the same scenario, but with the crack positioned at *x*=350mm, meaning the damage extremities x_1-x_2=350-400, are shown in Tables 3.7 to 3.9.

Table 3.5. Cantilever beam with T-shape crack of depth a=0.2 and extremities x_1-x_2=250-300

$F_{i\text{-}U}$ FEM	$F_{i\text{-}D}$ FEM	Area [-]			Reduction coefficient	$F_{i\text{-}D}$ [Hz]	Error [%]
[Hz]	[Hz]	$0 - x_1$	$x_1 - x_2$	$x_2 - L$	$c_i^{x_1-x_2}$	calculus using area	calculus vs. FEM
4.0812	4.06058	0.174	0.018	0.056	0.9970	4.0689	-0.21%
25.573	25.5602	0.070	0.003	0.177	0.9994	25.5576	0.01%
71.595	71.2565	0.059	0.018	0.171	0.9970	71.3798	-0.17%
140.27	139.7737	0.072	0.013	0.164	0.9976	139.9329	-0.11%
231.81	231.7524	0.068	0.001	0.181	0.9998	231.7636	0.00%

Table 3.6. Cantilever beam with T-shape crack of depth a=0.6 and extremities x_1-x_2=250-300

$F_{i\text{-}U}$ FEM	$F_{i\text{-}D}$ FEM	Area [-]			Reduction coefficient	$F_{i\text{-}D}$ [Hz]	Error [%]
[Hz]	[Hz]	$0 - x_1$	$x_1 - x_2$	$x_2 - L$	$c_i^{x_1-x_2}$	calculus using area	calculus vs. FEM
4.0812	4.0074	0.174	0.018	0.056	0.9911	4.0451	-0.94%
25.573	25.5146	0.070	0.003	0.177	0.9985	25.5371	-0.09%
71.595	70.3490	0.059	0.018	0.171	0.9909	70.9477	-0.85%
140.27	138.5761	0.072	0.013	0.164	0.9935	139.3693	-0.57%
231.81	231.5782	0.068	0.001	0.181	0.9995	231.7172	-0.06%

Table 3.7. Cantilever beam with T-shape crack of depth a=1 and extremities x_1-x_2=250-300

$F_{i\text{-}U}$ FEM	$F_{i\text{-}D}$ FEM	Area [-]			Reduction coefficient	$F_{i\text{-}D}$ [Hz]	Error [%]
[Hz]	[Hz]	$0 - x_1$	$x_1 - x_2$	$x_2 - L$	$c_i^{x_1-x_2}$	calculus using area	calculus vs. FEM
4.0812	3.9338	0.174	0.018	0.056	0.9859	4.0236	-2.28%
25.573	25.4511	0.070	0.003	0.177	0.9980	25.5218	-0.28%
71.595	69.1532	0.059	0.018	0.171	0.9857	70.5710	-2.05%
140.27	137.0856	0.072	0.013	0.164	0.9897	138.8318	-1.27%
231.81	231.3228	0.068	0.001	0.181	0.9992	231.6244	-0.13%

Table 3.8. Cantilever beam with T-shape crack of depth a=0.2 and extremities x_1-x_2=350-400

$F_{i\text{-}U}$ FEM	$F_{i\text{-}D}$ FEM	Area [-]			Reduction coefficient	$F_{i\text{-}D}$ [Hz]	Error [%]
[Hz]	[Hz]	$0 - x_1$	$x_1 - x_2$	$x_2 - L$	$c_i^{x_1-x_2}$	calculus using area	calculus vs. FEM
4.0812	4.0684	0.209	0.011	0.029	0.9981	4.0738	-0.13%
25.573	25.4884	0.081	0.013	0.155	0.9975	25.5115	-0.09%
71.595	71.3299	0.099	0.014	0.135	0.9975	71.4229	-0.13%
140.27	140.2145	0.089	0.001	0.159	0.9997	140.2419	-0.02%
231.81	230.2068	0.079	0.021	0.147	0.9964	230.974	-0.33%

Table 3.9. Cantilever beam with T-shape crack of depth a=0.6 and extremities x_1-x_2=350-400

$F_{i\text{-}U}$ FEM	$F_{i\text{-}D}$ FEM	Area [-]			Reduction coefficient	$F_{i\text{-}D}$ [Hz]	Error [%]
[Hz]	[Hz]	$0 - x_1$	$x_1 - x_2$	$x_2 - L$	$c_i^{x_1-x_2}$	calculus using area	calculus vs. FEM
4.0812	4.0350	0.209	0.009	0.029	0.9946	4.0591	-0.60%
25.573	25.2502	0.081	0.011	0.155	0.9934	25.4036	-0.61%
71.595	70.6292	0.100	0.012	0.135	0.9930	71.0920	-0.66%
140.27	140.0681	0.089	0.001	0.160	0.9994	140.1858	-0.08%
231.81	227.0758	0.079	0.018	0.147	0.9893	229.3396	-1.00%

Table 3.10. Cantilever beam with T-shape crack of depth a=1 and extremities x_1-x_2=350-400

$F_{i\text{-}U}$ FEM	$F_{i\text{-}D}$ FEM	Area [-]			Reduction coefficient	$F_{i\text{-}D}$ [Hz]	Error [%]
[Hz]	[Hz]	$0 - x_1$	$x_1 - x_2$	$x_2 - L$	$c_i^{x_1 - x_2}$	calculus using area	calculus vs. FEM
4.0812	3.9875	0.209	0.009	0.029	0.9913	4.0459	-1.47%
25.573	24.9250	0.081	0.011	0.155	0.9895	25.3056	-1.53%
71.595	69.7145	0.100	0.012	0.135	0.9889	70.8030	-1.56%
140.27	139.8548	0.089	0.001	0.160	0.9988	140.1015	-0.18%
231.81	222.9220	0.079	0.018	0.147	0.9830	227.8823	-2.23%

The percent differences between the developed analytical model and FEM simulations for the case where the crack is positioned at x=250 mm are shown in Tables 3.4 to 3.6. It was observed that the maximum error obtained is 2.05% for the crack having a depth of a=1 mm. As the crack has a smaller depth, one can observe that the error is decreased.

From the last three tables, it was observed that the maximum error obtained is 2.23% for the crack having a depth of a=1 mm. As the crack has a smaller depth, one can observe that the error is decreasing.

Judging from the results found, the error increases as the crack depth is increased, leading us to the conclusion that the developed algorithm should take into account the severity of the transversal component and the supplementary slope at the delamination ends of the complex-shaped crack.

3.1.3. Precision enhancement of the defined algorithm

In the current thesis a more accurate model is presented, in order to predict the natural frequencies of beams having complex-shaped cracks with different depths and placed on different location along the beam.

Firstly, our research team developed a simple algorithm for determining the severity $\gamma(a)$ for different transversal crack depths a, that consider only the undamaged and damaged beam deflections. Following mathematical relation applies [4]:

$$\gamma(0,a) = \frac{\sqrt{\delta_D(0,a)} - \sqrt{\delta_U}}{\sqrt{\delta_D(0,a)}} \tag{3.34}$$

In the above equation δ_U is the beam's free-end deflection under dead mass and $\delta_D(0,a)$ is the same deflection for the beam having a crack with depth a at the fastened end, i.e. $x=0$. Hence, from equation Eq. (3.34) results the relation of the pseudo-severity:

$$\gamma(x,a)=\frac{\sqrt{\delta_D(x,a)}-\sqrt{\delta_U}}{\sqrt{\delta_D(x,a)}} \tag{3.35}$$

The frequencies $f_i(x,a)$, which is calculated with equation:

$$f_{Ci}(x,a)=f_i\left\{1-\gamma(0,a)\left[\bar{\phi}_i''(x)\right]^2\right\} \tag{3.36}$$

It was illustrated in Figure 3.4 that the natural frequency of the first four transversal vibration modes for the healthy cantilever beam (dotted line) and the evolution of the frequency for the beam having a crack with depth $a=1$ mm which is replaced along the beam (blue continuous line).

The obtained frequencies are in good agreement with those obtained by simulation. An exception is found for the crack located at the fastened end $x=0$. Here, the frequency derived with both methods, analytically and by simulation, does not fit the trend depicted by the blue line but is significantly bigger as expected. However, the values, represented with a violet square in Figure 3.3, are very similar.

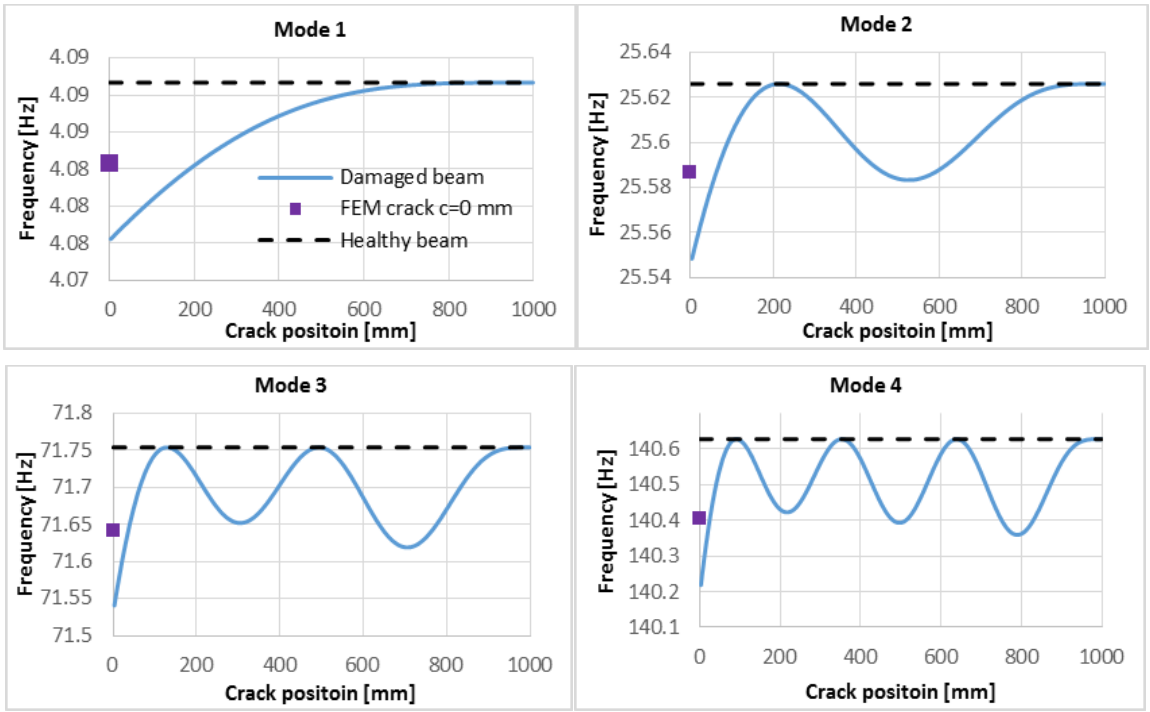

Figure 3.3. Natural frequencies evolution with the damage location, compared with the frequencies of the healthy beam and the frequency drop due to the crack located at the fixed end

Figure 3.4 illustrates the stress distribution around the cracks located at several locations near the fastened end.

For the crack positioned at the fixed end, just the beam segment to the right of the crack achieves bending, so that the frequency drop caused by the crack is smaller as those obtained for other locations in the area of the fixed end. This causes a lower deflection and frequency drop, even if theoretically the highest values of these features should be obtained.

This finding motivated us to obtain the frequencies for the locations where the effect of the boundary does not affect the normal beam behavior and to estimate the frequency at the fixed end from the achieved trend-line. To plot the trend-line and find the mathematical relation, a linear regression curve was used [44].

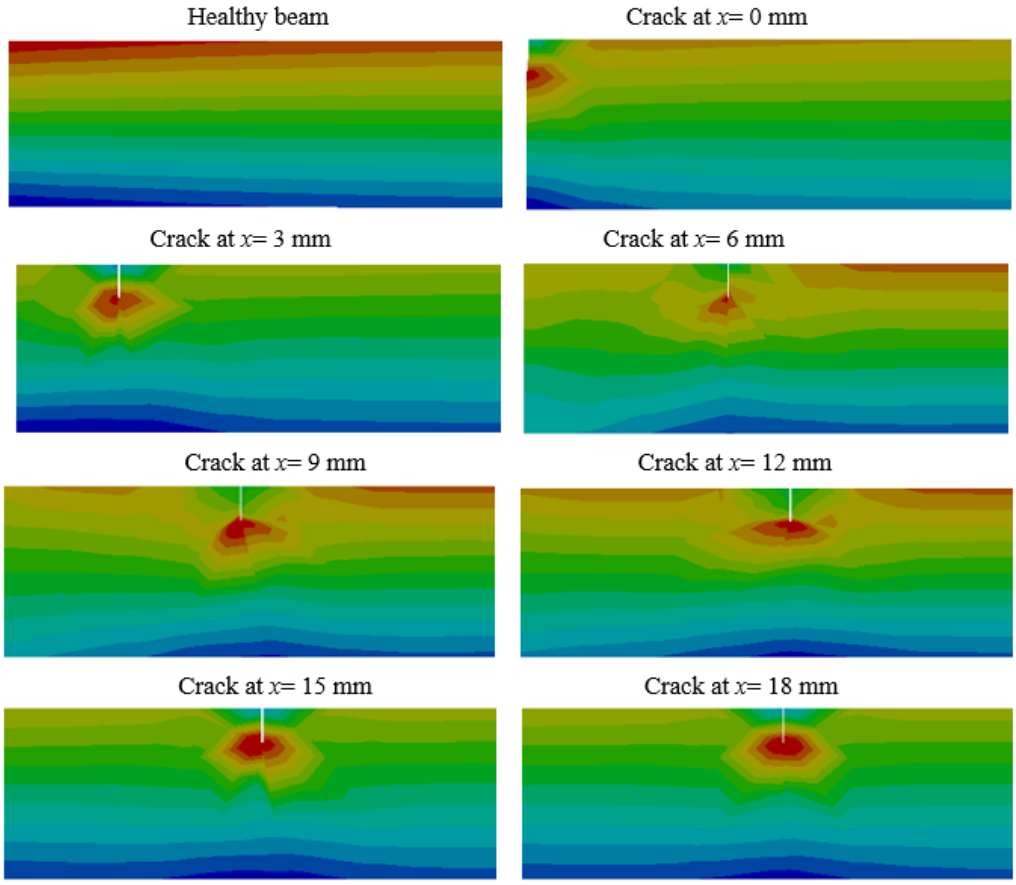

Figure 3.4. Eigenfrequency evolution with the damage location

As demonstrated, if too close to the fixed end, the crack determines deflections and frequencies that do not follow the analytical solutions. For this reason, for calculating the beam deflection in damaged state the location of the crack at $x=6$ mm from the fixed end was considered, and removed by a step of $s=2$ mm until it reaches $x=18$ mm from the fixed end as illustrated in Figure 3.5.

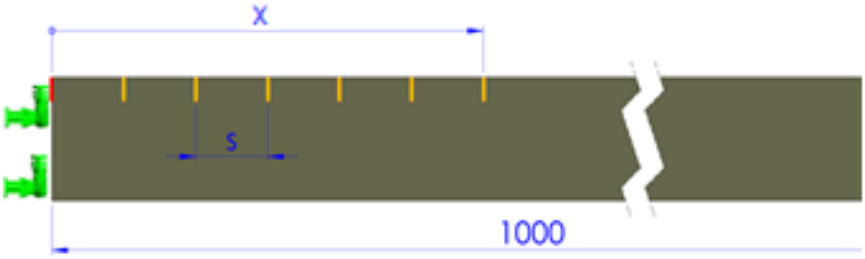

Figure 3.5. The beam with transversal crack replaced with a step *s*

The deflection is estimated from the regression curve plotted on the achieved points [23], which are given in Figure 3.6 for the cracks with depth *a= 0.2* mm and *a=1.2* mm. In these figures, the mathematical relation for the regression curve is also shown.

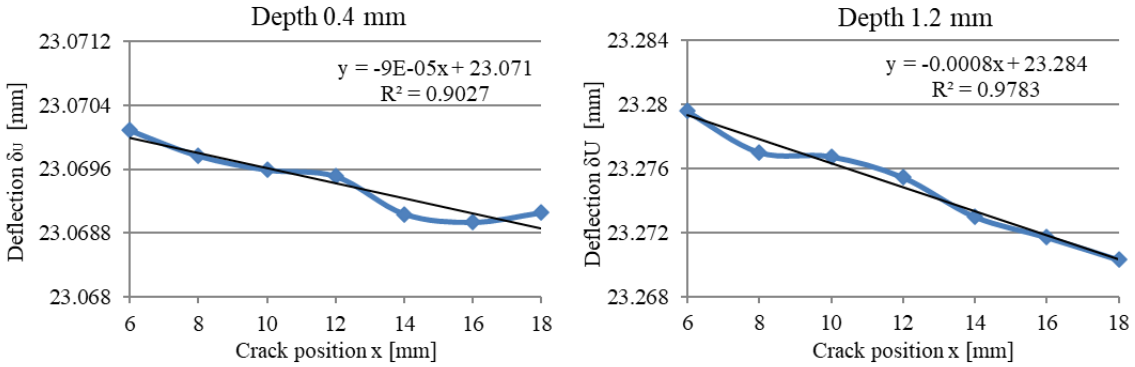

Figure 3.6. Regression curve representing the deflection of the beam with a transverse crack

After obtaining the static deflection values from the mathematical relation using the regression curve, the severity is calculated using relation (3.34).

The severity regression curve obtained for the beam with dimensions presented in Table 3.1 is illustrated in Figure 3.7. For other lengths or thickness the curve is simply adjusted by involving the radius of gyration.

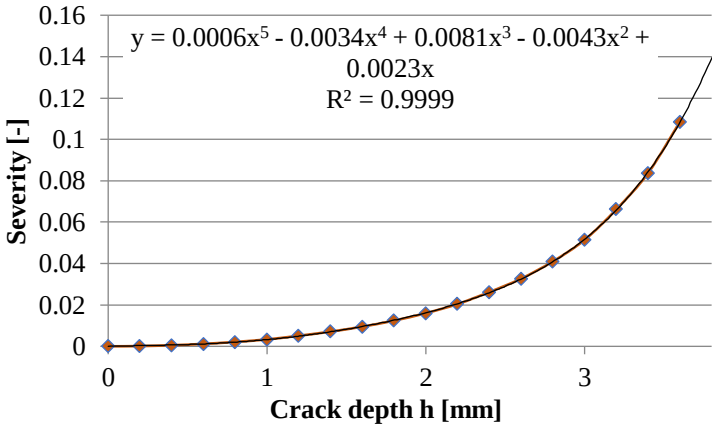

Figure 3.7. The curve representing the severity of a transverse crack.

Furthermore, to obtain more accurate results, the behavior of the damaged cantilever with T and L shaped cracks was studied, and a supplementary slope at the cross-section changes (at the crack ends) was observed. An image of the deformed state for the beam having a T-shaped crack is shown in Figure 3.8.

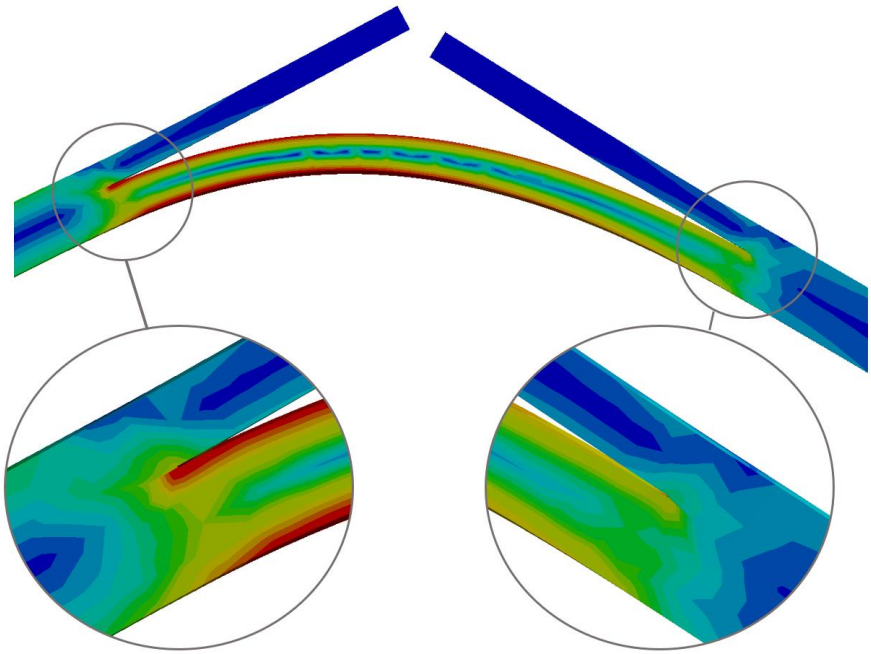

Figure 3.8. Supplementary bending moments at the damage location

In order to obtain the observed slope, a supplementary bending moment at each damage end was included in the model of the beam with a branched crack, shown in Figure 3.9. These moments are proportional with the squared normalized modal curvature at those locations and consequently with the pseudo-severity of the transverse crack positioned at the branched crack ends, corrected with a coefficient.

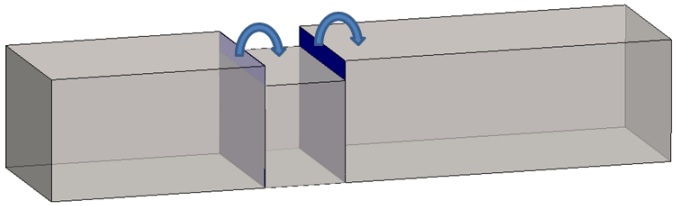

Figure 3.9. Supplementary bending moments at the damage location

The correction coefficient *c(a)*, are introduced to amplify the pseudo-severity *s(a)* as:

$$s(a) = c(a) \cdot \gamma(a) \tag{3.36}$$

With this correction coefficient, one can obtain pseudo-severity coefficients $c_i^{x_1}$ and $c_i^{x_2}$ that have a similar role as the coefficient $c_i^{x_1-x_2}$ in Eq. (3.33). These are calculated with the mathematical relations:

$$c_i^{x_1} = 1 - s(a)\left[\bar{\phi}_i''(x_1)\right]^2 = 1 - c(a)\cdot\gamma(a)\left[\bar{\phi}_i''(x_1)\right]^2 \tag{3.37}$$

$$c_i^{x_2} = 1 - s(a)\left[\bar{\phi}_i''(x_2)\right]^2 = 1 - c(a)\cdot\gamma(a)\left[\bar{\phi}_i''(x_2)\right]^2 \tag{3.38}$$

where: $\gamma(a)$ is the severity of the transverse crack with a given depth *a*, $\bar{\phi}_i''(x_1)$ and $\bar{\phi}_i''(x_2)$ are the normalized squares of the modal curvatures at locations x_1 and x_2. The correction coefficient *c(a)* is deduced empirically.

The coefficients $c_i^{x_1}$ and $c_i^{x_2}$ are used to multiply the coefficient $c_i^{x_1-x_2}$, in order to improve the results obtained with the proposed model. Now, the severity coefficient proposed for the beam with a branched crack is:

$$c_{Si}(a, x_1, x_2) = c_i^{x_1} \cdot c_i^{x_1-x_2} \cdot c_i^{x_2} \tag{3.39}$$

which considers the stiffness loss due to cross-section reduction between points x_1 *and* x_2 and the supplementary bending moments at the damage extremities. By applying the severity coefficients $c_{Si}(a, x_1, x_2)$, the frequency of the damaged beam becomes:

$$f_{Ci} = c_{Si}(a, x_1, x_2)\cdot f_i = c_i^{x_1} \cdot c_i^{x_1-x_2} \cdot c_i^{x_2} \cdot f_i \tag{3.40}$$

The correction coefficients *c(a)* were determined based on frequencies obtained from FEM simulation results. The coefficients are suitable for any complex-shaped crack if its depth and delamination extent remain constant. The empirical defined coefficient curve is presented in Figure 3.10.

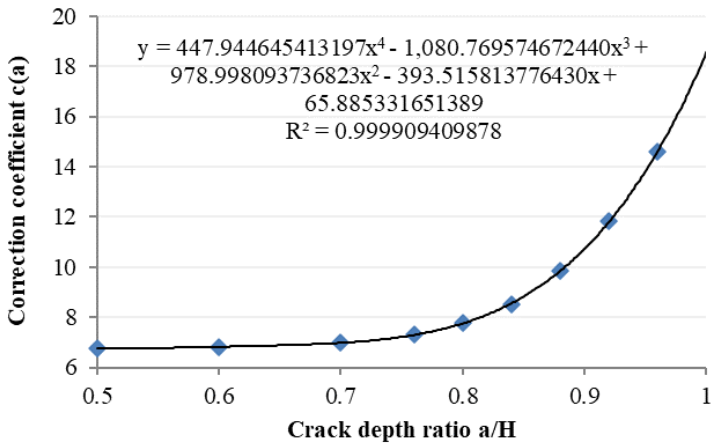

Figure 3.10. Empirical defined correction coefficient for severity estimation.

In the developed method the actual bending moment is considered, which is the moment that acts on the continuous section beam but having the same effect for the small section as a consequence of the apparent modification of the bending moment in the reduced area. Stating from the energy loss distribution along the beam and taking into account the energy fraction the stiffness reduction coefficients were obtained, which allow us to calculate the frequencies for the smaller section of the beam, a relation valid for any type of boundary.

Beside the stiffness reduction coefficients, the supplementary bending moments were applied for the reduced section in order to obtain an accurate prediction of the natural frequencies for the beam with a complex-shaped crack.

The flow chart for de introduced algorithm is presented in Figure 3.11.

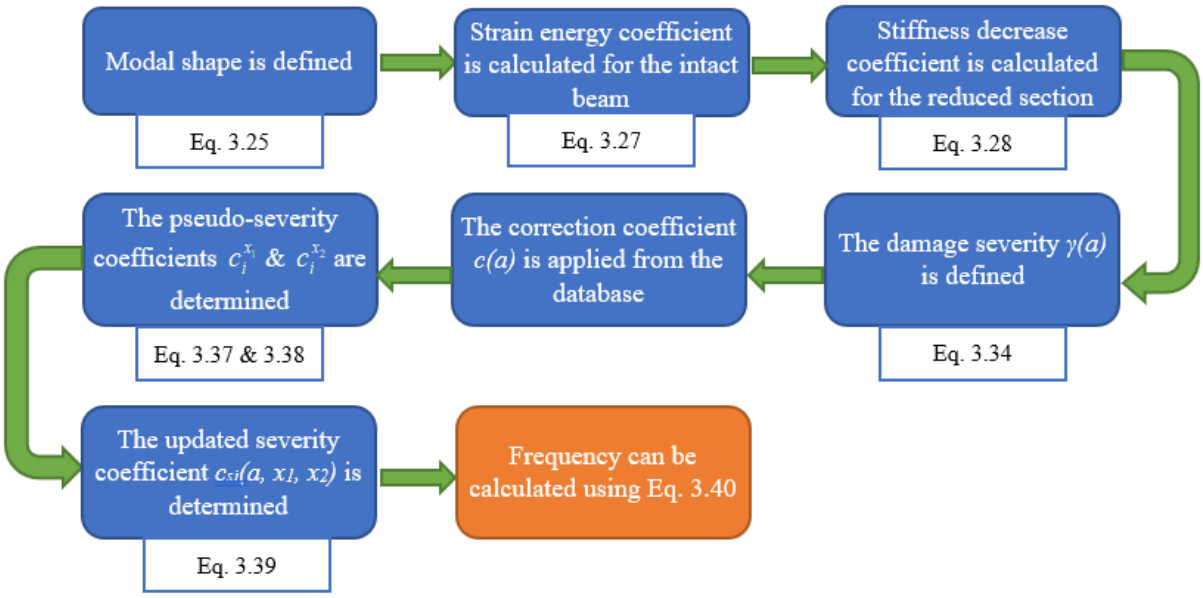

Figure 3.11. Workflow chart for the stiffness reduction algorithm

3.2. The developed PyDAM application

The algorithm proposed herein can be used to predict the impact of complex-shaped cracks on the natural frequencies of beams, by involving the damage severity coefficient presented in relation 3.39. It works for beams that can be modeled with the Euler-Bernoulli theory irrespective of the boundary conditions.

The algorithm is computerized by using the Python programming language resulting in the software named PyDAM. The developed software confers the possibility to use the Euler-Bernoulli model and it is capable of depicting the natural frequencies of beams with reduced sections, for several types of boundary conditions. The flowchart of the software is presented in Figure 3.12:

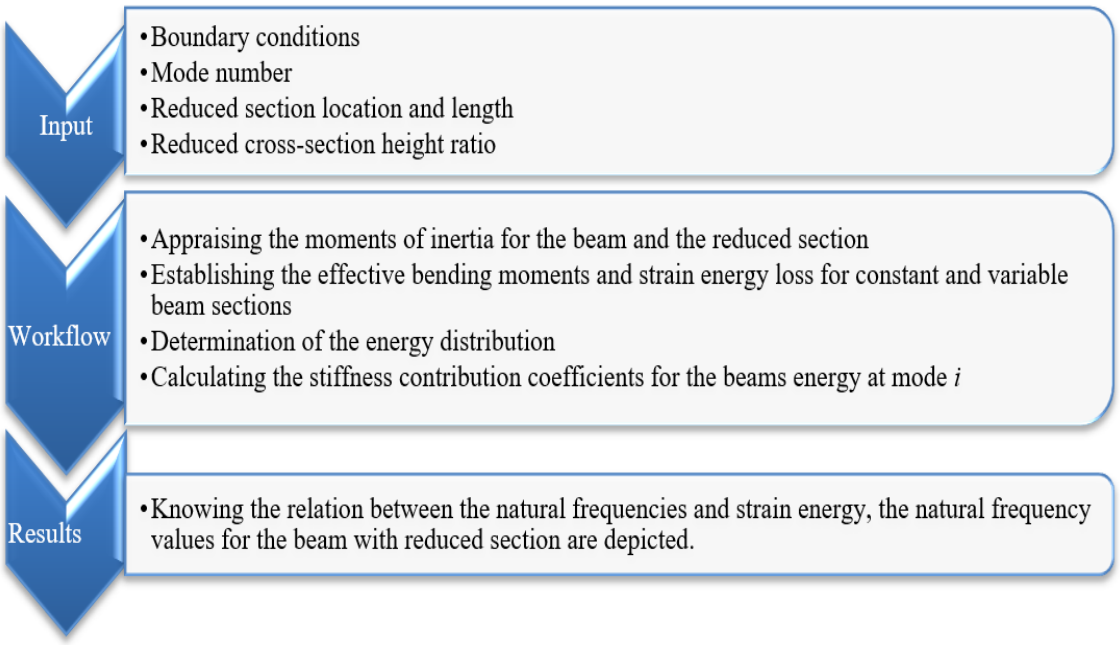

Figure 3.12. Algorithm flowchart

The PyDAM application interface used for determining the frequency estimation coefficients of the damaged beam is presented in Figure 3.13, and it consists in a drop-down menu for selecting the type of boundary condition, a second drop-down for selecting the transversal mode number used for calculus, and two type-in boxes for entering the damage location interval and damage depth ratio.

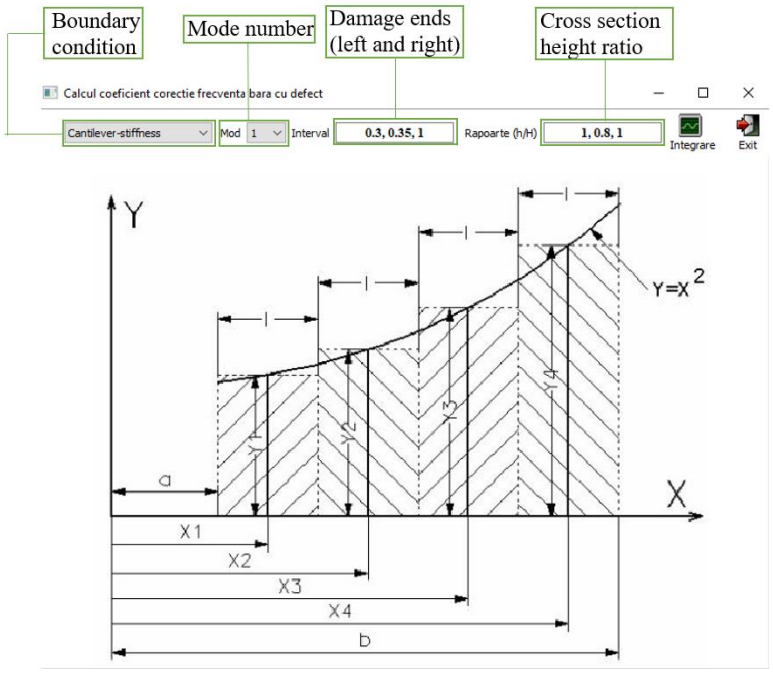

Figure 3.13. Developed PyDam interface

The steps for achieving the required set of results are as follows:

- Input:

a) Define the boundary conditions and mode number;

The boundary condition for the beam are selected from the drop-down menu, meaning: cantilever, double-clamped, free-free and simple-supported, as presented in Figure 3.14. For the current study, only the stiffness method is considered.

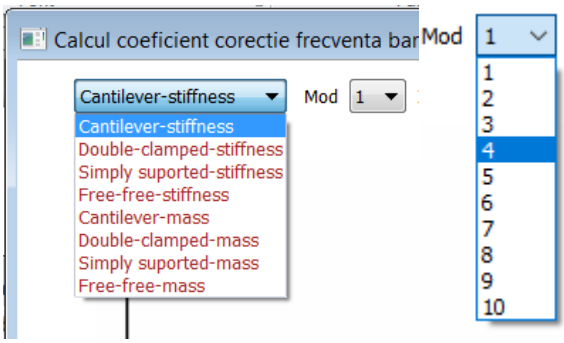

Figure 3.14. Boundary condition and mode number selection

b) The transversal vibration mode number is easily selected from the drop-down menu from mode number one to ten:

c) Introduce the damage limits, left and right;

The position of the section with a reduced stiffness is introduced as an interval value with the start of the damage location set up as the first value and the end as the second value. The values are normalized with the beam length. The third value in the input box is the normalized beam length, which obviously is one.

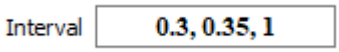

Figure 3.15. Type-in box for damage interval

d) Input reduced section height ratio, where $h = H - a$.

- Workflow

The algorithm works by implementing relations that permit:

a) The calculation of the modal curvature for any position along the beam. The Python code for calculating the modal curvature for a cantilever beam is illustrated in Figure 3.16:

```
# Liber-incastrat - cantilever.xls
def  functiel(x, Lambda):
        L=1.
        Alfa=Lambda/L
        coslam=math.cos(Lambda)
        coshlam=math.cosh(Lambda)
        sinlam=math.sin(Lambda)
        sinhlam=math.sinh(Lambda)
        ax=Alfa*x
        sinalx=math.sin(ax)
        cosalx=math.cos(ax)
        sinhalx=math.sinh(ax)
        coshalx=math.cosh(ax)
        fct = 0.5*( -(coslam+coshlam)/
        (sinlam+sinhlam)*(sinalx+sinhalx)+cosalx+coshalx )
        return fct**2
```

Figure 3.16. Section of the PyDAM backend code for calculating the normalized curvature of a cantilever beam

b) The calculation of the damage severity for defined depth of the crack:

```
# Returneaza severitatea defectului si un factor de corectie
def  SEVER_FUNCTIE(adanc_defect):
    # Severitate defect transversal 09.04.2020.xlsx
    x= adanc_defect
    if x==1:
        y = 0
    elif (x>=0.8 and x<1):
    y = 0.083999740436*x**2 - 0.167922059791*x + 0.083923096845
    else:
        y = -4.289323653114*x**5 + 13.718732250072*x**4 - 17.813742673584*x**3
        + 11.949919658823*x**2 - 4.275570129793*x + 0.682814548404

    # T50_ 0,4-1,5 mm  09.04.2020.xls   - sheet 'T diverse adancimi poz. 300'
    Factor_CORECTIE = 394.1*x**3 - 834.32*x**2 + 593.06*x - 134.5
    return y, Factor_CORECTIE
```

Figure 3.17. Section of the PyDAM backend code for severity calculation

c) The determination of the pseudo-severity coefficients by implementing the supplementary bending moments, with the help of Eq.3.36 and 3.37

d) The determination of the frequency estimation coefficient for the damaged beam with Eq. 3.38

Note that PyDAM permits calculating the frequencies for more branched cracks. In this case in the input boxes for the damage ends and cross-section height ratio must be inserted all crack ends.

The execution of the algorithm is done by pressing the button „Integrare”, which results in a separate window that indicates the normalized mode shape for the given mode number and

boundary conditions, as well as the stiffness reduction area, severity, slope at the crack extremities and coefficient values, as presented in figure 3.18.

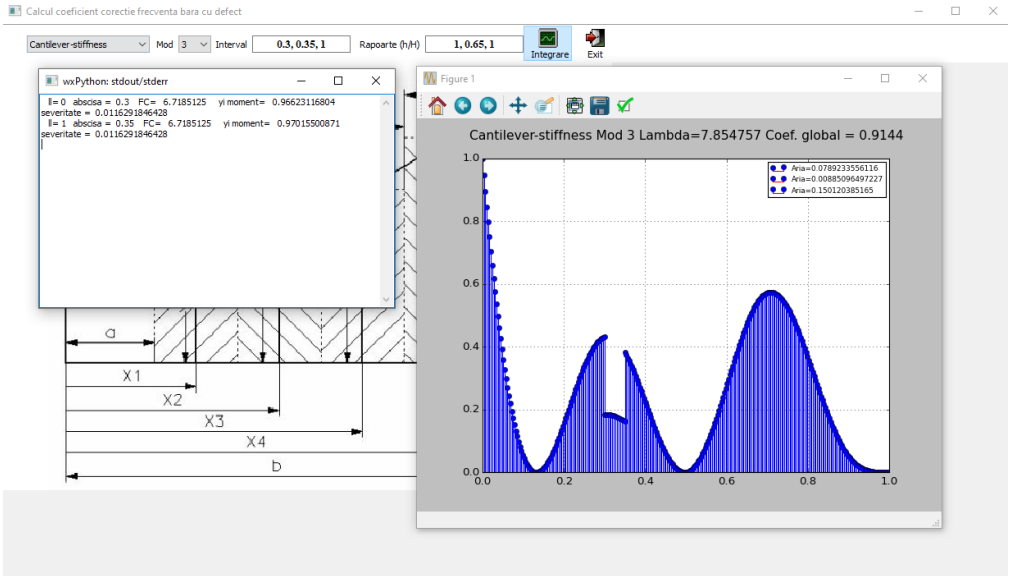

Figure 3.18. Results obtained using the Python developed software

3.3. The prediction accuracy of natural frequencies by using the developed algorithm on beams having complex-shaped cracks

In the current chapter, the aim was to show that the proposed model, implemented with the help of the Python programming language in the desktop application named PyDAM, leads to more accurate results, because it takes into consideration the severity of the transversal component of the damage as well as the slope at the ends of the longitudinal crack components. The achieved results were compared with the results obtained by using only the stiffness reduction model presented in Eq. 3.33 and with does obtained with the help of FEM for a cantilever beam having a T-shaped crack, presented in Table 3.4. Furthermore, in order to test the reliability of the proposed model for other damage types, the obtained results were compared with does calculated using FEM for the same cantilever, but with an L-shaped crack.

To this aim, several cracks have been considered, differing in depth and position. The crack depths a are: 0.2, 0.4, 0.6, 0.8, 1 and 1.2. The crack locations are x: 250, 300, 350, 400. Figures 3.19-3.23 show the calculated results using the PyDAM application, for a cantilever beam with reduced section depth a=1 mm and position x=*250* mm. The damage length has been considered to be 50 mm, meaning the stiffness reduction interval is set to x_1=*0.25* - x_2=*0.3*.

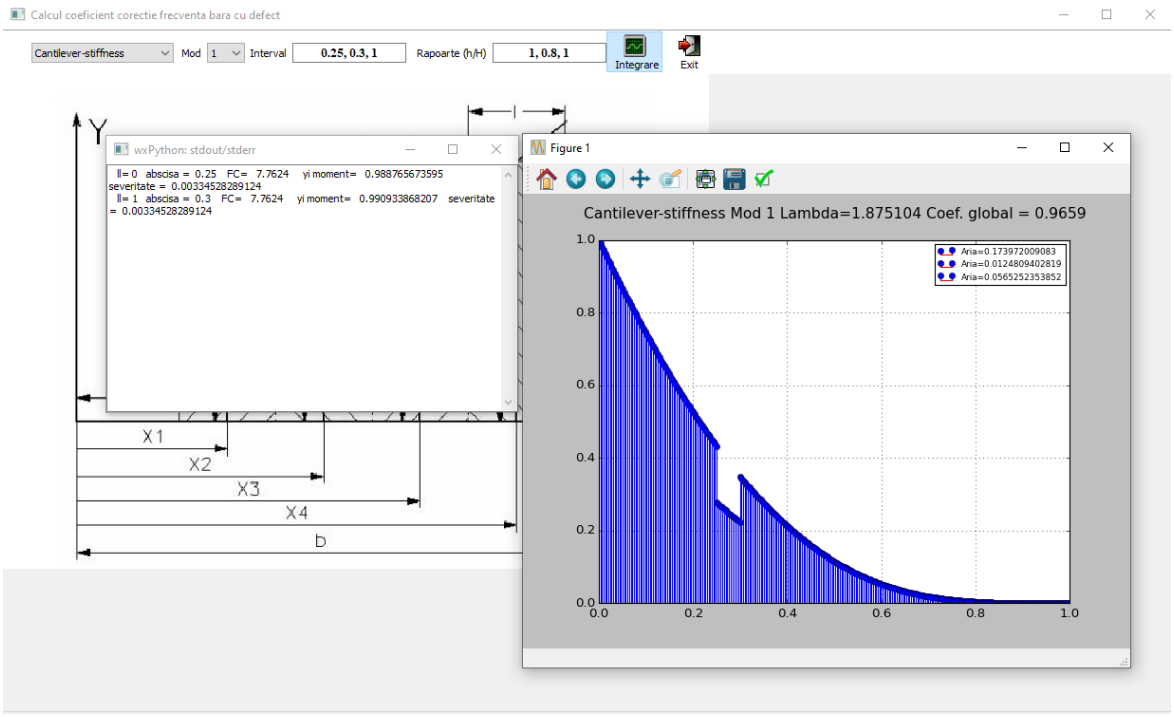

Figure 3.19. PyDAM application results for mode no. 1 of vibration for a cantilever beam having a reduced section of depth a=1 mm and interval x_1=0.25 x_2=0.3 mm.

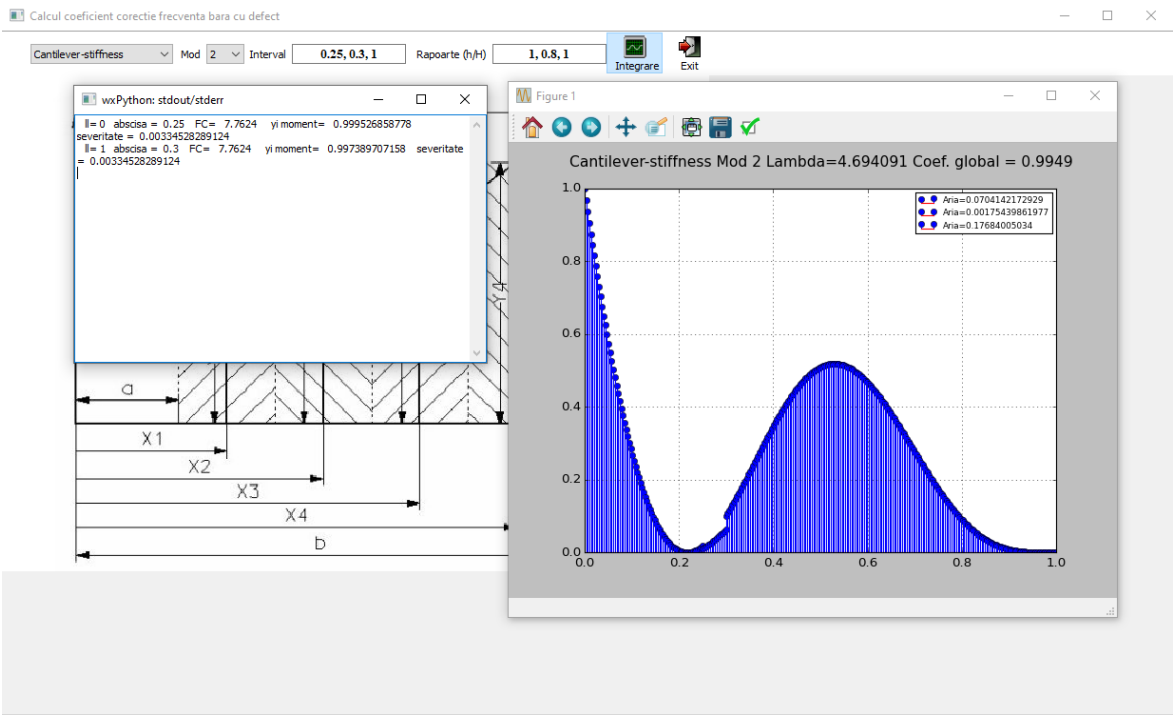

Figure 3.20. PyDAM application results for mode no. 2 of vibration for a cantilever beam having a reduced section of depth a=1 mm and interval x_1=0.25 x_2=0.3 mm.

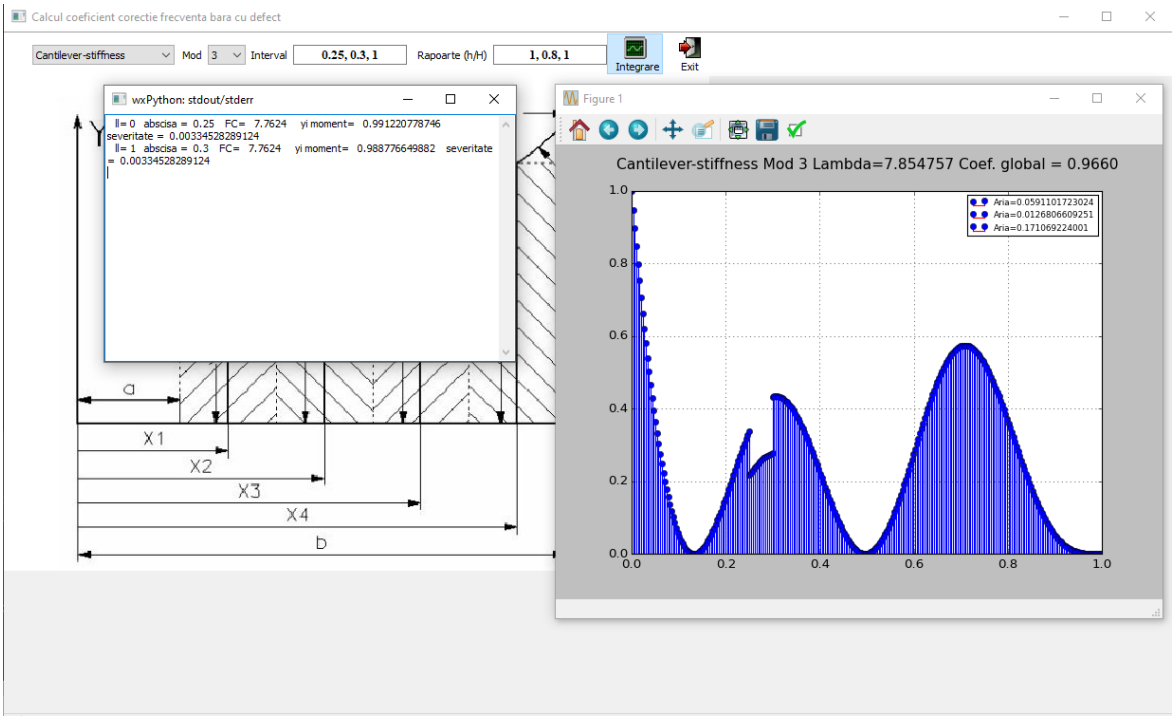

Figure 3.21. PyDAM application results for mode no. 3 of vibration for a cantilever beam having a reduced section of depth a=1 mm and interval x_1=*0.25* x_2=*0.3* mm.

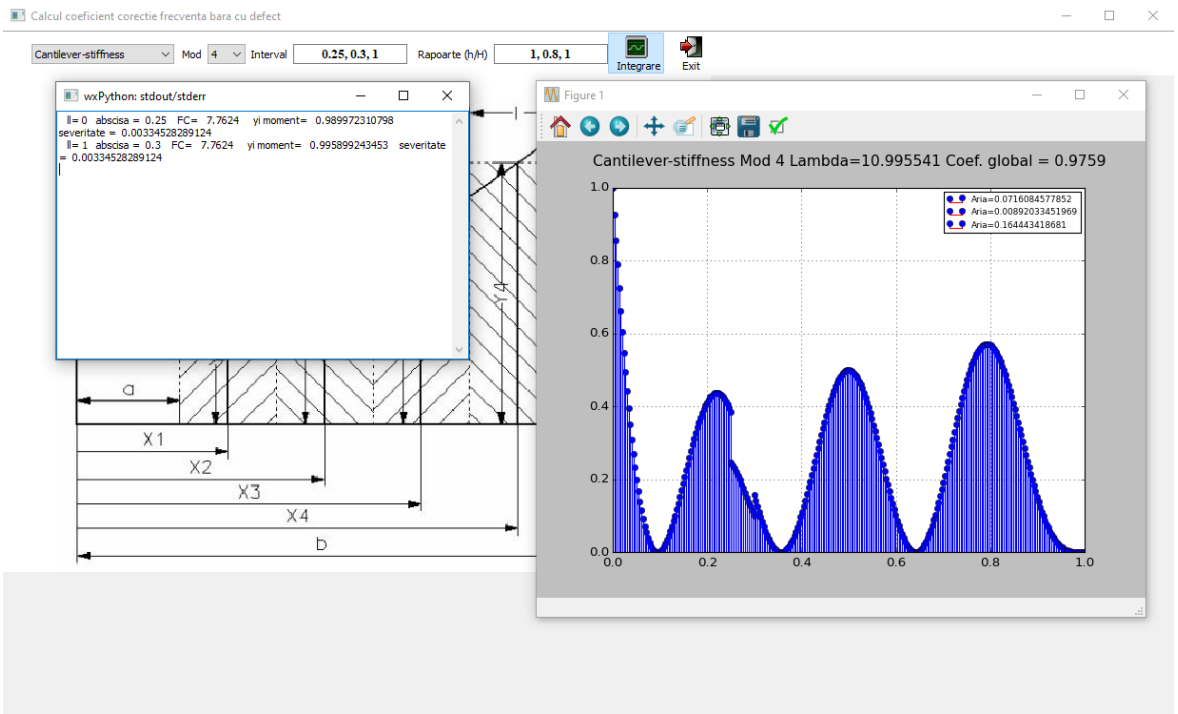

Figure 3.22. PyDAM application results for mode no. 4 of vibration for a cantilever beam having a reduced section of depth a=1 mm and interval x_1=*0.25* x_2=*0.3* mm.

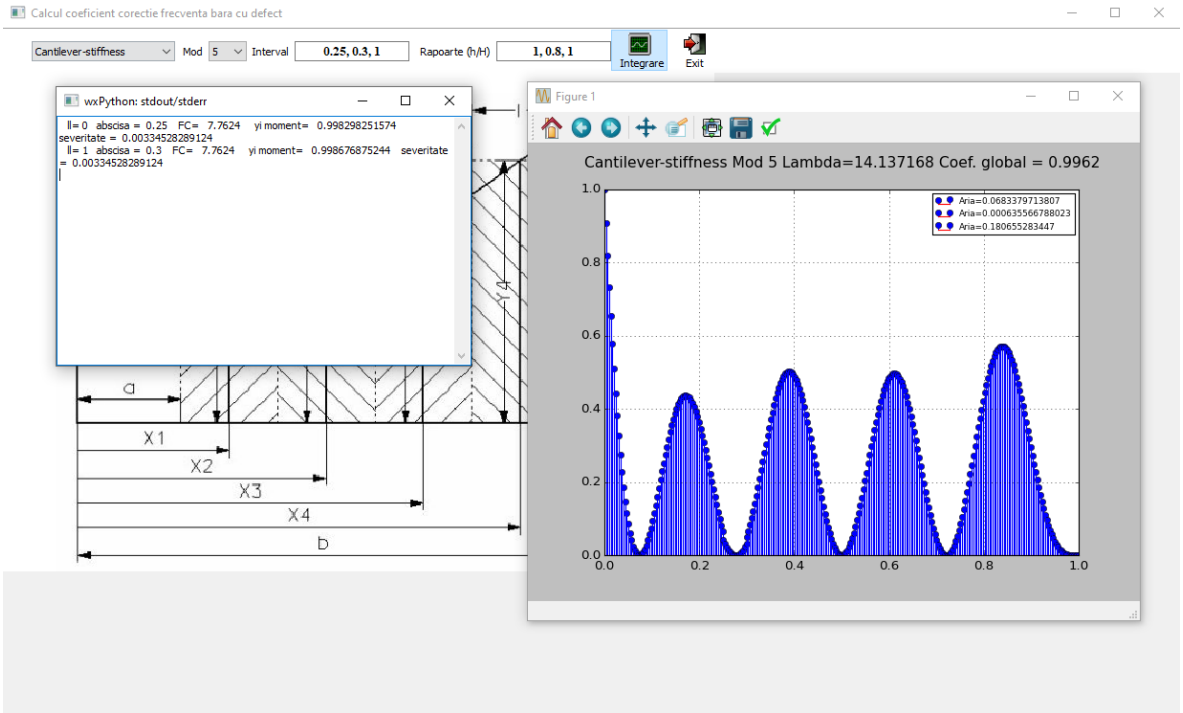

Figure 3.23. PyDAM application results for mode no. 5 of vibration for a cantilever beam having a reduced section of depth a=1 mm and interval x_1=*0.25* x_2=*0.3* mm.

The obtained results indicate the normalized mode shape for the given mode number and boundary conditions, as well as the stiffness reduction area, severity, slope at the crack extremities and coefficient values, as presented in figures 3.19-3.23.

After obtaining the correction coefficient described in Eq. 3.39 from the PyDAM application, namely the global coefficient one can calculate the natural frequencies with the help of Eq. 3.40 for the damaged cantilever beam with given dimensions by knowing its natural frequencies in healthy state.

The obtained natural frequencies are compared with the obtained results for the same cantilever having a T-shaped crack with dimensions presented in Table 3.4. It is shown in Tables 3.11 to 3.13. the cases where the crack depth is a=0.2, 0.6, and 1 mm positioned at x=250 mm, meaning the damage extremities x_1-x_2=250-300, which are identical with the damage scenarios presented in Tables 3.5 to 3.7.

In Tables 3.14 to 3.16, the cases where the crack depth is a=0.2, 0.6, and 1 mm positioned at x=350 mm are presented, meaning the damage extremities x_1-x_2=350-400, which are identical with the damage scenarios presented in Tables 3.8 to 3.10.

Table 3.11. Cantilever beam with T-shape crack of depth a=0.2 and extremities x_1-x_2=250-300

$F_{i\text{-}U}$ [Hz]	$F_{i\text{-}D}$ [Hz]	Reduct. coeff.	Severity	Correc-tion coeff.	Pseudo Severity	Squared curvature		$F_{i\text{-}D}$ [Hz]	Error
FEM	FEM	$c_{Si}(a,x_1,x_2)$	γ	*c(a)*	*s(a)*	$(\bar{\phi}_i''(x_1))^2$	$(\bar{\phi}_i''(x_2))^2$	proposed model	proposed model
4.0812	4.0606	0.9954	0.000132	14.6193	0.0019	0.4326	0.3491	4.06256	-0.05%
25.573	25.5602	0.9993				0.0182	0.1005	25.55592	0.02%
71.595	71.2566	0.9954				0.3380	0.4322	71.26521	-0.01%
140.27	139.7737	0.9967				0.3861	0.1579	139.8134	-0.03%
231.81	231.7525	0.9996				0.0655	0.0509	231.7154	0.02%

Table 3.12. Cantilever beam with T-shape crack of depth a=0.6 and extremities x_1-x_2=250-300

$F_{i\text{-}U}$ [Hz]	$F_{i\text{-}D}$ [Hz]	Reduct. coeff.	Severity	Correc-tion coeff.	Pseudo Severity	Squared curvature		$F_{i\text{-}D}$ [Hz]	Error
FEM	FEM	$c_{Si}(a,x_1,x_2)$	γ	*c(a)*	*s(a)*	$(\bar{\phi}_i''(x_1))^2$	$(\bar{\phi}_i''(x_2))^2$	proposed model	proposed model
4.0812	4.0074	0.9821	0.001191	9.8437	0.0117	0.4326	0.3491	4.0081	-0.02%
25.573	25.5147	0.9972				0.0182	0.1005	25.5016	0.05%
71.595	70.3490	0.9820				0.3381	0.4322	70.3083	0.06%
140.27	138.5762	0.9872				0.3862	0.1579	138.4814	0.07%
231.81	231.5783	0.9982				0.0655	0.0510	231.4008	0.08%

Table 3.13. Cantilever beam with T-shape crack of depth a=1 and extremities x_1-x_2=250-300

$F_{i\text{-}U}$ [Hz]	$F_{i\text{-}D}$ [Hz]	Reduct. coeff.	Severity	Correc-tion coeff.	Pseudo Severity	Squared curvature		$F_{i\text{-}D}$ [Hz]	Error
FEM	FEM	$c_{Si}(a,x_1,x_2)$	γ	*c(a)*	*s(a)*	$(\bar{\phi}_i''(x_1))^2$	$(\bar{\phi}_i''(x_2))^2$	proposed model	proposed model
4.0812	3.9339	0.9660	0.003345	7.7556	0.0259	0.4326	0.3491	3.94246	-0.22%
25.573	25.4511	0.9949				0.0182	0.1005	25.44321	0.03%
71.595	69.1533	0.9661				0.3381	0.4322	69.16761	-0.02%
140.27	137.0857	0.9758				0.3862	0.1579	136.8778	0.15%
231.81	231.3229	0.9962				0.0655	0.0510	230.9249	0.17%

Table 3.14. Cantilever beam with T-shape crack of depth a=0.2 and extremities x_1-x_2=350-400

$F_{i\text{-}U}$ [Hz]	$F_{i\text{-}D}$ [Hz]	Reduct. coeff.	Severity	Correc-tion coeff.	Pseudo Severity	Squared curvature		$F_{i\text{-}D}$ [Hz]	Error
FEM	FEM	$c_{Si}(a,x_1,x_2)$	γ	*c(a)*	*s(a)*	$(\bar{\phi}_i''(x_1))^2$	$(\bar{\phi}_i''(x_2))^2$	proposed model	proposed model
4.0812	4.0685	0.9973	0.000132	14.6193	0.0019	0.2758	0.2126	4.0700	-0.04%
25.573	25.4884	0.9965				0.2211	0.3475	25.4835	0.02%
71.595	71.3300	0.9964				0.3820	0.2245	71.3394	-0.01%
140.27	140.2145	0.9996				0.0020	0.1066	140.2125	0.00%
231.81	230.2069	0.9947				0.3679	0.4904	230.5914	-0.17%

Table 3.15. Cantilever beam with T-shape crack of depth a=0.6 and extremities x_1-x_2=350-400

$F_{i\text{-}U}$ [Hz]	$F_{i\text{-}D}$ [Hz]	Reduct. coeff.	Severity	Correc-tion coeff.	Pseudo Severity	Squared curvature		$F_{i\text{-}D}$ [Hz]	Error
FEM	FEM	$c_{Si}(a,x_1,x_2)$	γ	*c(a)*	*s(a)*	$(\bar{\phi}_i''(x_1))^2$	$(\bar{\phi}_i''(x_2))^2$	proposed model	proposed model
4.0812	4.0350	0.9889	0.001191	9.8437	0.0117	0.2758	0.2126	4.0359	-0.02%
25.573	25.2502	0.9868				0.2211	0.3475	25.2346	0.06%
71.595	70.6292	0.9859				0.3820	0.2245	70.5874	0.06%
140.27	140.0681	0.9981				0.0020	0.1066	140.0072	0.04%
231.81	227.0758	0.9794				0.3679	0.4904	227.0376	0.02%

Table 3.16. Cantilever beam with T-shape crack of depth a=1 and extremities x_1-x_2=350-400

$F_{i\text{-}U}$ [Hz]	$F_{i\text{-}D}$ [Hz]	Reduct. coeff.	Severity	Correc-tion coeff.	Pseudo Severity	Squared curvature		$F_{i\text{-}D}$ [Hz]	Error
FEM	FEM	$c_{Si}(a, x_1, x_2)$	γ	$c(a)$	$s(a)$	$(\bar{\phi}_i''(x_1))^2$	$(\bar{\phi}_i''(x_2))^2$	proposed model	proposed model
4.0812	3.9875	0.9788				0.2758	0.2126	3.9948	-0.18%
25.573	24.9251	0.9750				0.2211	0.3475	24.9337	-0.03%
71.595	69.7146	0.9734	0.003345	7.7556	0.0259	0.3820	0.2245	69.6932	0.03%
140.27	139.8548	0.9960				0.0020	0.1066	139.7067	0.11%
231.81	222.9220	0.9613				0.3679	0.4904	222.8360	0.04%

The percent differences between the developed PyDAM application and FEM simulations for the case where the crack is positioned at x=250 mm are shown in Tables 3.11 to 3.13. It was observed that the maximum error obtained is 0.22% for the crack having a depth of a=1 mm. For the scenarios with the T-shaped crack positioned at x=350 mm the largest error is 0.18%.

Furthermore, it is demonstrated that the enhanced method can be used for predicting the natural frequencies of other types of cracks also. In Figure 3.24 a comparison between the errors obtained by applying the earlier developed method with the help of relation 3.33 is presented, denoted Error-area and the results obtained by implementing the enhanced algorithm presented in Figure 3.12, denoted Error - proposed model for the cantilever beam with a T-shaped crack positioned at distance x=250 mm. The errors presented are referring to the calculated natural frequencies. The green line represents the reference error line for the natural frequencies obtained by means of FEM analysis.

Furthermore, in order to demonstrate that the developed model can be applied to other complex-shaped cracks also, in Figure 3.25 a comparison between the area method and the enhanced algorithm presented in Figure 3.11 is presented, for the cantilever beam having an L-shaped crack with dimensions presented in Table 3.17, positioned at distance x=250 mm.

Table 3.17. The T-shaped crack dimensions and geometry

Crack shape		Crack length		Crack depth	Crack angle		Crack geometry
		L_L [mm]	L_R [mm]	a [mm]	α	β	
c	L_L	25	25	0.2-1.2	no	90	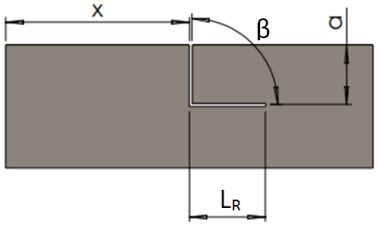

Figure 3.24. Errors obtained with the presented methods for a cantilever beam having a T-shaped crack

Figure 3.25. Errors obtained with the presented methods for a cantilever beam having a L-shaped crack

In order to evaluate the obtained frequencies, for the previous described damage cases, one can calculate the relative frequency shift (RFS), defined with the relation contrived by our research group [9]:

$$RFS_i(x,a) = \Delta\bar{f}_i(x,a) = \frac{f_{iU} - f_{iD}(x,a)}{f_{iU}} \tag{3.41}$$

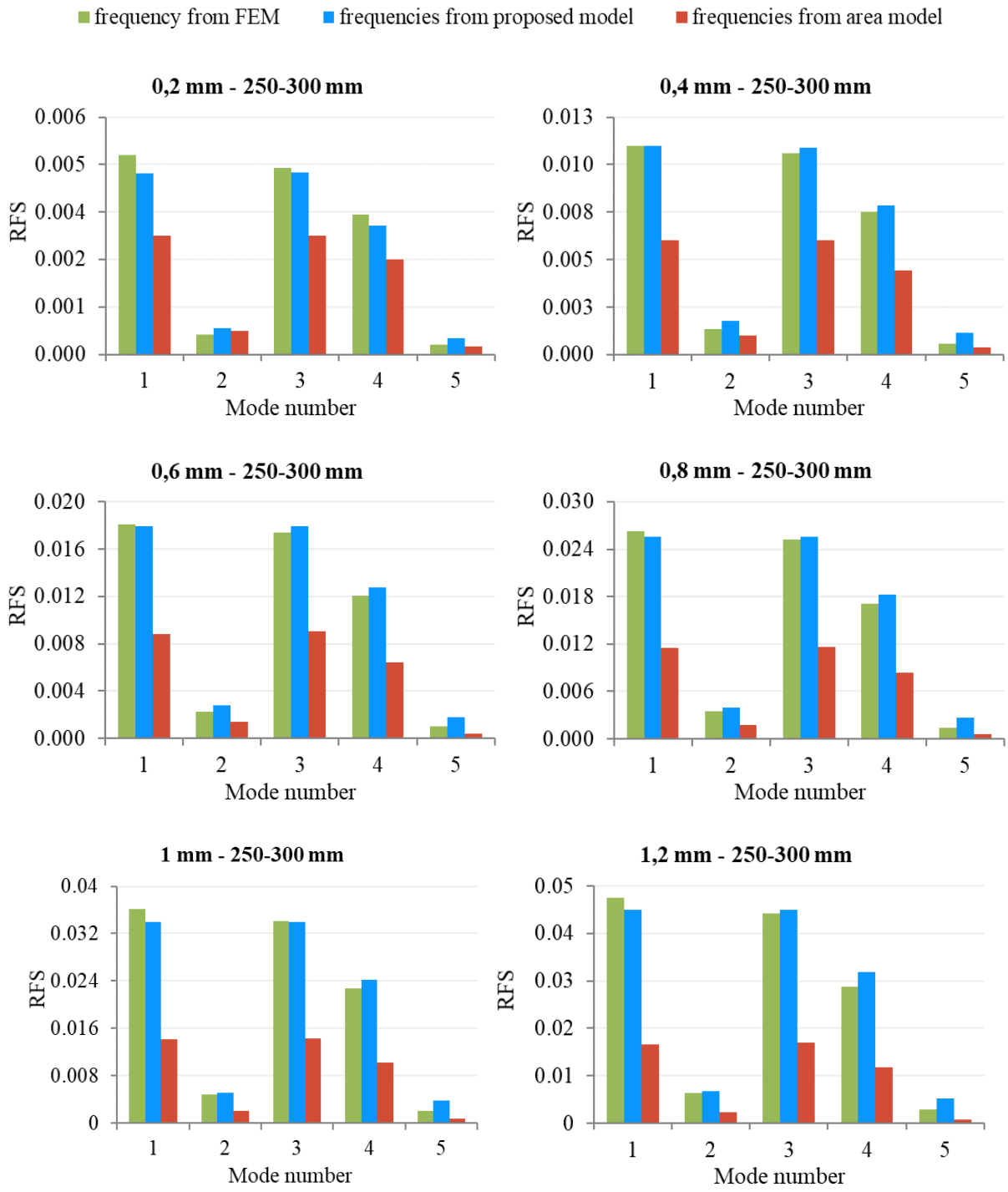

Figure 3.26. RFS comparison for the T-shaped crack located at *x*=250 mm at different depths

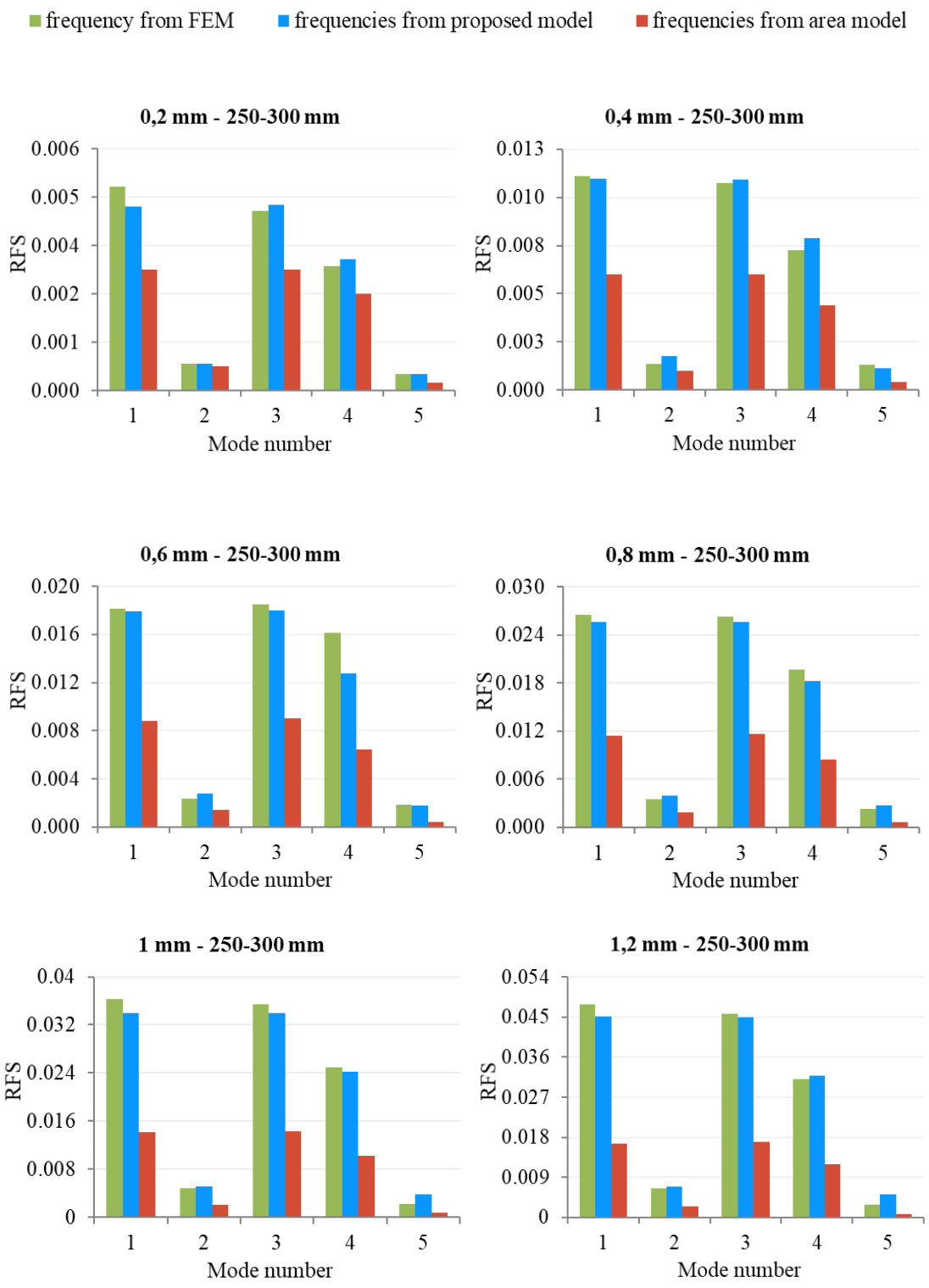

Figure 3.27. RFS comparison for the L-shaped crack located at *x*=250 mm at different depths

The obtained natural frequencies values, show that by using the squared modal curvature and by taking into account pseudo-severity produced by the stiffness reduction, lead to a more precise reading of the natural frequencies of beams with complex shaped damages.

The Damage Location Coefficients are calculated by dividing the values of the RFS for a given case to the biggest value in the series [22]. In general, the RFS for mode one achieves always the value one. This property makes finding the crack location independent of its severity estimation. If the crack position is found using DLCs, by dividing one of the RFSs to the corresponding DLC, one obtains the damage severity. This should be preferably made for the biggest RFS, to avoid small numbers, which are most susceptible to introduce errors. To have comparable values, it is convenient to work with normalized frequency values, which means that the frequency of the healthy beam for any mode is one.

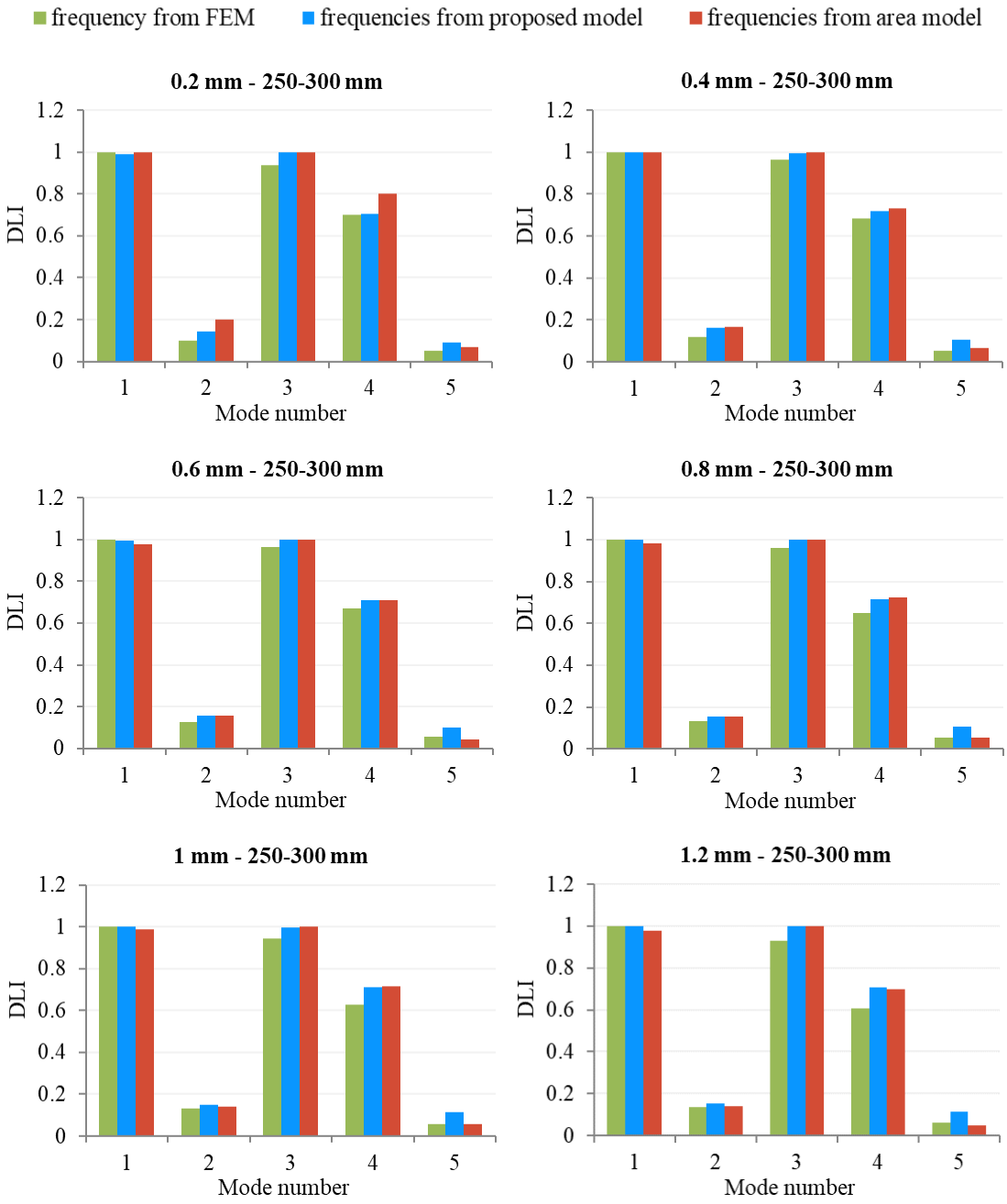

Figure 3.28. DLI comparison for the T-shaped crack located at *x*=250 mm at different depths

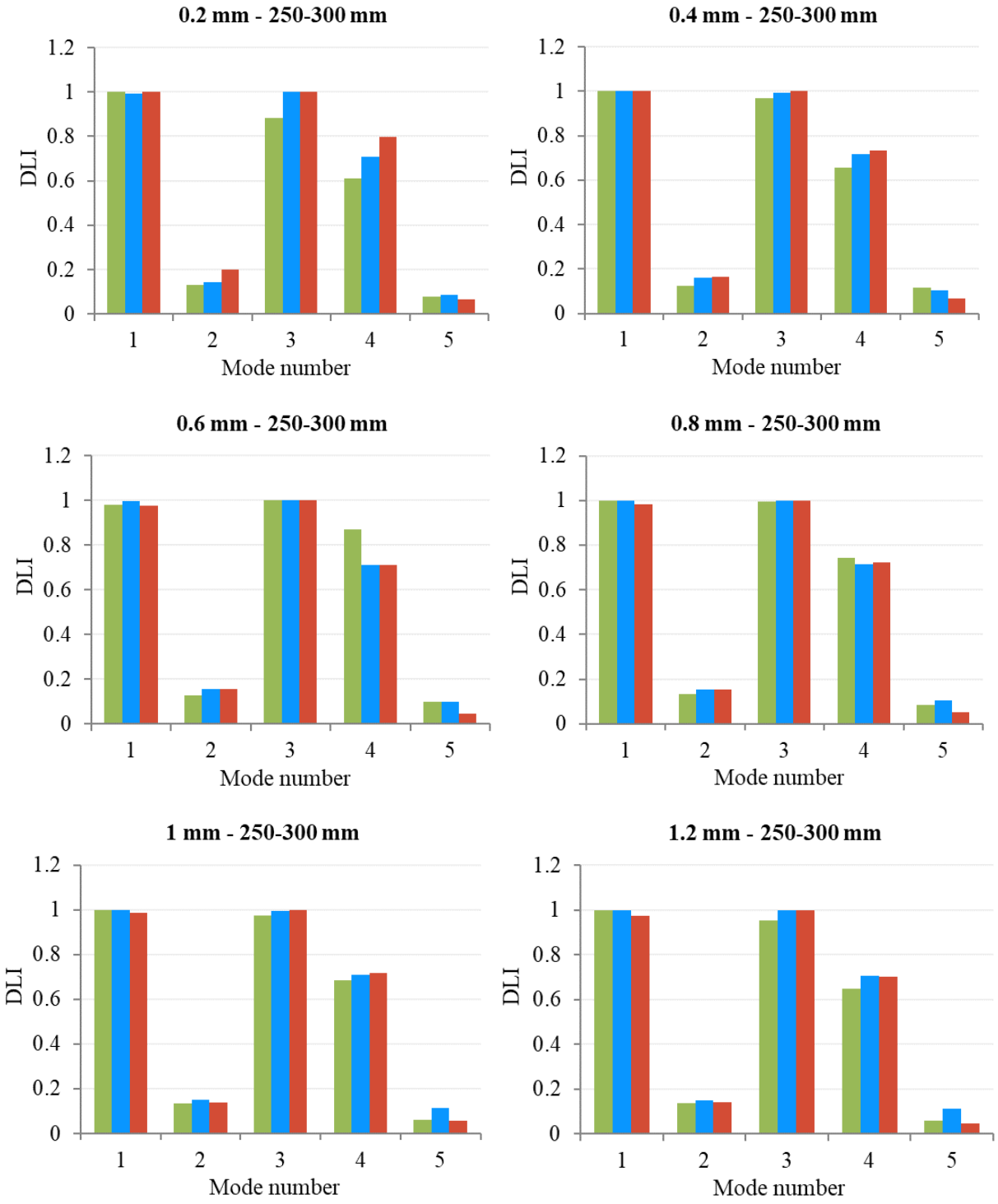

Figure 3.29. DLI comparison for the T-shaped crack located at *x*=250 mm at different depths

3.4. Conclusions

In the current study, a model reduced section model was proposed, that can be trustfully used to calculate the natural frequencies of beams affected by branched cracks when the crack depth, extent and position are known.

The algorithm considers the modal shape curvature which is the moment that acts on the constant section of the beam but having the similar effect for the reduced section as a consequence of the apparent modification of the bending moment in the reduced area. Stating from the distribution of energy loss along the beam and taking into account the energy ratio, the stiffness reduction coefficients have been obtained, which allow us to calculate the frequencies for the narrow section beam, a relation valid for any type of support.

The obtained results using Eq. 3.33, were compared with the results obtained with the help of FEM analysis for a beam having a T-shaped crack. The percent differences between the developed analytical model and FEM simulations are shown in Tables 3.4 to 3.9. It was observed that the error increases as the crack depth is increased, leading us to the conclusion that the developed algorithm should take into account the severity of the transversal component and the supplementary slope at the delamination ends of the complex-shaped crack.

The precision of the described algorithm was enhanced, by taking into consideration the stiffness reduction in the affected beam segment, and in addition the supplementary slope at the ends of the longitudinal component of the crack. Involving this model, one could predict the natural frequencies with high precision, the error being smaller than 1%.

Furthermore, in order to demonstrate that the developed model can be applied to other complex-shaped cracks, in Figure 3.25 a comparison between the area method and the enhanced algorithm is presented, for the cantilever beam having an L-shaped crack with dimensions presented in Table 3.17, positioned at distance x=250 mm.

Different results are shown in the appendix section for T and L -shaped cracks at different locations and depths, denoting the small errors obtained in predicting the natural frequencies using the PyDAM software. This qualifies the proposed model to be used to develop damage patterns as benchmarks to be used in damage detection.

4. EXPERIMENTAL RESEARCH AND VALIDATION

4.1. Materials and methods

In order to test the precision of the presented algorithm to detect and quantify complex shaped damages, experimental tests have been conducted in the Eftimie Murgu laboratory on cantilever beams both in damaged and undamaged state, by measuring their first five natural frequencies and comparing the obtained damage signatures by those obtained using FEM and the developed PyDAM application.

The experimental study was carried out for two test beams made of plain carbon steel bands, grade S355 with dimensions and material properties presented in Table 4.1.

Table 4.1. Physical-mechanical properties of the structural steel used

Length L [mm]	Width B [mm]	Thick. H [mm]	Mass density [kg/m^3]	Young modulus [N/m^2]	Poisson ratio [-]	Tensile strength [MPa]	Yield strength [MPa]	Min. elongation [%]
1000	20	5	7850	$2 \cdot 10^{11}$	0.3	470-630	355	20

The cantilever was fixed in a vise, by taking the necessary precautions for the specimen to be aligned accordingly. The experimental setup is presented in Figure 4.1:

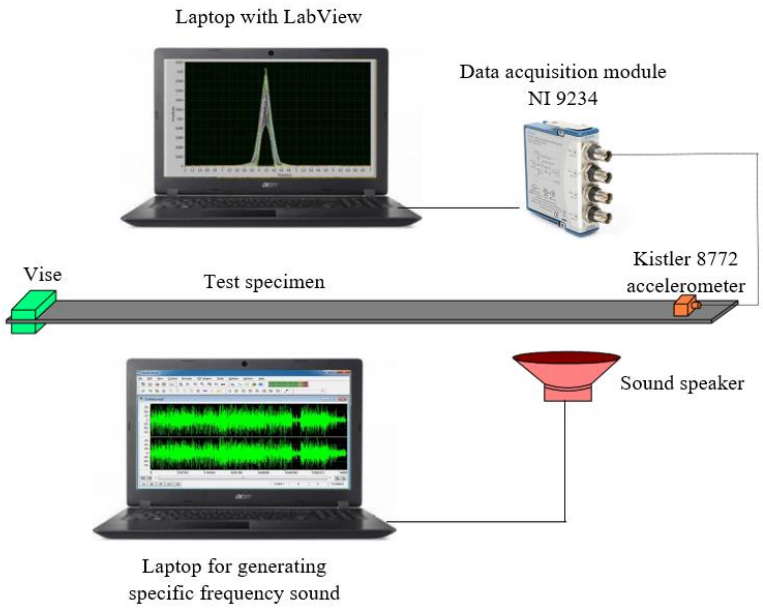

Figure 4.1. Experimental setup schematic for measuring the natural frequencies of cantilever beams

The study was performed in six steps for every test beam:

- Mounting in a rigid support and excitation of the test specimen;
- Measurement and processing of the signal; the eigenfrequency of the un-damaged beam is determined and recorded;
- The chosen damages are developed in each test beam by means of electrical discharge machining EDM.
- New measurement and processing of the signal, the eigenfrequencies of the damaged beams are determined and recorded;
- Comparison of the obtained natural frequencies.
- Identification of the damage position.

The equipment used for experimental validation is located in the laboratory of University Eftimie Murgu and it is presented in Figure 4.2.

Figure 4.2. Experimental setup for measuring the natural frequencies of cantilever beams

4.1.1. The excitation system

The excitation system is composed from a sound speaker of 100 W power, linked to an amplifier which is connected to a laptop. Through the described system the desired frequencies have been generated by using the installed software AudioDope. In order for the excitation to be flawless a few guidelines have been taken into account, such as excitation time, the distance from the cantilever beam has been kept constant at 10-15 mm, and more important the position of the speaker along the longitudinal direction of the beam has been adjusted as such not to coincide with a vibration node for a given mode. It is important to calibrate the excitation frequency as such not to stimulate other unwanted modes, as presented in Figure 4.3, one can observe that along mode 4 of vibration, several other modes are excited and the signal is distorted:

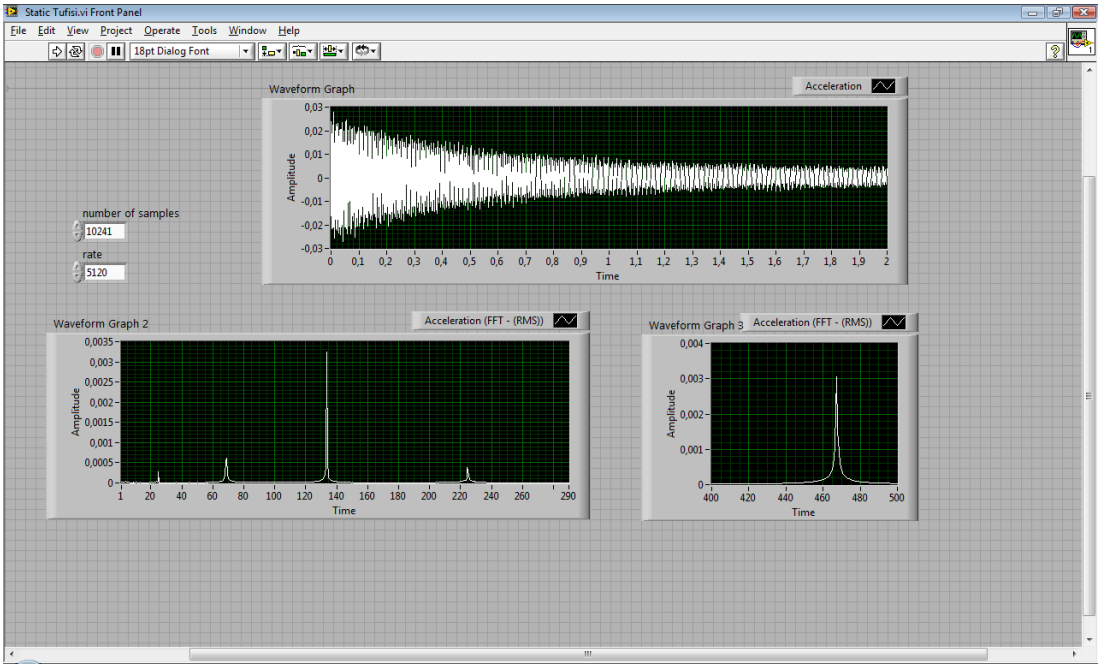

Figure 4.3. Distorted signal due to improper excitation

This excitation error is fixed by setting the appropriate excitation frequency with a precision of two decimals:

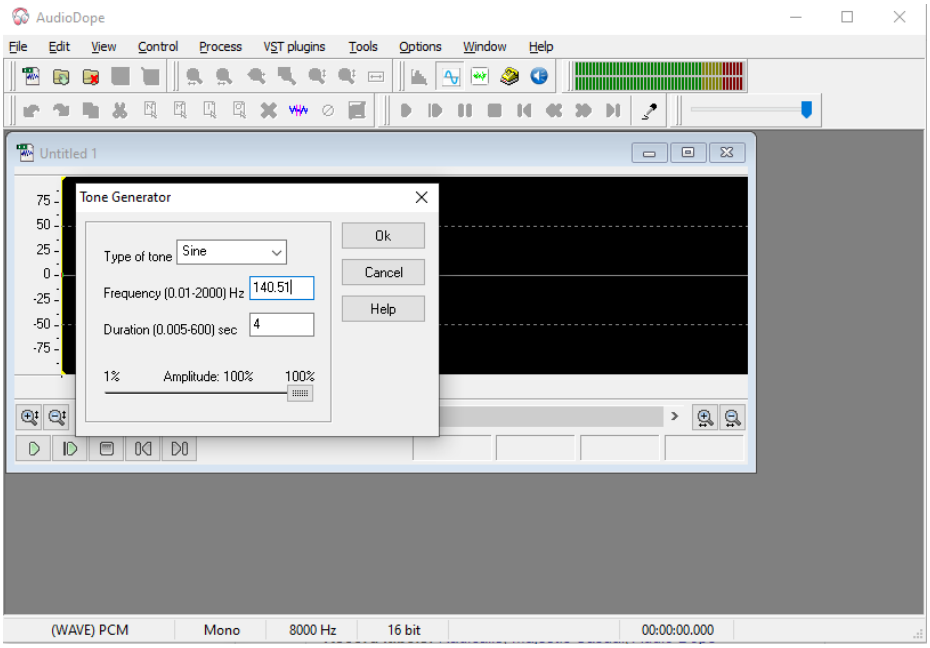

Figure 4.4. Software interface used for sound excitation

For low frequencies, e.g., 4 Hz in the first mode of vibration, the beams could not be excited with the described speaker; thus, it was necessary to stimulate the test specimens by hitting (impulse excitation).

The measurement system is composed of a Kistler 8772 accelerometer, mounted on the test beam by using adhesive as presented in Figure 4.5, and the data acquisition module NI cDAQ-9175 with NI9234 four-channel dynamic signal acquisition modules connected to a laptop through the USB port.

Figure 4.5. An accelerometer mounted on the test specimen

The accelerometer is a light weight cube shaped vibration measurement device of the piezoelectric type, presented in Figure 4.6.

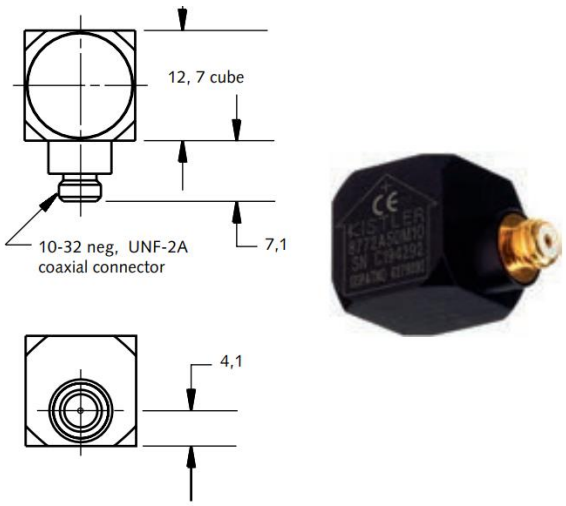

Figure 4.6. Model of the accelerometer used

A piezoelectric accelerometer consists essentially of three elements: the accelerometer body, the piezoelectric sensor and seismic mass. Due to the fact that the seismic mass is constant, the force acting on the element to be measured is proportional to the acceleration, according to Newtons law. In proportion to this acceleration, an electrical impulse is generated and transmitted to the acquisition system. The mass of the accelerometer is 8 grams, practically negligible in the process of measuring the natural frequencies of steel beams.

The NI 9234 acquisition module (AC/DC converter) produced by National Instruments, takes the signal from the accelerometer and transmits it to the NI cDAQ-9172 compact chasis. The

module has four channels (fig. 4.7a), i.e. it can pick up and transmit the signal from four simultaneous accelerometers.

a. b.

Figure 4.7. The NI 9234 acquisition module and the NI cDAQ-9172 compact chasis

The compact chasis (fig. 4.7b) produced by National Instruments makes the connection between the acquisition module and the laptop.

For realizing the spectral analysis, the LabVIEW programming environment was used to develop the virtual tools which acquire the time history acceleration. LabVIEW is a specialized software that allows the reading of acquired signals during vibration measurements, their analysis and visualization.

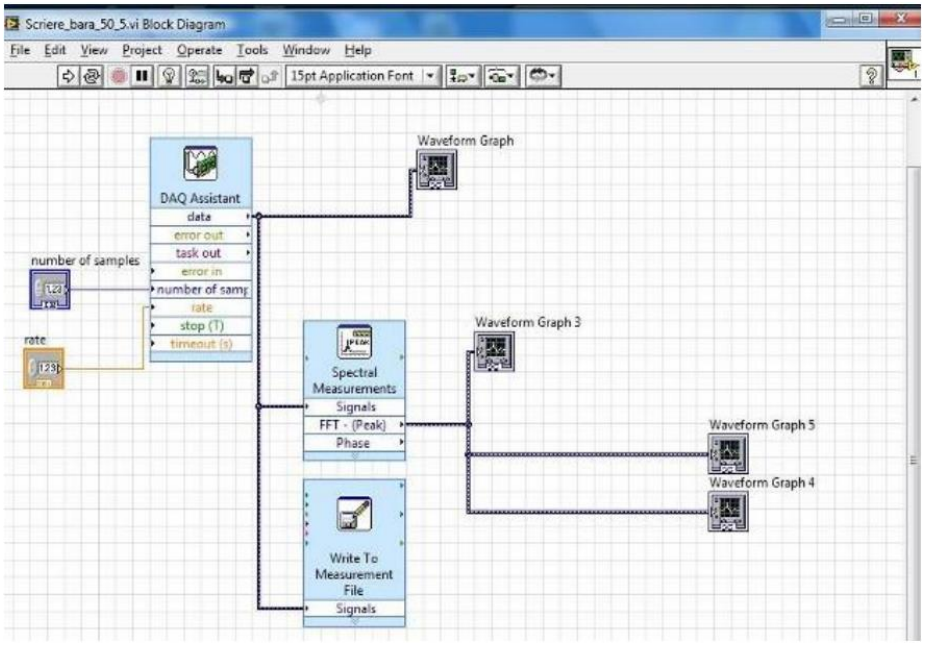

Figure 4.8. Virtual instrument schematic for signal acquirement

The virtual instruments are designed to allow the acquisition of the vibration signal, from which the natural frequencies of the test specimens will be accurately extracted. In Figure 4.10 the

extracted vibration signal is illustrated with the help of the virtual instruments for a cantilever beam.

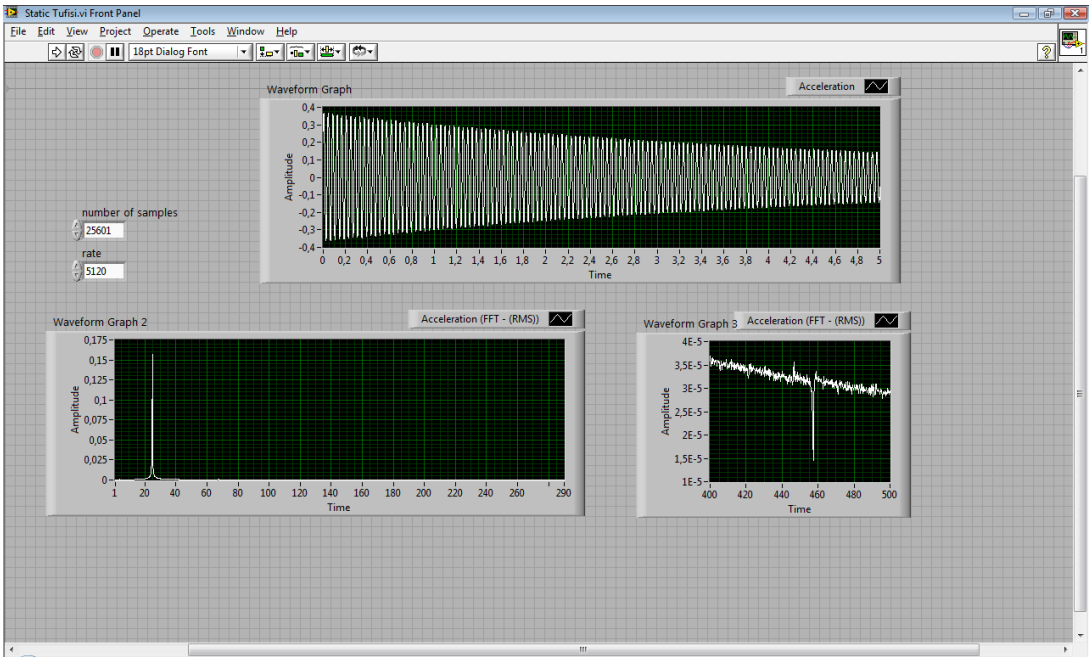

Figure 4.9. Extracted signal using LabVIEW

Given that only the first five modes of vibration are of interest, the signal reading time, at a single excitation of the beam, is limited to maximum 5 seconds for 5121 to 25601 samples submitted, depending on the measured mode of vibration. A longer reading time helps to determine the eigenfrequencies for mode 1, because during this time it has been managed to read several periods (cycles) of the eigenfrequency. Reducing the sampling number greatly decreases the accuracy of the signal read for high frequencies. As a consequence, in order to have sufficient cycles in the small modes, respectively sufficient samples transmitted in the large modes, the optimal reading time and number of samples for the studied beams was set different for every mode. In Table 4.2 the measurement parameters used for the intact beams are presented.

Table 4.2. Parameters used for measuring the vibration signal for a given mode

Mode no.	Excitation			Measurement			
	Type	Time [s]	Frequency Hz]	Sample no. [-]	Rate [-]	Reading time [s]	Time range [s]
1	Impulse	20	-	25601	5120	5	3-5
2	Speaker	4	25	25601	5120	5	3-5
3	Speaker	4	70	10241	5120	2	1-2
4	Speaker	4	138	5121	5120	1	0.5-1
5	Speaker	4	227	5121	5120	1	0-1

The acquired signal is imported in a Python programmed software, named PyFEST, developed by our research team [51] that uses a method of rectangular windows which truncates the acquired reading and calculates the DFT values for different frequency resolutions. The regression curves and maximum peaks are found by interpolating the three largest amplitudes found for the targeted frequency.

Furthermore, the algorithm and necessary stepts for using the developed application are shown [51]:

a. Import the acquired or generated original signal

b. Define the maximum frequency of interest. The standard DFT is showed in a separate window.

d. By right clicking on the maximum amplitude point, the frequency for which the analysis should be made is selected (Figure 4.12).

e. The signal is cropped by applying a rectangular window and the DFTs are calculated for each resulted signal.

f. The number of cycles that will be analyzed is selected by right-clicking the desired point on the top of the curve.

g. The maximum amplitude is found and the selected number of cycles is displayed.

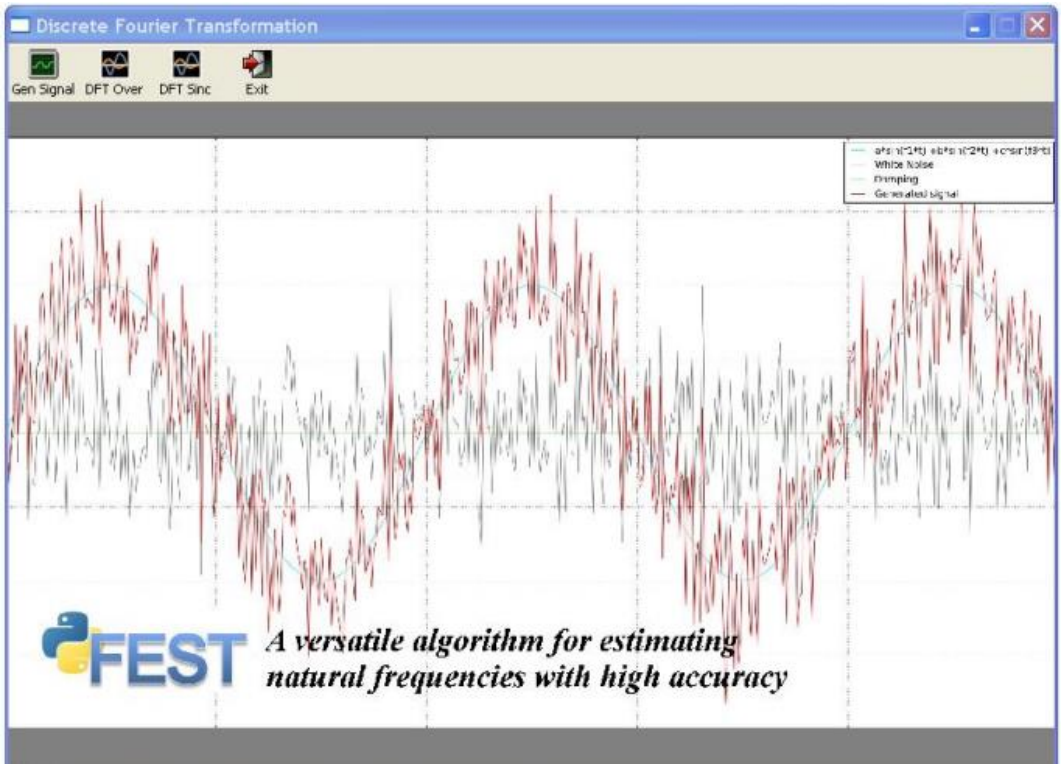

Figure 4.10. PyFEST software interface [51]

The signal is imported and the highest frequency of interest is introduced. By right-clicking the OK button a new window opens.

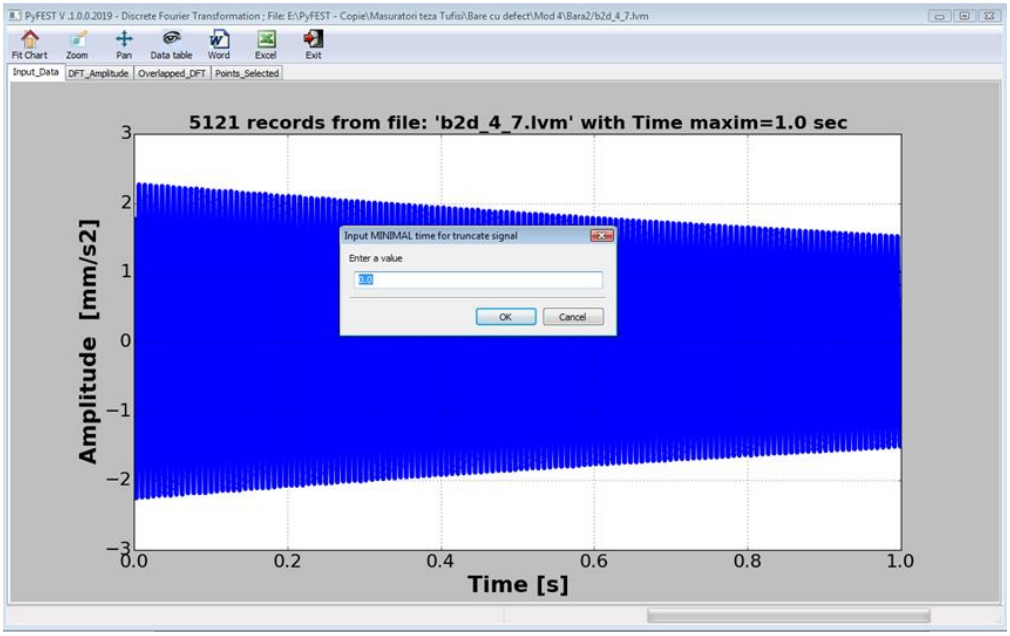

Figure 4.11. Imported signal

The largest amplitude and the matching raw frequency are shown By taking the necessary step, described at point f, starts the signal processing and the results are displayed in a new window.

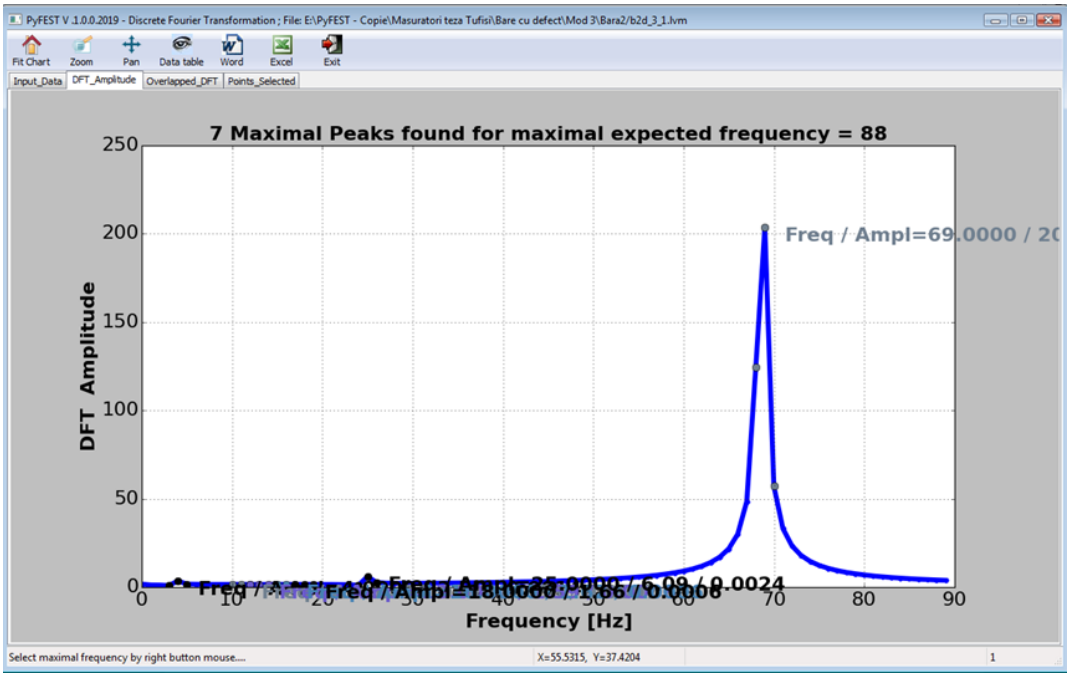

Figure 4.12. Acquired standard DFT signal

The calculated peaks are showed using diverse colors in relation with the number of cycles contained in the cut signal.

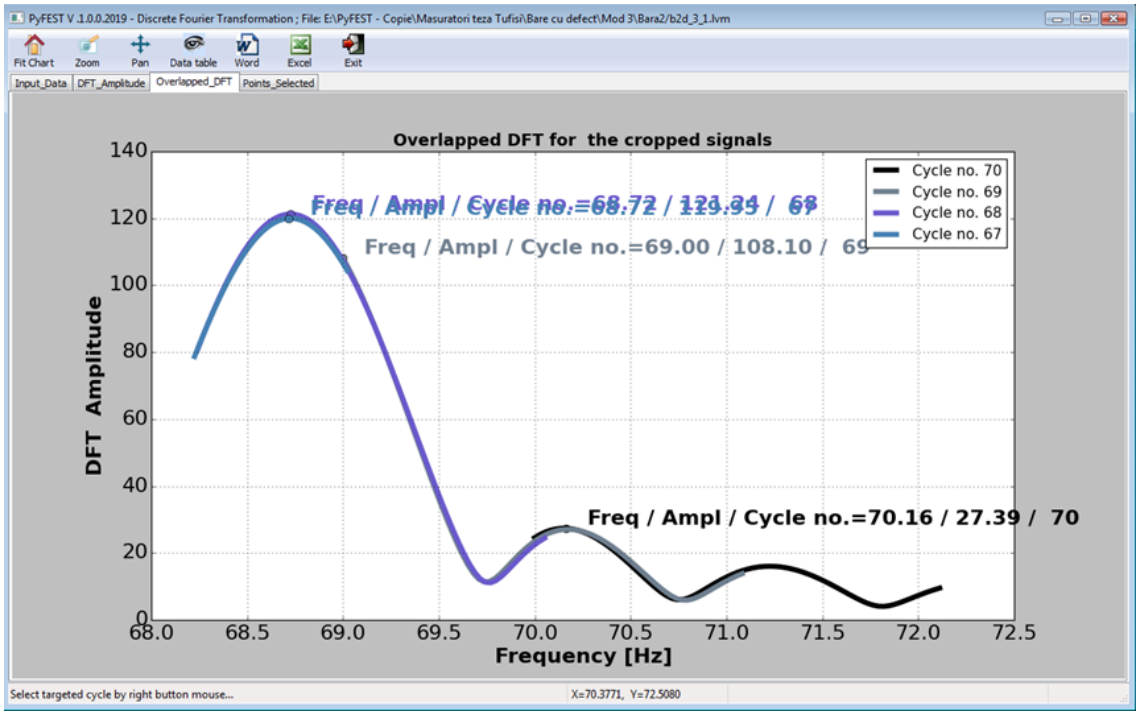

Figure 4.13. A window displaying the overlapped DFT

Figure 5.14 illustrates the window displaying the amplitudes calculated for the selected number of cycles and the maximum derived from the regression curve. The estimated frequency, the amplitude and the real amplitude calculated in function of the number of samples contained in the signal are displayed.

4.1.2. The developed damages

The fabrication process used for generating the damages in the beams is Wire-cut electrical discharge machining, due to the fact that the desired geometry needs to replicate a real crack caused by natural degradation of structures. The specimens were machined at a company situated near Resita, namely s.c. Centrul de Prelucrari Mecanice Bocsa s.r.l.

EDM is a machining process based on erosion caused by electrical discharge sparks developed by the tool electrode which is basically a brass wire that is fed through the workpiece submerged in a tank of dielectric fluid. The wire is constantly fed from a spool and held by upper and lower diamond guides that are allowed to move in the x-y plane.

This method was chosen because of its high precision of 0.004 mm, and because of the obtained kerf of 0.335 mm obtained by using a Ø0.25 wire, which makes it suitable for developing small width cracks. This process causes low residual stress in the material, then other methods and little change in the mechanical properties is expected due to the low stress. In figure 4.15 the machined T-shaped crack in Beam 2 using the described process is illustrated.

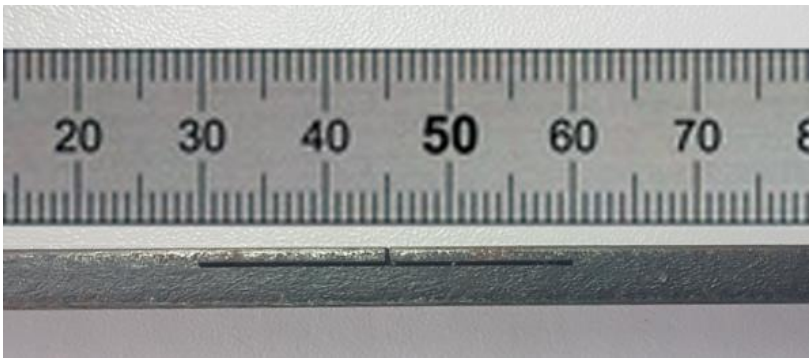

Figure 4.14. Machined T-shaped crack in Beam 2

For the current experiments T-shaped cracks positioned at x=210 mm from the clamping end of the beam were considered. The crack positions and dimensions are shown in Figure 4.16 for Beam 1 and in figure 4.17 for Beam 2.

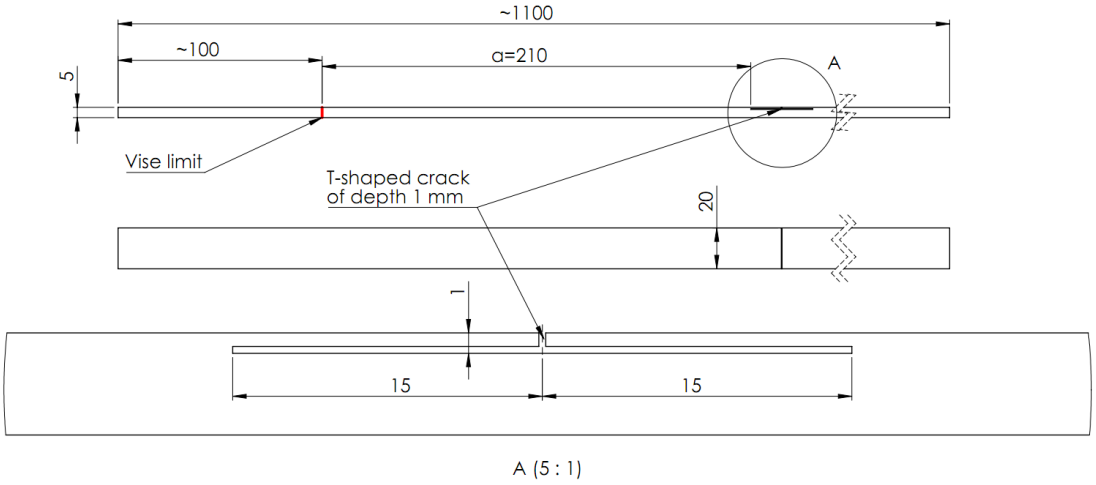

Figure 4.15. Crack geometry generated in Beam 1

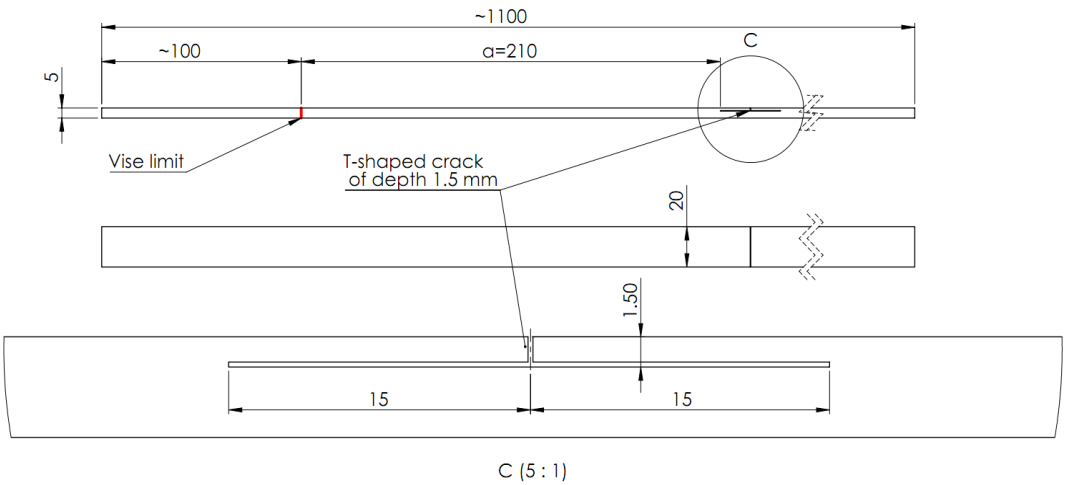

Figure 4.16. Crack geometry generated in Beam 2

As one can observe from the previous figures, the cracks generated in both beams are composed from a transversal element of defined depth followed by two equal and opposite branches oriented at 90°, only difference is the depth of the crack, for the first beam the depth is a=1 mm and for the second a=1.5 mm. In order to have a good fixing of the cantilever, the test specimens have been cut to a length of L=1100 mm, in order to grip 100 mm of the beam's length.

It is true that transversal cracks followed by 90° branches are most commonly to occur in composite materials, at the bonding interface, but for the purpose of this study the aim is to replicate these crack geometries in steel beams in the scope of evaluating the developed algorithm to detect complex-shaped cracks in isotropic materials.

4.2. Obtained results

Natural frequency measurements were performed on the two steel beams, cut from 20x5 mm flat strip with a length of ~ 1100 mm. To identify the measurements, the beams were marked with dots corresponding to the beam number. Given that the length of the beam for which the measurements were made is 1000 mm, the remaining ~ 100 mm being the embedded portion (caught in the vise), each beam was drawn and measured at 1000 mm from each end. Thus, for a single beam two sets of natural frequency measurements were obtained, two for the undamaged beams and two for the damaged ones. The accelerometer was mounted by using special adhesive and the frequencies for every mode of vibration have been measured and recorded using the virtual instruments.

At least ten natural frequency readings were made for each specimen, for each reading the first five natural frequencies of the beam were extracted, and the values were entered in a table. For each mode of vibration, the arithmetic mean of the their ten read values were compared with the value obtained from the PyDAM application, respectively from the numerical modal analysis.

Figure 4.17. Measurement of the natural frequencies of Beam 1 on the experimental stand

The measured values are the natural frequencies and amplitudes for the undamaged cantilevers presented in table 4.3 for Beam 1 and in table 4.4 for Beam 2.

Table 4.3. Natural frequency measurements for undamaged Beam 1

Mode 1		Mode 2		Mode 3		Mode 4		Mode 5	
Freq.	Ampl.	Freq.	Ampl.	Freq.	Ampl.	Freq.	Ampl.	Freq.	Ampl.
3.9099	0.013	25.0336	0.0955	70.0312	1.0589	136.9726	0.4013	226.9272	1.0113
3.9122	0.03	25.0298	0.1982	70.0469	0.83	136.9774	0.2866	226.9023	2.3885
3.9189	0.0308	25.0362	0.1608	70.0833	0.5255	136.9767	0.2532	226.8998	2.3408
-	-	25.031	0.2174	70.0618	0.6986	136.9842	0.166	226.9186	1.1823
-	-	25.031	0.215	70.0721	0.621	136.9849	0.3523	226.9197	0.9275
-	-	25.0309	0.2221	70.0613	0.7106	136.9856	0.4347	226.9098	1.3734
-	-	25.0325	0.2197	70.0753	0.5934	137.001	0.3443	226.9157	0.8838
-	-	25.0313	0.2245	70.0758	0.5934	137.0082	0.3284	226.9181	0.832

Except for mode number one, at least ten natural frequency readings were made for each mode of vibration and the values were recorded.

Table 4.4. Natural frequency measurements for undamaged Beam 2

Mode 1		Mode 2		Mode 3		Mode 4		Mode 5	
Freq.	Ampl.	Freq.	Ampl.	Freq.	Ampl.	Freq.	Ampl.	Freq.	Ampl.
3.91	0.0327	24.7539	0.3089	69.2201	0.1791	135.8909	2.6911	224.3852	0.2544
3.8973	0.0401	24.7568	0.1959	69.2194	0.1692	135.8952	2.6115	224.3985	0.5111
3.8998	0.0413	24.755	0.2349	69.2152	0.2245	135.8996	2.5318	224.3606	0.371
-	-	24.7545	0.2269	69.2177	0.1982	135.8981	2.5796	224.3677	0.2305
-	-	24.7545	0.2349	69.2147	0.2006	135.8975	2.4721	224.379	0.414
-	-	24.7559	0.1911	69.2156	0.1959	135.9935	0.5414	224.3708	0.1871
-	-	24.7576	0.1576	69.2145	0.2126	135.9721	0.836	224.3845	0.422
-	-	24.7528	0.3121	69.2137	0.215	135.875	3.4833	224.3945	0.4777

After measuring the natural frequencies for the undamaged cantilever beams, the mean value was calculated and is further considered for comparison with the results obtained by analytic and FEM calculations for the same idealized beams. The comparison is presented in Table 4.5.

Table 4.5. Comparison between the obtained natural frequencies

Mode no.	Measured Beam 1	Measured Beam 2	FEM	Analytical
1	3.913667	3.902367	4.0813	4.076903
2	25.0332	24.75523	25.574	25.54952
3	70.0538	69.21823	71.597	71.53938
4	136.9756	135.8952	140.27	140.1886
5	226.9098	224.3814	231.81	231.7419

It can be observed from table 4.5 that the measured frequencies are smaller than the ones obtained by FEM and calculation, this is due to the test specimens' homogeneity, unperfect surface quality and edge radius, however the damage signature should remain the same.

After each undamaged beam has been analyzed, the corresponding T-shape crack was made using EDM with the help of the company Machining Center Bocsa, thus generating the cracks with a very high level of precision, resulting for a single beam two sets of measurements, respectively two cases to be analyzed.

The two test beams were rigourously verified for any imperfections or unwanted damages that may have occurred in the machining process. The measured frequencies and amplitudes for the two damaged beams are presented in Tables 4.6 and 4.7.

Table 4.6. Natural frequency measurements for damaged Beam 1

Mode 1		Mode 2		Mode 3		Mode 4		Mode 5	
Freq.	Ampl.	Freq.	Ampl.	Freq.	Ampl.	Freq.	Ampl.	Freq.	Ampl.
3.7761	0.0955	25.0305	0.1409	68.7153	0.0753	133.5249	0.0589	224.5396	0.1027
3.7927	0.0312	25.0310	0.1576	68.6995	0.078	133.4732	2.8025	224.5334	0.1967
3.774	0.0384	25.0332	0.0502	68.5635	0.5912	133.5109	1.3296	224.5446	0.2866
3.7785	0.0354	25.0309	0.2054	68.5651	0.6628	133.5156	0.7683	224.5078	0.1799
		25.0325	0.1791	68.5618	0.8181	133.5272	0.5541	224.4531	0.1081
		25.0313	0.1505	68.5595	0.8539	133.5253	0.2691	224.4639	0.1451
		25.0342	0.1194	68.5651	0.7345	133.4994	1.8989	224.4730	0.1191
		25.0311	0.1911	68.5634	0.8061	133.4897	2.2333	224.4629	0.1461

Table 4.7. Natural frequency measurements for damaged Beam 2

Mode 1		Mode 2		Mode 3		Mode 4		Mode 5	
Freq.	Ampl.	Freq.	Ampl.	Freq.	Ampl.	Freq.	Ampl.	Freq.	Ampl.
3.6451	0.215	24.7404	0.3201	67.0957	0.1473	130.0769	0.042	220.0171	0.1105
3.6468	0.203	24.7437	0.3344	67.0815	0.4554	130.0533	0.3328	220.0803	0.4849
3.6608	0.0304	24.7536	0.4045	67.0743	0.9954	129.9767	3.2643	220.0171	0.1099
3.6553	0.0402	24.7545	0.4076	67.09	0.209	129.9921	1.9586	220.0604	0.4359
-	-	24.7541	0.4204	67.0747	0.621	130.0267	0.8559	220.1006	1.2122
-	-	24.7313	0.3535	67.0745	0.8897	130.0074	1.2838	220.0577	0.4538
-	-	25.7342	0.3044	67.0802	0.3392	129.9874	2.2572	220.0111	1.5318
-	-	25.7311	0.3045	67.0834	0.2946	129.9802	3.1688	220.0895	0.8838

The values of the measured natural frequencies for the damaged beams were compared to the same intact beams and the measurements have been plotted and illustrated for Beam 1 in Figure 4.19 and for Beam 2 in Figure 4.20. Here, the blue points represent the measured frequency and amplitude values for the undamaged beam cases and the orange dots represent the frequency and amplitude values for the damaged beam cases.

It was observed from the plotted graph, that the frequency values follow a strate line, for any measured amplitude value, validating that the obtained results are correct and follow the analytical and FEM achieved results.

For the second mode of vibration the frequency values for the damaged beams are close to those achieved for the undamaged cantilever; this is because the damage is positioned at an inflection point. The FEM results show the same fenomen.

Comparing the results regarding the location of the damage on the beam obtained by measurements and the undamaged beams in Figures 4.18 and 4 it was found that by using a single accelerometer placed on a tes, the comparison of measured frequencies, with a database previously determined by the location and assessment of the depth of the damage by the proposed method is very efficient.

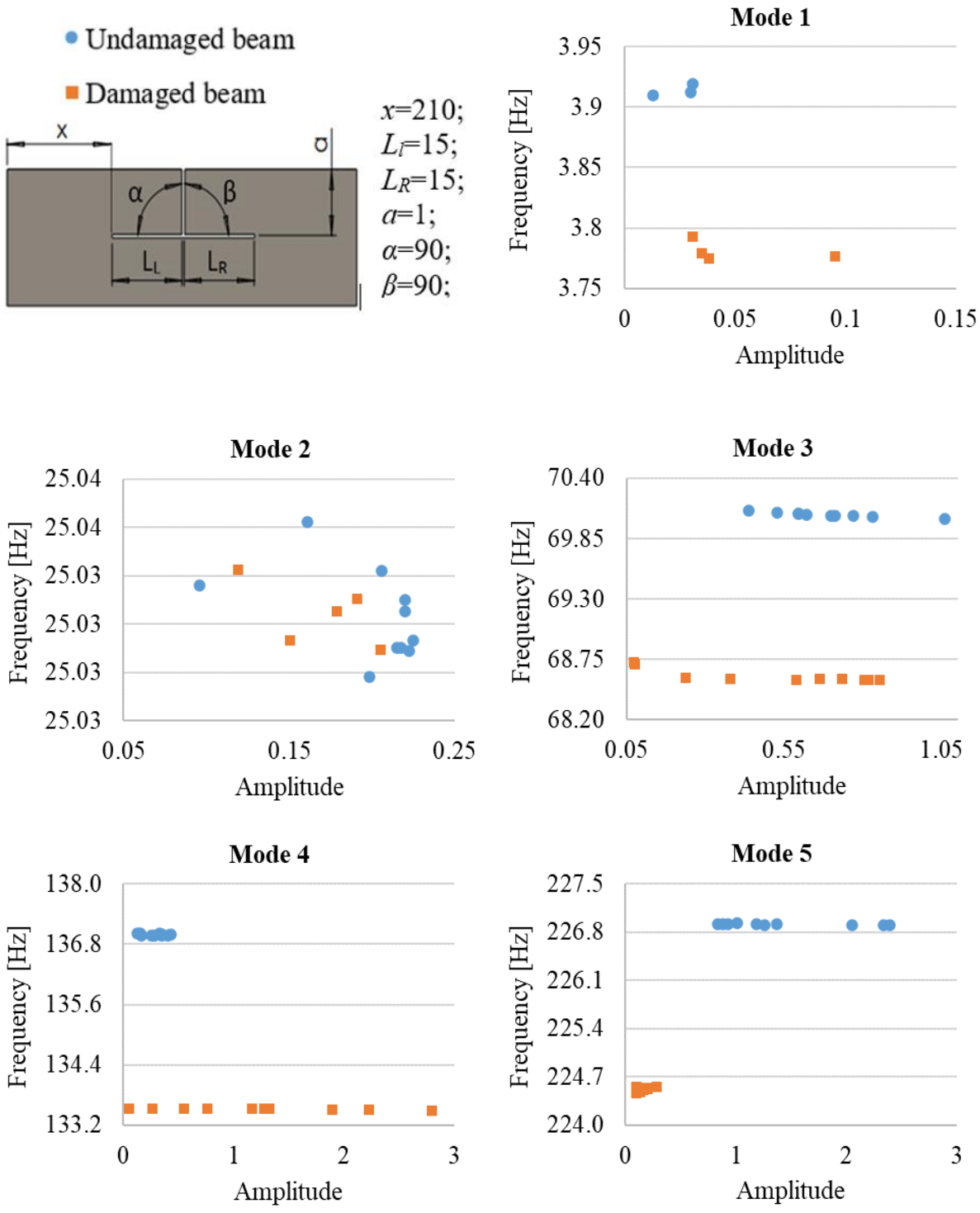

Figure 4.18. Measurement of the natural frequencies of Beam 1 on the experimental stand

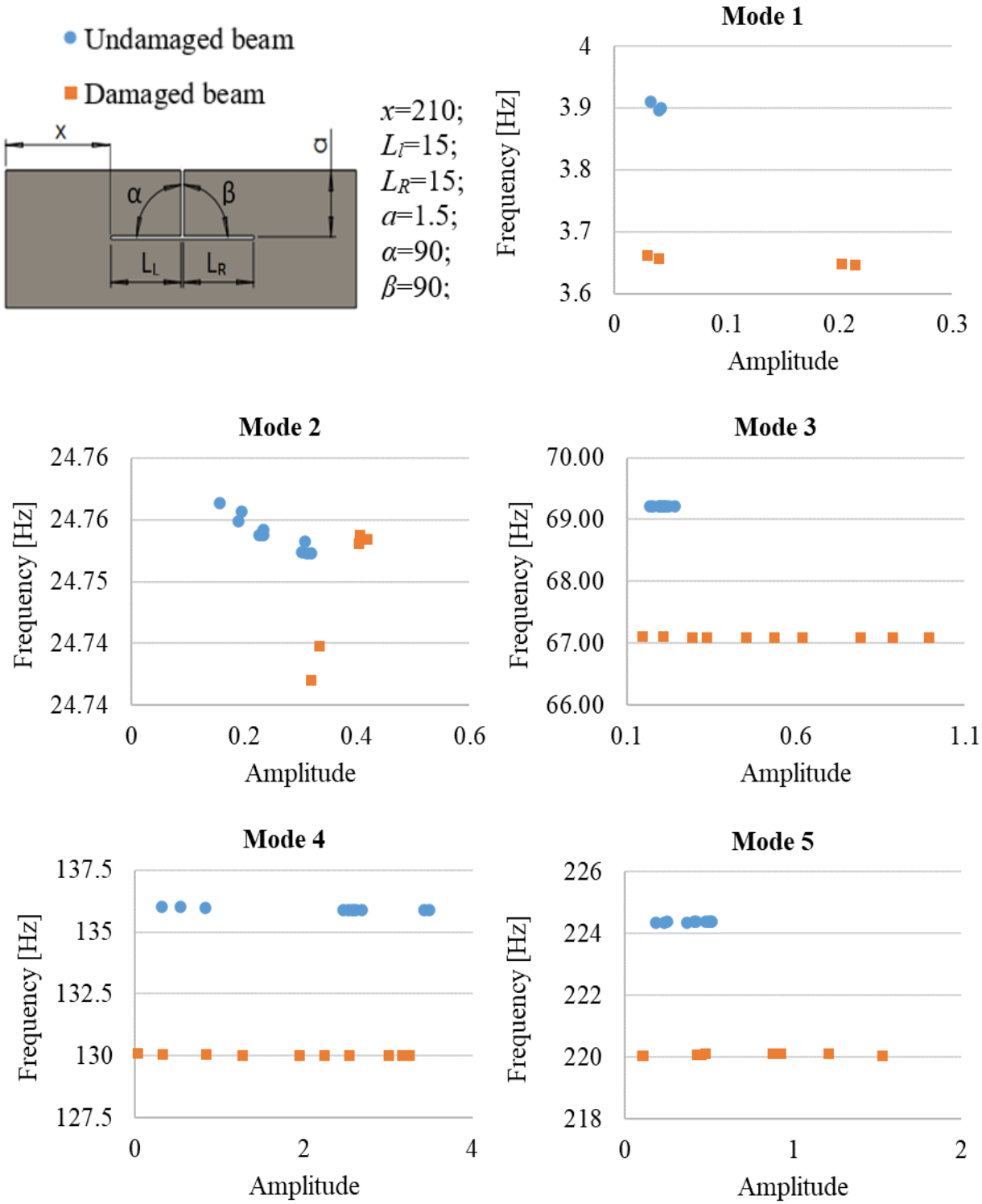

Figure 4.19. Measurement of the natural frequencies of Beam 2 on the experimental stand

The average frequency values for the two beams, both in damaged and healthy state, have been compared in tables 4.8 and 4.9:

Table 4.8. Natural frequency measurements for the two tests

Mode number	Beam 1			Beam 2		
	Undamaged frequency [Hz]	Damaged frequency [Hz]	Percent difference	Undamaged frequency [Hz]	Damaged frequency [Hz]	Percent difference
1	3.91366	3.78093	3.39%	3.90236	3.65090	6.44%
2	25.0332	25.0038	0.12%	24.7552	24.7459	0.04%
3	70.0538	68.6594	1.99%	69.2182	67.0838	3.08%
4	136.975	133.503	2.54%	135.895	130.035	4.31%
5	226.909	224.539	1.04%	224.381	220.038	1.94%

The comparison between the measured natural frequency, FEM and PyDAM results for the two damaged cantilevers are presented in Table 4.9 for Beam 1 and in Table 4.10 for Beam 2.

Table 4.9. Natural frequency measurements for damaged Beam 1

Mode no.	Measured natural frequencies [Hz]	Natural frequencies obtained using FEM [Hz]	Natural frequencies obtained using PyDAM [Hz]
1	3.78093	3.969208	3.934873
2	25.0038	25.57969	25.54136
3	68.6594	70.69365	70.23043
4	133.503	137.2701	135.8413
5	224.539	229.4407	228.146

Table 4.10. Natural frequency measurements for damaged Beam 2

Mode no.	Measured natural frequencies [Hz]	Natural frequencies obtained using FEM [Hz]	Natural frequencies obtained using PyDAM [Hz]
1	3.65090	3.864119	3.798414
2	24.7459	25.57532	25.53281
3	67.0838	69.78494	68.96101
4	130.035	134.61	131.6721
5	220.038	227.491	224.649

The set of values calculated from the measured frequencies for the relative deviation are passedin the table and compared with the numerically determined sets of values in the database previously created and the results obtained using the PyDAM application.

Representing graphically the values of the relative frequency shift for every corresponding vibration mode one can obtain the graph of the tendency of the relative deviation of natural frequencies. This graph allows us to accurately assess the location of the damage along the beam.

In order to evaluate the obtained frequencies, the relative frequency shift (RFS) values were calculated using relation 3.41 for the obtained frequencies, and compared them graphically in figures 4.21 and 4.22.

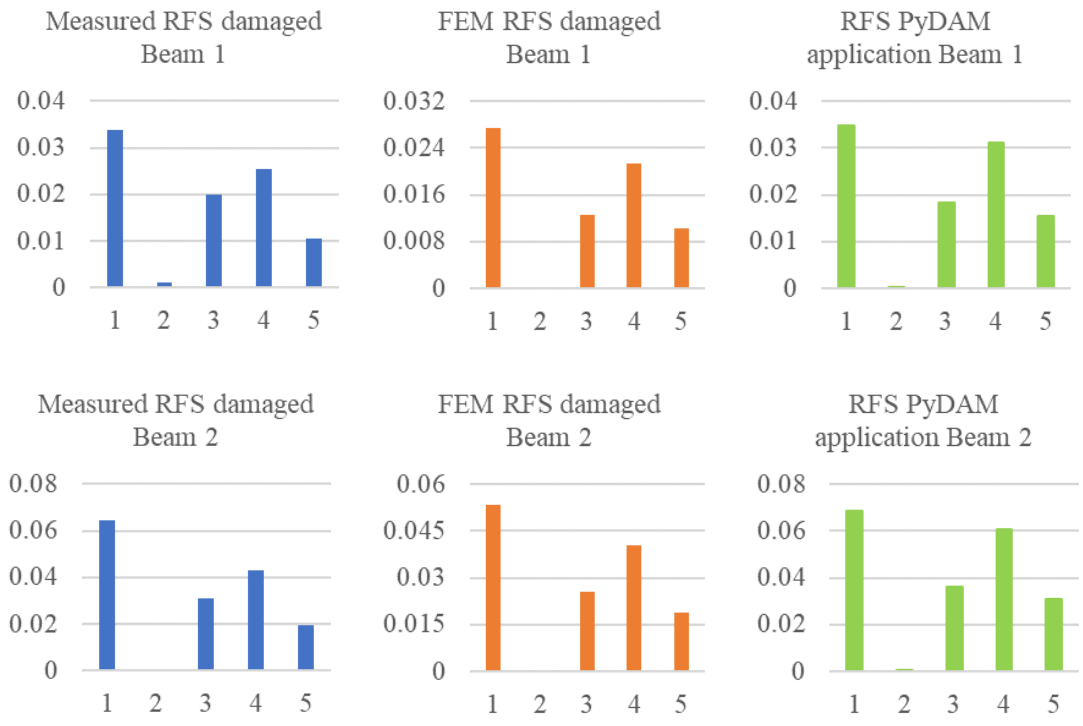

Figure 4.20. Obtained RFS values for the damaged beams

To have comparable values, the Damage Location Coefficients are calculated by dividing the values of the RFS for a given case to the biggest value in the series.

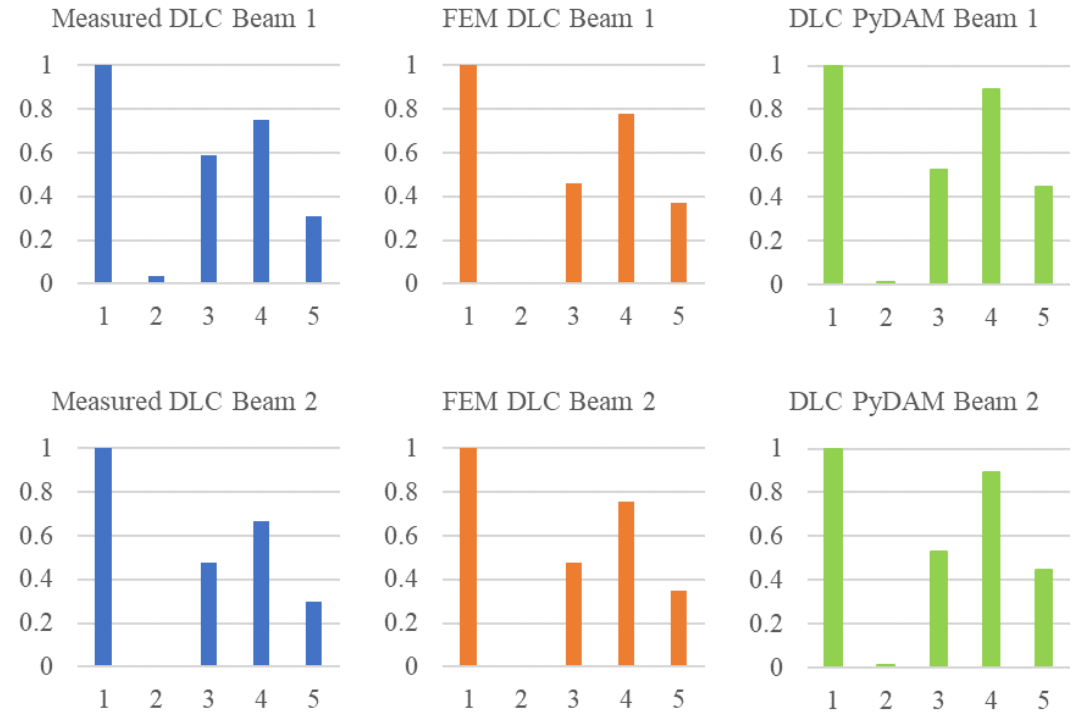

Figure 4.21. Obtained DLC values for the damaged beams

4.3. Conclusions

By applying the frequency estimation method with the help of the PyDAM software, it was observed that small changes in frequency values are easely depicted. A very good example is the obtained frequency values, concerning the second mode of vibration, for the two damaged beams from the plotted RFS graphs in Figures 4.21 and 4.22 which show that the frequency drop obtained with the help of the PyDAM software is the same with the measured frequency drop.

Through the described excitation system the resonant frequencies are generated in the test specimens, which allow attaining large amplitudes, however, using this method, in the same time they do not exceed the resonance limit, avoiding nonlinear vibrations.

In order to ensure that the measured frequency values are constant despite the obtained amplitude, different recording delay times were taken into consideration. This means that after the excitation is stopped, different waiting intervals, between 0 and 5 seconds are taken in order to achieve different amplitudes, before the frequency is recorded.

For the small frequency values, such as the first mode of vibration it was not possible to stimulate the beams using the developed system, thus it was necessary to excite the test specimens by using impulse excitation.

The experimental results confirmed the validity of the developed theoretical model and allowed the recognition of the damage and the determination of the respective position of the longitudinal branch of the crack.

5. General conclusions and original contribution

5.1. Conclusions

The doctoral thesis addresses the topic of vibration-based methods for assessing complex-shaped cracks, which take into account the modifications of the modal parameters of structures. In this respect, the simulations aimed to contribute to a better understanding of the dynamic behavior of beams whith various types of geometrical discontinuities. Whith this knowledge, a analytical model of a beam with branched cracks is developed and implemented in a robust and accurate damage detection method, which permits observation of the crack occurrence and assessment of its depth and longitudinal extent. Laboratory experiments confirmed the validity of the model and it was possible to assess branched cracks.

Each step of the research was designed to cover the specific thesis objectives. The research outcomes have led to the following conclusions:

- The longitudinal extent increses significantly the frequency shift produced by branched cracks, so that the branched cracks are easier observable as the transverse cracks.
- The delamination position has the significant contribution to the frequency drop.
- The position of the transverse component of the crack (located between the delamination ends) has a small effect on the frequency decrease, and so relative frequency shift curve evolution is defined by the delamination position rather than by the position of the transverse component of the crack.
- The dimension of the transverse component of the crack is less important as depth at the delamination ends in defining the frequency drop.
- The smallest frequency changes were found for the delamination located around the inflection points, where the beam faces less stress, thus the crack has a low effect.
- The analytic model has to consider along with the stiffness decrease in the affected segment also the margin effects, since at the delamination ends, on the ‘healthy segments’, are slices that do not contribute to the global stiffness.
- The crack depth determines the damage severity, which is a parameter independent to the crack location, hence it controls the amplitude of the frequency shift curves. On the other hand, the shape of these curves is controlled by the crack location and the vibration mode number. A crack with a given depth differently affects the natural frequency of a vibration

mode if it is placed in different beam slices. Regarding the crack with defined depth and position, it differently affects the natural frequencies of different vibration modes.

- The proposed model works until the extent of the longitudinal crack component exceeds a given length. That diferes for cracks located on nodes and on antinodes. For the beam analysed in this thesis, the maxim number for bending vibration modes for which the model works is five.
- The natural frequency shifts of beams due to branched cracks constitute a reliable indicator, signalizing the appearance of damage and information about the position and severity. From this indicator, it is possible to observe when the crack changes the propagation direction.
- Each branched crack damage has its own signature, so it is possible to define a database that can be used as a reference base for use in damage detection methods.

In this thesis, the personal original contributions are:

- The proper approach was defined after a comprehensive literature analysis, and the *natural frequencies were selected* as the relevant modal parameter.
- Typical branched cracks are idealized and parameters (dimensions and angles) associated to them, resulting in *geometric models* with higher or lower degree of generality.
- An *analytic model* was designed, which can be used to calculate the natural frequencies of beams affected by branched cracks when the crack depth, extent and position are known. The model is valid for any type of the beam's supports.
- A *coeffcients* to calculate the effect of the stiffness reduction on the beam segment with the longitudinal component is deduced analytically.
- The effect of the stress distribution at the ends of the longitudinal component of the crack is highlighted and *coefficients* to calculate this effect are determined empirically.
- An *application in Python language* to calculate the coefficients contained in the analytical beam model was developed.
- An informatical-instrumental *method for estimating the natural frequencies* of beams was and developed; it involves controlled acoustical excitation of the beam and estimation of the frequencies on an interline position in the spectrum.
- The *analytical model is validated* by comparing the frequencies obtained with it with the results achieved by simulation and laboratory experiments.
- The *damage detection method is validated* since branched cracks are succefully assessed by laboratory experiemnts on real beams.

The results of the research were disseminated in journals (3 ISI and 2 BDI) and conferences (8 Scopus and 3 BDI), as presented below:

Journal aricles

1. Gillich G.R., **Tufisi C.**, Lupu D., Hamat C.O., *Assessing the accuracy of a new model for T-shaped cracks*, Romanian Journal of Acoustics and Vibration, 16(2), 2019, pp. 119-124 (ISI)

2. Gillich N., **Tufisi C.**, Vasile O., Gillich G.R., *Statistical method for damage severity and frequency drop estimation for a cracked beam using static test data*, Romanian Journal of Acoustics and Vibration, 16(1), 2019, pp.47-51 (ISI)

3. **Tufisi C.**, Gillich G.R., Hamat C.O., Gillich N., Praisach Z.I., *Numerical Study of the Stiffness Degradation Caused by Branched Cracks and its Influence on the Natural Frequency Drop*, Romanian Journal of Acoustics and Vibration, 15(1), 2018, pp. 53-57 (ISI)

4. **Tufisi C.**, Gillich G.R., *A numerical study regarding the influence of the longitudinal extent of a T-shaped crack on the eigenfrequency decrease of cantilever beams*, Journal of Engineering Studies and Research, 24(4), 2018, pp. 50-55 (Index Copernicus)

5. **Tufisi C.**, Gillich G.R., *Modeling of complex shaped cracks*, Analele Universitatii Eftimie Murgu. Fascicula de Inginerie, 25(2), 2018, pp. 155-162 (Index Copernicus)

Conference proceedings papers

1. **Tufisi C.**, Gillich G.R., *A new concept regarding the modeling of beams with branched cracks*, European Workshop on Structural Health Monitoring, Palermo, Italy, Special Collection of 2020 papers, to be published by November 2020

2. **Tufisi C.**, Gillich G.R., Hamat C.O., Manescu T., *Study Regarding the Effect of Crack Branching on the Eigenfrequencies of Beams*, 13th International Conference on Damage Assessment of Structures, 9-10 July 2019, Porto, Portugal, Published in: Lecture Notes in Mechanical Engineering, 2020, pp. 79-91 (Scopus)

3. Gillich G.R., Aman A.T., Abdel Wahab M., **Tufisi C.**, *Detection of Multiple Cracks Using an Energy Method Applied to the Concept of Equivalent Healthy Beam*, 13th International Conference on Damage Assessment of Structures, 9-10 July 2019, Porto, Portugal, Published in: Lecture Notes in Mechanical Engineering, 2020, pp. 63-78 (Scopus)

4. Barbinta C.I., **Tufisi C.**, Hamat C.O., Nedelcu D., Gillich G.R., *Sensitivity analysis for frequency-based prediction of cracks in open cross-section beams*, 41st International JVE Conference, 30 September – 1 October, 2019, Leipzig, Germany, Published in: Vibroengineering Procedia, Vol. 27, 2019, pp.7-12 (Scopus)

5. **Tufisi C.**, Gillich G.R., Hamat C.O., Gillich N., Nedelcu D., *Exact solution for the severity of transverse cracks in prismatic beams*, International Conference on Applied Sciences, 9–11 May 2019, Hunedoara, Romania, Published in: Journal of Physics: Conference Series, Vol. 1426, 2020, art. no. 012023 (Scopus)

6. **Tufisi C.**, Gillich G.R., Aman A.T., *The effect of a crack near the fixed end on the natural frequencies of a cantilever beam*, 37th International JVE Conference, 25-26 April 2019, Bratislava, Slovakia, Published in: Vibroengineering Procedia, Vol. 23, 2019, pp. 37-42 (Scopus)

7. **Tufisi C.**; Nedelcu D., Gillich G.R., *Appraising the accuracy of a novel model for L-shaped cracks*, 43rd International Conference on Mechanics of Solids, 21-22 November 2019, Brasov, Romania, Published in: COMEC 2019, Vol. I, pp. 133-139 (Index Copernicus)

8. **Tufisi C.**, Gillich G.R., Nedelcu D., *Effect of the orientation of an oblique crack branches on the beam eigenfrequencies*, 1st International Conference on Circuits, ICMSAV 2018 & COMAT 2018 & eMECH 2018, 25-26 October 2018, Brasov, Romania, Published in: COMAT 2018, pp. 97-102 (Index Copernicus)

9. **Tufisi C.**, Gillich G.R., Nedelcu D., Hamat C.O., *Numerical study on complex shaped cracks in cantilever beams concerning frequency and stiffness changes*, 33rd International Conference on Vibroengineering, 24-26 September 2018, Zittau, Germany, Published in: Vibroengineering Procedia, Vol. 19, 2018, pp. 253-258 (Scopus)

10. Gillich G.R., **Tufisi C.**, Korka Z.I., Hamat C.O., Gillich N., *Automatic detection of L and T shaped cracks in semifinished casting products*, The 10th International Symposium Machine and Industrial Design in Mechanical Engineering (KOD 2018), 6–8 June 2018, Novi Sad, Serbia, Published in: IOP Conference Series: Materials Science and Engineering, Vol. 393, 2018, art. no. 012016 (Scopus)

11. **Tufisi C.**, Gillich,G.R., Vasile O., Korka Z.I., Hamat, C.O., *Identification of Delamination in Multilayered Composites*, 7th International Conference on Advanced Materials and Structures - AMS 2018, 28–31 March 2018, Timisoara, Romania, Published in: IOP Conference Series: Materials Science and Engineering, Vol. 416, 2018, art. no. 012045 (Scopus)

References

1. Actis R.T.; A.D. Dimarogonas. *"Non-linear Effects Due to Closing Cracks in Vibrating Beams"*, ASME Design Engineering Division Publication DE-Srructural Vibration and Acoustics, V. 18, No.3, pp. 99-104, 1989;
2. Allemang R.J.; Brown D.L., *A correlation coefficient for modal vector analysis*, Proceedings of the 1st International Modal Analysis Conference, SEM Orlando, p.110-116, 1982;
3. Al-Waily M., Theoretical *and Experimental Vibration Study of Continuous Beam With Crack Depth and Location Effect*, Indian Journal of Applied Research, Volume 3, Issue 9, ISSN-2249-555X, 2013;
4. Arvid H., *Structural Health of Bridges, Monitor, Assess and Retrofit*, Unpublished Licentiate Thesis, Department of Civil and Environmental Engineering, Division of Structural Engineering, 2004;
5. Baardman R.H., *3D Ultrasonic Imaging of Defects in Welds by Inverse Wave Field Extrapolation*, M.Sc.Thesis, Faculty of Applied Physiscs Delft University of Technology, 2007;
6. Balageas, D.; Fritzen C-P.; Guemes A., *Structural Health Monitoring*, ISBN-13: 978-1-905209-01-9, ISTE Ltd., 2006;
7. Banks H.T.; Inman D.J.; Leo D.J.; Wang, Y.,'*An experimentally validated damage detection theory in smart structures*, Journal of Sound and Vibration, vol. 191, no. 5, pp. 859-880, 1996;
8. Baughurst L.,*Welding Defects, Causes & Correction*, The ASEAN Patent Examination Co-operation (ASPEC), Engineering Technical Article, October, 2011;
9. Bratu P., *Elastic systems vibrations*, Technical Publishing House, Bucharest, 2000;
10. Catbas N.; Aktan A.E.; Allemang R.J., Brown D.L., *A Correlation Function for Spatial Locations of Scaled Mode Shapes (COMEF)*, Proceedings of SPIE - The International Society for Optical Engineering Vol. 2, pp.690-695, January 1998;
11. Cawley P.; Adams R.D., *The locations of defects in structures from measurements of natural frequencies*, The Journal of Strain Analysis for Engineering Design, Vol. 14(2), p.49-57, 1979;

12. Choi S.; Park S.; Stubbs N., *Non-destructive Damage Detection in Structures using Changes in Compliance'*, International Journal of Solids and Structures, Vol. 42 p.4494-4513, 2005;
13. Chondros T.J.; Dimarogonas A.D; Yao J., *A continuous cracked beam vibration theory*, Journal of Sound and Vibration, Vol. 215(1), p. 17–34, 1998;
14. Clark A. B. J.; Irwin G. R., *Crack-propagation behaviors,* Experimental Mechanics, Vol. 6, p.321-330, 1996;
15. Crema L.B.; Castellani A.; Coppotelli G., *Damage localization in composite material structures by using eigenvalue measurements.* Materials and Design Technology ASME PD-71, pp. 201–205, 1995;
16. De Alba Alvarez R.O.; Ferguson N.S.; Mace B.R., *A robust spot weld model for structural vibration analysis*, Finite Element Analysis Design, 89:1–7, 2014;
17. Doquet V.; Bertolino G., *Local approach to fatigue cracks bifurcation" LMS, Ecole Polytechnique, UMR CNRS 7649, 91128 Palaiseau cedex, France,2007;*
18. Farrar C.R.; James G.H., *System identification from ambient vibration measurements on a bridge*, Journal of Sound and Vibratiuon, Vol. 205, p.1–18, 1997;
19. Friswell M.I.; Penny J.E.T.; Wilson D.A.L., *Using Vibration data and Statistical Measures to Locate Damage in Structures*, Modal Analysis: The International Journal of Analytical and Experimental Modal Analysis, Vol.9(4), p. 239–254, 1994;
20. Friswell, M.I., *Damage identification using inverse methods*, Philosophical Transactionsof the Royal Society A, Vol. 365, p. 393-410, 2007;
21. Gibson R.F., *Modal vibration response measurements for characterization of composite materials and structures*, Composite Science and Technology, Vol. 15(60), p. 2769–2780, 2000;
22. Gillich G.R., *Dinamica masinilor*, Vibratii, Editura AGIR, Bucuresti, 2005;
23. Gillich G.R.; Gillich N.; Birdeanu E.D.; Iancu V., *Detection of damages in simple elements*, Annals of DAAAM and Proceedings of the International DAAAM Symposium, Vol. 20, 2009, pp. 623-624, 2000;
24. Gillich G.R.; Praisach Z.I.; Onchis D., *About the Effectiveness of Damage Detection Methods Based on Vibration Measurements*, Proceedings of the 3rd WSEAS International Conference on Engineering Mechanics, Structures, Engineering Geology (EMESEG'10), Corfu, pp. 22-24, 2010;

25. Gillich G.R.; Praisach Z.I.; Minda P.F.; Negru I., *The influence of damage location on the change of natural frequencies of beams*, Proceedings of the XI-th symposium, Acoustics and Vibrations Mechanical Structures AVMS-2011, Timişoara, ISSN: 1843-0902, 2011;
26. Gillich G.R.; Praisach Z.I.; Negru I.; Bîrdeanu E.D.; Gillich N., *Weak-Axis Bending Vibrations of Beams with Variable Cross-Section*, 1st International Conference on Circuits, Systems, Communications, Computers and Applications (CSCCA '12), "G. Enescu" University Iaşi, Romania, 2012;
27. Gillich G.R.; Praisach Z.I.; Iavornic C.M., *Reliable method to detect and assess damages in beams based on frequency changes*, Proceedings of the ASME 2012 International Design Engineering Technical Conferences & Computers and Information in Engineering Conference, IDETC/CIE 2012, Chicago, Illinois, USA, 2012;
28. Gillich G.R.; Praisach Z.I.; Amariei D.; *A method to detect and assess damage in beams based on frequency changes,* Proceedings of the Eleventh International Conference on Computational Structures Technology, Paper 77, Dubrovnik, Croatia, 2012;
29. Gillich G.R.; Minda P.F.; Praisach Z.I.; Minda A.A., *Natural frequencies of damaged beams - a new approach,* Romanian Journal of Acoustic and Vibration, Vol. IX, issue 2, pp.101-108, 2012;
30. Gillich G.R.; Praisach Z.I.; Negru I., *The relationship between changes of deflection and natural frequencies of damaged beams,* Proceedings of the 5th WSEAS International Conference on Finite Differences - Finite Elements - Finite Volumes - Boundary Elements (F-andB '12), Praga, Cehia, pp.38-42, 2012;
31. Gillich G.R.; Praisach Z.I., *Robust method to identify defects in beams based on frequency shift analysis*, SPIE Smart Structures and Materials & Nondestructive Evaluation and Health Monitoring, 83481D-12, San Diego, CL, USA. pp.12-15 march 2012;
32. Gillich G.R.; Praisach Z.I.; Bobos D.; Hatiegan C., *Assessment of corrosion damages with important loss of mass and influences on the natural frequencies of bending vibration modes,* Applied Mechanics and Materials Vol. 430, pp. 95-100, Trans Tech Publications, Switzerland, doi:10.4028/www.scietific.net/AMM.430.95, 2013;
33. Praisach Z.I.; Gillich G.R.; Ovidiu V.; Birdeanu D.E.; Protocsil C., *Assessment of damages in sandwich panels based on the damage location indexes Department of Mechanics, "Eftimie Murgu" University of Resita 2013;*

34. Gillich, G.R.; Praisach Z.I., *Damage-patterns based method to locate discontinuities in beams,* SPIE Smart Structures and Materials & Nondestructive Evaluation and Health Monitoring, Vol. 8695, March 2013, San Diego CA, 2013;
35. Gillich. G.R.; Praisach, Z-I., *Modal identification and damage detection in beam-like structures using the power spectrum and time–frequency analysis,* Signall Processing, Vol. 96, pp. 29-44, Elsevier, 2014;
36. Gillich G.R.; Wahab M.A., Praisach Z-I.; Htakpe J.L., *The influence of transversal crack geometry on the frequency changes of beams,* International Conference on Noise and Vibration Engineering, ISMA 2014, ID 666, 2014;
37. Gillich, G.R.; Praisach, Z.I.; Wahab, M.A.; *A new modal-based damage location indicator*, Conference: International Conference on Noise and Vibration Engineering (ISMA) Location: Leuven, Belgium, Date: SEP 15-17, 2014, Proceedings of International Conference on Noise and Vibration Engineering (ISMA2014) and International Conference on Uncertainty in Strucutral Dynamics (USD2014), pp. 499-512, 2014;
38. Gillich G.R.; Frunzaverde D.; Gillich N.; Ntakpe J.L.; Muntean F., *On the Influence of Damage-Caused Global Stiffness Decrease upon Structural Modal Parameters,* Advanced Materials Research Vol 1111 (2015), pp. 139-144, Trans Tech Publications, Switzerland, doi: 10.4028/ www.scientific.net/AMR.1111.139, 2015;
39. Gillich G.R.; Maia N.; Mituletu I.C.; Praisach Z.I.; Tufoi M.; Negru I., *Early structural damage assessment by using an improved frequency evaluation algorithm,* Latin American Journal of Solids and Structures, 12(12), pp. 2311-2329, 2015;
40. Gillich G.R.; Maia N.M.M.; Mituletu I.C.; Tufoi M.; Iancu V.; Korka Z.I., *A New Approach for Severity Estimation of Transversal Cracks in Multi-layered Beams,* Latin American Journal of Solids and Structures, 13(8, pp. 1526-1544), 2016;
41. Gillich G.R.; Praisach Z.I.; Iancu V.; Furdui H.; Negru I., *Natural frequency changes due to severe corrosion in metallic structures,* Journal of Mechanical Engineering, DOI:10.5545/sv-jme.2015.2674, Strojniski vestnik-Journal of Mechanical Engineering 61(2015)12, pp. 721-730, 2015;
42. Gillich; G.R., Muntean F.; Niţescu C.N.; Iancu V.; Prais```````ach Z.I.; Korka Z.I., *On the use of higher-order frequencies in crack identification in columns subjected to important tip mass,* Applied Mechanics and Materials (Volume 801), pp. 148-153, doi:10.4028/www.scientific.net/AMM.801.148, 2015;

43. Gillich G.R.; Praisach Z.I.; Wahab M.A.; Gillich N.; Mituleţu I.C.; Niţescu C.N., *Free vibration of a perfectly clamped-free beam with stepwise eccentric distributed masses,* Shock and Vibration Vol. 2016, Article ID 2086274, 2016;
44. Gillich G.R.; Tufoi M.; Korka Z.I.; Stanciu E.; Petrica A. *The relations between deflection, stored energy and natural frequencies, with application in damage detection*, Romanian Journal of Acoustics and Vibration, 13(2), pp. 87-93, 2016;
45. Gillich G.R.; Negru I.; Stanciu E.; Protocsil C.; Minda P. F., *Evaluarea integritatii structurilor mecanice,* Colectia Orizonturi Tehnice, Editura Eftimie Murgu Resita 2018;
46. Gillich G.R.; Tufisi C.; Gillich N., *Automatic detection of L and T shaped cracks in semifinished casting products*, IOP Conf. Series: Materials Science and Engineering, Vol. 393, 2018, art. 012016;
47. Gillich G.R.; Tufisi C.; Lupu D.; Hamat O. C., *Assessing the Accuracy of a New Model for T-Shaped Cracks,* Romanian Journal of Acoustics and Vibration, Vol. 16(2), pp. 119-124, 2019;
48. Gillich N.; Tufisi C.; Vasile O.; Gillich G.R., *Statistical Method for Damage Severity and Frequency Drop Estimation for a Cracked Beam using Static Test Data,* Romanian Journal of Acoustics and Vibration, 16(1), pp. 47-51, 2019;
49. Gillich G. R.; Tufisi C.; Maia N. M. M.; Aman A. T.; Korka Z. I., *Multiple crack detection in beams using the modal strain energy distribution,* Proceedings of the 13th International Conference on Damage Assessment of Structures: DAMAS 2019, 9-10 July 2019, Porto, Portugal;
50. Gillich G.R.; Aman A. T.; Wahab M. A.; Tufisi C., *Detection of multiple cracks using an energy method applied to the equivalent healthy beam* – Proceedings of the 13th International Conference on Damage Assessment of Structures: DAMAS 2019, 9-10 July 2019, Porto, Portugal;
51. Gillich G.R.; Nedelcu D.; Iancu V.; Gillich N., About the accuracy of estimated frequencies with the PyFest software, Annals of the „Constantin Brancusi" University of Targu Jiu, Engineering Series, No. 4 /2019;
52. Horia Furdui., *"Contributii privind influenta sarcinilor operationale si de mediu asupra detectării defectelor in grinzi,"* Universitatea „Eftimie Murgu" Reşiţa Facultatea De Inginerie si Management Departamentul De Mecanică si Ingineria Materialelor., Reşiţa 2016;

53. Hussam Saleem, *Vibration Based Damage Identification For Plate-Like Structures*, Washington State University Department Of Civil And Environmental Engineering, December 2011;
54. Kerkhof F., *Bruchvorgange* in Glasern, *Verlag der Deutschen Glastechnischen Gesellschaft*, Frankfurt am Main, 1970;
55. Kenley R. M.; Dodds C. J., *West Sole we platform: detection of damage by structural* response *measurements,*Proceedings of the 12th Annual Offshore Tech. Conf., pp. 111–118, 1980;
56. Kessler S.S.; Spearing S.M.; Atalla M.J.; Cesnik C.E.S.; and Soutis, *Damage detection in composite materials using frequency response methods*. Composites Part B: Engineering,Vol. 33, pp. 87–95, 2001;
57. Kim J.T.; Stubbs; N., *Model-uncertainty and damage-detection accuracy in plate girder,* Journal of Structural Engineering, vol. 121, no. 10, pp. 1409-1417, 1995;
58. Kim, J.T.; Stubbs N., *Improved damage identification method based on modal informatio',* Journal of Sound and Vibration, vol. 252, no. 2, pp. 223-238, 2002 ;
59. Kim J.T.; Stubbs N., *Crack detection in Beam-type Structures using frequency Data,* Journal of Sound and Vibration, vol. 259, no.1, pp. 145-160, 2013;
60. Kim T.H.; Lee K.M.; Chung, Y.S.; Shin H.M., *Seismic Damage Assessment of Reinforced Concrete Bridge Columns',* Engineering Structures, Vol. 27, pp. 576-592, 2005;
61. Khatir S.; Wahab M. A.; Boutchicha D.; Khatir T., *Structural health monitoring using modal strain energy damage indicator coupled with teaching-learning-based optimization algorithm and isogeometric analysis*, Journal of Sound and Vibration, Vol. 448, pp. 230-246, 2019;
62. Krawczuk M.; Ostachowicz W.M., *Parametric Vibration of Beam with Crack*, Archives of Applied Mechanics, Vol. 62, pp. 46-473, 1992;
63. Krawczuk M.; Ostachowicz W.M., *Forced Vibrations of a Cantilever Timoshenko Beam* with *a Closing Crack*, ISMA 19-Tools for Noise and Vibration Analysis, pp. 1067-1078, 1994;
64. Lichun B.; Farid T., *A proposed maximum ratio criterion applied to mixed mode fatigue crack propagation"* School of Mechanics, Yanshan University, Qinhuangdao, Hebei 066004, PR China / Department of Civil Engineering, Dalhousie University, Halifax, Canada NS B3J 1Z1, 2011;

65. Mehrisadat M. A., *Vibration-Based Structural Health Monitoring*, University of Technology, Sydney Faculty of Engineering and Information Technology, School of Civil and Environmental Engineering, 2015;
66. Mituleţu; I.C.; Gillich N.; Nițescu C.N.; Chincel C.P., *A multi-resolution based method to precise identify the natural frequencies of beams with application in damage detection*, Journal of Physics: Conference Series, Volume 628 , 11th International Conference on Damage Assessment of Structures, IOP Publishing, doi: 10.1088/1742-6596/628/1/012020; 2015;
67. Minda F.P.; Praisach Z.I.; Minda A.A.; Gillich G.R., *Methods of interpreting the Results of Vibration Measurements to Locate Damages in Beams*, Applied Mechanics and Materials Vol. 430, pp. 84-89, Trans Tech Publications, Switzerland, doi:10.4028/www.scietific.net/AMM.430.84, 2013;
68. Minda P.F.; Praisach Z.I.; Gillich N.; Minda A.A.; Gillich G.R., *On the Efficiency of Different Dissimilarity Estimators Used in Damage Detection*, Romanian Journal of Acoustics and Vibration, Vol. 10(1), pp. 15-18, 2013;
69. M.A.Wahab, "*Effect Of Modal Curvatures On Damage Detection Using Model Updating''* Mechanical Systems and Signal Processing, Vol. 15(2), pp. 439-445), 2001;
70. Niţescu C.N., *Cercetări privind identificarea defectelor la structuri sudate prin metode globale de control"* Universitatea „Eftimie Murgu" Reşiţa Facultatea De Inginerie si Management, Departamentul De Mecanică şi Ingineria Materialelor., Reşiţa 2017 ;
71. Oldrtich S.; Raul Bermejo, et al., *Prediction of the crack bifurcation in layered ceramics with high residual stresses"* Faculty of Mechanical Engineering, Brno University of Technology, Engineering Fracture Mechanics Vol. 108, pp.120–138, 2000 ;
72. Ostachowicz W.M.; Krawczuk M., *"Vibration Analysis of a Cracked Beam"*, Computers andStruetures. V. 36, No.2, pp. 245-250, 1990;
73. Pandey A.K.; Biswas M.; Samman M. M., *Damage detection from changes in curvature mode shapes*, Journal of sound and vibration, vol. 145(2), pp. 321-332, 1991;
74. Paolozzi A.; Peroni I., *Detection of Debonding Damage in a Composite Plate through Natural Frequency Variations*, Journal of Reinforced Plastics and Composites, vol. 9, no. 4, pp. 369-389, 1990;
75. Praisach Z.I.; Gillich G.R.; Birdeanu D.E., *Considerations on Natural Frequency Changes in Damaged Cantilever Beams Using FEM*, Conference: 3rd WSEAS International Conference on Engineering Mechanics, Structures, Engineering

Geology/International Conference on Geography and Geology Location: Corfu Island, Greece, Date: JUL 22-24, 2010, Latest Trends on Engineering Mechanics, Structures, Engineering Geology, Book Series: Mathematics and Computers in Science and Engineering, pp. 214-219, 2010;

76. Praisach Z.I.; Gillich G.R.; Protocsil C., Muntean F., *Evaluation of Crack Depth in Beams for known Damage Location based on Vibration Mode Analysis,* Applied Mechanics and Materials Vol. 430,(2013), pp. 90-94, (2013) Trans Tech Publications, Switzerland, doi:10.4028/www.scietific.net/AMM.430.90, 2013;
77. Qian G. L.; Gu S. N.; Jiang J.S., *The Dynamic Behavior and Crack Detection of a Beam with a Crack"*, Journal of Sound and Vibration. Vol. 38, No.2, 1990;
78. Radeş, M., *Vibraţii mecanice,* Ed. Printech, 2008;
79. Raúl Bermejo; Robert Danzer, *High failure resistance layered ceramics using crack bifurcation and interface delamination as reinforcement mechanisms*" Institut für Struktur- und Funktionskeramik, Peter-Tunner Straße 5, Montanuniversität Leoben, 8700 Leoben, Austria., Engineering Fracture Mechanics 77 (2010) 2126–2135 ;
80. Ravi J.T.; Nidhan S.; Muthu N.; Maiti S.K., *Analytical and experimental studies on detection of longitudinal, L and inverted T cracks in isotropic and bi-material beams based on changes in natural frequencies,* Mechanical Systems and Signal Processing, 101(15), pp. 67-96), 2018;
81. Rizos P.F.; Aspragathos N.; Dimarogonas A.D., *Identification of crack location and magnitude in a cantilever beam from the vibration modes,* Journal of Sound and Vibration, 138(3), pp. 381–388, 1990;
82. Rytter A., *Vibration based inspection of civil engineering structures,* Dept. of Building Technology and Structural Engineering, Aalborg University, Fracture and Dynamics, No. 44, Vol. R9314, 1993;
83. Schardin H., *Velocity Effects in Fracture*, (edited by B. L. Averbach et al.) Technology Press of Massachusetts, Institute of Technology and John Wiley & Sons, Inc., New York pp. 297-330, 1959;
84. Sinha J.K.; Friswell M.I.; Edwards S., *Simplified models for the location of cracks in beam structures using measured vibration data*, Journal of Sound and Vibration, 251(1), pp. 13-38, 2002;

85. Soham S. V.; Raikar V. A., *Crack detection in composite cantilever beam by Vibration analysis and Numerical method,* International Research Journal of Engineering and Technology (IRJET), Vol. 4(04), pp. 1776-1785, 2017;
86. Songsong Lu; Bao Rui; Zhang Thing; Fei Binjun, *Mechanism of crack branching in the fatigue crack growth path of 2324-T39 Aluminium alloy*, Institute of Solid Mechanics, Beihang University (BUAA), 100191, Beijing, China L. Songsong et alii, Frattura ed Integrità Strutturale, Vol. 35, pp. 74-81; DOI: 10.3221/IGF-ESIS.35.09, 2016;
87. Srinivas V.; Ramanjaneyulu K.; Jeyasehar C.A., *Multi-stage aprroach for structural damage identification using modal strain energy and evolutionary optimisation techniques*, Structural Health Monitoring, DOI: 10.1177/1475921710373291, 10(2) pp. 219-230, 2010;
88. Stubbs N.; Kim J. T.; Topole K., *An efficient and robust algorithm for damage localization in offshore platforms* Proceedings of the ASCE 10th Structures Congress, Vol. 1, pp. 543-546, 1992;
89. Tahreer M. F.; Janet M. L*., "Experimental investigation of crack propagation and crack branching in lightly reinforced concrete beams using digital image correlation"* Engineering Department, University of Cambridge, United Kingdom, Engineering Fracture Mechanics 182, pp. 487–505, 2017;
90. Timoshenko S., *History of strength of materials*, McGraw-Hill New York, 1953;
91. Tracy J.J., Gerard C.P., *Effect of delamination on the natural frequencies of composite laminates,* Journal of *Composite* Materials, Vol. 23: p. 1200–1215, 1989;
92. Tufoi M.; Hatiegan C.; Vasile O.; Gillich G.R., *Dynamic Analysis of Thin Plates with Defects by Experimental and FEM Methods*, Romanian Journal of Acoustics and Vibration 10(2), pp. 83-88, 2013;
93. Tufisi C.; Gillich G.R.; Nedelcu D; Hamat C.O., *Numerical study on complex shaped cracks in cantilever beams concerning frequency and stiffness changes*, Vibroengineering procedia, Vol. 19, pp. 253-258, 2018;
94. Tufisi C.; Gillich G.R.; Hamat C.O.; Gillich N.; Praisach Z.I., *Numerical Study of the Stiffness Degradation Caused by Branched Cracks and its Influence on the Natural Frequency Drop*, Romanian Journal of Acoustics and Vibration, 15(1), pp. 53-57, 2018;

95. Tufisi C.; Gillich G.R.; Nedelcu D., *Effect of the orientation of an oblique crack branches on the beam eigenfrequencies,* 1st International Conference on Circuits, ICMSAV 2018 & COMAT 2018 & Emech 2018, Brasov, Romania, October 2018;
96. Tufisi C.; Gillich G.R.; Vasile O.; Korka Z.I.; Hamat C.O., *Identification of delamination in multilayered composites,* 7th International Conference on Advanced Materials and Structures AMS'18, pp. 28-31, Timisoara, 2018;
97. Tufisi C.; Gillich G.R., *Modeling of complex shaped cracks,* Analele Universitatii Eftimie Murgu. Fascicula de Inginerie, Vol. 25, 2018;
98. Tufisi C.; Gillich G.R.; Hamat C.O.; Gillich N.; Manescu T., *Study regarding the effect of crack branching on the eigenfrequencies of beams,* DAMAS 2019;
99. Vandiver J.K., "*Detection of Structural Failure on Fixed Platforms by Measurement of Dynamic Response,*" in Proc. of the 7th Annual Offshore Tech. Conf., pp. 243–252, 1975;
100. Wahab M.A.; De Roeck Guido, *Damage detection in bridges using modal curvatures: Application to a real damage scenario,* Journal Of Sound And Vibration, Vol. 226 (2), p.217-235, 1999;
101. Wang Z.; Lin R.M.; Lim M.K., *'Structural Damage Detection using Measured FRF Data*'. Computer Methods in Applied Mechanics and Engineering, Vol. 147, 187-197, 1997;
102. Yun-Lai Zhou; Wahab M.A., "*Rapid Early Damage Detection Using Transmissibility With Distance Measure Analysis Under Unknown Excitation In Long-Term Health Monitoring*", Jve International Ltd. Journal Of Vibroengineering, Vol. 20, ISSUE 1. ISSN 1392-8716, Feb 2018;
103. Zhang K.; Yan X., *Multi-cracks identification method for cantilever beam structure with variable cross-sections based on measured natural frequency changes,* Journal of Sound and Vibration, 387, pp.53-65, 2017;
104. Zou Y.; Tong L.; Steven G.P., *Vibration-Based Model-Dependent Damage (Delamination) Identification and Health Monitoring For Composite Structures* - A Review. Journal of Sound and Vibration, 230(2): p. 357-378, 2000;
105. https://en.wikipedia.org/wiki/Modal_analysis [17.08.2020];
106. https://www.simscale.com/docs/content/simwiki/fea/whatisfea.html [17.08.2020];

Appendix

Figure 1. Errors obtained with the presented methods for a cantilever beam having a T-shaped crack at position x=300 mm

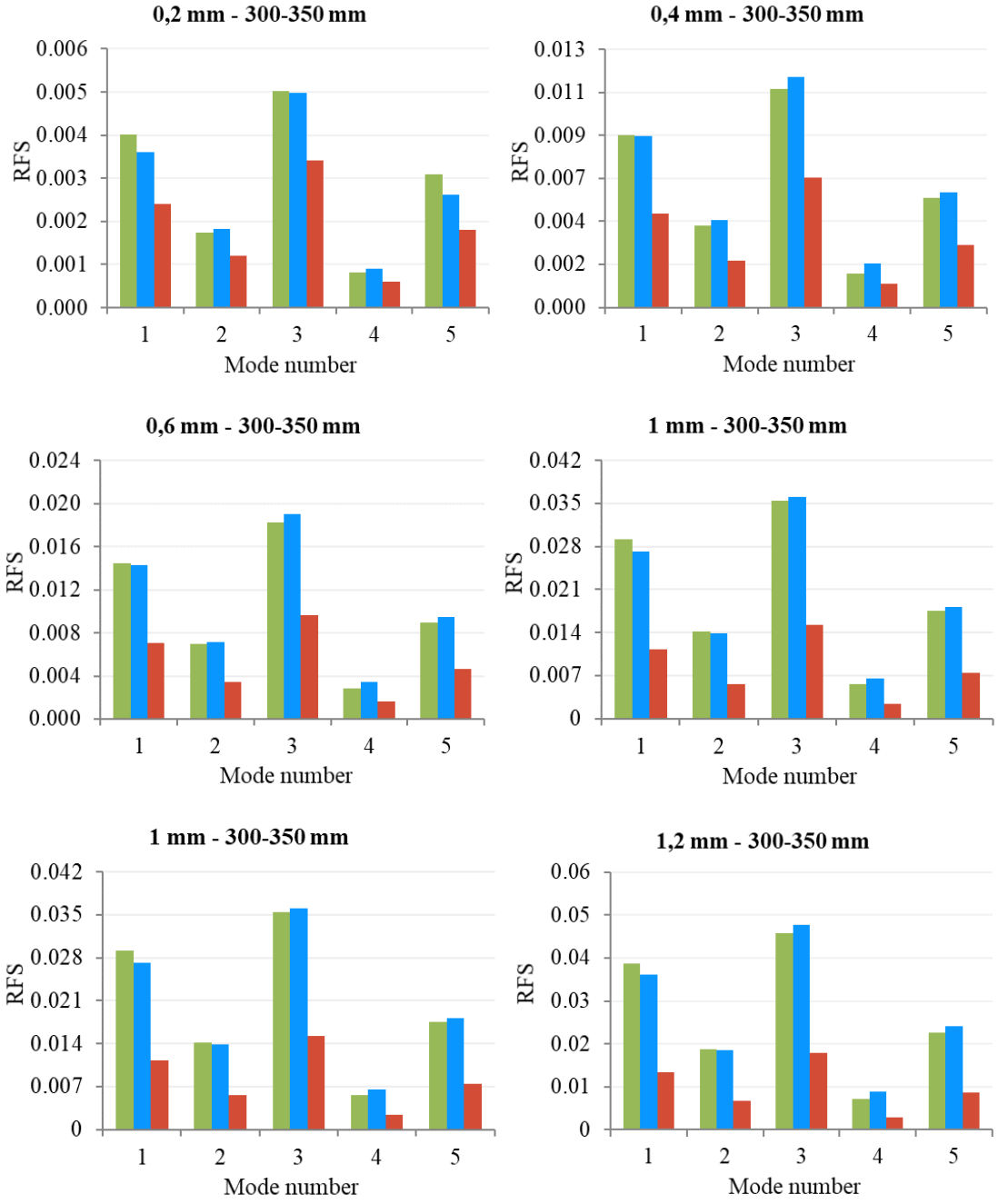

Figure 2. RFS comparison for the T-shaped crack positioned at *x*=300 mm at different depths

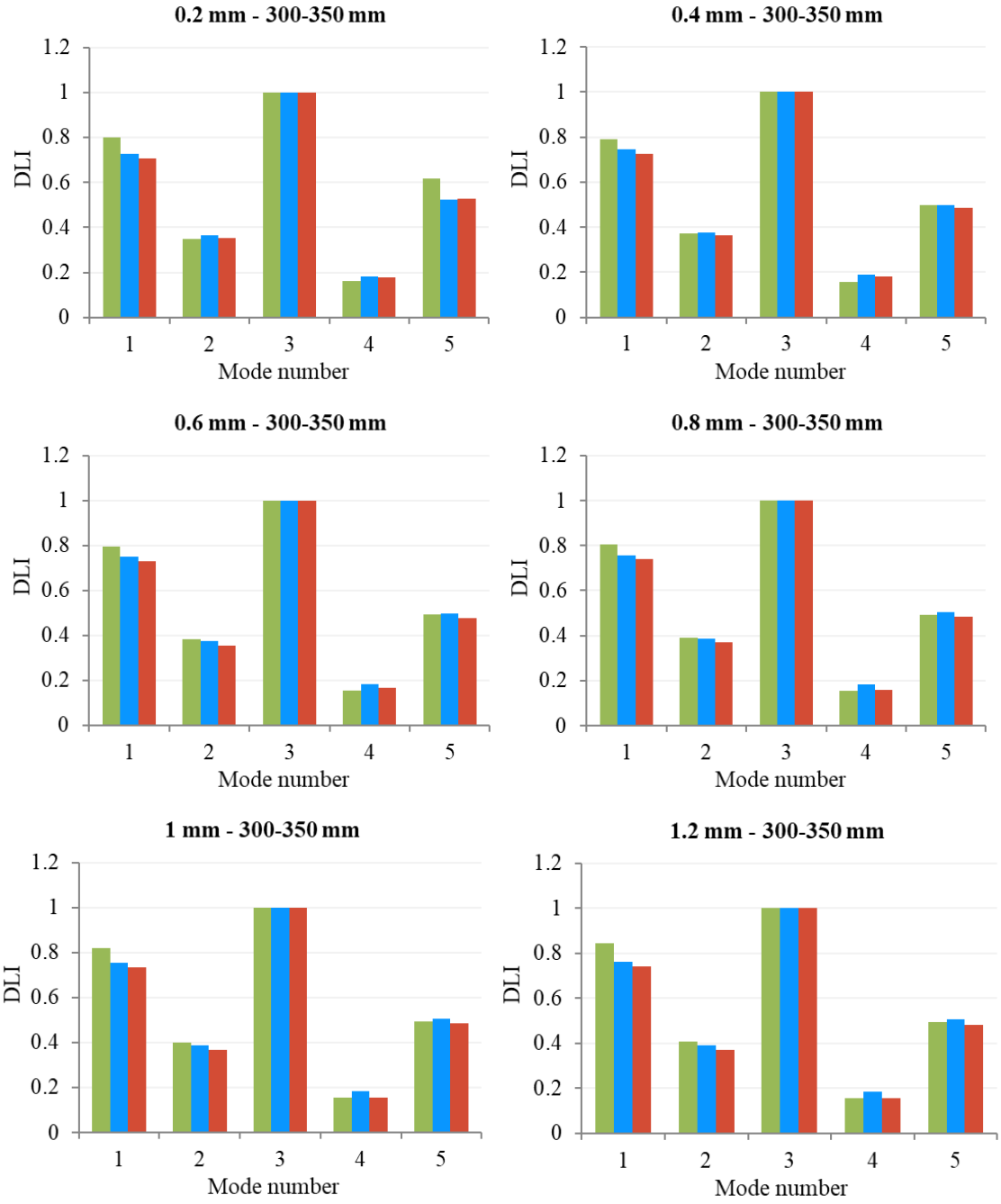

Figure 3. DLI comparison for the T-shaped crack positioned at *x*=300 mm at different depths

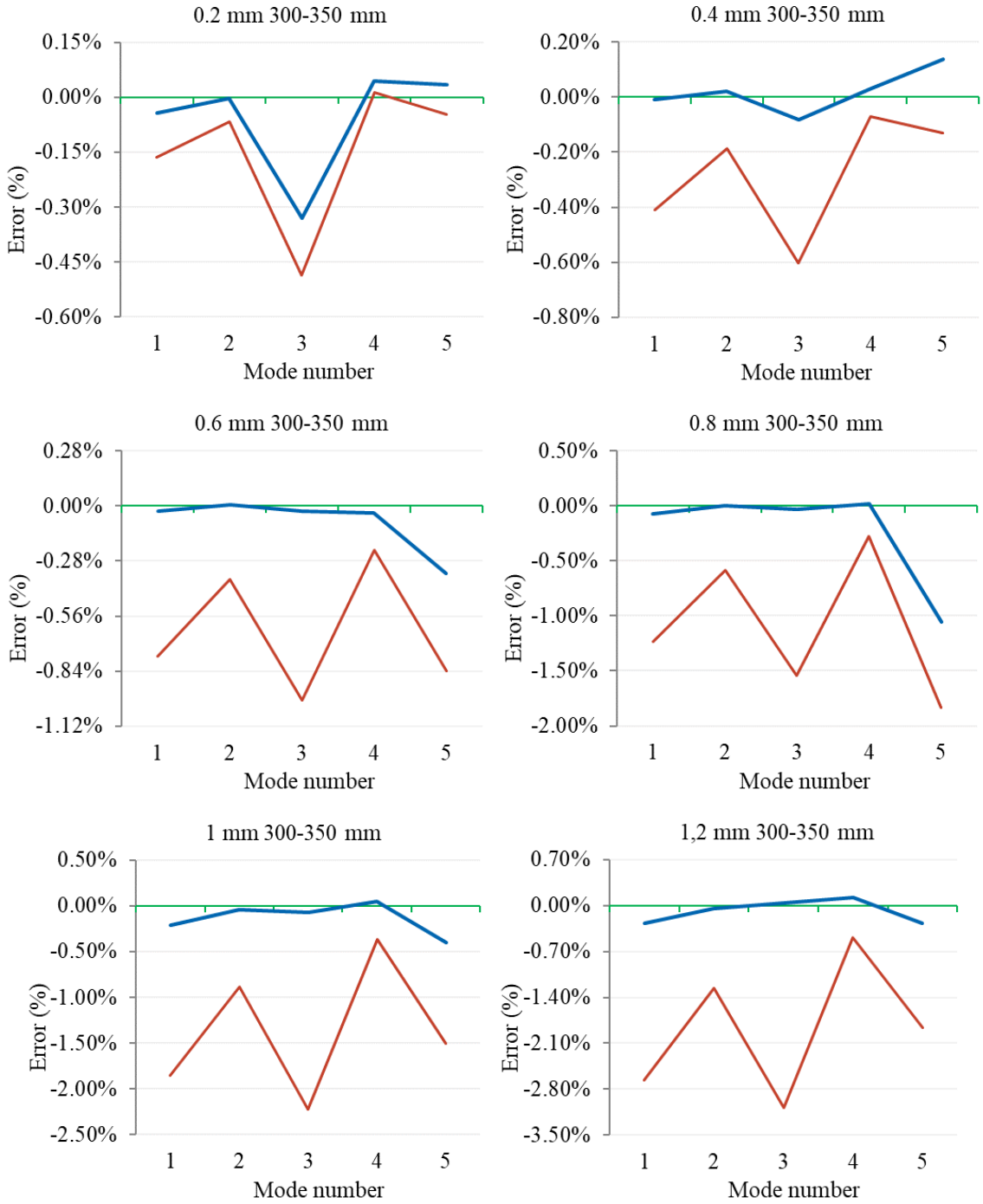

Figure 4. Errors obtained with the presented methods for a cantilever beam having a L-shaped crack at position x=300 mm

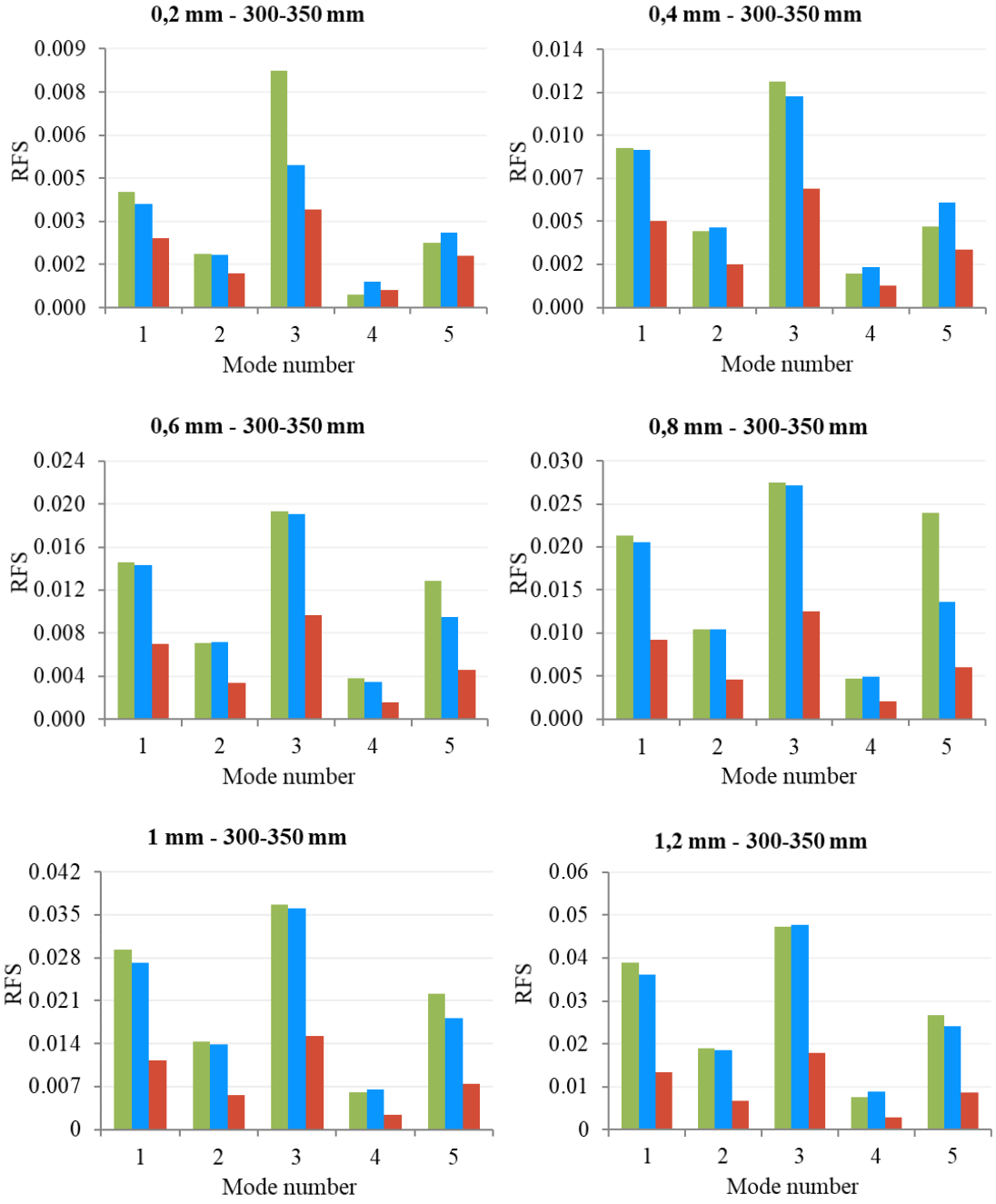

Figure 5. RFS comparison for the L-shaped crack positioned at *x*=300 mm at different depths

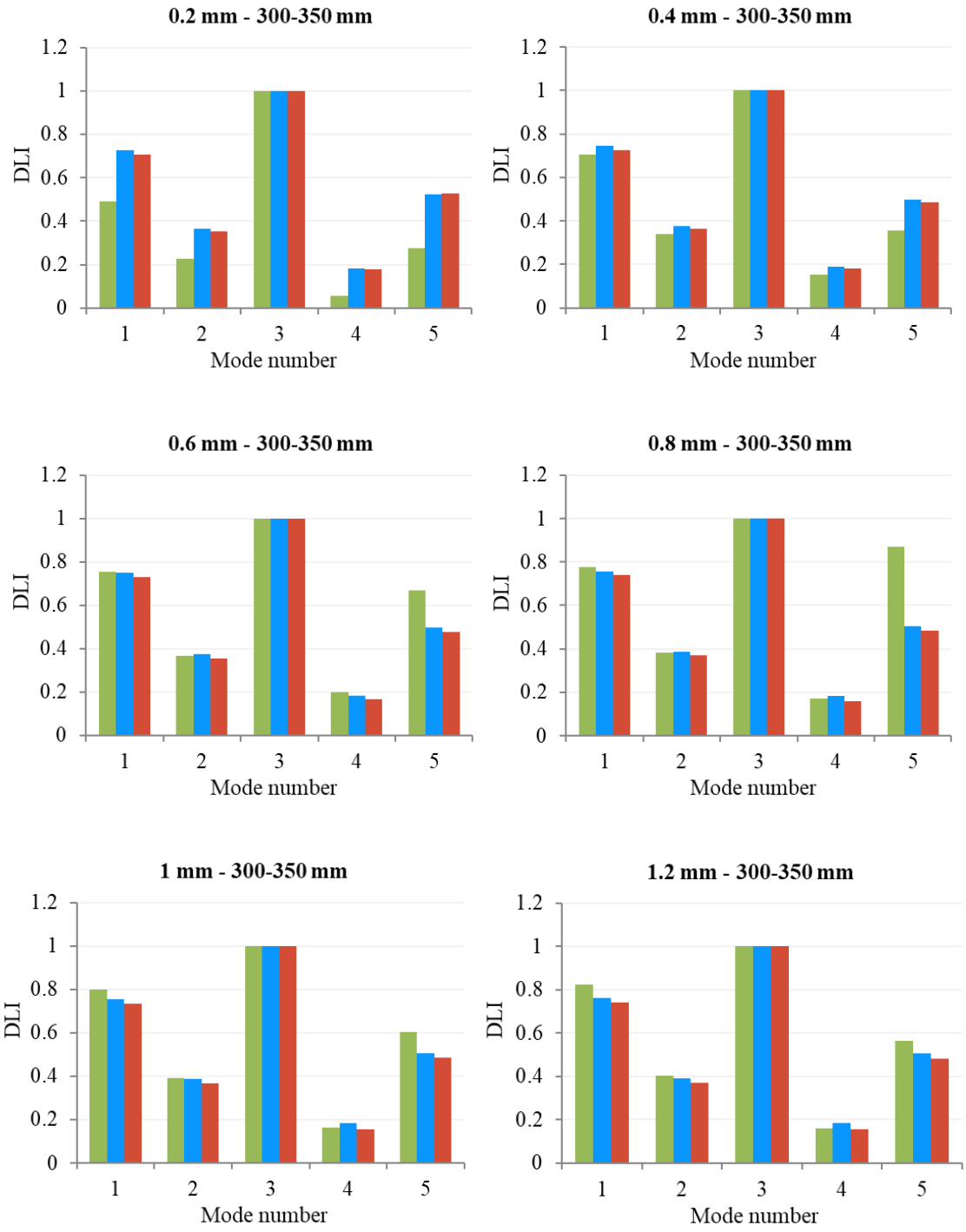

Figure 6. DLI comparison for the L-shaped crack positioned at *x*=300 mm at different depths

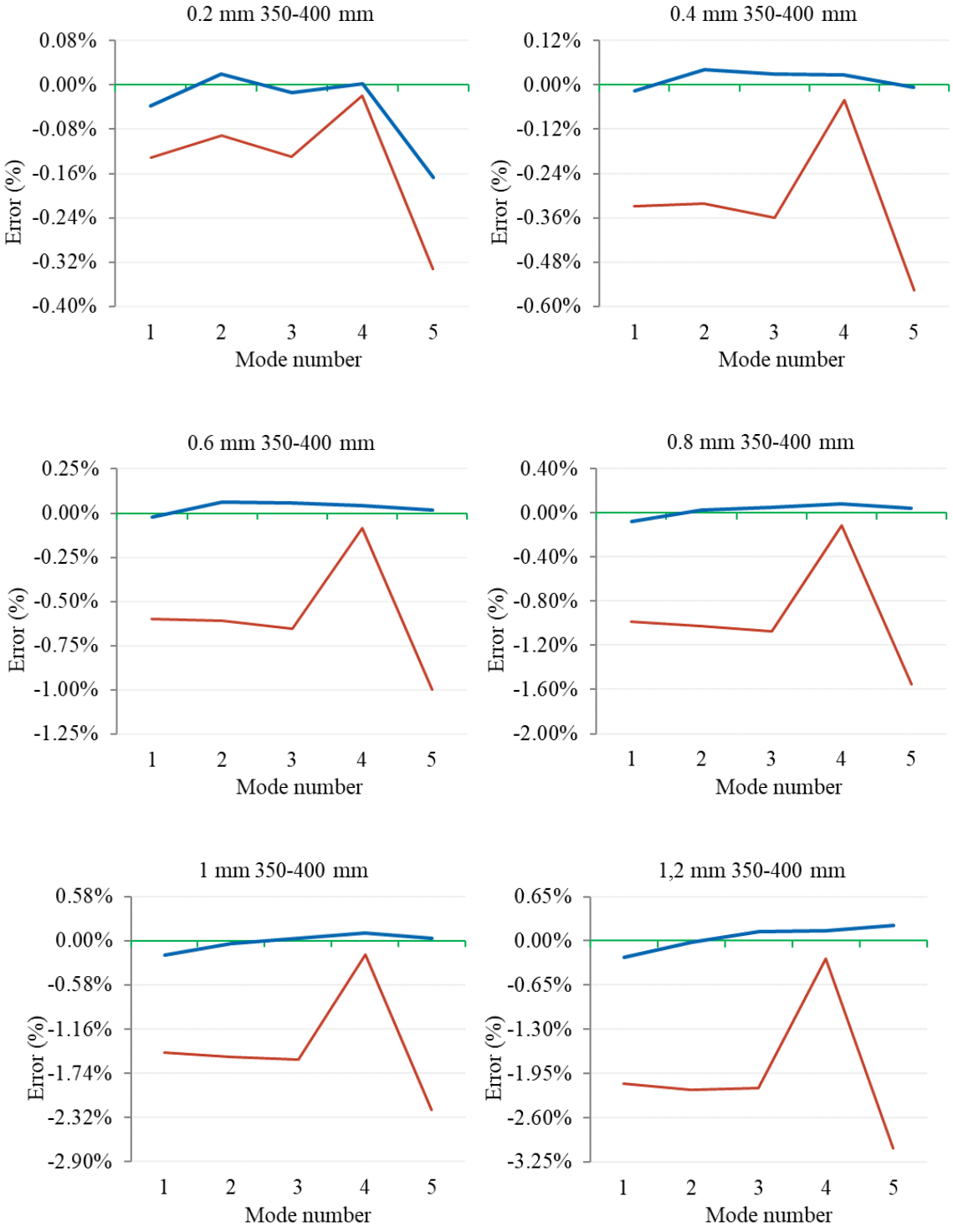

Figure 7. Errors obtained with the presented methods for a cantilever beam having a T-shaped crack at position x=350 mm

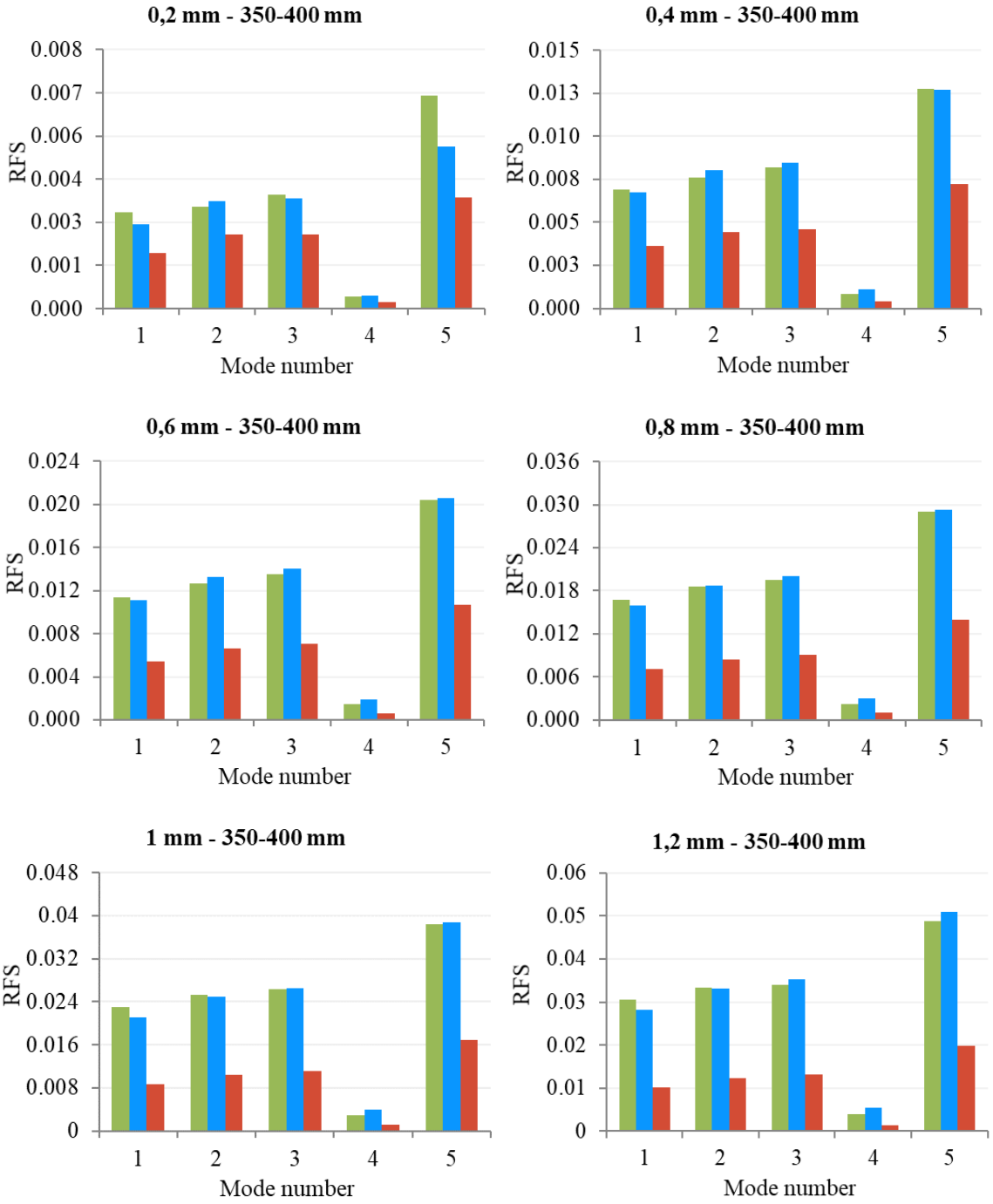

Figure 8. RFS comparison for the T-shaped crack positioned at *x*=350 mm at different depths

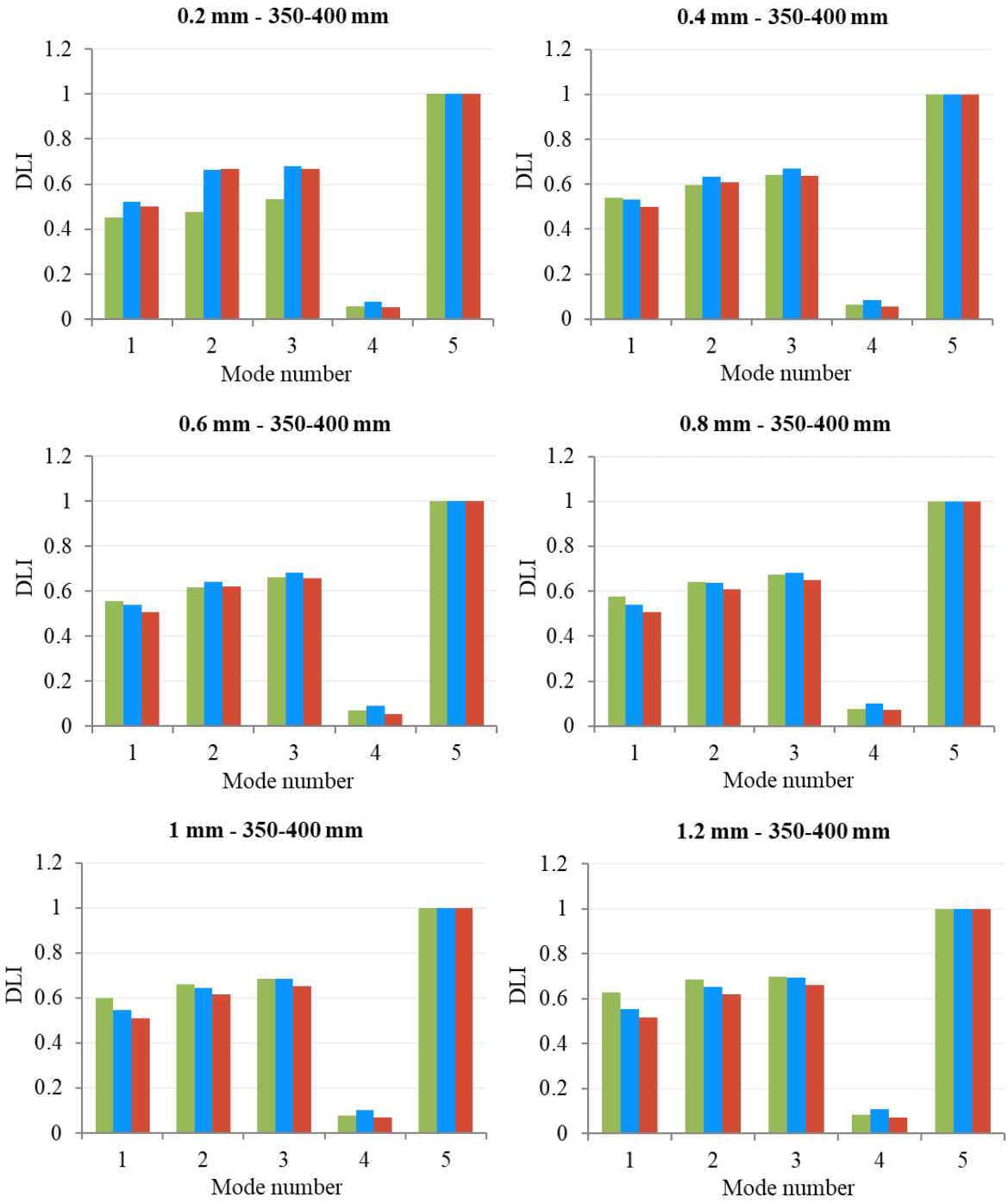

Figure 9. DLI comparison for the T-shaped crack positioned at *x*=350 mm at different depths

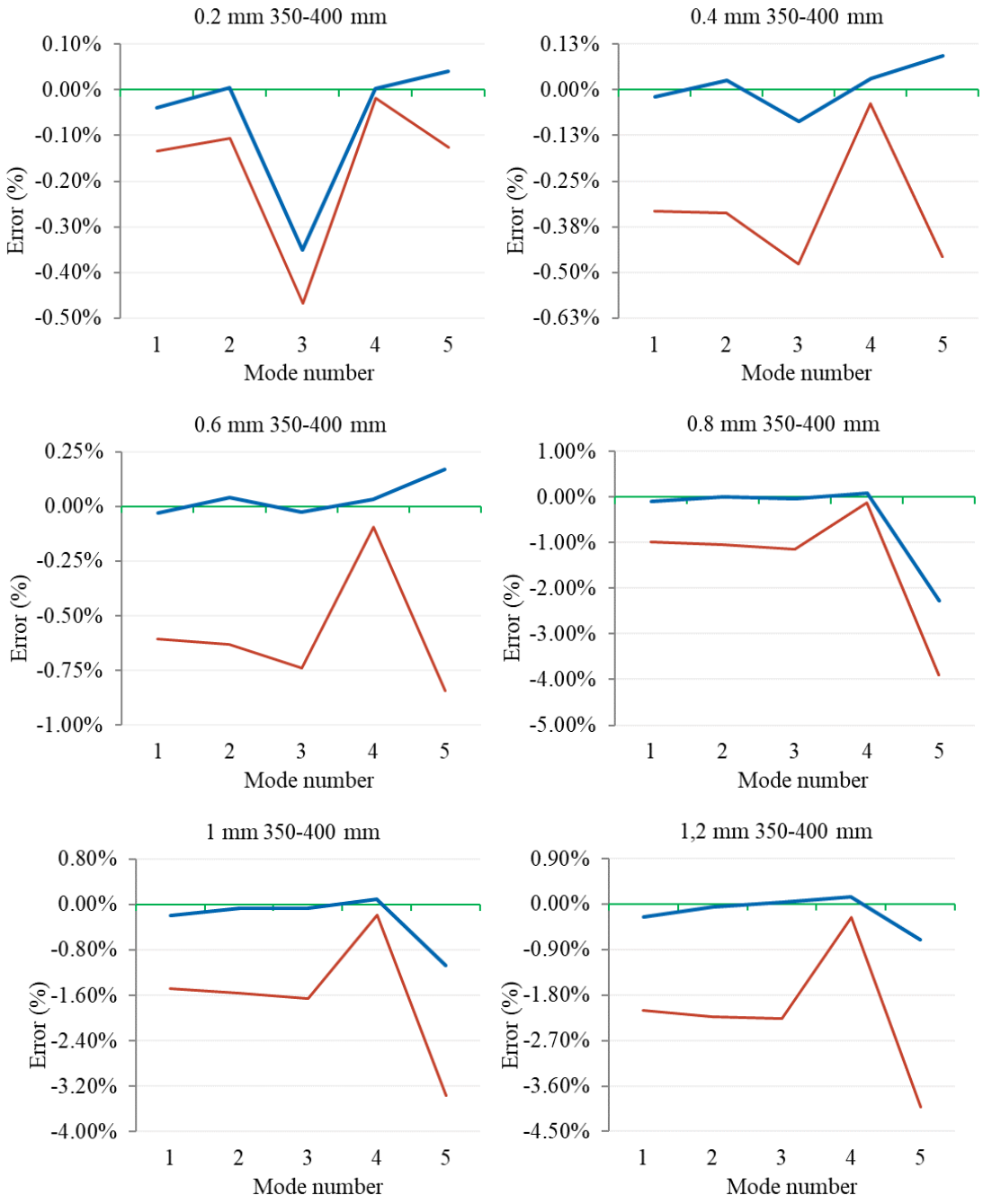

Figure 10. Errors obtained with the presented methods for a cantilever beam having a L-shaped crack at position x=350 mm

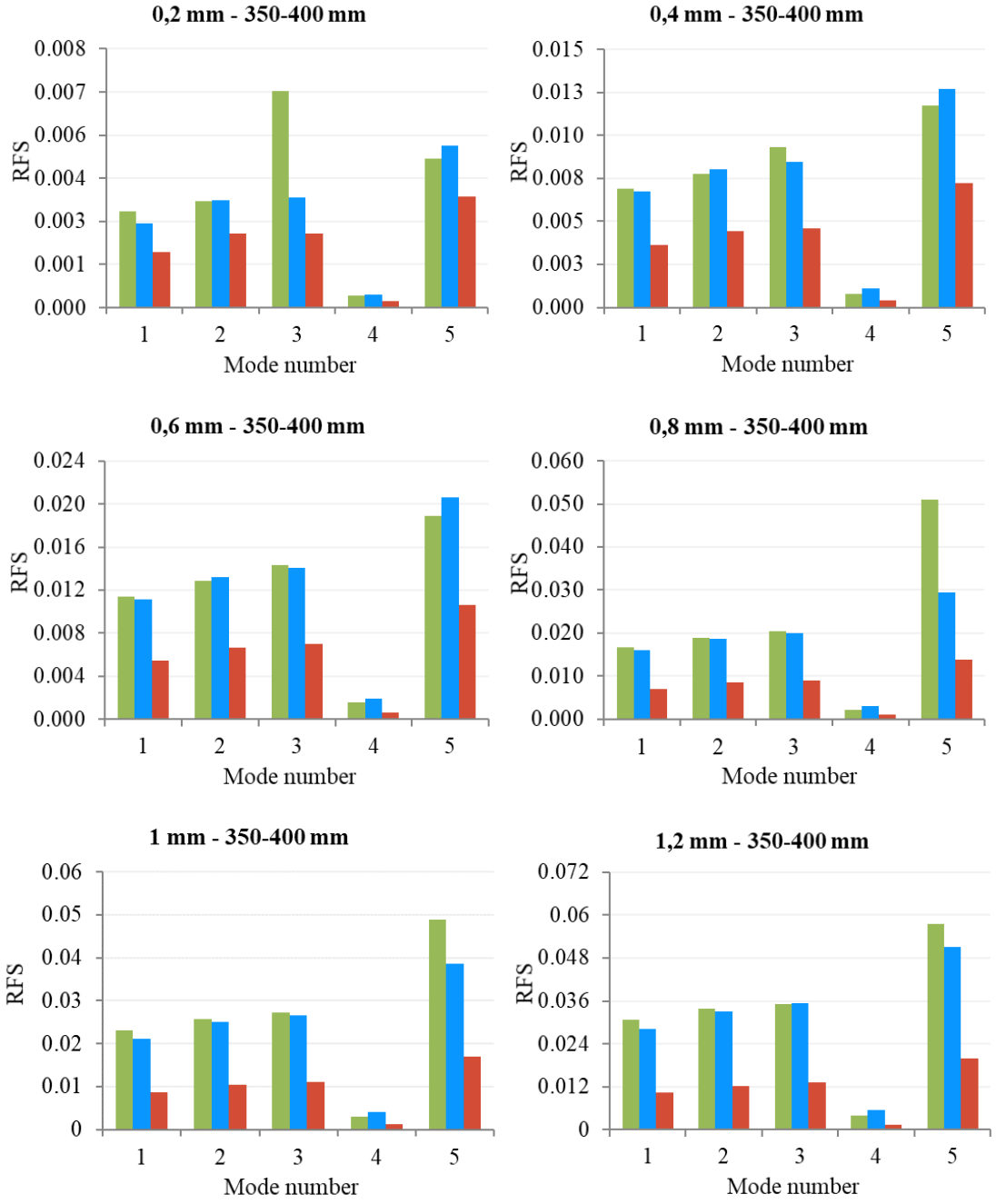

Figure 11. RFS comparison for the L-shaped crack positioned at *x*=350 mm at different depths

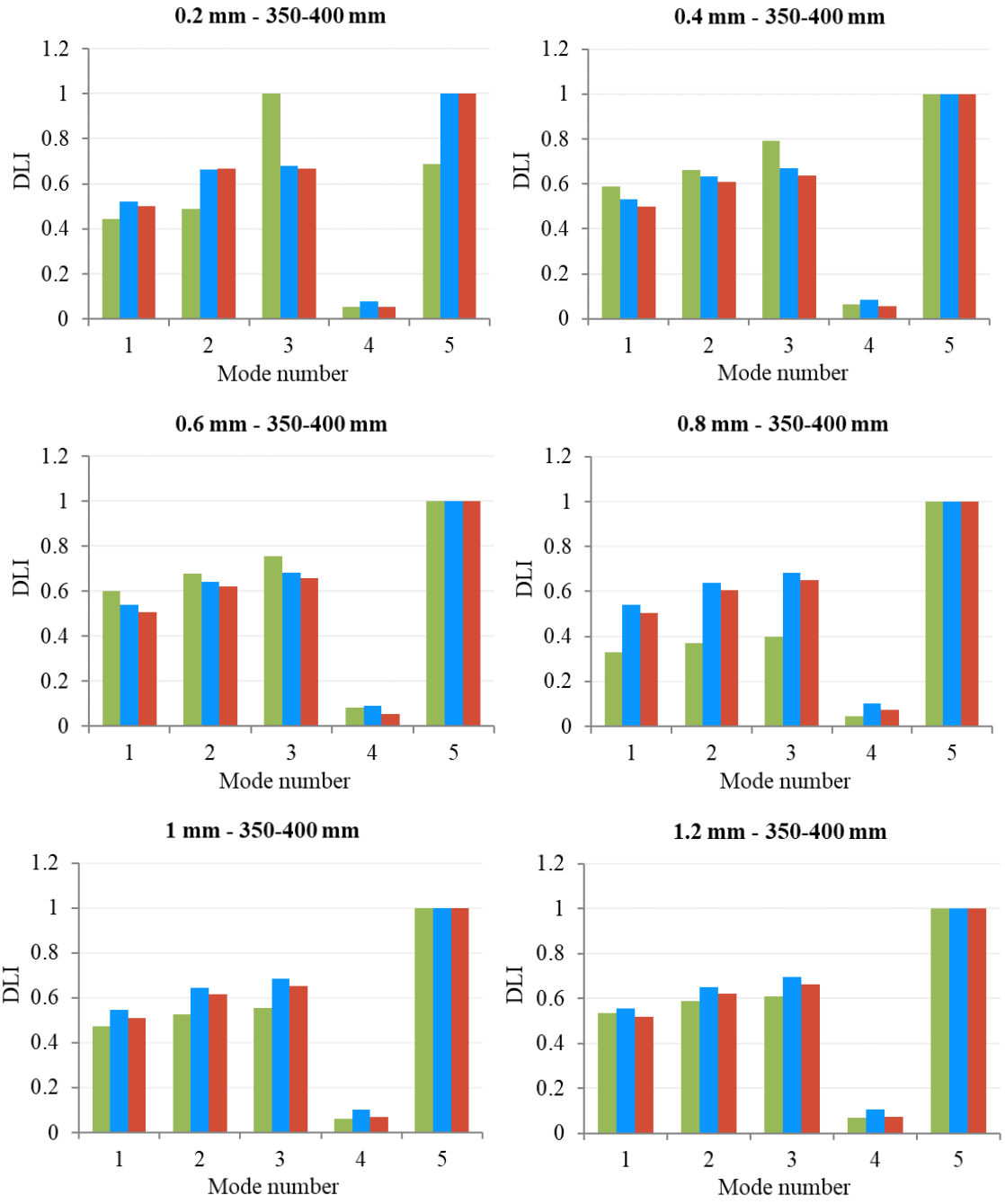

Figure 12. DLI comparison for the L-shaped crack positioned at *x*=350 mm at different depths